FACIES ARCHITECTURAL STUDY OF INCISED VALLEYS, DISTRIBUTARY CHANNELS, AND MOUTH BARS IN THE CRETACEOUS FERRON NOTOM DELTA, SOUTHERN CENTRAL UTAH, USA.

A Dissertation Presented to

the Faculty of the Department of Earth and Atmospheric Sciences

University of Houston

In Partial Fulfillment

of the Requirements for the Degree

Doctor of Philosophy

By

Yangyang Li

December 2012

FACIES ARCHITECTURAL STUDY OF INCISED VALLEYS, DISTRIBUTARY CHANNELS, AND MOUTH BARS IN THE CRETACEOUS FERRON NOTOM DELTA, SOUTHERN CENTRAL UTAH, USA.

_____

Yangyang Li

APPROVED:

_____

Dr. Janok P. Bhattacharya, Chairman

_____

Dr. William R. Dupré, Committte Member

_____

Dr. Julia Wellner, Committee Member

_____

Dr. Brian Willis, Committee Member

_____

Dr. Mark A. Smith, Dean

College of Natural Sciences and Mathematics

ACKNOWLEGEMENTS

Firstly, I would like to express my deepest gratitude to my advisor, Dr. Janok P. Bhattacharya, who has guided, encouraged and inspired me throughout this graduate career in University of Houston. I am deeply influenced by his way of critical thinking, passion in geology, and enthusiasm in life. He not only teaches me how to be a good scientific researcher, but also a way of living life. I feel so lucky working with an advisor and a friend like him. I would like to thank Dr. William R. Dupré, Dr. Julia S. Wellner, and Dr. Brian Willis for serving on my committee. Thanks for their valuable suggestions and discussions at different stages of my research.

Thanks to Ben Browning and Danfix D'Souza for being field assistants for me and making the field works in the Utah desert more fun and enjoyable. Thanks also go to my other colleagues Sumiyah Ahmed, Jarratt Kelso, Petter Dischington, Yijie Zhu, Weiguo Li, Oyebode Famubode, Omar Montes, Darsel Seepsard, Jianqiao Wang, Chenliang Wu, Cameron Griffin, Ben Hilton, Shahidullah Apu, and friends Mark Barton, and Chris Modica for insightful discussions on the Ferron.

I would like here to thank my Mom Chunping Xu and Dad Yingxiang Li for supporting me throughout my study career and especially when I am in the US. And thank you for their understanding that I did not go back to see them in almost four and a half years. Thank to my sister and brother and all other family members for always being supporting and caring. Special thanks to my girlfriend Linyi Wu, for her patience and care to me during the period I was working hard on my thesis.

This work was made possible by funding to Dr. Bhattacharya's Quantitative Sedimentology Consortium sponsored by Anadarko, BP, Chevron, Nexen, Shell, ExxonMobil, Pioneer, EcoPetrol, Inpex, and BHP Billiton.

FACIES ARCHITECTURAL STUDY OF INCISED VALLEYS, DISTRIBUTARY CHANNELS, AND MOUTH BARS IN THE CRETACEOUS FERRON NOTOM DELTA, SOUTHERN CENTRAL UTAH, USA.

A Dissertation Presented to

the Faculty of the Department of Earth and Atmospheric Sciences

University of Houston

In Partial Fulfillment

of the Requirements for the Degree

Doctor of Philosophy

By

Yangyang Li

December 2012

ABSTRACT

This dissertation is focused on analysing architectural elements to understand the formative processes in linked fluvial and deltaic depositional systems in an ancient system. A compound incised valley system (IVS) and distributary channel and crevasse delta system are documented in successively more distal positions within outcrops of the Cretaceous Ferron Notom Delta in central Utah.

The compound IVS is composed of three simple IVS systems, IVS3, IVS2 and IVS1 (oldest to youngest). IVS3 consists of tidally influenced deposits that form a terrace cut into lower shoreface deposits. IVS2 consists of multi-storey fluvial deposits with minor tidally influenced fluvial deposits in the upper 10%. IVS1 consists entirely of medium-grained fluvial deposits. The composite valley fill records generally increasing fluvial-dominance and decreasing tide-influence during successive cut-and-fill episodes associated with each simple valley fill. These changes are interpreted to correlate with a longer term, stepped relative fall of sea level, punctuated by stillstands, or minor rises of sea level.

A lower delta-plain distributary channel system is mapped in 3-D outcrop exposures in Parasequence 5a, Sequence 2. A main channel belt about 250 m wide narrows to 200 m downstream of the branching point. The subordinate channel belt is 80 m wide. Water discharge from the main distributary channel, upstream of the branching point, is estimated to be 85-170 m^3/s. Compared to paleodischarge of trunk rivers mapped in previous studies in the Notom Delta, the branching is estimated to be a 4th order split.

A crevasse delta that prograded toward the west is mapped in Parasequence 6a Sequence 2, while the regional delta prograded toward the east. The crevasse delta

was protected from marine influence by a wave-dominated barrier system. The proximal delta-front facies consists of planar beds which pass upward into meter-scale low-angle cross beds, which decrease in dimensions upward and finally change to decimeter-scale cross beds. Planar-stratified sandstones are interpreted to be deposited in an inertia-dominated environment and cross-stratified sandstones are interpreted to be deposits in a friction-dominated environment. The upward decrease of cross set dimensions is mainly due to the filling of accommodation and shallowing of the water.

TABLE OF CONTENTS

CHAPTER 1 Introduction

1.1 Overview

This dissertation provides documentation of compound incised valley systems, delta-plain distributary channel systems and river-dominated mouth-bar deposits in a fluvial-deltaic system in the Cretaceous Ferron Notom Delta in Utah.

1.2 Dissertation Organization

Chapter 2 is mainly from a paper submitted to the Journal of Sedimentary Research, and coauthored by me and my advisor Janok Bhattacharya (Li and Bhattacharya in review). I have collected all the data, drafted all the figures, and written most part of the paper and Dr. Bhattcharya did primarily the editing of the paper. This paper was accepted with minor revision.

This chapter describes a compound incised valley system, which is interpreted to have formed during a stepped force regression. Detailed outcrop facies architectural study of a portion of a >10 kilometer-wide compound incised valley system in the Turonian Ferron Notom Delta shows three simple incised valley systems filled with different facies associations. The valley fill deposits were mapped with 30 detailed measured sections, photomosaics and bedding diagrams. The oldest, IVS 3 forms a terrace deposit that erodes directly into hummocky cross-stratified lower shoreface deposits. It is filled with fine- to medium-grained tidally influenced deposits, characterized by abundant mud-draped cross beds, sparse burrowing, and a bimodal paleocurrent-direction pattern. The next youngest IVS 2 locally cuts through the valley 3 terrace and also into the lower shoreface deposits. The valley 2 fill comprises multi-storey, medium-grained fluvial deposits with minor finer grained, tidally

influenced fluvial deposits in the upper 10% of the fill. The youngest, IVS 1, also locally cuts into the lower shoreface deposits, partially removing the terraces formed by valley 2 and 3. Valley 1 is filled entirely with medium-grained fluvial deposits. The composite valley fill records generally increasing fluvial dominance and decreasing tidal influence during successive cut-and-fill episodes associated with each simple valley fill. This is hypothesized to correlate with a longer term, stepped relative fall of sea level, punctuated by standstills, or rises of decreasing amplitudes.

Chapter 3 is mainly from a paper submitted to Sedimentology, which is coauthored by me and my advisor Dr. Janok Bhattacharya and is now in the second round of review (Li and Bhattacharya in review). I have collected all the data, drafted all the figures, and written most part of the paper and Dr. Bhattcharya did primarily the editing of the paper.

This chapter illustrates a lower delta-plain distributary channel system. Distributary channel systems are an important component of deltaic systems, but details of their branching pattern, internal variability, complexity, and relationship with adjacent levee, bay, and crevasse splays, are rather poorly documented in ancient examples. A gooseneck-shaped canyon in the Coalmine Wash area in southern Utah, U.S.A. provides 3-D outcrop exposures of a lower delta-plain distributary channel system of the Late Turonian Ferron Notom delta. Thirty-two measured sections and 9 cross sections allow direct mapping and documentation of the branching pattern of a distributary system. A main channel belt about 250 m wide narrows to about 200 m downstream of the branching point. The subordinate channel belt is about 80 m wide. Water discharge from the main channel belt, upstream of the branching point, is estimated to be 85-170 m^3/s. Compared to paleohydraulic estimates of trunk rivers

mapped in previous studies (Li et al. 2010), the branching documented in this study is probably a 4th order split. The distributary channels are characterized by a U-shaped geometry in oblique and strike-oriented cross sections. They are filled with medium-grained, cross-bedded sandstone, meter-scale inclined beds, ripple-cross-laminated sandstone, and muddy abandoned channel deposits with local tide- and wave-influenced deposits. Detailed bedding diagrams indicate a meandering channel pattern with local braided threads within the main channel belt. Distributary channels erode into adjacent levee and underlying heterolithic bayfill deposits. The subordinate channel belt fed a crevasse splay, which is characterized by a coarsening upward facies succession consisting of interbedded wave-rippled, current-rippled and planar-bedded, very fine-grained sandstone and thin mudstones.

Chapter 4 is mainly from a paper that co-authored by me, my advisor Janok Bhattacharya, Daniel Garza and Sumiyah Ahmed (Li et al. in review). It documents a crevasse delta system and discussed the processes of mouth-bar deposition. I have collected most of the data used in this paper and part of the data is from Daniel Garza and Sumiyah Ahmed. This paper was submitted to Journal of Sedimentary Research for review. A crevasse delta is mapped with 18 detailed measured sections, 10 high-resolution photomosaics and associated bedding diagrams, more than a thousand paleocurrent measurements, and 10 clinoform dip directions. The crevasse delta prograded toward the west, while the regional delta generally prograded toward the east. The crevasse delta was protected from marine influence (wave/tide) by a wave-dominated barrier system basinward of the crevasse delta. Facies analysis shows that the crevasse delta is river-dominated and is characterized by a coarsening upward succession, composing muddy prodelta, heterolithic distal delta front, sandy

proximal delta front, and distributary channel deposits. The proximal delta-front facies is composed of planar beds which pass upward into meter-scale low-angle cross strata, which gradually decrease in dimensions (thickness and width) upward and finally change to dune-scale cross beds. Planar bedded and cross-bedded sandstones are interpreted respectively to be deposited in inertia-dominated and friction-dominated environments. The decrease in dimensions upward of the cross-bed sets above the planar beds is interpreted to represent a transition from an inertia-dominated to a friction-dominated environment, which is interpreted to be mainly due to the filling of accommodation and shallowing of the water.

Chapter 5 is a summarization of the results of this thesis and suggestions about future work.

CHAPTER 2 Facies Architectural Study of a Stepped Forced Regressive Compound Incised Valley System in the Ferron Notom Delta, Southern Central Utah

2.1 Introduction

Incised valleys are defined as elongate topographic features, floored by rivers that are unable to routinely flood their walls (Zaitlin et al. 1994). In the stratigraphic record, incised valley depositional systems are important because their erosional margins are assumed to have chronostratigraphic significance as sequence bounding unconformities, and the associated overlying fills have economic significance in hosting oil and gas reservoirs (Van Wagoner et al. 1990; Dalrymple et al. 1994; Posamentier and Allen 1999; Boyd et al. 2006; Dalrymple 2010). However, recent studies have questioned the idea that such regional fluvial incision surfaces actually represent a geomorphic valley or form a sequence boundary (Holbrook et al. 2006; Strong and Paola 2008; Bhattacharya 2011; Holbrook and Bhattacharya 2012). In the original sequence stratigraphic literature (e.g. Posamentier et al. 1988; Van Wagoner et al. 1990; Shanley and McCabe 1994), it was assumed that degradational landscapes were largely eroded during sea-level falls, forming a geomorphic valley-shaped regional surface of erosion (i.e. the sequence boundary). These models assumed that sediments were largely bypassed across these surfaces into more distal environments, such as shelf-edge deltas and lowstand submarine fans. This “bypass model” also suggests that valleys are only later filled primarily during base-level rise (Boyd and Diessel 1994).

Holbrook and Bhattacharya (2012) proposed an alternate “cut-and cover” model,

in which significant fluvial sediments can be stored on the evolving surface, forming falling-stage terraces. True geomorphic valleys form in the areas in between these exposed terraces and form a small part of the broader stratigraphic discontinuity. Later, these falling-stage terraces may be reworked and covered during rising-stage. Such regional erosional surfaces are highly composite and potentially highly diachronous stratigraphic discontinuities, which may be covered by a variety of fluvial to marine-influenced facies (e.g. transgressive estuarine deposits) that vary widely in age. In reality, erosional drainage networks may form basin-scale features with a great degree of regional variability in morphology and associated fills.

The focus of this paper is to document and interpret the detailed facies architecture and complex cut-and-fill relationships of part of a regional compound ancient valley system, which is well exposed in a series of closely spaced canyon walls in the Notom Delta Complex of the Ferron Sandstone Member of the Mancos Shale Formation in southern central Utah. Previous sequence stratigraphic studies (Li 2009; Zhu et al. 2012) indicate that this compound valley system was linked to a shoreline and formed over a relatively short time interval, probably in less than 100, 000 years, within a Milankovitch frequency range. The Ferron valleys were within 150 km of the shoreline with a costal prism angle of 0.006^0 (Li et al. 2010); the incision depth of the valleys is about 15 m in this study. These information allow us to investigate the response of the valley system to relative changes of sea level (Ainsworth and Walker 1994; Dalrymple et al. 1994; Garrison and Van Den Bergh 2006), similar to those documented in studies of Quaternary-age compound valleys (Blum 1993).

Simple incised valley systems are formed through one cycle of incision and

deposition, compared to compound incised valley systems which record multiple cycles of cut-and-fills (Zaitlin et al. 1994). Incised valley fills can be divided into a marine-dominated segment 1 (seaward outer portion); estuarine-dominated segment 2 (middle portion), and fluvial-dominated segment 3 (landward inner portion) along their depositional dip profile (Zaitlin et al. 1994; Boyd et al. 2006). Although there are numerous case studies that documented facies organizations of incised valley fills (Allen and Posamentier 1993; Blum 1993; Aitken and Flint 1994; Ashley and Sheridan 1994; Belknap et al. 1994; Simms et al. 2006; Maynard et al. 2010), there are relatively few detailed facies architectural studies of ancient examples in outcrop (Martinsen 1994; Willis 1997; Barton et al. 2004; Garrison and Van Den Bergh 2006; Plink-Bjorklund and Steel 2006; Li et al. 2010).

Many examples of stepped forced regressions, associated with marine depositional systems, have been documented in the literature (Plint 1988; Posamentier et al. 1992; Hamberg and Nielsen 2000; Azeredo et al. 2002; Tamura et al. 2007), including the Ferron Notom Delta (Li and Bhattacharya 2011; Zhu et al. 2012), but there are far fewer examples that show how coeval valleys evolve during such stepped relative sea-level falls (Blum 1993; Zaitlin et al. 1994; Hamilton et al. 2001; Ardies et al. 2002). This study attempts to evaluate the possibility of the origin of the Ferron compound valley system as a function of a high-frequency, stepped forced regression.

2.2 Geological Setting and Previous Ferron Work

The Ferron Sandstone Member of the Mancos Shale Formation consists of a series of northeast prograding clastic wedges, shed from the Sevier orogenic belt to the west and deposited at the western margin of the late Cretaceous Western Interior

Seaway (Hale 1972; Cotter 1975; DeCelles and Giles 1996; Ryer and Anderson 2004) (Fig. 1A). Three fluvial deltaic complexes have been identified in the Ferron Sandstone, including the informally named "Notom Delta", the "Last Chance Delta" and the less well exposed "Vernal Delta" (Hale and Van De Graaff 1964; Hale 1972; Cotter 1975; Hill 1982) (Fig. 1B). The Notom Delta is bounded by the Blue Gate Shale Member above and Tununk Shale Member below and passes from sandy fluvial deltaic facies into muddy marine facies northeastward (Li 2009; Zhu et al. 2012) (Fig. 1A).

A recent regional sequence stratigraphic synthesis of the Ferron Notom Delta documented 43 parasequences, 18 parasequence sets, and 6 sequences (Li 2009; Zhu et al. 2012) (Fig. 2). The compound incised valley system examined in this study is placed in Parasequence set 3 of Sequence 1 (Fig. 2B). Based on $^{40}Ar/^{39}Ar$ dating of sanidine crystals in associated bentonites, the entire Ferron Delta complex is estimated as deposited between 91.25 Ma and 90.63 Ma, a total of ~620,000 years (Zhu 2010). Sequence 1 is thus estimated to have been deposited in approximately 100, 000 years.

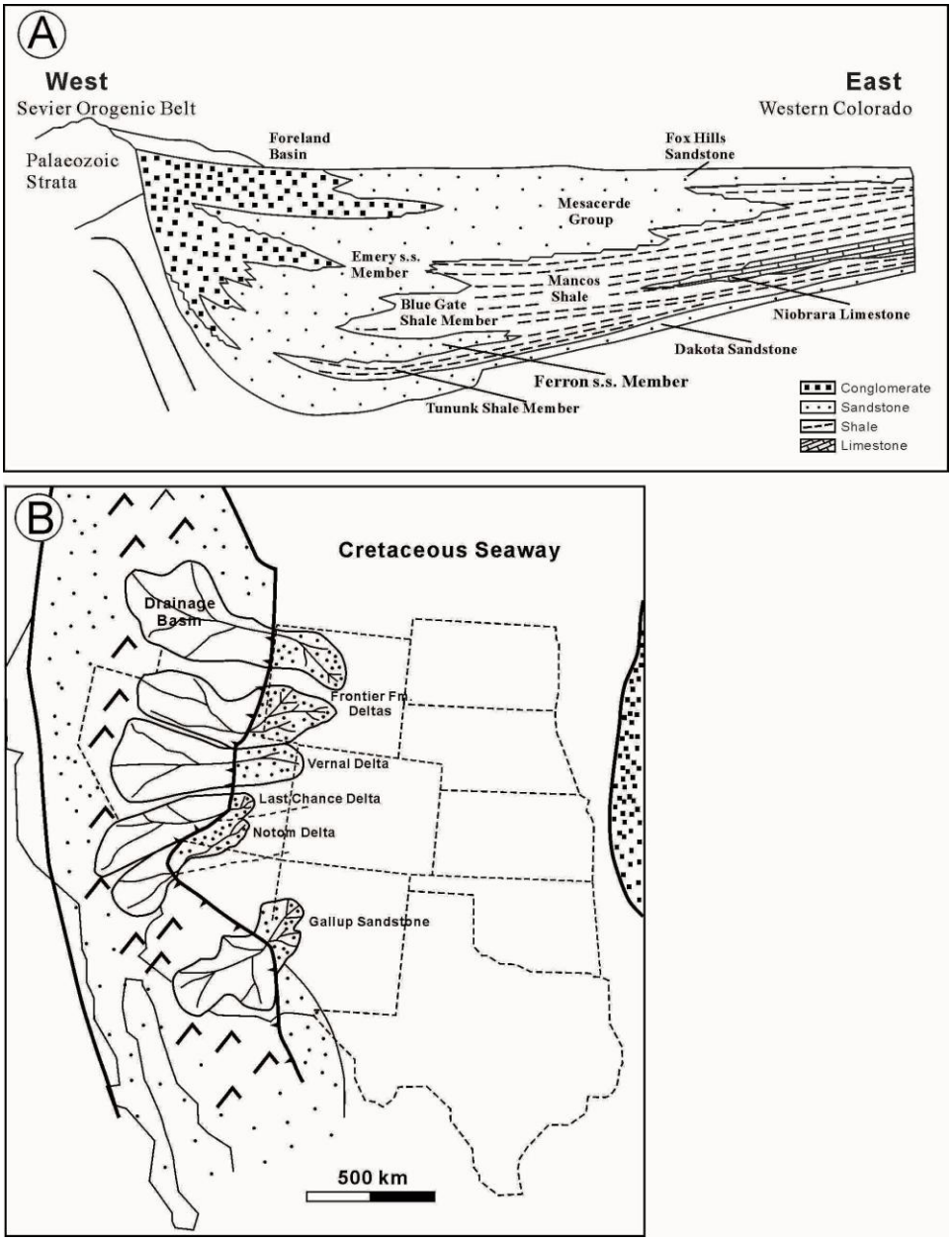

Figure 1. Geological setting of the study area. A) Schematic cross section showing the regional stratigraphy of the study area. The Ferron Sandstone Member of the Mancos Shale Formation was deposited in the Cordillera foreland basin with the thrusting of the Sevier Orogenic Belt. It is bounded below by the Tununk Shale and above by the Blue Gate Shale and pinches out toward east into the Mancos Shale (modified after Armstrong 1968). B) Paleogeographic reconstruction of the Western Interior Seaway in the late Cretaceous, showing the delta complexes that deposited in the Seaway and their associated drainage basins. Notom Delta is one of the delta complexes developed in late Turonian and was prograding generally toward northeast as shown (modified after Bhattacharya and Tye 2004). Reconstructions are primarily based on Gardner (1995) and Williams and Stelck (1975).

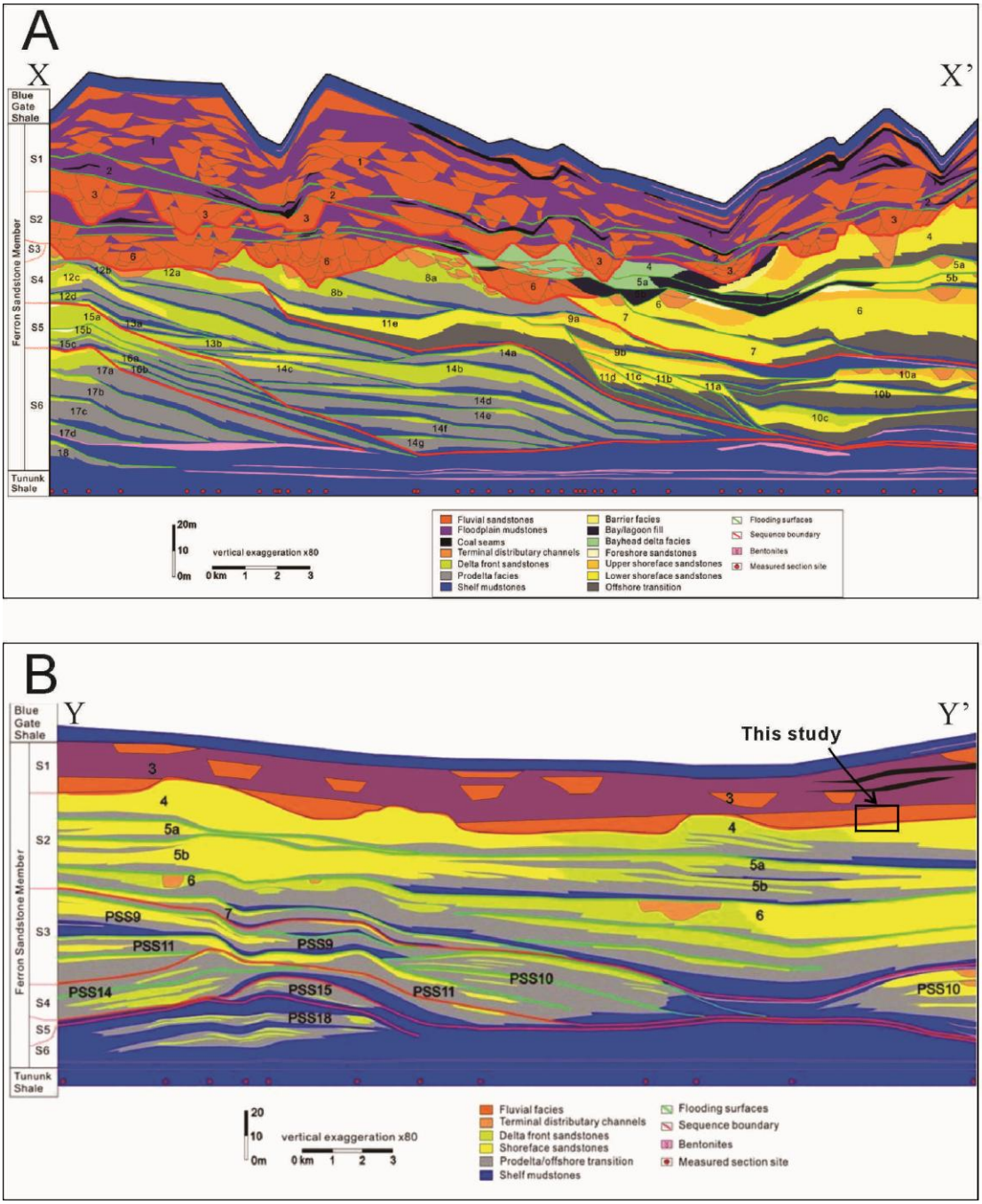

Figure 2. Cross sections showing the regional sequence stratigraphy of the Ferron Notom Delta. See Figure 3B for locations of the two cross sections. A) Oblique depositional dip cross section of the Notom Delta Zhu (2010). B) Oblique depositional strike cross section of the Notom delta Li (2009). This study primarily focused on Parasequence 3. The black rectangle marks the stratigraphic location of the study area. See Figure 3 for the locations of the two cross sections.

Li et al. (2010) completed a detailed facies architectural study of the compound incised valley system of Sequence 1 in the Notom Delta and provided the regional framework for the more detailed study presented in this paper. Focusing on outcrops extending from Neilson Wash south to the Fremont River, Li et al. (2010) showed a regionally extensive erosional surface, marked by significant truncation and superposition of coarse-grained fluvial deposits onto marine shoreface deposits, which they interpreted to be a sequence boundary (SB1) (Figs. 3 and 4). The erosional surface, with a relief of up to 17 m, can be traced for the entire extent of the exposed outcrops, suggesting that it is over 10 km in width (Fig. 4). Li et al. (2010) also documented 3 episodes of valley incision-and-deposition. They showed the older valleys to be finer grained and more tidally influenced throughout their study area (Fig. 4). Extraformational conglomerate facies are primarily confined to the youngest valley 1 of Li et al. (2010). This study is focused on determining whether the same valley architecture and cut-and-fill episodes can be documented in outcrop exposures further north along Coalmine Wash (Fig. 3). Detailed descriptions and interpretations of environmental lithofacies of the Ferron Notom Delta have been provided by Li et al. (2009, 2010), Fielding (2010) and Zhu et al. (2012).

2.3 Study Area, Methodology, and Data Set

The study area is located in the Coalmine Wash area near Hanksville in southern central Utah and lies about 8 km north of the area studied in detail by Li et al. (2010) (Figs. 3 and 4). Thirty measured sections and 5 photomosaics were collected. Paleocurrent data were collected and analyzed using the program “GEOrient”. Technical climbing gear was used to access vertical cliff faces where outcrops were difficult to walk out. Lithology, sedimentary structure, sediment grain size, bed

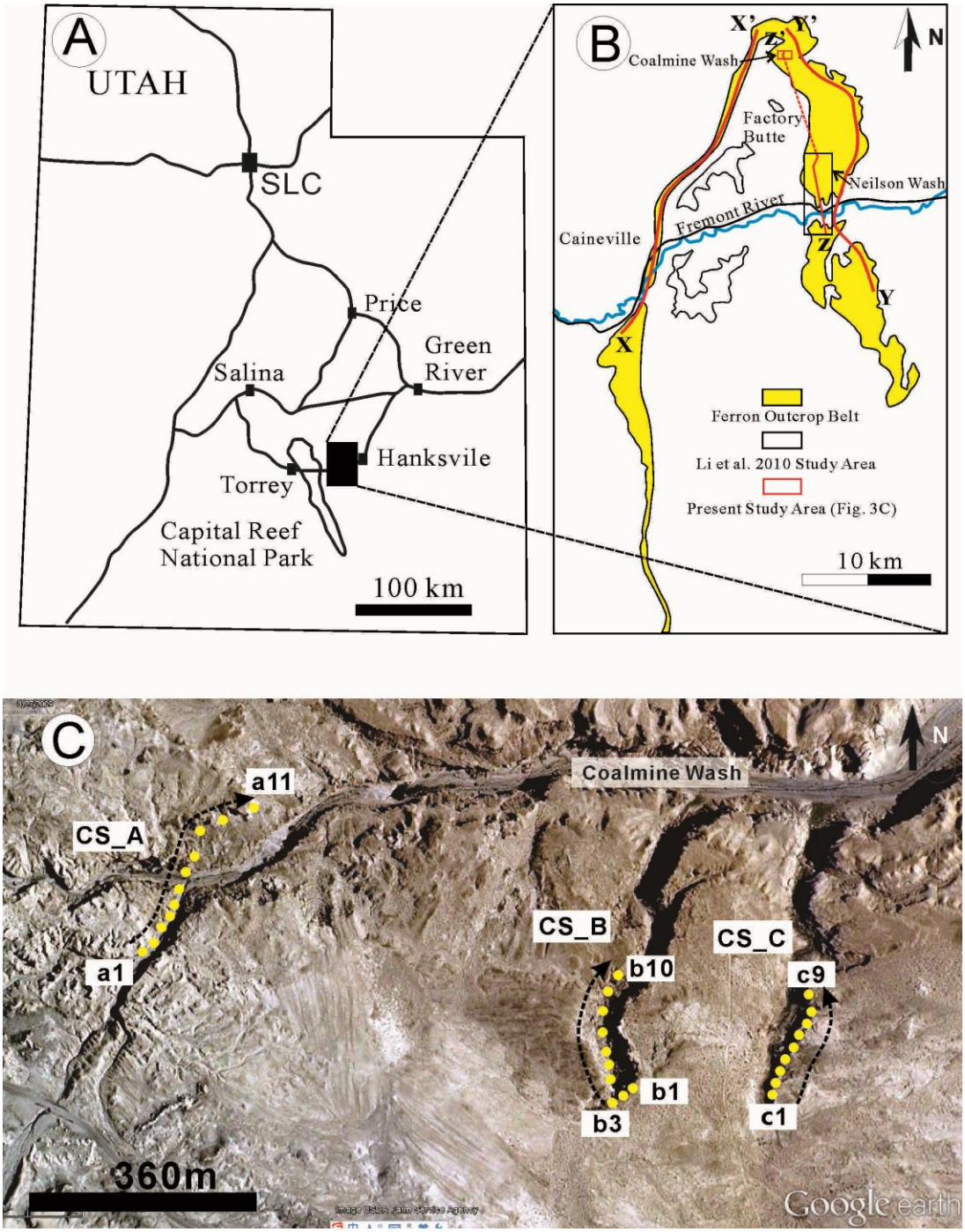

Figure 3. Basemaps showing the study area. A) Basemap showing Utah and the location of Ferron Notom Delta outcrop, which is marked with a black rectangle. B) Basemap showing the distribution of Ferron Notom Delta outcrops, the location of this study area which is marked with a red rectangle and the location of the study area of Li et al. (2010). XX' and YY' mark the locations of cross sections shown in Figure 2. C) Google Earth image of the study area in Coalmine Wash showing the locations of outcrop exposures, measured sections, and cross sections (CS).

thickness, paleocurrent direction, and trace fossils were recorded in the measured sections. Correlation of measured sections is based on tracing of erosional surfaces in the field and interpretation of high-resolution photomosaics matched to measured sections. Sediments in and below the incised valleys are subdivided into different lithofacies, according to their overall lithology, biota, and sedimentary characteristics, and further combined into depositional facies associations based on their interpreted depositional environments. Fluvial and tidally influenced fluvial deposits are analyzed by defining and correlating bounding surfaces and associated architectural elements using the methodology described by Miall (1986). Channel depths were estimated from preserved channel morphology and bar geometry and cross-bed thicknesses (Bridge 2000; Leclair and Bridge 2001; Bridge 2003).

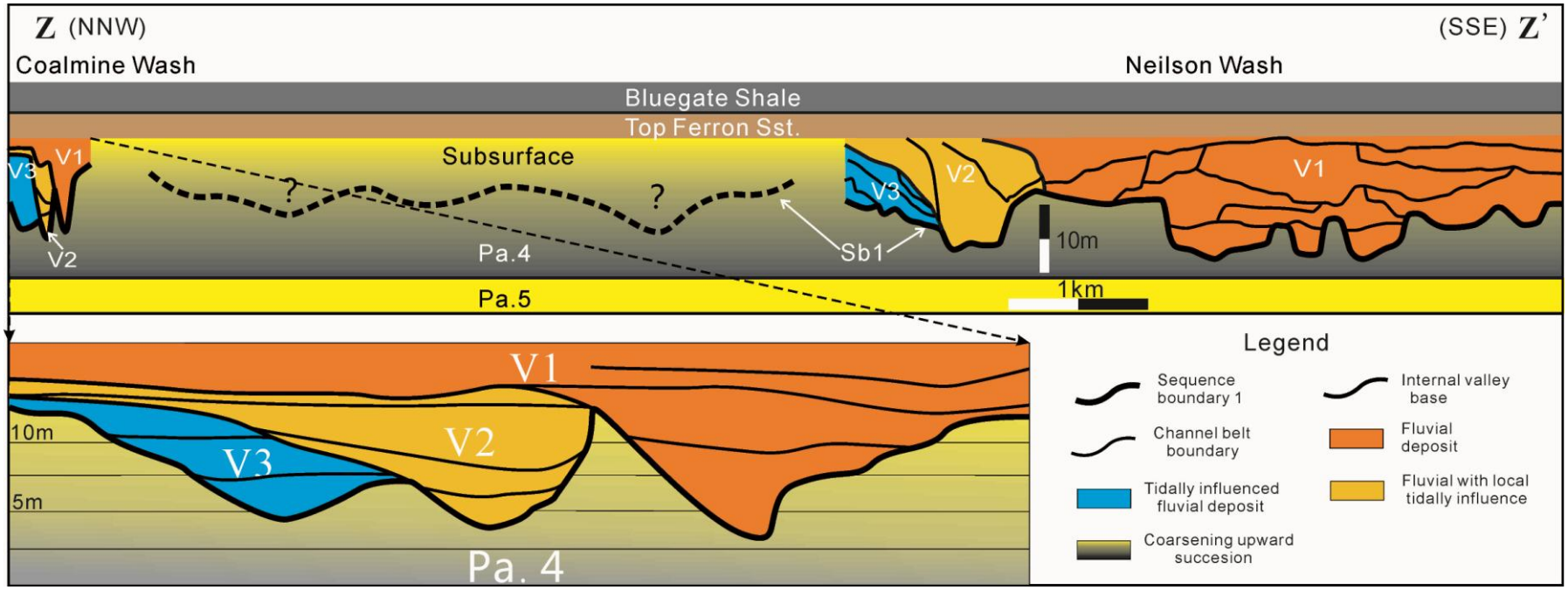

Figure 4. Composite cross section showing the context of the study area. It shows that the composite incised valley (SB1), which cuts into the lower shoreface deposits in Parasequence 4 can be correlated for more than 10 km in an depositional oblique-strike direction from this study area in Coalmine Wash area to Li et al. (2010)'s study area in Neilson Wash to the south (see also Fig. 2). Three simple incised valley systems with similar facies organization are identified in both Coalmine Wash and Neilson Wash. It shows that older valleys are more tidally-influenced, while younger valleys are filled with more proximal fluvial facies. Valley fill between Coalmine Wash and Neilson Wash are in subsurface, the morphology and filling pattern are uncertain. Data are from Li et al. (2010) and this study. See Figure 3B for the location of the cross section.

2.4 Lithofacies

Three depositional facies associations are identified within and outside of the incised valley system They include lower shoreface deposits below the incised valley system, fluvial channel deposits, and tidally influenced fluvial deposits within the incised valley system. Each depositional facies is characterized by distinctive lithology, biota, and sedimentary structures. Facies description and interpretations are summarized in TABLE 1 and are essentially the same as have been documented by Li et al. (2010), Fielding (2010), and Zhu et al. (2012). The essential descriptions and interpretations are briefly summarized below.

2.4.1 Facies Association 1: Shoreface

Description: Facies association 1 comprises upward coarsening facies successions that range from several meters up to 10 m thick, depending on the erosional depth of the overlying incised valleys. Thin-bedded bioturbated mudstones interbedded with very fine-grained wave-cross-laminated sandstones pass upward into thicker hummocky-cross-stratified (HCS) sandstone with thin mudstones (Fig. 5A). *Chondrites* (Fig. 5B), *Asterosoma, Thalassinoides* (Fig. 5C), *Diplocarterion* (Fig. 5D), *Paleophycus, Planolites* (Fig. 5E), *Rhizocorallium*, and *Ophiomorpha*, define a *Cruziana* ichnofacies (MacEachern et al. 2010). Bioturbation decreases upwards.

Interpretation: The predominance of wave-rippled and HCS sandstones in a coarsening upwards succession with a *Cruziana* ichnofacies, is typical of a prograding, storm-dominated shoreface, as are well described globally (Clifton 2006; Plint 2010).

TABLE 1. —Summery of the major facies recognized below and within the compound incised valley system. See Figure 5, 6, 7 for photos of these facies. See Figure 10, 11, 12, 13, 14, 15 and 16 for detailed facies organization in measured sections and bedding diagrams.

Facies	Interpretation	Lithology	Sedimentary Structures	Biota
1	Lower shoreface (below the incised valley)	Heterolithic, interbedded mudstone and thin bedded very fine grained sandstone, which thickens and coarsens upward to interbedded very fine grained sandstone and thin bedded mudstone and then amalgamated sandstone.	Abundant planar lamination and wave cross lamination in thin bedded sandstone layer, thick sandstones commonly show hummocky/swaley cross stratification, which sometimes grades upward to wave cross laminations, mudstones are mostly massive due to bioturbation, sometimes show normal grading.	Bioturbation is diverse and abundant. Common ichnogenera include: *Chondrites*, *Thalassinoides*, *Planolites*, *Paleophycus*, *Asterosoma*, *Rhizocorallium* and *Diplocraterion*, the assemblage of which suggests a *Cruziana* Ichnofacies.
2	Fluvial channel (within the incised valley)	Erosionally based, coarse to fine grained sandstone with local small pebbles, sometimes capped with thin silty mudstone. Fining upward pattern is obvious in some channel fills. Locally abundant intraformational mud clasts up to cobble size are present.	Flutes and tool marks on basal erosional surfaces, dune-scale trough and tabular cross bedding, large-scale (1-6m) solitary cross bedding (lateral accretion surfaces), planar bedding, current ripple cross lamination.	Plant debris, logs, and or their impressions at the channel base. No apparent burrows.
3	Tidally-influenced deposits (within the incised valley)	Erosionally based, mostly fine grained sandstone with locally intraformational mud clasts at the base. Sandstones are separated by a relatively thin layer of mudstone. Interbedded fine-grained sandstone and mudstone are present at the upper part of the sandy facies.	Meter-scale (up to 5m) solitary cross bedding (lateral accretion) with mud drapes, dune scale cross bedding (sometimes herringbone cross bedding) with double mud drapes and occasional reactivation surfaces, which sometimes pass laterally into flaser bedding. Local soft sediment deformation. Mudstones are mostly laminated, rarely with lenticular bedding.	Plant debris. Sparse burrowing in the heterolithic interbedded sandstone and mudstone, including *Planolites* and *Paleophycus.*

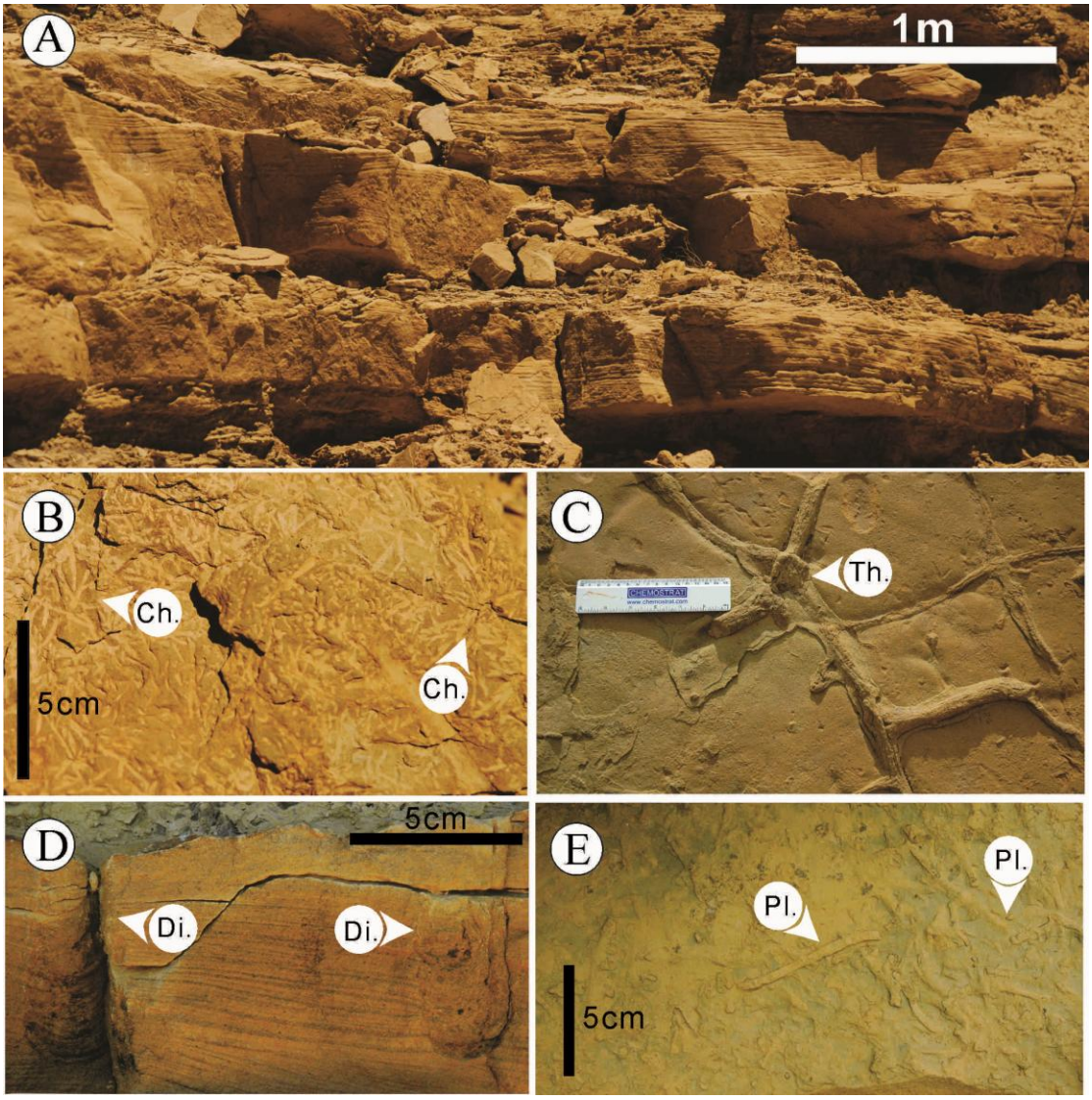

Figure 5. Photos showing lower shoreface deposits in Parasequence 4. A) hummocky cross stratification and swaley cross stratification. B) *Chondrites.* C) *Thalassinoides.* D) *Diplocraterion. E) Planolites.*

2.4.2 Facies Association 2: Fluvial Deposits

Description: Facies association 2 comprises stacked, fining upward sandy facies successions, bounded by concave-up scour surfaces. Thickness of fining upward units ranges from 1-5 m. Basal facies may comprise localized massive medium- to coarse-grained sandstone with abundant extraformational quartz, feldspar, and chert pebbles and intraformational mud clasts (Figs. 6A and 6B). Wood logs and coal

fragments are also locally observed. These are overlain by dune-scale cross-bedded medium-lower to fine-upper-grained sandstones (Fig. 6C). Thickness of cross sets range from 3-31 cm and average 15 cm. locally there are solitary cross beds which are thicker than 1 m. Upper parts of fining-upward successions may comprise fine-grained planar-bedded to ripple-cross laminated, fine-grained sandstone (Fig. 6D), in places interbedded with thin mudstone beds containing abundant plant material (Fig. 6E). These heterolithic units of interbedded mudstone and sandstone can reach 5 meters thick and locally show channel-form geometry. No distinctive bioturbation is observed.

Interpretation: Facies association 2 is interpreted as classic fluvial deposits (Miall 1996; Bridge 2006; Miall 2010). The massive medium- to coarse-grained sandstone with abundant pebbles and mud clasts is interpreted to be channel thalweg deposits. The pebble-sized mud clasts represent bank collapse material, formed in a cut bank and deposited at the channel base. The dune-scale cross bedding indicates formation by unidirectional river flows, and the capping finer grained parallel-laminated to ripple-cross-laminated indicate waning river floods. The solitary cross beds that are thicker than 1 m may indicate deposition in unit bars (Smith 1974; Bridge 2003; Bridge 2006; Sambrook Smith et al. 2006; Rice et al. 2008). Heterolithic intervals capping the successions may represent abandoned channels. Individual fining-upward successions likely define channel storeys, which can be used as a proxy for formative channel depth (Bridge 2006; Miall 2010). The scale of top-preserved channel storeys and the thicknesses of cross-bed sets suggest channel depth is on the order of about 5 m (Leclair and Bridge 2001).

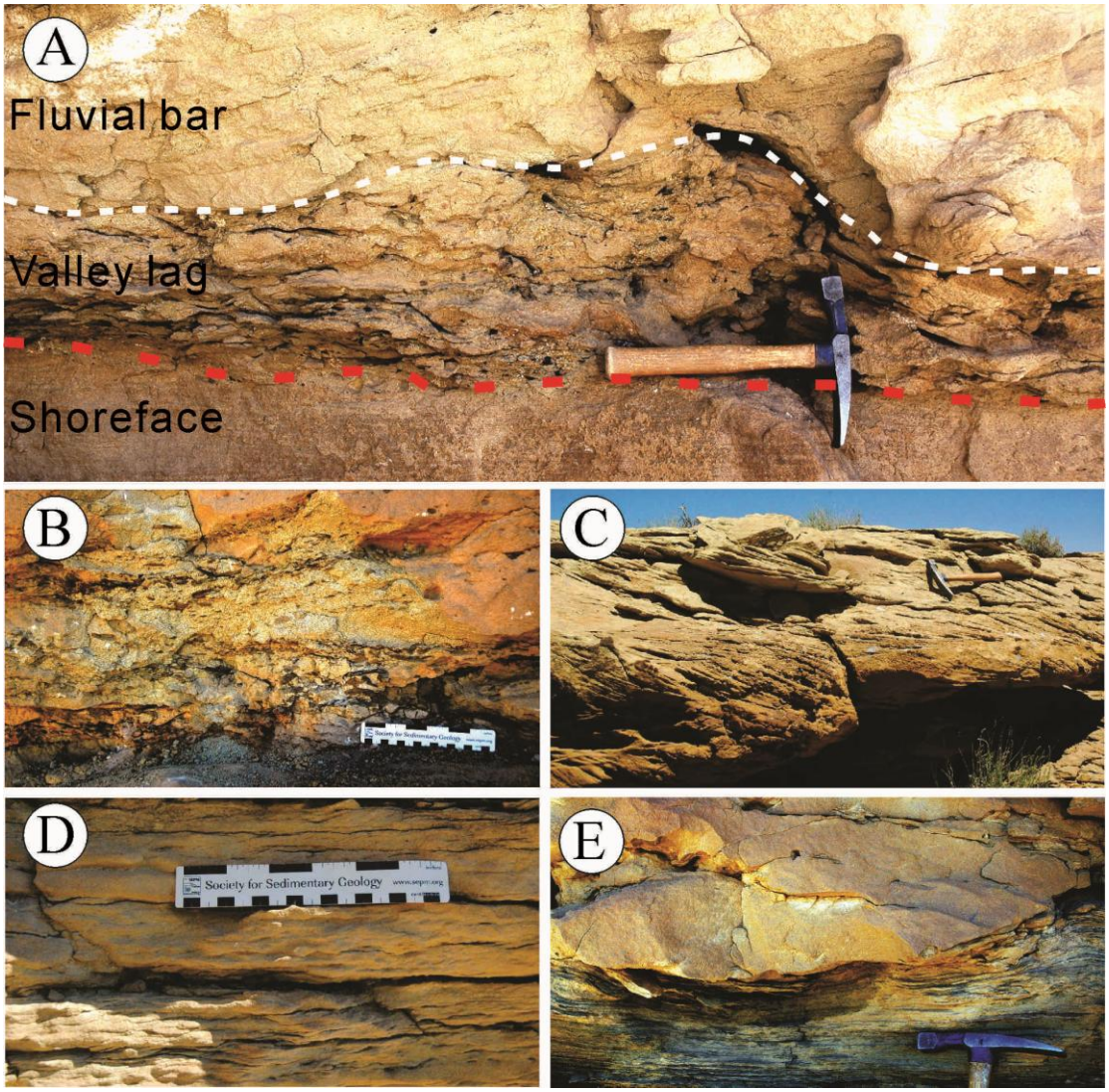

Figure 6. Photos of typical fluvial facies. A) Base of incised valley, marked by a red dashed line, is overlain by a layer of coaly lag with extraformational pebbles and intraformational rip-up mud-clasts. White dashed line marks the top of the valley lag and the base of cross-bedded fluvial bar deposits. B) Massive medium-grained sandstone with abundant intraformational mud clasts. C) Cross bedded sandstone. D) Current ripple-cross-laminated sandstone. E) planar/current-ripple cross-laminated muddy sandstone cut by a younger channel storey.

2.4.3 Facies Association 3: Tidally Influenced Deposits

Description: Facies association 3 is generally composed of fining upward successions, with fine- to medium-grained cross-bedded sandstones passing upward into interbedded mudstone and fine-grained sandstone. Cross beds are characterized

by abundant mud drapes, some of which are paired and bound tidal bundles (Figs. 7A, 7B and 7C). Mud-draped cross beds may pass laterally into flaser beds or lenticular beds, forming heterolithic bottom sets (Figs.7C and 7D). Double mud drapes separate relatively thin sandstone from thicker sandstone, showing a cyclical pattern of alternating thin-bedded and thick-bedded sandstones (Fig. 7B). Thin sandstones between double mud drapes sometimes are cross laminated with lamina dipping in an opposite direction to the dip of dune-scale cross bedding (Fig. 7B). The cross-bedded sandstone is locally interbedded with centimeter- to decimeter-thick cross-laminated mudstone (Fig. 7E), which are sparsely bioturbated. These mud-draped cross-bedded sandstone are commonly capped by a heterolithic unit up to 2 meters, composing interbedded fine-grained ripple-cross-laminated sandstone and silty mudstone (Fig. 7F). Sparse bioturbation is observed in the mudstone and heterolithic units, including *Planolites and Paleophycus*. Paleocurrent data collected from these dune-scale cross-beds show a bimodal pattern with a major component dipping toward northwest and a minor component dipping toward southeast (See IVS 3 in Fig. 8).

Interpretation: The presence of abundant mud drapes, flaser bedding, lenticular bedding and bimodal paleocurrent pattern all indicate strong tidal influence. Double mud-draped cross beds and tidal bundles indicate a subtidal depositional environment (Visser 1980). The alternating thin and thick sandstones bounded by thin mud layers are interpreted to be the product of tidal inequality (Ainsworth and Walker 1994). The thin laminated mudstones separating cross-bedded sandstones are interpreted to be deposited mainly out of suspension during lower flow stages. Capping muddy heterolithic strata may represent abandoned channels or tidally influenced mud flats. Sparse bioturbation indicates a brackish water environment.

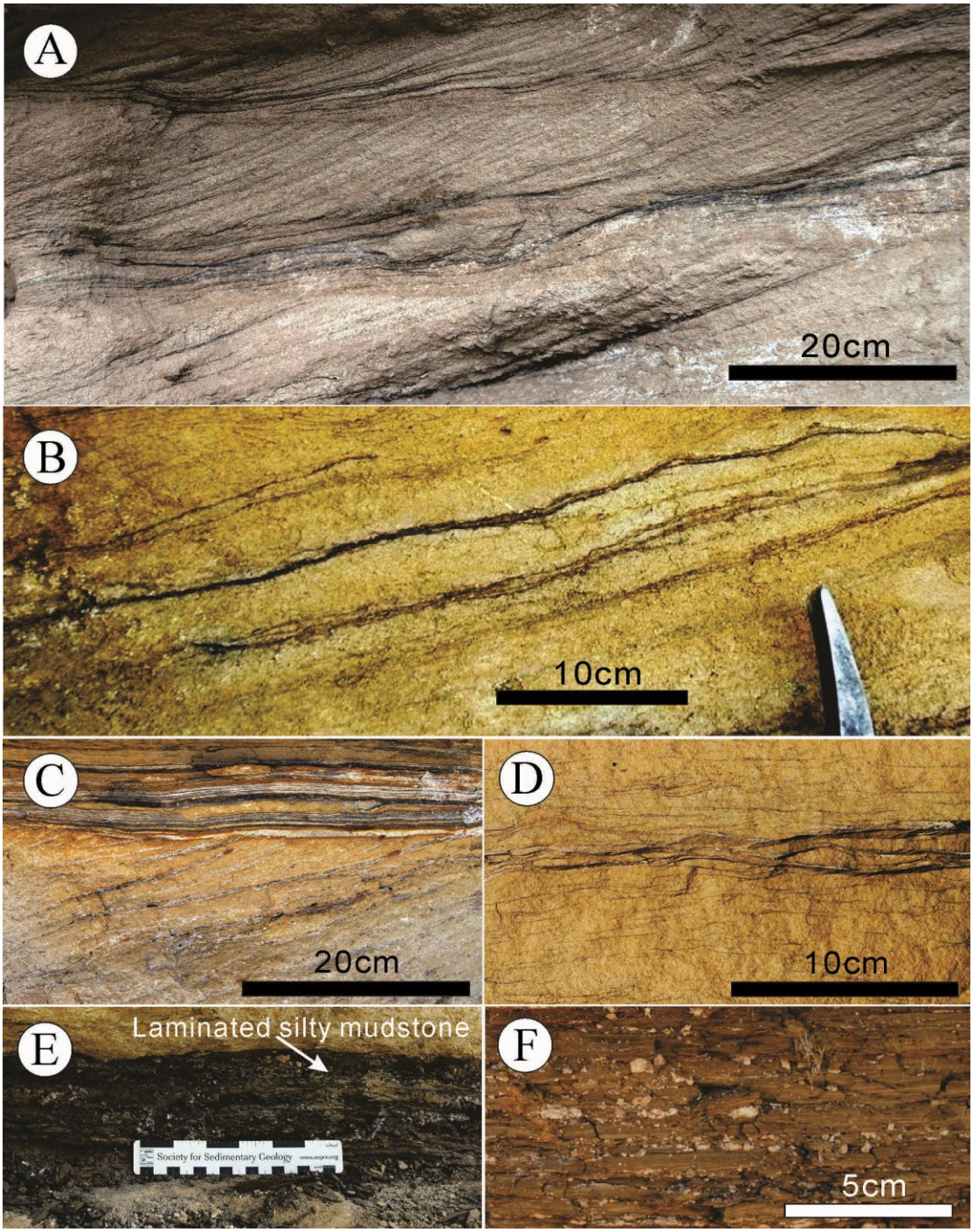

Figure 7. Photos of typical tidally influenced facies. A) Dune-scale cross beds with tidal bundles. B) Dune-scale cross beds with double mud drapes, showing a pattern of alternating thin- and thick-bedded sandstones. Thin-bedded sandstones between paired mud drapes show cross laminations which dip in an opposite direction to the dune-scale cross beddings. C) Mud-draped cross beds capped by wavy and lenticular beds. D) Flaser bedding. E) Laminated mudstone. F) Laminated silty mudstone.

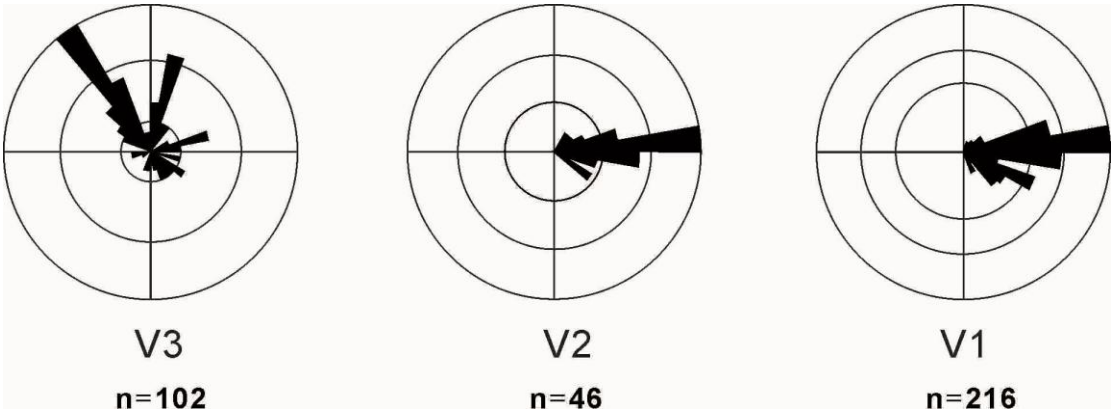

Figure 8. Rose diagrams showing paleocurrent directions for each simple incised valley system.

2.5 Evidence for a Compound Valley in Coalmine Wash

The essential nature of the basal erosional surface as an incised valley is interpreted based on the anomalous juxtaposition of truncating fluvial and tidal facies on distal shoreface deposits of Parasequence 4, forming a surface that violates Walther's Law. The fact that the surface cuts into Parasequence 4 also indicates that it correlates with the regional surface defining the base of Sequence 1, defined in the previous studies (Li et al 2010; Zhu et al. 2012). The position of this study area with respect to the regional studies (Li et al. 2010, Zhu et al. 2012), suggests that it is near the valley margin, and thus depths of erosion may be less than seen in Neilsen Wash farther south (Fig.4). The composite nature of the overlying deposits is indicated by cross-cutting relationships of multi-storey bodies, as well as comparison with the correlative areas to the south in Neilson Wash. Three distinct simple valleys were identified, although these could not be directly traced to the Neilsen Wash area as the valley fill dives into the subsurface (Fig. 4). The relative age of the three IVSs is established based on cross cutting relationships. IVS 1 is younger than IVS 2, which is younger than IVS 3 (Fig. 4), and is illustrated in the following section. Details of the architecture of each valley fill are described below.

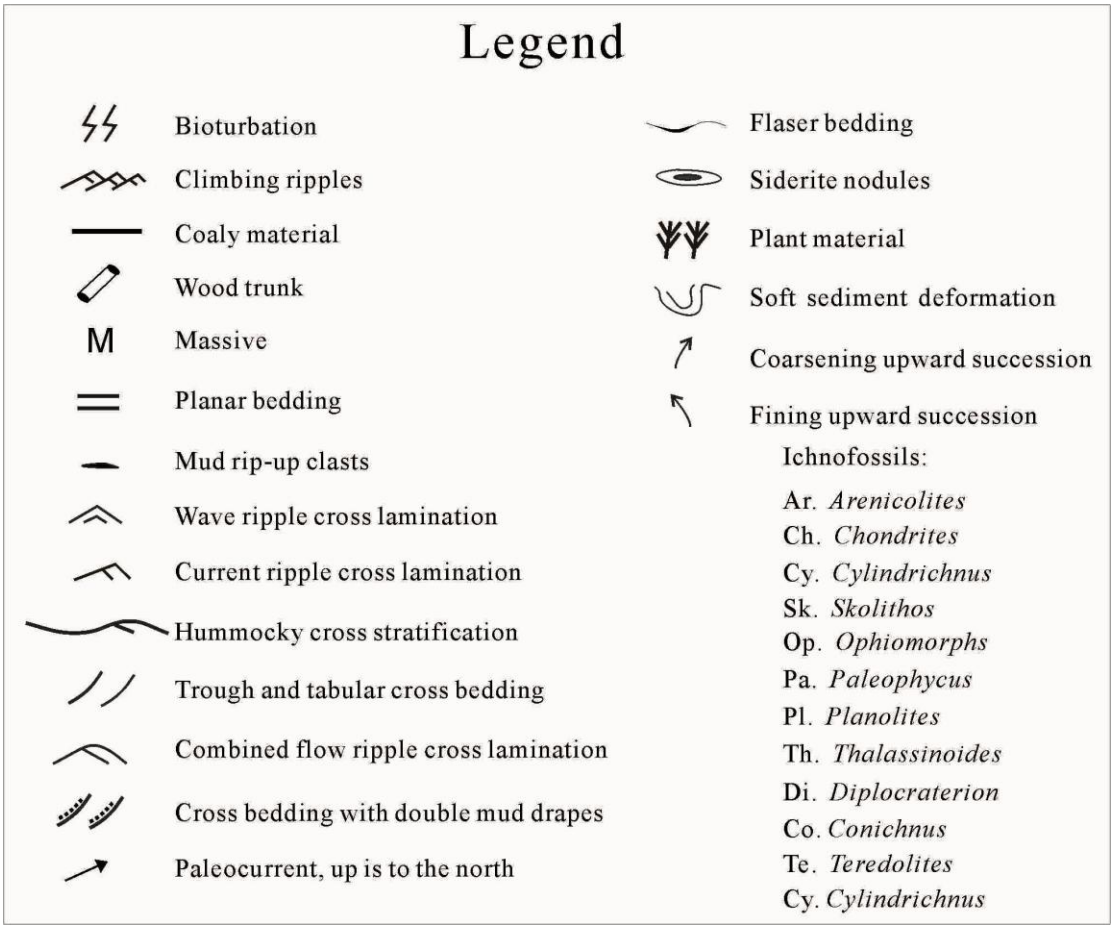

Figure 9. Legend for the geological sections presented in Figures 10, 11, 12 and 13.

2.6 Facies Organization

2.6.1 Incised Valley System 3 (IVS 3)

Description: IVS 3 is exposed at cross sections A and B (Fig. 3). It directly cuts into the lower shoreface deposits (FA. 1) of Parasequence 4 below and it is differentially eroded by younger incised valley 2 and 1 (Figs. 10 and 11). No distinct lag facies is observed at the base of IVS 3, except for a few mud chips. The maximum preserved relief of IVS 3 is about 10 m. It shows a general fining upward trend and it is mostly filled with tidally influenced deposits, composing mud-draped cross beds capped by interbedded laminated mudstone and fine-grained sandstone with sparse bioturbation (FA. 3). Vertically stacked storeys can be seen locally, with each storey

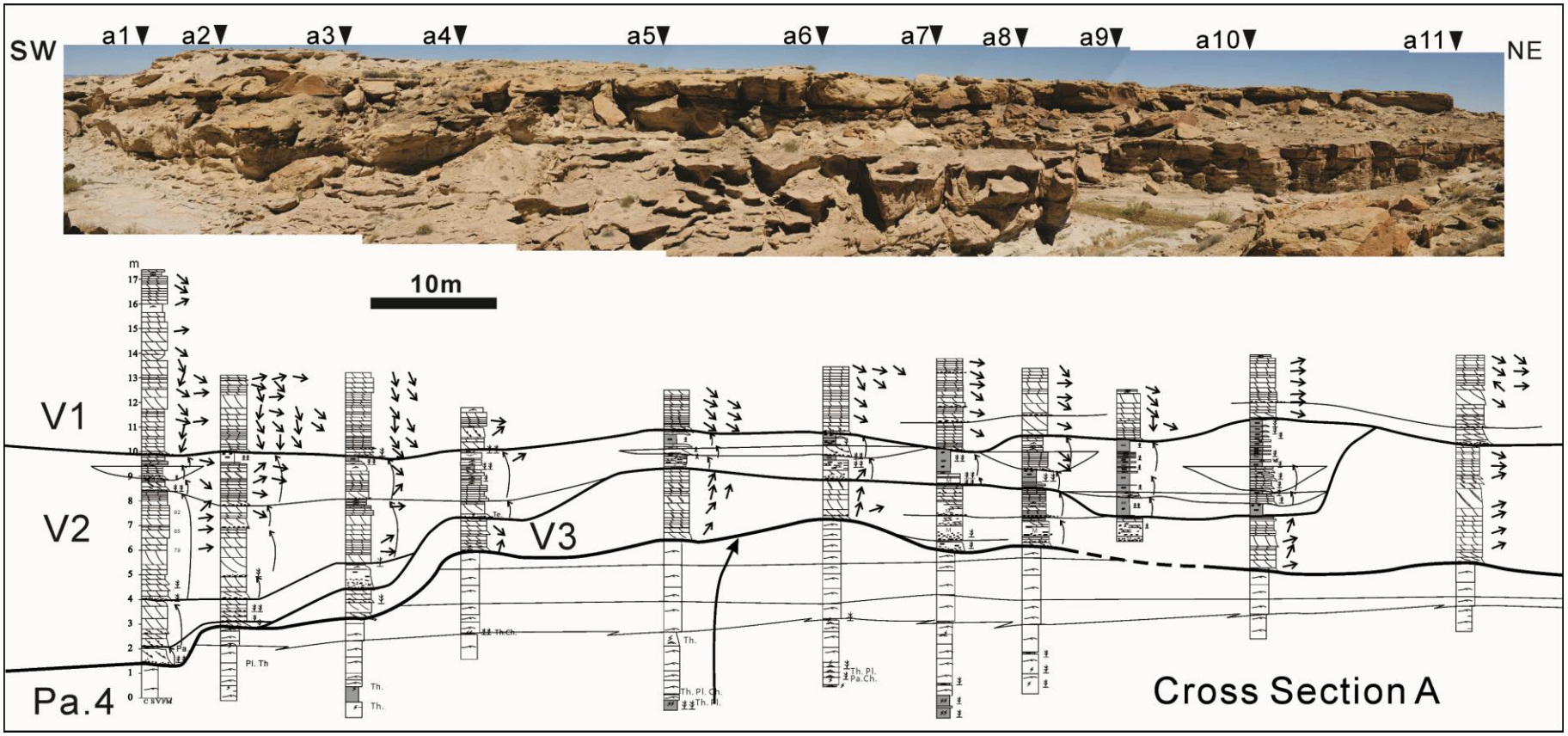

Figure 10. Photomosaic, measured sections and their correlation, showing facies organization and strata bounding surfaces in the incised valleys exposed at cross section A. Both fining-upward and coarsening-upward successions are marked with arrows. Possible channel storeys are interpreted and correlated, some of which are drawn out with a channel form (undulating base and flat top). IVS 2 shows a multi-storey fill pattern. Mudstones are shaded with a grey color. See Figure 3C for location of the cross section. See Figure 9 for legend for measured sections.

characterized by a fining upward succession (Fig. 11). A bimodal paleocurrent pattern is recognized as described above with major component dipping toward northwest and a minor component dipping toward southeast (Fig. 8). An oblique-strike cut of IVS 3 at the southern end of cross section B shows lens-shaped sandbodies accreting toward northeast (Fig. 12). These lens-shaped sandbodies have thicknesses ranging from 1 to 6 m and lengths of a few tens of meters. They are mostly composed of mud-draped fine-grained cross beds and flaser beds (FA. 3). These lens-shaped sandbodies are separated by thin laminated mudstone layers (Fig. 7E), forming large inclined heterolithic strata (IHS).

Interpretation: The justaposition of tidally influenced deposits (FA. 3) over lower shoreface deposits (FA. 1) indicates a basinward shift in depositional facies. The overall fining-upward trend of the valley fill suggests either simple waning flow conditions or a transgressive fill developed in a possible estuary environment (Dalrymple et al. 1992; Boyd et al. 2006; Dalrymple and Choi 2007; Dalrymple 2010). However, the extensiveness of the fining upward trend through the study area supports more of the interpretation of a transgressive fill rather than commonly localized waning flow deposits. Since the Ferron River was flowing east and northeast (Li et al. 2010; Zhu 2010), the predominant northwest-directed paleocurrent component indicates a flood-dominated flow regime. The abundant tidally influenced facies, flood-dominated flow regime, and lateral accretion pattern suggest that the lens-shaped sandbodies are part of sandy tidal bars deposited in a tidally dominated estuary (Dalrymple et al. 1992; Boyd et al. 2006). The thin laminated mudstones draping accreting sandbodies are interpreted to be deposited during river low stage or abandoned phase of tidal bars. Formative channels are interpreted to be at the scale of

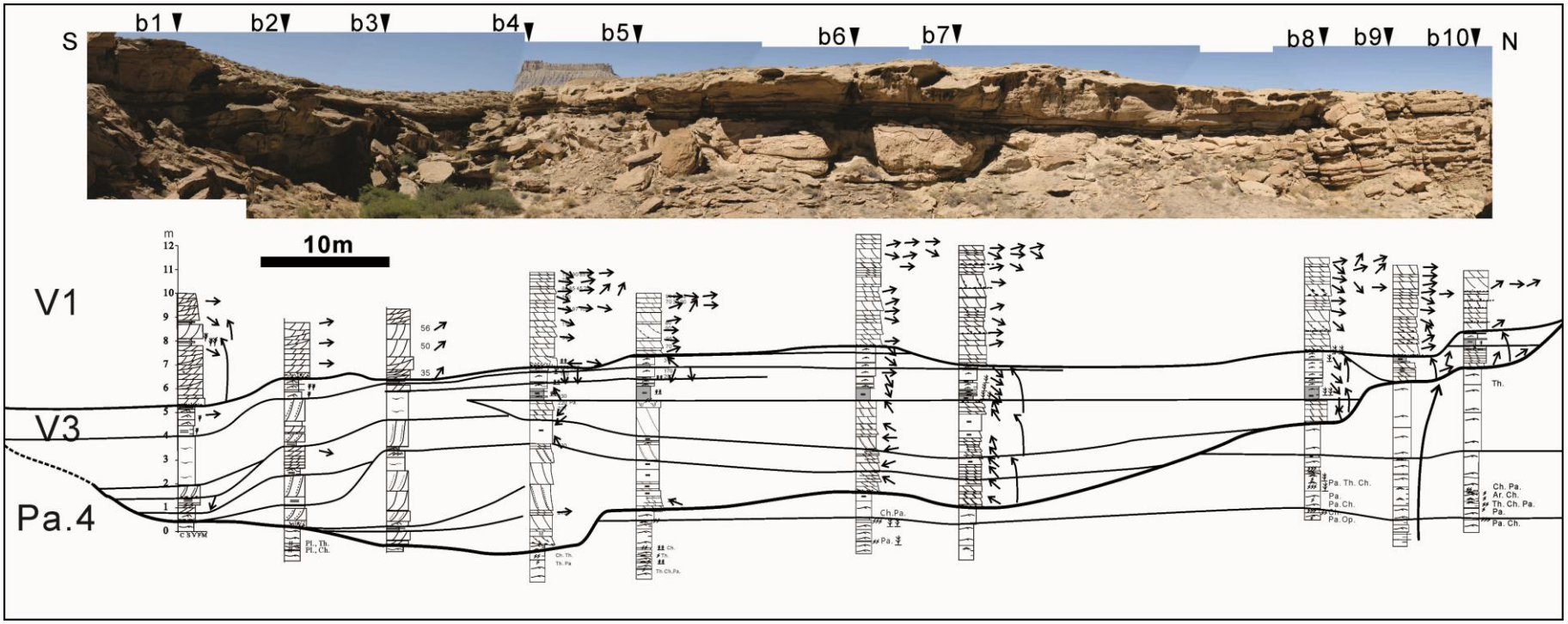

Figure 11. Photomosaic, measured sections and their correlation, showing facies organization and strata bounding surfaces in the incised valleys exposed at cross section B. Both fining-upward and coarsening-upward successions are marked with arrows. Possible channel storeys are interpreted and correlated, some of which are drawn out with a channel form (undulating base and flat top). IVS 3 shows lateral accreting bar forms on the southern part of the cross section (b1-b3) and multi-storey fill pattern on the northern part of the cross section (b4-b10). Mudstones are shaded with a grey color. See Figure 3C for location of the cross section. See Figure 9 for legend for measured sections.

the lateral accreting sandy tidal bars, which suggest flow depths on the order of 6-7 m. The preserved valley relief (10m) is about 1.6 times deeper than the inferred flow depth of the associated channels and tidally influenced bars. The locally preserved multistory pattern and the anomalous juxtaposition of tidally influenced facies cutting into lower shoreface deposits also support the interpretation as an incised valley system.

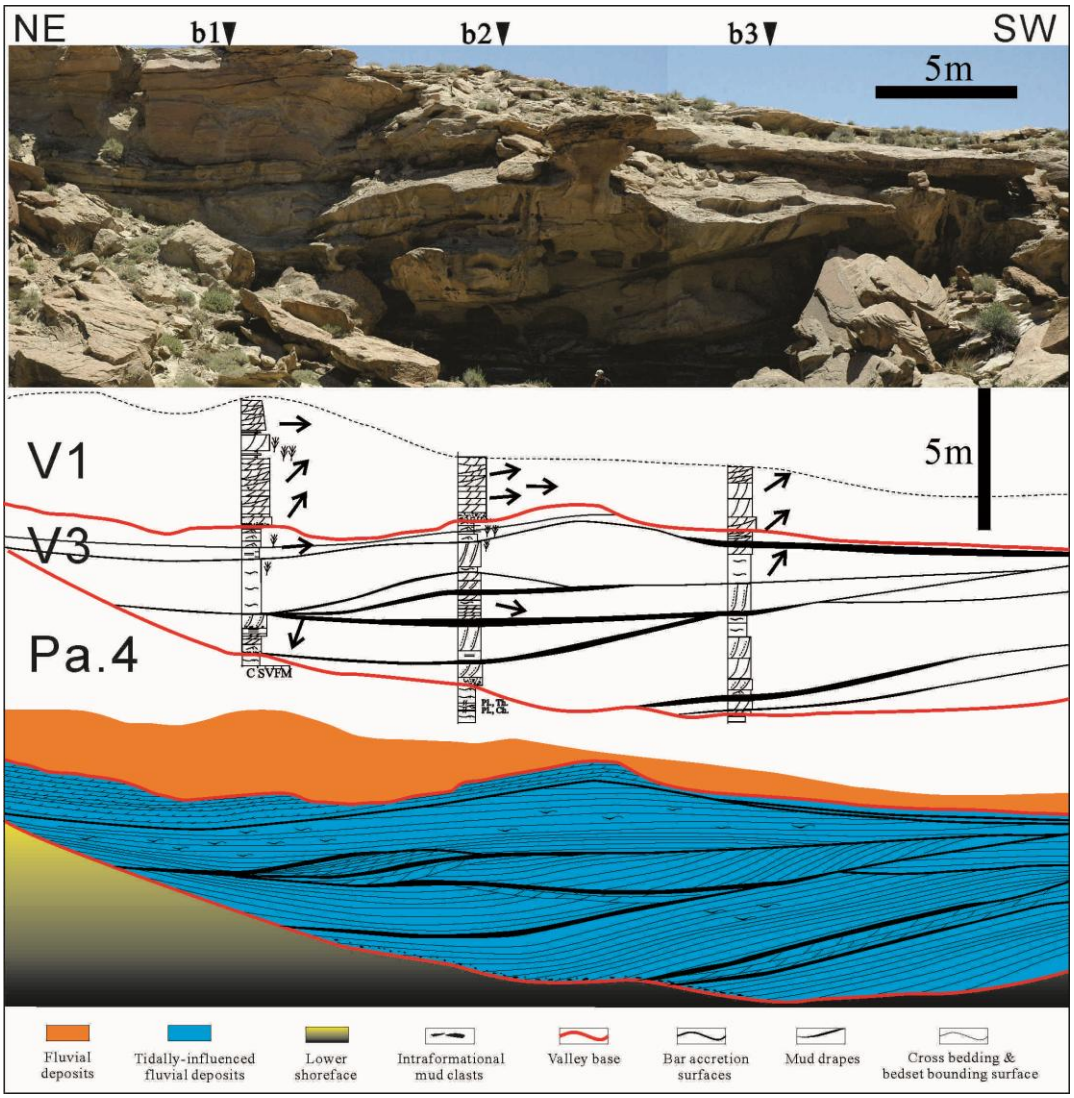

Figure 12. Photomosaic, bedding diagram and measured sections of IVS 3 exposed at the southern end of cross section B. It shows that IVS 3 is filled with lens-shaped accreting sandbodies, which are composed of double mud-draped cross beds and flaser beds. Incised valley system cuts into the lower shoreface below and it is cut by IVS 1 on top. See Figure 9 for legend for measured sections.

2.6.2 Incised Valley System 2 (IVS 2)

Description: IVS 2 is exposed at cross sections A and C (Fig. 3). At cross section A, it cuts into older IVS 3 described above and locally it cuts through valley 3 into the lower shoreface deposits (between section a1 and a2) (Fig. 10). At cross section C, it cuts directly into the lower shoreface deposits (Fig. 13). IVS 3 was either cut off by IVS 2 or was not deposited there. The top of IVS 2 is truncated by younger IVS 1 at both cross sections A and C (Figs 10 and 13). Preserved valley fill is up to 12 m. A layer of massive medium-grained sandstone with extraformational pebbles, intraformational pebble- to cobble-sized mud clast and locally wood logs is observed at the base of IVS 2, varying in thicknesses from a few centimeters up to 1 m. IVS 2 is mainly filled with fluvial deposits (FA. 2), with only the upper 10% filled with tidally influenced deposits (FA. 3) (Figs. 10 and 13). Up to 6 fining upward successions are identified in IVS 2, showing cross-bedded medium-grained sandstone pass upward to fine-grained ripple-cross-laminated sandstone and carbonaceous silty mudstone (Figs. 10, 13). In Figure 14, at least 6 fining upward successions, which are characterized by a lateral accretion pattern, are recognized. Their thicknesses range from 1 to 5 m. Each fining upward succession is bounded below be an undulating erosional surface, which shows a channel geometry and cuts into strata below. The general paleocurrent direction as indicated by angle-of-repose dune-scale cross beds is east (Fig. 8). At cross section C, incised valley 2 shows a “V” -shaped geometry and is filled with 4 fining upward successions. A detailed bedding diagram of the fining upward succession 2 is constructed to illustrate its internal architecture (Fig. 15). The base of succession 2 shows concave-up morphology, with a maximum relief of about 7 m and an apparent width about 85 m (Fig. 15). The lower left part of succession 4 is

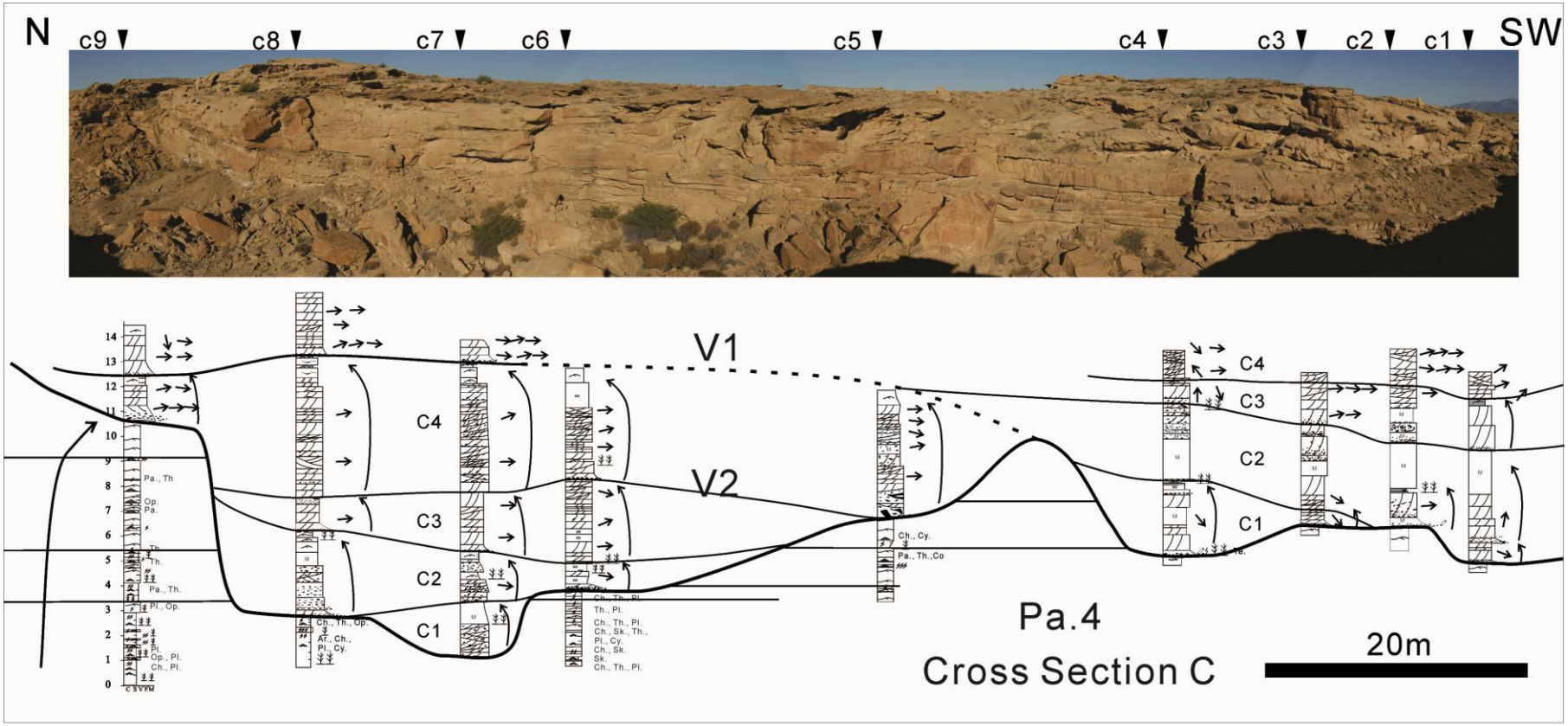

Figure 13. Photomosaic, measured sections and their correlation, showing facies organization and strata bounding surfaces in the incised valleys exposed at cross section C. Both fining-upward and coarsening-upward successions are marked with arrows. Possible channel storeys are interpreted and correlated. Four channel storeys are recognized in IVS 2 and 4 storeys are recognized in IVS 1. See Figure 3C for the location of the cross section. See Figure 9 for legend for measured sections.

composed of large-scale inclined beds dipping to the north (Fig. 16). Internally, these inclined beds are composed of dune-scale cross-bedded medium-grained sandstone, showing generally east-directed paleocurrent (Fig. 8). No bioturbation is observed in the fill of incised valley 2.

Interpretation: The local juxtaposition of medium-grained cross-bedded fluvial deposits over lower shoreface deposits indicates a basinward facies change across the base of incised valley 2. The massive mud-clasts-rich sandstone at the base of the valley is interpreted to be a thalweg deposit. The fining upward successions are interpreted as typical fluvial channel storeys as described and interpreted in FA. 2. Consequently, IVS 2 shows a multi-storey fill pattern. Based on well-preserved bar geometry, a schematic channel form is drawn to show the estimated formative channel dimensions of channel belt 2 in Figure 14. The depth of the formative channel is estimated to be about 2 m, which is much less than the relief of the valley (>10 m). Paleocurrent data indicate that the river was flowing generally toward east (Fig. 8). The large inclined beds in channel storey 3 at cross section C, which dip toward north, are interpreted to be lateral accreting point bars, suggesting a classic meandering fluvial style (Miall 1985) (Fig. 15). Bankful water depth is estimate to be 5-7 m from well-preserved channel morphology and bar dimensions, indicating that rivers were underfit relative to the larger incised valley. This result is also confirmed by taking field measurements of dune-scale cross-bed thicknesses and applying the methodology of Leclair and Bridge (2001). The general fining upward trend and changing from fluvial to tidally influenced deposits may indicate a transgressive fill. The overall low ratio of tidally influenced deposits, however, indicates a more proximal facies succession compared with IVS 3.

2.6.3 Incised Valley System 1 (IVS 1)

Description: IVS 1 is exposed at cross sections A, B, and C (Fig. 3). It truncates IVS 2 at cross sections A and C (Figs. 10 and 13), and it cuts into IVS 3 at cross section B (Fig. 11). It also locally cuts into the lower shoreface deposits in Parasequence 4 at cross section C (Fig. 13). A layer of medium- to coarse-grained sandstone containing extraformational pebble-sized quartz, chert, and feldspar clasts and intraformational mud-clasts is observed at the base of incised valley 1. Incised valley 1 is entirely filled with fluvial deposits (FA. 2), consisting mostly of medium- to coarse-grained dune-scale cross-bedded sandstone (Figs. 10, 11, and 13). The general paleocurrent direction as indicated by angle-of-repose dune-scale cross beds and ribs and furrows structure is east (Fig. 8). At cross section C, 4 fining upward successions are recognized (Fig. 13), showing massive or cross-bedded medium-grained sandstone passing upward into fine-grained cross-bedded sandstone. No apparent tidal signature and bioturbation was observed.

Interpretation: A basinward shift in depositional facies from lower shoreface to fluvial deposits is also observed across the base of incised valley 1. Fining upward successions observed at cross section C are interpreted to be fluvial storeys similar to those observed in IVS 2, which indicate a multistory fill of incised valley 1. The absence of apparent marine influence and the lack of fine-grained sediments, as well as the common presence of coarse-grained sandstone and extraformational pebbles, indicate a more proximal fluvial depositional environment than IVSs 2 and 3.

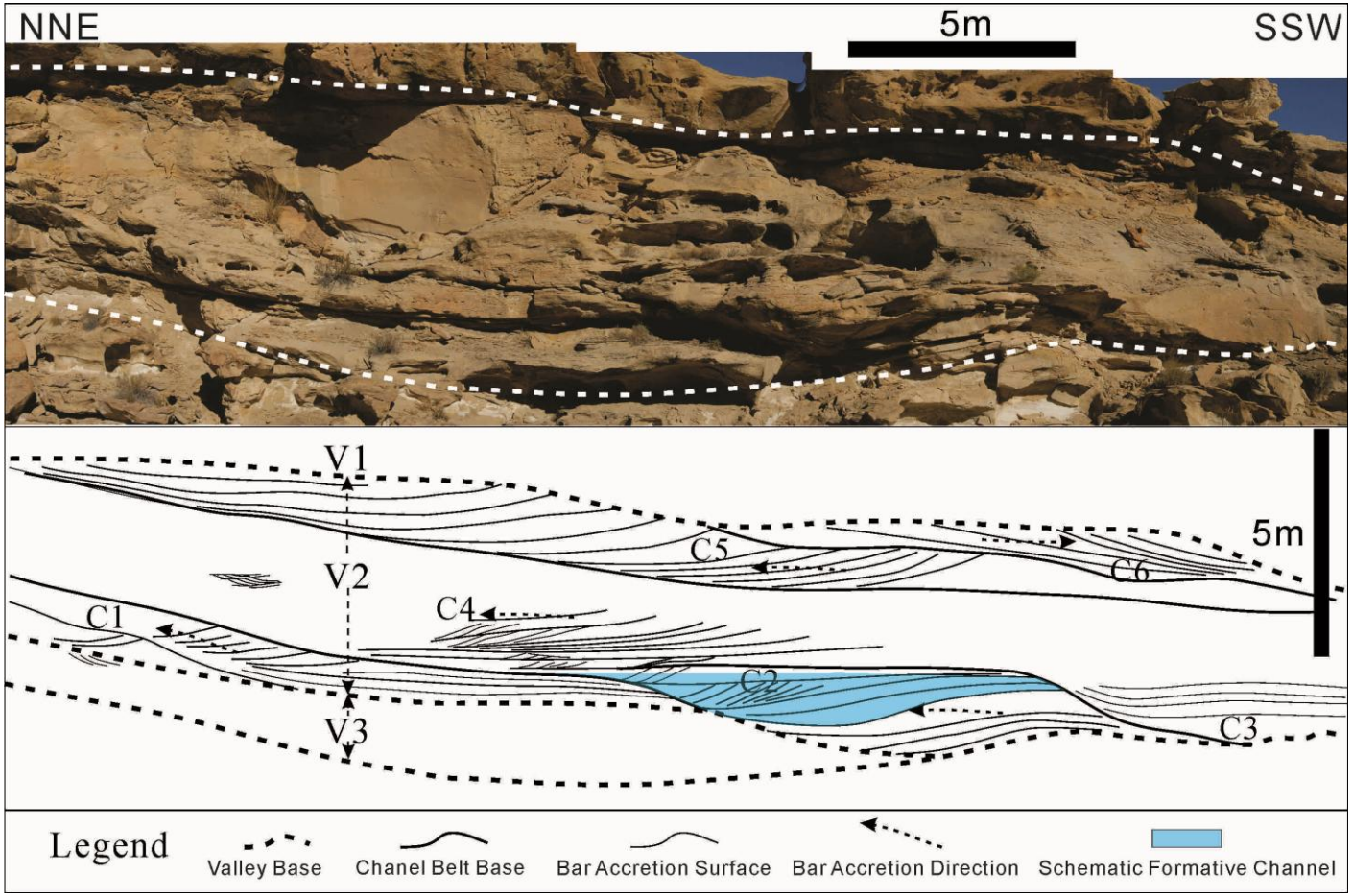

Figure 14. Photomosaic and bedding diagram of part of IVS 2 exposed at the eastern side of the cliff where cross section A is located, showing a multi-storey filling pattern. Six channel belts showing lateral accretion were identified stacking vertically. Light-blue colored semi-transparent channel forms are drawn to show the estimated dimension of the formative channel from well-preserved channel belt 2.

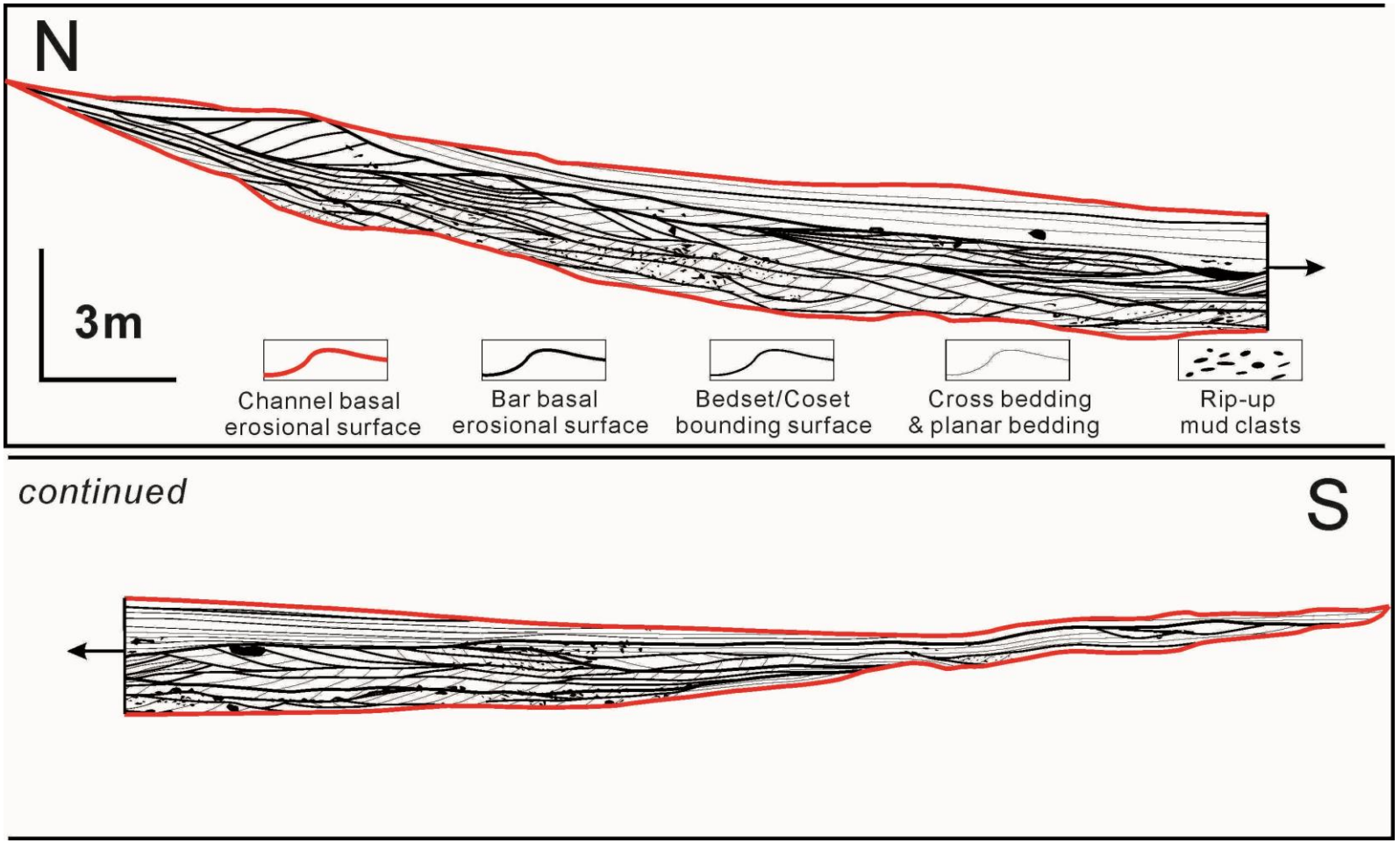

Figure 15. Detailed bedding diagram showing the internal facies architecture of channel storey 2 in IVS 2 at cross section C. A regular upward change of facies from intraformational mud-clasts-rich cross-bedded to planar-bedded to current-ripple cross-laminated sandstone is seen, which is associated with a fining upward trend in grain size from medium grained at the base to muddy siltstone on top.

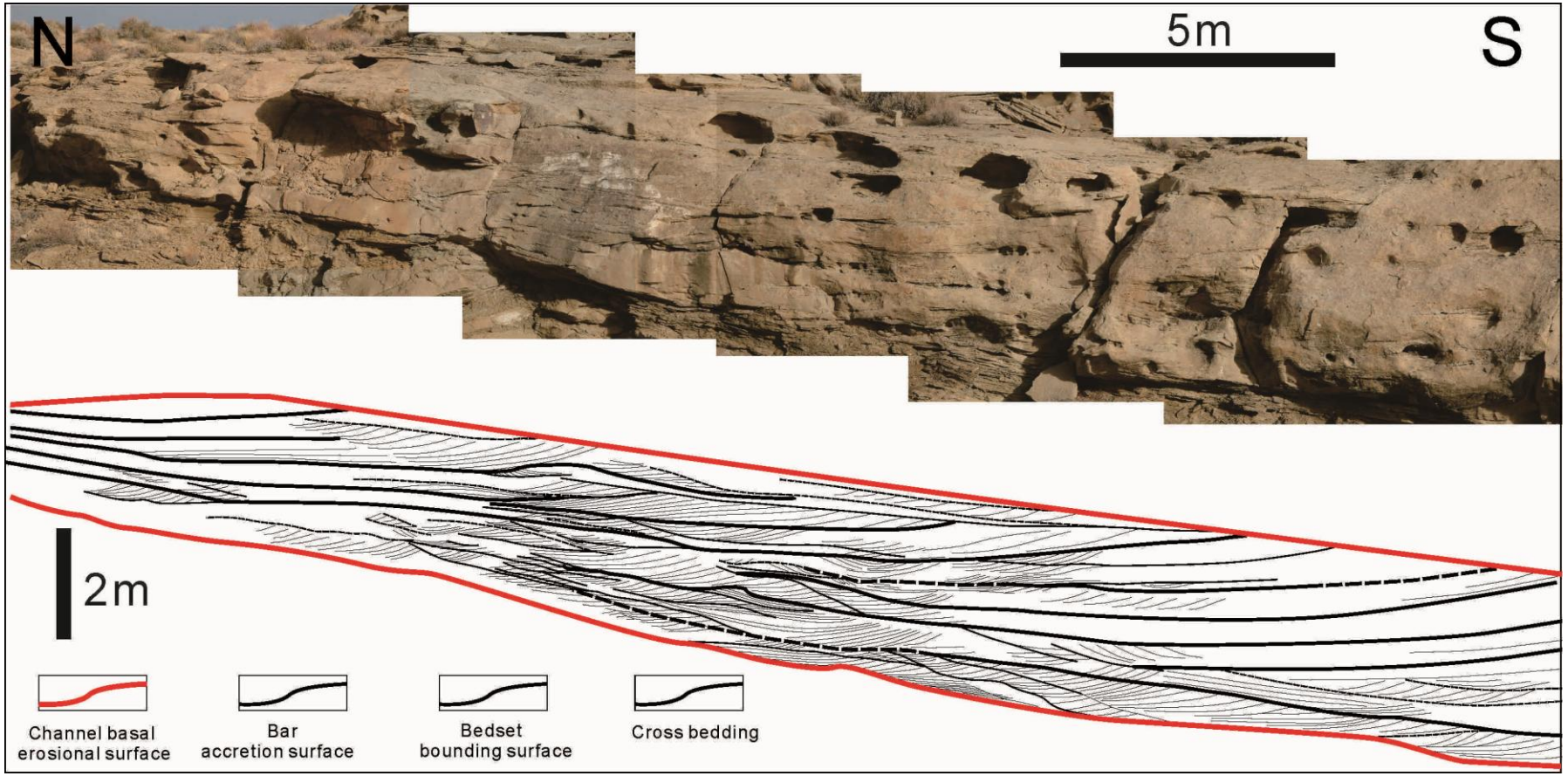

Figure 16. Photomosaic and bedding diagram of part of channel storey 3 in IVS 2 at cross section C, showing a laterally accreting point bar deposit, where large inclined beds dip to the north and internal dune-scale cross beds dip into the outcrop and toward east (See Figures. 8 and 13).

2.7 Sequence Stratigraphic Interpretation

2.7.1 Evolution of the Compound Incised Valley

Figure 17 schematically illustrates a strike-oriented cross section showing the cross cutting relationships between the three simple incised valley systems and their internal facies types and organization. Figure 18 shows a schematic dip cross section that illustrates the evolution of the compound valley through time. The three simple incised valley systems, record three cycles of incision and deposition.

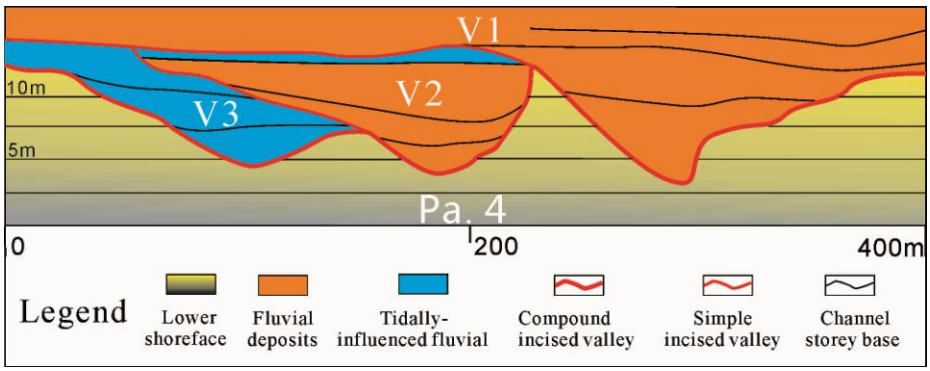

Figure 17. A schematic diagram showing the cutting relationship between the three incised valley systems in depositional strike direction and their internal facies organization. The oldest IVS 3 cuts into the lower shoreface deposits and is filled entirely with tidally-influenced deposits. The younger IVS 2, which cuts into IVS 3 and locally into the lower shoreface deposits, is filled with mostly fluvial deposits and a minor component of tidally-influenced deposits. The youngest IVS 1, which cuts into older IVSs 2 and 3, is completely filled with tidally influenced deposits.

Incised valley 3 is filled with tidally influenced deposits (Figs. 10 and 11), associated with seaward portion of segment 2 of Zaitlin et al. (1994) and which lacks a distinctive lag. There are many other examples of incised valleys, which are filled entirely with estuarine or marine deposits and do not contain fluvial deposits at the valley base, even though they are inferred to have been cut by fluvial action (Wilson 1948; Rahmani 1988; Ainsworth and Walker 1994; Pattison and Walker 1998). Several possible explanations for the absence of fluvial deposits at a valley base

include: 1) deposition in a tidal-fluvial environment close to lowstand river mouth (Boyd et al. 2006); 2) transgressive ravinement and coincidence of a flooding surface with a sequence boundary (Van Wagoner et al. 1990); or 3) a low ratio of sediment supply over transgression (Dalrymple et al. 1994; Willis 1997). The lack of a distinct lag deposit (either transgressive lag or fluvial lag) at the base of the valley suggests that there is unlikely to be a coincidence of a flooding surface with a sequence boundary. The fill of incised valley 3 with sandy tidally-influenced deposits (up to 90% of sandstone) indicates a fairly high rate of sediment supply. However, the fining-upward trend, interpreted tidal-dominance nature and flood-dominated tidal regime, may indicate a transgressive setting. Consequently, we argue that incised valley 3 was filled in a transgressive tidal-fluvial river mouth environment. According to the terminology of Willis et al. (1997), IVS 3 would be "flood-based", in which the flooding surface is located at the basal part of the valley.

Incised valley 2 is mostly filled with fluvial deposits (Figs. 10 and 13), except for the most upper part of the valley, which is filled with tidally-influenced facies and accounts for only a minor portion (less than 10%) of the valley fill. IVS 2 is thus "flood-topped", wherein the first significant flooding surface is located at the upper part of the valley, separating basal fluvial facies from upper tidal facies (Willis 1997). The dominance of fluvial deposits and minor tidally influenced deposits indicate deposition in landward portion of segment 2 of Zaitlin et al. (1994).

Incised valley 1 is completely filled with fluvial deposits, without any tide or wave signature (Figs. 10, 11 and 13). It is interpreted to be associated with segment 3 of Zaitlin et al. (1994), where fluvial deposits characterize the entire valley fill. According to Simms et al. 2006, it is an "overfilled" incised valley system similar to

the fill of the Brazos, the Rio Grande, and the Colorado incised valleys in the Gulf of Mexico. The extraformational pebbles, which are not present in IVSs 2 and 3, also indicate that it is the most proximal of the three fills. Compared to incised valley 2, which was finally flooded at the late stage of transgression, the absence of direct marine signature in IVS 3 suggests that it was never flooded prior to filling.

As a whole, successive valley fills record an overall stepped "basinward shift in depositional facies" in which there is progressively less marine influence. A normal regression, which occurs during relative sea-level rise and stillstand, when sediment supply exceeds accommodation creation, would not explain the incision of the valleys and the abrupt basinward shift in depositional facies across the composite sequence boundary (Posamentier et al. 1992). Olariu and Bhattacharya (2006) suggest that during normal regressions, rivers build across underlying units as shallowly scoured distributive channel systems, rather than deep incisions, and are more likely to avulse elsewhere rather than incise. River incision, in contrast, is favored by negative shoreline trajectories and exposure of nickpoints (Posamentier et al. 1988; Wescott 1993; Helland-Hansen and Gjelberg 1994; Posamentier and Allen 1999). Consequently, we argue that the three simple incised valley systems, with a progressively more fluvial-dominated character in each successive valley fill, record a longer-term stepped relative sea-level fall, punctuated by transgressions of decreasing amplitudes. Such a stepped-fall is consistent with observation in the underlying marine sequences and parasequences, which also show evidence of stepped-forced regressions (Li and Bhattacharya 2011; Zhu et al. 2012). Unfortunately, the equivalent marine units to Sequence 1 are not preserved due to modern erosion, and thus a direct comparison or correlation to the equivalent marine strata can not be made.

The evolution of the cut and fill of the compound incised valley system and its associated schematic relative sea-level change is illustrated in a schematic dip-cross section (Fig. 18) and in a Wheeler Diagram (Fig. 19). Fluvial incision is interpreted to have begun in response to the first episode of relative sea-level fall (Figs. 18A and 19). Following the first episode of incision, the incised valley was flooded during a subsequent possible stillstand or minor transgression. The incised valley was then turned into a tidally dominated estuary as discussed above, in which sediments likely transported from the river were reworked into tidally influenced deposits (FA. 3) (Fig. 18B). The second episode of fluvial incision occurred in response to another cycle of relative sea-level fall, which eroded a large part of previous tidal estuarine deposits in incised valley 3 and locally cut into the lower shoreface deposits. The erosional remnants of IVS 3 formed a terrace. The paleo-shoreline fell further and retreated from the study area. Consequently, during the subsequent transgression, the area was further away from the shoreline and did not experienced marine influence until a later stage of filling (Fig. 18C). Fluvial aggradation occurred before the final flooding of the incised valley, which deposited amalgamated fluvial deposits. The thin tidally influenced deposits capping IVS 2 were deposited after the flooding, possibly reflecting attenuated flooding at a later stage of transgression than IVS 3 experienced. Incised valley 1 was formed in response to the third episode of relative sea-level fall. The fact that IVS 1 contains the coarsest material suggests that it was formed at the maximum lowstand and it was filled during a subsequent stillstand or rise of sea level with the most proximal fluvial facies over older valley terraces. The paleo-shoreline at maximum lowstand was further away and this valley segment shows no evidence of marine influence and was never flooded as it was filled (Fig. 18D).

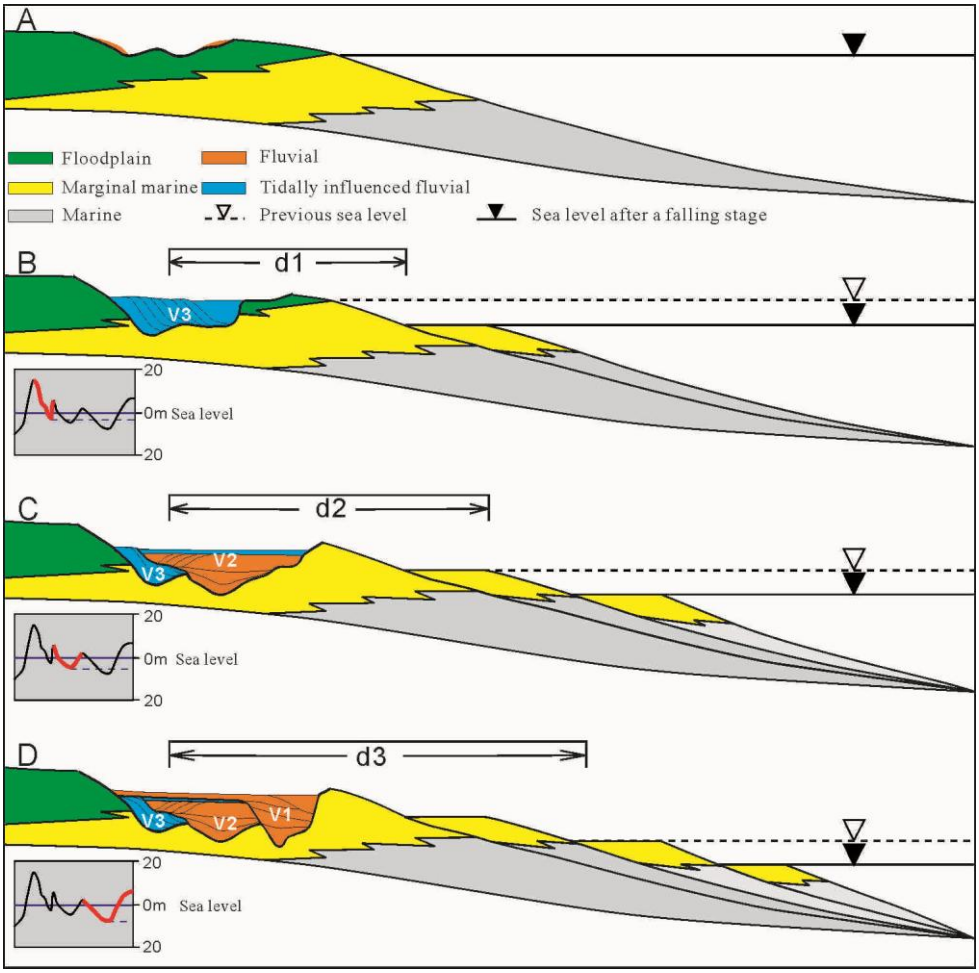

Figure 18. Cartoon illustrating the evolutionary history of the compound incised valley system in depositional dip direction and corresponding relative sea level change. d1, d2, and d3 mark the distance from the paleo-shoreline to the incised valley segment after each falling stage. Notice that d1<d2<d3, which means that the paleo-shoreline was further away from the incised valley in successive cycles of relative sea-level fall and rise. Solid lines mark the sea level after the falling stage and dashed lines mark the previous sea level. A) Depositional profile before sea level fall. Fluvial channel cuts into its own floodplain and shows no distinctive incision. B) Depositional profile after the first cycle of sea-level fall and rise. River started to incise and cut into lower marginal marine deposits. The incised valley was flooded and turned into a tide dominated estuary due to its relative closeness to the paleo-shoreline (d1) C) Depositional profile after the second cycle of relative sea-level fall and rise. Fluvial aggradation occurred before flooding of the incised valley segment due to further retreat of the paleo-shoreline (d2) and lowering of relative sea level. D) Depositional profile after the third cycle of relative sea-level fall and rise. The valley segment was not flooded due to further retreating of the paleo-shoreline (d3) and lowering of relative sea level. Fluvial aggradation occurred in response to relative sea-level rise that was further basinward.

2.8 Discussion

2.8.1 Criteria for Identifying Stepped Regression in a Compound Incised Valley

Stepped relative sea-level fall, punctuated with transgressions of various magnitudes, is a common phenomenon in geological history (Imbrie et al. 1984; Shackleton 1987). Stepped forced regression has been widely documented in the geological record in near shore depositional environments (e.g. deltaic, shoreface) and particularly in Cretaceous examples (Plint 1988; Posamentier et al. 1992; Fitzsimmons and Johnson 2000; Hamberg and Nielsen 2000; Azeredo et al. 2002; Tamura et al. 2007). However, it is poorly documented in fluvial deposits (but see Blum and Valastro 1994 and Hamilton et al. 2001), which may be due to low preservation potential and lack of recognition criteria. Within the Ferron Notom Delta complex, several stepped forced regressive deposits have been documented within the marine systems (Li et al. 2011; Zhu et al. 2012), but this is only the second study to document forced regressions in the non-marine facies (Li et al. 2010).

Based on this study, the following criteria may be used to identify a stepped forced regressive valley fill. 1) Successively more fluvial-dominated nature of each simple valley fill (from flood-based to flood-topped and then to non-flooded in this study); 2) Decreasing marine or tidal influence in successive fills; 3) Increase in proportion of extraformational material in successive valley fills; 4) Formation of terrace deposits. In addition, Blum (1993) and Miall and Arush (2001) documented intra-valley paleosols, associated with abandoned terraces. Li et al. (2010) observed rooted paleosols on top of the terrace deposits associated with valleys 2 and 3 in Nielsen Wash, but these were not observed in the Coalmine Wash area.

The formation and preservation of falling stage terraces supports the idea that rivers are not particularly efficient at wholesale sediment removal (Holbrook and Bhattacharya 2012). Storage of sediment during periods of falling base level supports the idea that rivers preserve some of their own sediment as they migrate within a valley (cut–and-cover model) rather than transferring all eroded sediment to more distal environments (bypass model). The observation of finer grained terraces (valleys 2 and 3) only partially eroded by later coarse-grained fluvial deposits of valley 1 indicates that significant sediment may be stored in a valley during falling stage. Our data are also consistent with the hypothesis of Strong and Paola (2008) that compound incised valleys are floored by complex erosional discontinuities that may form over several base-level cycles, and whose topography never represented a geomorphic surface. These are thus "stratigraphic" versus "topographic" valleys systems. The Wheeler analysis (Fig. 19) also emphasizes the diachronous nature of the overlying valley fill facies. Zhu et al. (2012) and Bhattacharya (2011) suggested that the erosional discontinuities also may not have chronostratigraphic significance, especially with respect to the shallow marine facies that the valleys override, although that is hard to prove in Sequence 1 with the data at hand.

2.8.2 Origin of High Frequency Non-marine Sequences

The composite erosional surface at the base of Sequence 1, as documented in this paper, and by Li et al (2010), shows at least three cycles of incision and deposition. Given that this composite erosional surface forms only a small part of the Sequence 1, which we estimate was deposited in about 100,000 years, each cycle probably occurred during a period of < 20 thousand years, which correlates with the

shortest, high-frequency Milankovitch cycles. The depths of fluvial incision suggest that these high-frequency sea-level changes were on the order of 10-20 meters and were thus likely climato-eustatic in origin (see discussion in Zhu et al. 2012).

Tectonically driven fluvial incisions have been documented in the foreland basin adjacent to the Sevier orogeny during the Cretaceous Period (Willis 2000; Yoshida 2000; Vakarelov et al. 2006), however, these events are all orders of magnitude slower than the cycles documented in this study (10^4-year). Fielding (in press), in a study of the Ferron Notom delta immediately south of our study area, documented a low relief angular unconformity associated with a small peripheral bulge or local uplift at the base of Sequence 2. However, it is challenging to explain the higher-frequency complex cut and fill patterns, and especially the more fluvial-dominated character in each successive valley fill documented in this study, using a tectonic model. We suspect that the higher-frequency events documented in this study were superimposed over a basin that experienced slower tectonic deformation resulting in unconformities that have multiple origins. A full geodynamic study may be required to tease out the relative importance of tectonic versus eustatic controls.

Climate-induced water and sediment discharge variations could lead to high-frequency cycles of fluvial incision and deposition that are independent of relative sea-level changes (Blum 1993; Goodbred and Kuehl 2000; Blum and Aslan 2006; Holbrook et al. 2006). However, climate control is mostly dominant upstream and diminishes towards the downstream buffer, which in our case is sea level (Blum and Valastro 1994; Blum and Aslan 2006; Holbrook et al. 2006). It is not clear how climate-controlled discharge changes would explain the abrupt basinward shift in

depositional facies and in particular the extensive incision surface that marks the base of Sequence 1. Discharge changes would more likely control sediment supply, which would increase or decrease the rate of normal (sediment-supply) regression. Such discharge increases would likely initiate enhanced deltaic progradation or avulsions, rather than deep incision (Olariu and Bhattacharya 2006) . The observation of tidal facies in this study is compelling evidence that these IVSs were directly linked to the sea, and can thus be considered as downstream buttress valleys (Holbrook and Bhattacharya 2012). Preliminary results from an ongoing study of the overlying floodplain paleosols in Sequence 1 show seven pedostratigraphic cycles characterized by gleyed paleosols with horizon development, which suggests that high-frequency climate cycles were important in Ferron time (Famubode et al. 2012).

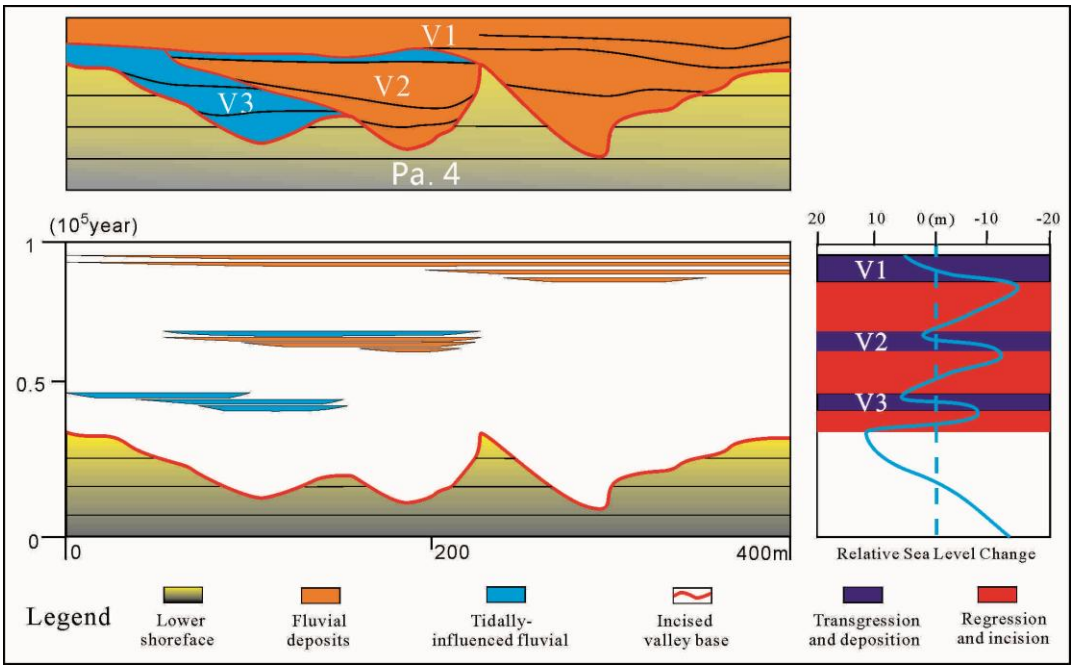

Figure 19. Wheeler diagram illustrating the history of the compound IVS and fluctuations of relative sea level, which is interpreted to be the major driving force of the IVS. A stepped relative sea-level fall punctuated by relative rises is illustrated in the right diagram. Incised valleys were cut during relative sea-level falls and filled during relative sea-level rises. The magnitude of relative change was estimated based on the relief of each incised valley.

2.9 Conclusions

1) The margin of a over 10 km-wide compound IVS was documented in outcrop exposures of the Ferron Sandstone in southern central Utah using measured sections and photomosaics. The "stratigraphic" valley is characterized by an abrupt basinward shift in depositional facies, a multi-storey fill, and significantly larger dimensions than the formative channels.

2) Facies analysis shows that the three simple incised valleys are characterized by different fill patterns. The oldest incised valley 3 is filled completely with tidally influenced deposits and represents a flood-based valley fill, deposited at the seaward portion of segment 2 of Zaitlin et al. (1994). Incised valley 2 is dominantly fluvial with minor tidally influenced deposits at the upper part of the valley. Valley 2 is flood-topped and interpreted to be deposited at the landward portion of segment 2 of Zaitlin et al. (1994). Incised valley 3 is filled with purely fluvial deposits without any marine influence. It represents an "overfilled' valley, deposited within the proximal inner segment 3 of Zaitlin et al. (1994).

3) The successively more fluvial dominated nature of each successive valley fill is interpreted to correlate with a prolonged stepped Milankovitch-scale sea-level fall, punctuated by transgressions of decreasingly amplitudes. Chronometric control suggests that the entire stratigraphic valley was formed over < 100,000 years and depth of incision suggest 10-20 meters of base-level change. This suggests a climato-eustatic control. However, simple climate-controlled changes in paleo-river discharge are unlikely to be able to explain the extensive incised nature in the basal discontinuity, and thus base-level changes are deemed to be required.

4) Storage of sediment during periods of falling base level, as indicated by the preservation of finer grained terraces, supports the idea that rivers preserve their own sediment as they migrate within a valley (cut-and-cover model) rather than transferring all eroded sediment to more distal environments (bypass model). The cut-and-cover model implies that overlying valley fill deposits are highly diachronous and suggests that the basal erosional discontinuity is a complex stratigraphic feature that never had any topographic expression.

CHAPTER 3 Facies Architecture, Branching Pattern, and Paleodischarge of a Lower Delta-plain Distributary Channel System in the Cretaceous Ferron Notom Delta, Southern Utah, U.S.A.

3.1 Introduction

Distributary channel networks are a crucial component in defining deltaic depositional systems, but are remarkably poorly documented in ancient sedimentary systems (Bhattacharya 2010). In modern deltas, distributary channels are characterized by successive downstream branching, which subsequently splits the trunk river discharge and sediment loads among a variable number of smaller-scale channels downstream (Bhattacharya 2010) . The smallest terminal distributary channels form by bifurcation around mouth bars, whereas larger upstream delta-plain distributary networks form by incomplete or partial avulsion (Bates 1953; Wright 1977; DuMars 2002; Slingerland and Smith 2004; Jerolmack and Swenson 2007; Edmonds et al. 2009; Bhattacharya 2010). The number and scale of terminal distributary channels depends on delta type and may also be controlled by numerous other factors such as slope-gradient advantage, substrate erodability, and trunk-channel discharge (Olariu and Bhattacharya 2006).

Distributary channels on the upper delta plain are purely fluvial, although they may show some indirect tidal influence, and interfinger with floodplain deposits, whereas distributary channels on the marine-influenced lower delta plain are characterized by tidal fluctuation and salt-water wedge intrusion and may be

associated with brackish bay or lagoonal environments that grade into delta-front and prodelta facies (Coleman and Prior 1982; Bhattacharya 2010). Studies of upper delta-plain distributary channels show meandering to be dominant (Elliott 1976; Cherven 1978; Fielding 1984; Hopkins 1984), however Coleman and Prior (1982) suggest that upper delta-plain channels may also be braided, presumably due to higher slopes. Distributary channels on lower delta plains, however, are commonly regarded as generally straight with limited migration and expansion (Coleman and Prior 1982). There are very few studies that documented migration patterns of ancient lower delta-plain channels (e.g. Corbeanu et al., 2004).

Recognition of the distributive nature of distributary channels in an ancient deltaic depositional environment is difficult but may be indicated by progressive downstream decrease in channel dimensions (e.g. widths and thicknesses of channel sandbodies), as is commonly observed in modern deltaic systems (Bhattacharya 2006; Olariu and Bhattacharya 2006; Bhattacharya 2010). Bridge (2000) documented systematic decrease in channel dimensions in more distal facies within the Devonian “Catskill” deltaic wedge of the Appalachian basin, U.S.A. Due to the limitation of many outcrop exposures (mostly 2-D), examples that use this method in recognition of ancient distributary systems, are rare. Direct documentation of channel branching in outcrop examples requires multiple strike-oriented outcrop exposures in successively updip and down-dip positions, such that upstream and downstream changes can be documented. North and Warwick (2007) point out the challenges of distinguishing ancient "distributive fluvial system" (DFS, Hartley et al., 2010) characterized by a single avulsing river, versus a system that has multiple active channel threads, such as dominates deltaic distributary channels and some "fluvial

fans".

Consequently, there are very few examples that document channel branching in the field. One exception is the branching pattern documented in the incised valley system of the Cretaceous Last Chance Delta in Utah (Garrison and Van Den Bergh 2006). Most studies of ancient delta systems interpret distributary channel deposits based on characteristics of their adjacent, associated strata (e.g. linked to upward coarsening deltaic succession) versus documentation of downstream decreasing channel dimensions (Bhattacharya 2010; Fielding 2010) . Studies of modern deltas also indicate that delta-plain distributary channel branching is commonly uneven, consequently forming asymmetrical channel belts (Yalin 1992; Olariu and Bhattacharya 2006; Edmonds and Slingerland 2008). However, the asymmetrical nature of distributary channel branching has not yet been documented within an ancient example.

Goal of this Study

The goal of this study is to document avulsion-dominated distributary channels in a lower delta-plain setting in an ancient storm- and wave-influenced deltaic depositional system. This study will evaluate the style and migration history of ancient delta-plain channels, which can be compared to purely fluvial channels in the same systems. This paper documents an ancient example of a lower delta-plain distributary channel network and its associated deposits within the Cretaceous Ferron Sandstone in central Utah. Three-dimensional outcrop exposures of the distributary channel system both upstream and downstream of the branching point provide an opportunity for accurate measurement of channel belt dimensions, which allow for testing of the uneven branching model. With accurate measurements of channel

dimensions, water discharge can be estimated. This can be used to infer the characteristics of distal delta-front or prodelta deposits fed by these distributary channels in as much as discharge may be linked to the threshold for producing hyperpycnal and other delta-plume types (e.g. frictional, inertial) (Bhattacharya and MacEachern 2009). Paleodischarge estimates also make it possible to estimate the branching order of specific channels within the entire deltaic distributary channel network, especially since trunk river dimensions, associated with incised valleys, have been estimated in previous studies (Li et al. 2010). Cross sections with measured sections, high-resolution photomosaics, and detailed bedding diagrams were made to illustrate internal facies architecture and migration patterns of distributary channel deposits. These allow interpretation of the relationship between distributary channels and their associated environmental facies, such as interdistributary bay, levee, crevasse splays; and their heterogeneity as analogs for hydrocarbon reservoirs. Barforms are identified and illustrated to show the variability and complexity of the distributary channel system.

3.2 Geological Setting

The Ferron Sandstone Member of the Mancos Shale Formation consists of a series of clastic wedges deposited on the western margin of the Cretaceous Western Interior Seaway during the late Turonian (Hale 1972; Cotter 1975). The Ferron Sandstone was developed as a result of the continued thrusting of the Sevier orogenic belt to the west and associated subsidence of the Cordilleran foreland basin as sediments were shed from the highland to the seaway eastward (DeCelles and Giles 1996; Ryer and Anderson 2004) (Fig. 1A). Three east- to northeast-prograding fluvial

deltaic clastic complexes were identified in the Ferron Sandstone, corresponding to the “Last Chance”, “Notom”, and “Vernal” deltas (Hale and Van De Graaff 1964; Hale 1972; Hill 1982) (Fig. 1B). The Notom delta complex is well exposed in the north of the Henry Mountains in south central Utah. A recent sequence stratigraphic study of the Notom Delta has divided it into 6 sequences, 18 parasequence sets and 43 parasequences (Li 2009; Zhu 2010; Zhu et al. 2012) (Fig. 20). Based on $^{40}Ar/^{39}Ar$ dating of sanidine crystals in associated bentonites, the entire Ferron Notom Delta is estimated to have been deposited between 91.25 and 90.63 Ma, a total of ~620,000 years. Consequently, on average each parasequence was deposited in about 15, 000 years. This study is focused on Parasequence 5a in Parasequence set 5 and Sequence 2 (Fig. 20B) (Zhu et al. 2012).

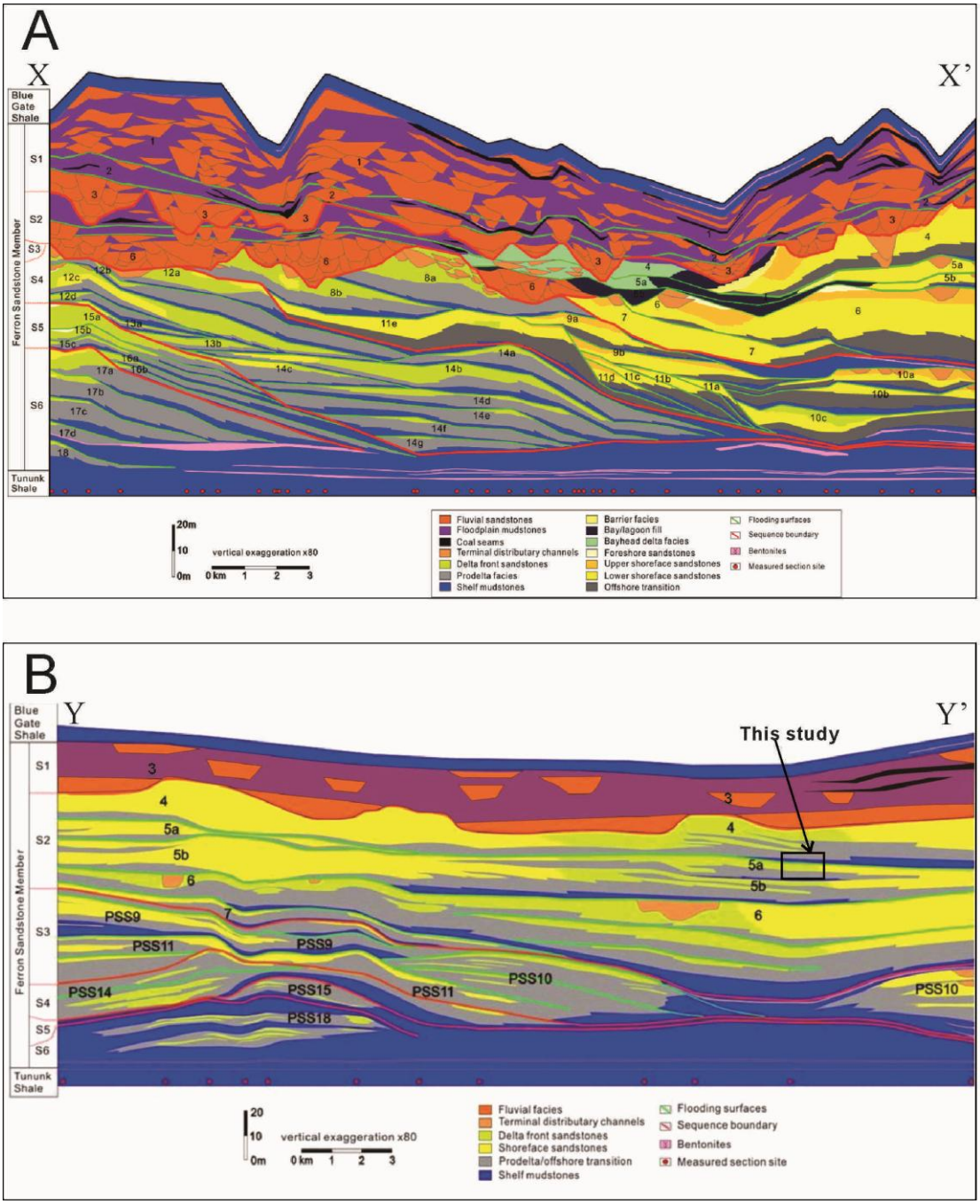

Figure 20. A) Cross section showing oblique regional depositional dip sequence stratigraphy of Notom Delta by Zhu, (2010). B) Cross section showing oblique regional depositional strike sequence stratigraphy of the Notom Delta by Li, (2009). Parasequence 5a of Sequence 2, which is interpreted as dominated by shoreface and delta-front deposits, is the focus of this study. See Figure 22 for the locations of the cross sections.

3.3 Previous Studies

Li (2009) and Zhu (2010) documented two parasequences in Parasequence set 5 (Parasequence 5a and 5b), and noticed a lateral facies change from river-dominated delta-front deposits to storm/wave-dominated shoreface deposits (Fig.20). Parasequence 5a is thus interpreted as a storm- and wave-influenced river delta. The tidal range is interpreted to be micro-tidal, and the system is thus only weakly influenced by tides. Zhu et al. (2012), based on their aggradational stacking pattern, assigned them to the highstand systems tract of Sequence 2. Based on the regional stratigraphy by Li (2009) and Zhu (2010), a paleogeography is constructed (Fig. 21). Parasequence 5a is interpreted to be a river-dominated delta prograding toward northeast. The delta shows a transition from proximal upper delta plain distributary channel and floodplain facies to lower delta plain interdistributary bay and lagoonal facies to delta-front mouth-bar and terminal distributary channel facies. In the regional strike direction, river-dominated delta facies laterally change to wave- and storm-dominated shoreface deposits (Fig. 21).

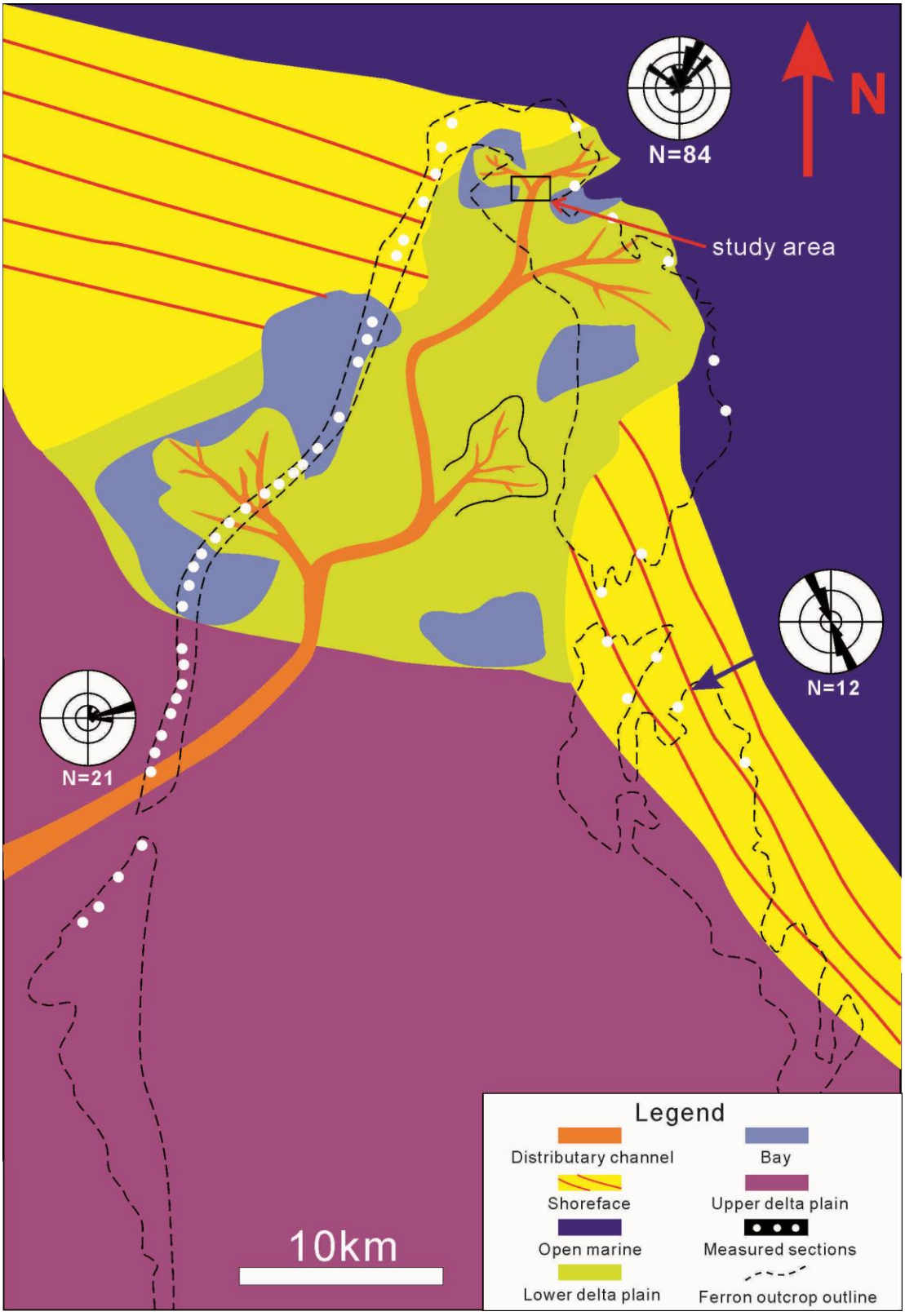

Figure 21. Paleogeographic reconstruction of Parasequence 5a based on the regional stratigraphy documented by Zhu, (2010) and Li, (2009) and data from this study. Black rectangle marks this study area.

3.4 Methodology and Data Set

The study area is located in Coalmine Wash in southern central Utah, west of Hanksville and close to Factory Butte (Figs. 22A and 22B). A gooseneck-shaped canyon provides a 3-D outcrop exposure of a distributary channel system and its associated levee, crevasse splay, and bayfill deposits within Parasequence 5a, allowing detailed mapping of sandbody dimensions and internal facies architecture (Fig. 22C).

Data used for this study were collected in the field by measuring detailed sections, in which lithology, sedimentary structures, grain size, bed thickness, paleocurrent direction, and trace fossils were recorded. The locations for measured sections were located by GPS (Fig. 22C). Measured sections were correlated based on tracing of erosional surfaces and macroform-bounding surfaces in the field and similarity of facies successions. Gigapan hardware and software and telephoto zoom lenses were used to compose photomosaics of sub-centimeter resolution, which were in turn used to make detailed bedding diagrams, illustrating internal bed geometry and facies architecture.

Paleocurrent data measured from directions of angle-of-repose cross-stratification and “rib and furrow” structures in bedding plane view were plotted in rose diagrams with a program named “Georient” (Fig. 22C). Documenting macroform geometry and their accretion patterns are key in interpreting channel pattern, river behavior, and evolutionary history. Consequently, in each bedding diagram and cross section, internal erosional surfaces and large inclined surfaces are illustrated.

In total, 32 measured sections (ranging from 5-9 m) and 8 high-resolution

photomosaics were collected. Seven detailed bedding diagrams and 7 cross sections with measured sections were made (Fig. 22C).

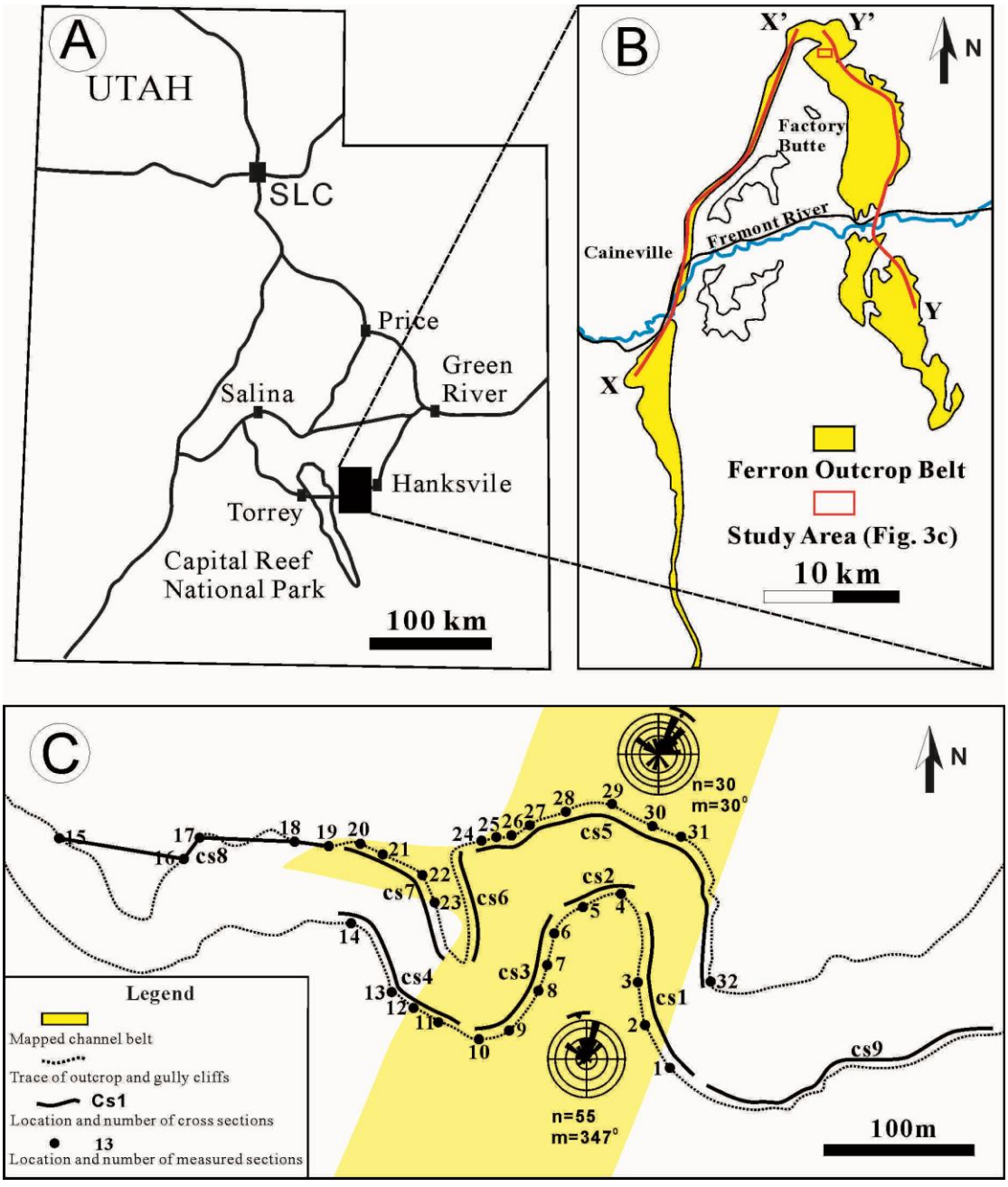

Figure 22. Basemaps showing the study area. A) Basemap showing Utah and the location of Ferron Notom delta outcrop, which is marked with a black rectangle. B) Basemap showing the distribution of Ferron Notom delta outcrop and the location of this study area (in the red rectangle). XX' marks the location of cross section shown in Fig. 20. C) Basemap of the study area showing the location of outcrop exposures, measured sections, and cross sections. Rose diagrams showing general paleocurrent directions are shown.

3.5 Facies Analysis

In total, 7 facies associations are identified based on their lithology, sedimentary structures, ichnofacies, geometry, and vertical and lateral relationships. They are: 1) distributary channel, 2) abandoned channel, 3) levee, 4) crevasse splay, 5) bayfill, 6) shoreface, and 7) transgressive lag. These facies associations are summarized in TABLE 2 and described below.

3.5.1 FA1: Distributary Channel Belt

Description: Facies association 1 is mostly composed of fine- to medium-grained sandstones confined in U-shaped concave-up channel forms, which erosionally cut into adjacent strata (Fig. 23A). Channel forms are commonly 4-5 m thick and 80-250 m wide. The basal erosional surfaces are locally overlain by massive, carbonaceous medium- to coarse-grained sandstones with abundant intraformational rip-up-mud-clasts and extraformational pebbles (Fig. 23A). Dune-scale cross-bedded medium-grained sandstone is the most abundant facies (Fig. 23B). Thicknesses of cross-bed sets range from a few centimeters to tens of centimeters. Current-ripple cross-laminated fine-grained sandstones, although uncommon (Fig. 23C), typically overlie cross beds and are relatively finer grained and more heterolithic. Meter-scale angle-of-repose inclined beds are the second most abundant facies (Fig. 23D). These large inclined beds are 1-2 m thick and are commonly a few meters wide, with individual beds of uniform thickness accreting laterally or downstream. Locally, dune-scale cross beds dip in opposite directions and show abundant mud drapes (sometimes paired) (Fig. 23F). Sparse bioturbation was observed within these mud drapes (Fig. 23F). Ichnogenera include *Paleophycus, Cylindrichnus, and Planolites*.

TABLE 2. —Summary of the major facies associations (FA)

FA	Interpretation	Lithology	Sedimentary Structures	Biota	Lateral & vertical relationships
1	Distributary channel	Erosionally based, fine- to medium-grained sandstone bodies with local pebbles, <5m thick, local intraformational conglomerates at the base, Thalweg deposits at the base, Internal minor erosional surfaces.	Flutes and tool marks at the channel base, large-scale macroform accretion surfaces, meter-scale unit bar accretion surface, dune-scale cross bedding, planar bedding, ripple cross lamination, local convolute bedding. Locally paleocurrent reversal, double mud drapes.	Plant debris	Sometimes have multi-lateral stacking pattern, with single storey sandstone bodies typically 3-5 meter thick and 50-100m wide.
2	Abandoned channel	Carbonaceous silty mudstone or interbeded mudstone and silty sandstone.	Mostly planar lamination, with silt; sandstones sometimes show current ripple cross lamination.	Plant debris	Mostly less than 10 m wide and less than 1 meter thick, no vertical trend or gradually coarsening upward, sometimes vertically cut by another channel storey.
3	Levee	Conformable with bayfill deposits (FA5), very fine-grained sandstone interbedded locally with thin mudstones.	Planar laminated, climbing ripple-cross laminated.	Sandstone are commonly not bioturbated, thin mudstones contain Pl. Ch. Th.	About 1-1.5 m thick, gradually thins away from the channel in a perpendicular direction, width is estimated to be a few hundred meters.
4	Crevasse Splay	Heterolithic very fine- to fine-grained sandstone interbedded with thin mudstone, abundant internal minor erosional surfaces with thickness up to 3 m.	Current ripple-cross lamination, wave ripple-cross lamination, hummocky cross stratification, planar bedding.	As FA.3	Gradually coarsens upward and thins away from crevasse channel, locally show lens shaped sandbodies, and foresets dipping away from the crevasse channel.

TABLE 2. –continued

Facies	Interpretation	Lithology	Sedimentary Structures	Biota	Lateral & vertical relationships
5	Bayfill	Heterolithic thin silty mudstone interbedded with very fine grained sandstone.	Wave ripple cross lamination, hummocky cross stratification are common, locally inverse grading.	Lightly to moderately bioturbated (BI= 0-4) with Pl., Th., Ar., Sk., Ch., Di.	Relatively uniform through out the study area, thins toward the distributary channel.
6	Shoreface	Very fine grained sandstone.	Swaley cross stratification, Hummocky cross stratification.	Moderately to highly bioturbated (BI-2-6) with Ar., Op., Sk., Cy..	Very local, laterally adjacent to a distributary channel cut bank.
7	Transgressive lag	Fine to medium grained sandstone.	Cross bedding.	*Glossifungites* ichnofacies with Op. Sk. Th.	Continuous and extensive through out the study area about 10-30 cm thick.

Interpretation: The erosionally based U-shaped sandstone bodies are interpreted to be channel belt deposits. The basal carbonaceous sandstone with intraformational mud clasts and extraformational pebbles are interpreted to be channel thalweg deposits. Dune-scale cross beds are formed by migration of dunes. The capping finer grained, more heterolithic laminated sandstone indicates waning river floods. The fining upward succession from dune-scale cross beds up to cross laminated beds are interpreted to represent river flood deposits. Meter-scale inclined beds are interpreted to be unit bar deposits (Smith 1974; Bridge 2003; Bridge 2006; Rice et al. 2008; Reesink and Bridge 2011). They could either be part of a compound bar form or a separate bar form. Oppositely dipping cross beds with double mud drapes indicate flow reversal and suggest some tidal influence (Visser 1980). The trace fossils indicate a brackish water environment (MacEachern et al. 2005; MacEachern et al. 2010).

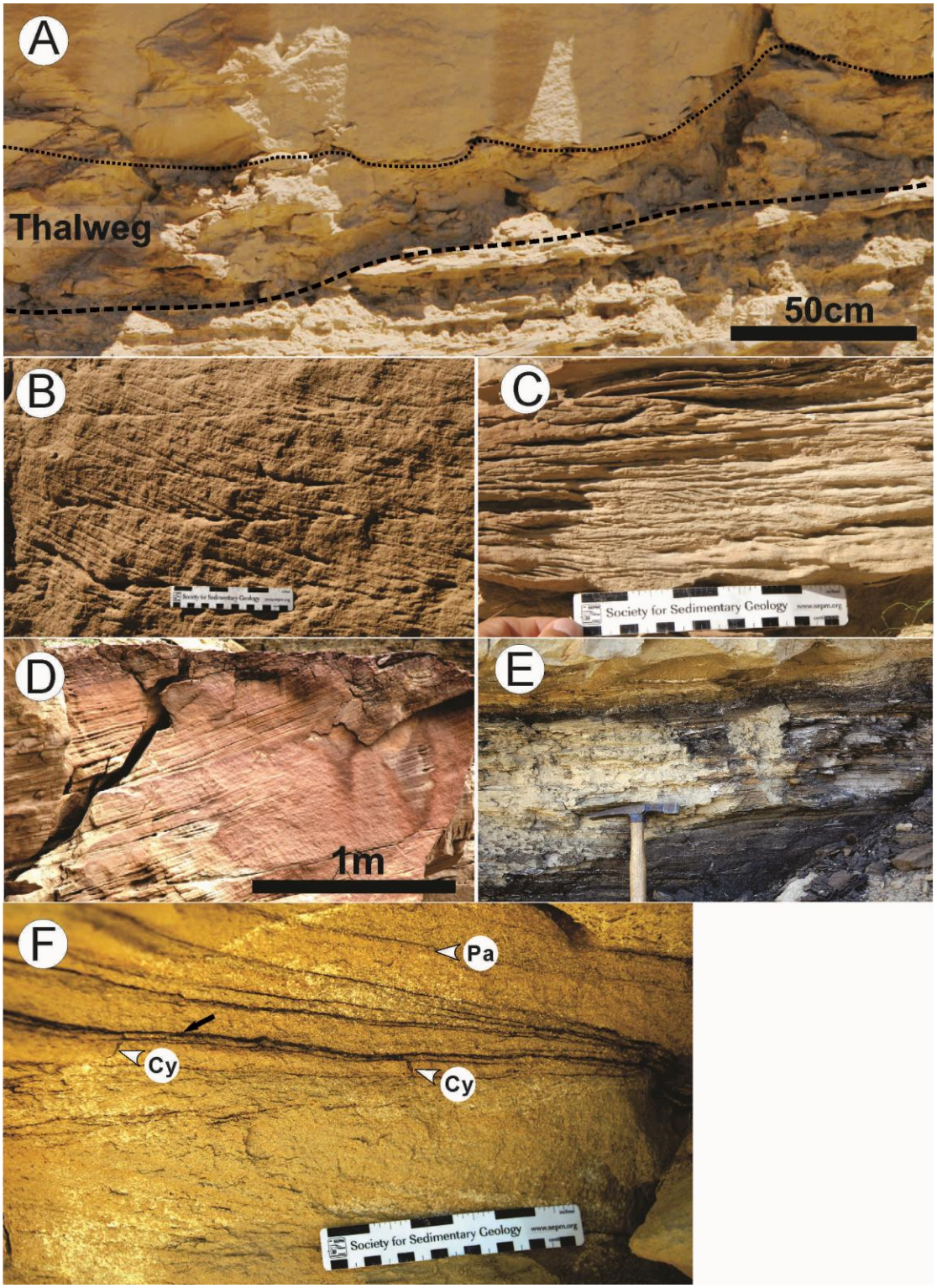
A
Thalweg
50cm
B
C
Society for Sedimentary Geology
D
1m
E
F
Pa
Cy
Cy
Society for Sedimentary Geology

Figure 23. Distributary channel and abandoned channel facies. A) A thalweg deposit at the base of a channel, characterized by mottles without any sedimentary structures. It is composed of carbonaceous, pebbly medium-grained sandstone with abundant rip-up-mud-clasts. The thin black dashed line marks the base of fluvial bar deposits and the thick black dashed line marks the base of the channel. B) Dune-scale tabular cross-bedded fine-upper to medium-grained sandstone. C) Current-ripple cross-laminated sandstone. D) Meter-scale cross-bedded medium-grained sandstone interpreted to be unit bar deposits. E) Abandoned channel deposits. The abandoned channel is filled with interbedded carbonaceous mudstone and silty sandstone, indicating that the channel was still receiving minor discharge during floods after abandonment. It was erosionally cut by another channel storey. F) Photo showing tide-influenced facies in the distributary channel fill. Five cross-bed sets or lamina sets were identified and illustrated. The lower one dips to the right, the middle three dip toward the left and the upper one dips toward the right again, indicating reversal of paleocurrrent direction. The thicknesses of three middle bed sets are much thinner than those above and below. Double mud drapes separating tidal bundles can be seen in the upper bed set. Ripple-cross laminations dipping to the left can be seen in the tidal bundles in the upper bed set. Based on the observation above, dominant flow is interpreted as toward the right, while subordinated flow was toward the left. Burrows associated with mud drapes can be seen. Pa. *Palaeophycus.* Cy. *Cylindrichnus.*

3.5.2 FA 2: Abandoned Channel Deposit

Description: Facies association 2 is also characterized by an erosional channel-form geometry with a basal erosional surface. It is mostly composed of carbonaceous laminated silty mudstone, which is commonly interbedded with thin bedded fine-grained sandstone (Fig. 23E). The strata filling the channel forms are commonly conformable with the adjacent macroforms on one side and are erosional on the other side. Sediments filling the channel forms are generally muddier than adjacent strata. They are, however, not necessarily always mudstones. Rarely, only a thin layer of mudstone lines the entire channel form and it is overlain by cross-bedded sandstone. These mud-filled channel forms are commonly less than 1 m thick and less than 30 m wide. No bioturbation was observed in these muddy deposits.

Interpretation: This facies association is interpreted as abandoned channel deposits. The thin bedded sandstones indicate gradual rather than abrupt abandonment. The channel-lining mudstone overlain by cross bedded sandstone is interpreted to indicate temporary abandonment followed by river rejuvenation, similar to that described by Lynds and Hajek (2005). The abandoned channel widths indicate that the channels were about 30 m wide.

3.5.3 FA 3: Levees

Description: Facies association 3 is present adjacent to and erosionally cut by the channel deposits described above. It ranges from 1-3 m thick adjacent to the channel belts and thins away from them. It is mostly composed of unidirectional climbing ripple cross-laminated sandstone with minor scour surfaces (Figs. 24A, 24B, 24D) and planar-bedded very fine-grained sandstone (Fig. 24C). Ripples are weakly asymmetrical. The angles of climb are commonly larger than 60^0 (Figs. 24A and 24B). The rippled and planar-bedded sandstones are commonly interbedded with very thin silty mudstone layers (Fig. 24D). The mudstones show sporadic bioturbation, including *Planolites*, *Chondrites,* and *Thalassinoides (*Fig. 24E*).* Symmetrical ripples and sporadic bioturbation also occurs in the mudstone layers.

Interpretation: The observation that this facies lies adjacent to and consistently thins away from channel belt deposits suggests that they are the associated levee deposits. The weakly asymmetrical nature of the climbing ripples indicates possible combined flows with some wave influence. The high angles of climb (type S of Allen, 1973), indicate a very high rate of sedimentation. Minor erosional surfaces indicate possible strong flood events, during which erosion occurred. The sporadic

bioturbation in the mudstone layers indicates that they were deposited in a subaqueous and probably brackish water environment, such as an interdistributary bay, as opposed to a non-marine floodplain lake (MacEachern et al. 2005; MacEachern et al. 2010). This also suggests a lower delta plain setting, as opposed to fully fluvial channels in a non-marine floodplain (Bhattacharya 2006; Bhattacharya 2010)

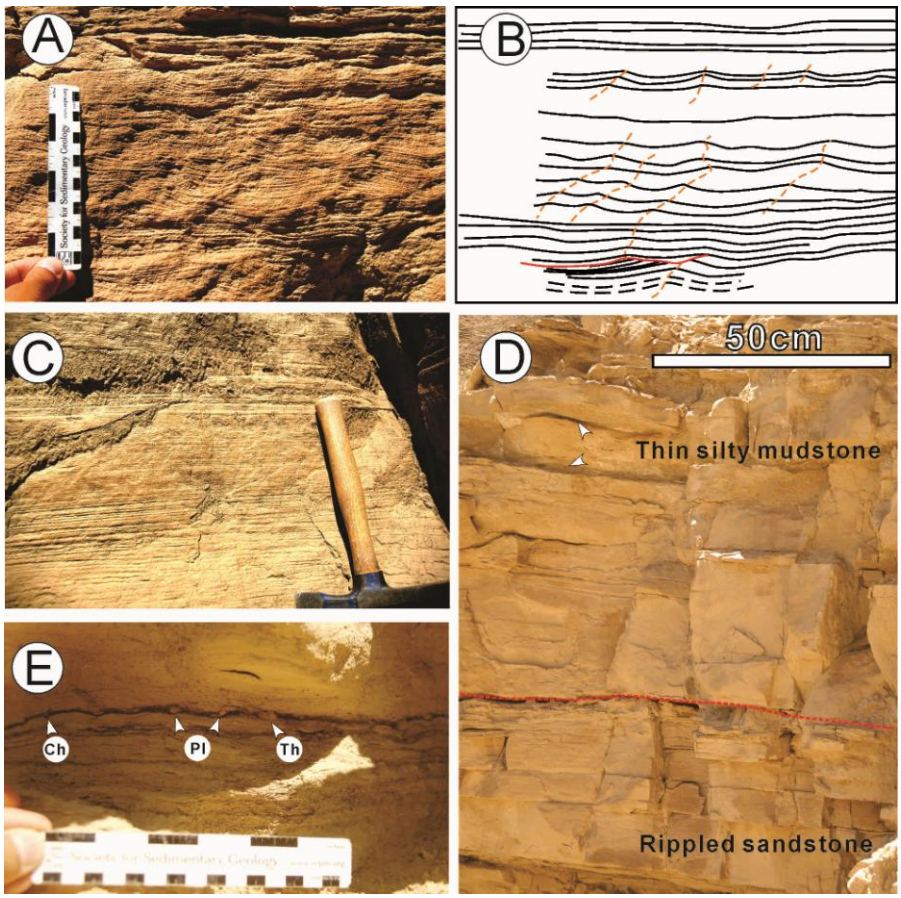

Figure 24. Photos showing typical levee facies. A) Climbing ripples with angle of climb larger than 60^0 (Type S of Allen, 1973) indicating extremely high rate of aggradation. B) Bedding diagram made based on the photo in Fig. 24A, showing the ripple geometry (solid black lines) and traces of ripple crests (dashed brown lines). A minor erosional surface can be seen at the basal part of photo Fig 24A, and is marked with a red solid line, indicating lower rate of sediment supply relative to water discharge. C) Very fine-grained planar-bedded sandstone. D) A photo showing a complete vertical section of levee facies. It shows rippled sandstone overlain by planar-bedded sandstone which is interbedded with thin layers of silty mudstones (marked with white arrows). The red dashed line marks a minor erosional surface. E) Burrows in the thin mudstone layers of levee facies. Ch. *Chondrites*, Th. *Thalassinoides*, Pl. *Planolites.*

3.5.4 FA 4: Crevasse Splay

Description: Facies association 4 is characterized by a general coarsening upward and is more heterolithic than the levee facies described above (Fig. 25A). It is composed of interbedded very fine-grained sandstone with thin mudstone. Sandstones are characterized by planar lamination, wave-ripple cross lamination (Fig. 25B), current-ripple cross lamination (Fig. 25C), and less commonly hummocky cross stratification (Fig. 25A). Minor erosional surfaces are common (Fig. 25A) Climbing ripples are locally seen (Fig. 25D). A succession of planar-laminated sandstones capped by wave ripples, which are overlain by laminated silty mudstone, is very common (Fig. 25B). The paleocurrent direction, as indicated by the current ripple cross laminations, is generally laterally away from the main channel belt and in accordance with the dip direction of the smaller subordinate channel belt, which it is associated with. The thin mudstone layers are commonly bioturbated (BI of 2-5), with *Planolites, Chondrites,* and *Palaeophycus,* which are commonly small in size, compared to those in normal shoreface deposits (Li et al. 2011).

Interpretation: The heterolithic coarsening upward succession at the distal end of subordinated channels is interpreted to be crevasse splay deposits. Current ripples indicate unidirectional river flows. The heterolithic coarsening upward succession indicates progradation into a shallow brackish bay, as opposed to a non-marine floodpain. The successions of planar sandstone overlain by rippled sandstone and mudstone are interpreted to be waning flood deposits, which are possibly related to major storm flood events. Climbing ripples indicate temporarily high rate of sedimentation during strong flood events. The wave cross lamination and HCS indicates occasional storm influence. The bioturbation (BI of 1-3) suggests significant

marine influence, although the reduced size of trace fossils indicates a stressed and probably brackish environment (Willis 1997; MacEachern et al. 2005). Consequently, these crevasse splays were probably developed in a semi-enclosed brackish, interdistributary bay in a lower delta plain setting.

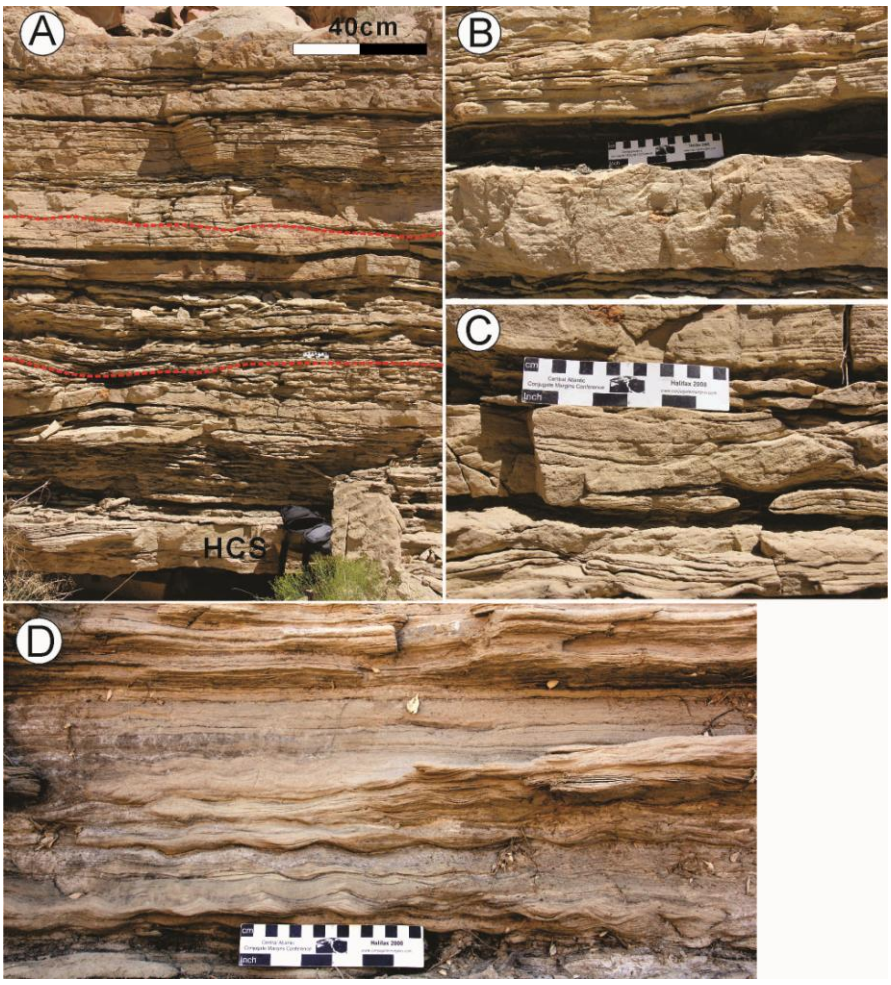

Figure 25. Photos showing typical crevasse splay facies. A) A complete vertical section showing that crevasse splay deposits are characterized by a general upward coarsening succession composing of heterolithic interbedded mudstone and very fine-grained sandstone. Minor erosional surfaces marked with red dashed lines, are common. The whole section is about 2.5 m. B) Photo showing a typical vertical facies succession in crevasse splay deposits comprising planar bedded sandstone capped by a layer of wave-ripple cross-laminated sandstone, which is overlain by a layer of laminated silty mudstone. C) Photo showing unidirectional current-ripple cross-lamination which is overlain by wave-cross lamination. D) Climbing ripple cross lamination gradually changes upward into planar lamination, indicating a possibly decreasing rate of sediment supply.

3.5.5 FA 5: Bay Fill

Description: Facies association 5 is commonly present at the basal part of Parasequence 5a. It is erosionally cut into by the channel belt deposits. It is characterized by a general coarsening upward pattern, containing silty mudstone in the basal part changing upward into heterolithic, interbedded very fine-grained sandstone and mudstone (Fig. 26A). Sandstones are commonly wave cross-laminated and sometimes hummocky cross-stratified, with their bases and tops lightly bioturbated (Fig. 26A). The mudstone layers are commonly bioturbated to different degrees (Fig. 26B). Ichnogenera are more diverse than in the previously described facies associations and include *Teichichnus*, *Planolites, Paleaophycus, Chondrites, Diplocraterion,* and *Asterosoma.*

Interpretation: These silty mudstone at the basal part of Parasequence 5a are interpreted to be proximal prodelta and bay fill deposits. The coarsening upward pattern may indicate progradation of a bayhead delta. Wave ripples and HCS indicates wave and storm influence. The trace fossil assemblage indicates a brackish water environment, also indicating a more protected bay, versus a fully open marine environment (MacEachern et al., 2005; MacEachern, 2011).

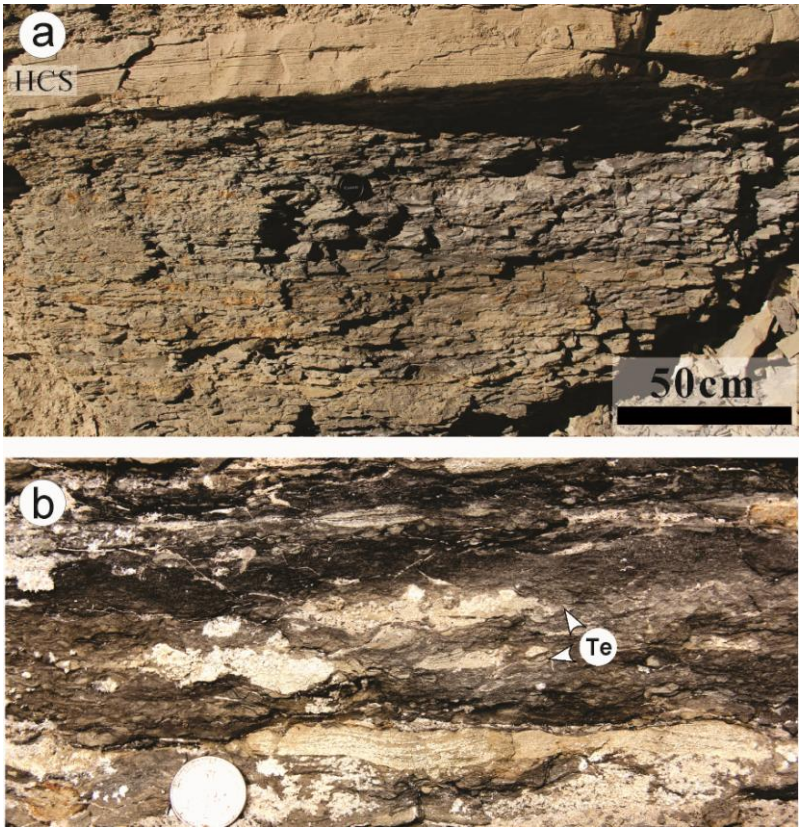

Figure 26. Photo showing typical bayfill deposits, which are composed of carbonaceous, silty mudstone and are mostly massive, with locally cross laminations. They are sharply overlain by a layer of hummocky cross stratified very fine grained sandstone. B) A close-up photo of the muddy bayfill deposits, showing the internal bioturbation. Bioturbation index ranges from 1-5.Te. *Teichichnus.*

3.5.6 FA 6: Shoreface Facies

Description: Facies association 6 is only found locally, on one side of the subordinate channel belt replacing the levee facies that usually occur adjacent to the mapped channel belt. It is about 1-2 m thick and less than 10 m long. It is mostly composed of swaley cross stratified and hummocky cross stratified very fine-grained sandstone, bioturbated to different degrees (BI of 1-6) (Fig. 27). Sometimes beds show a cyclic pattern of highly bioturbated sandstone interbedded with lightly bioturbated sandstone (Fig. 27). Ichnogenera include *Ophiomorpha, Palaeophycus,*

Skolithos, *Cylindrichnus*, and *Arenicolites* (Fig. 27). These facies laterally change to typical levee or bay fill deposits.

Interpretation: The hummocky and swaley cross bedded very fine grained sandstone beds are interpreted to be storm/wave-reworked shoreface deposits (may be from formerly developed crevasse splay deposits) but the localized nature of the deposit suggests that it formed as a subaqueous barrier spit deposit, possibly representing re-worked levee or crevasse splay sands that it replaces. The trace fossil assemblage is interpreted to represent a *Skolithos* ichonofacies typical of a shoreface environment (MacEachern et al. 2010). The cyclic pattern of bioturbated to less burrowed beds is interpreted to have resulted from storm deposits followed by inter-storm organism reworking.

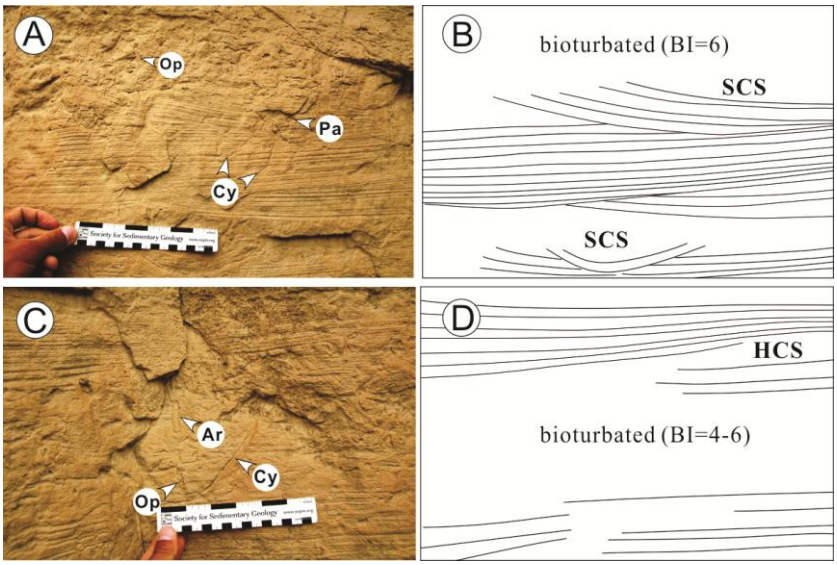

Figure 27. Lower shoreface deposits. A) Lightly bioturbated very fine-grained swaley cross-bedded sandstone overlain by highly bioturbated sandstone. B) Bedding diagram of photo 27A, illustrating the swaley cross stratification (SCS). C) A photo showing an example of lightly bioturbated sandstone overlain by highly bioturbated sandstone in the middle which is overlain by lightly bioturbated hummocky cross stratified (HCS) sandstone on the top, indicating two separate storm events. D) Bedding diagram of photo 27C, illustrating the cyclic pattern of the shoreface deposits in terms of degree of biotrubation. Op. *Ophiomorpha,* Pa. *Palaeophycus*, Cy. *Cylindrichnus*, Ar. *Arenicolites*.

3.5.7 FA 7: Transgressive Lag

Description: Facies association 7 is present throughout the study area and overlies parasquence 5a. It is composed of massive medium- to coarse-grained highly bioturbated sandstone about 20 cm thick (Fig. 28). The massive sandstone is erosionally based and is locally underlain by vertically and inclined burrowed cross-bedded sandstone (Fig. 28). The massive sandstone is in turn overlain by a fining upward bioturbated muddy sandstone. Ichnogenera include *Cylindrichnus, Skolithos, and Thalassinoides*.

Interpretation: The 20 cm thick fining upward facies succession is interpreted to represent a transgressive lag deposit. The erosional surface below the transgressive lag is interpreted to be a transgressive surface of erosion. The trace fossil assemblage represents a *Glossifungites* ichnofacies, implying firmground burrowing (MacEachern, 2011)

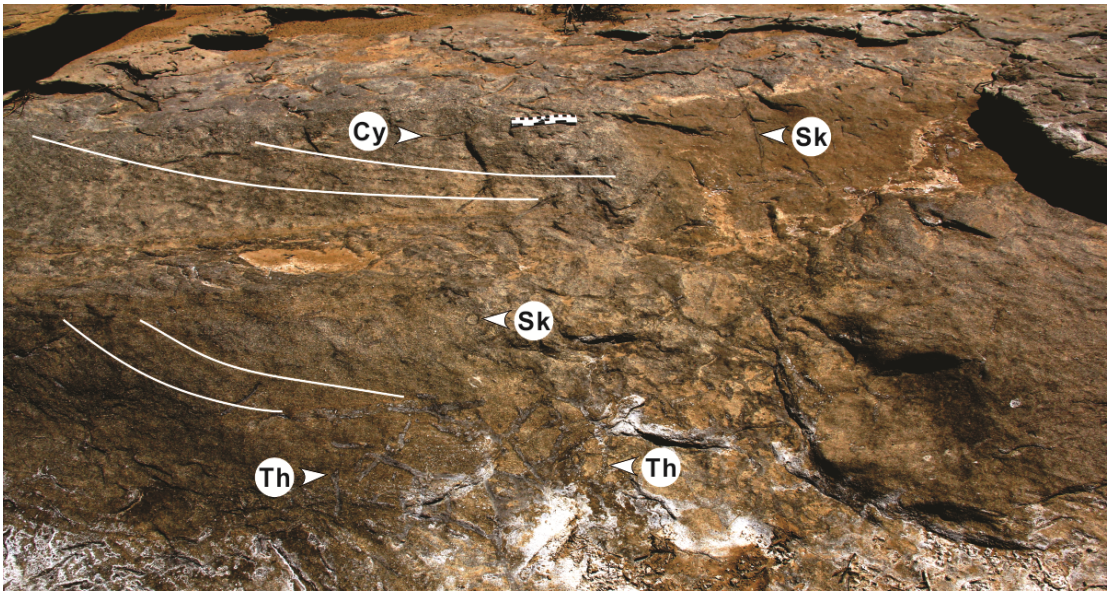

Figure 28. A Photo showing Glossifungites ichnofacies on top of Parasequence 5a in an oblique view, where vertical and inclined burrows penetrate cross-bedded sandstone. Sk. *Skolithos*, Cy. *Cylindrichnus*, Th. *Thalassinoides.*

3.6 Facies Architectural Analysis

Here we outline our overall interpretation of the facies architectural relationships, in order to provide context for the detailed documentation of its components.

Within the 3-D outcrop exposure, a main channel belt and a subordinate channel belt are recognized and correlated across the canyon (Fig. 22C). The channel belts erode into and are laterally associated with moderately wave- and storm-influenced levee, splay, and bay fill deposits. Brackish to marine trace fossils indicate a lower delta-plain environment, and suggest that the channels flowed into and were associated with inter-distributary bays that grade seaward into wave- and storm-influenced prodelta and delta-front deposits. This overall facies association suggests that these are distributary channels on the lower delta plain. A lack of mouth-bar deposits suggests that this is not the terminus of the delta, which is presumed to lie several kilometers or more seaward of our study area.

The main channel belt has a general northeast trend with four cut banks exposed respectively near sections 1,13, 24, and the middle of sections 31 and 32 (Fig. 22C). The subordinate channel belt has a general northwest trend with four cut banks exposed respectively near sections 20 and 23, and close to the two ends of cross section 6 (Fig. 22C). The downstream subordinate channel belt is interpreted to branch from the main channel belt, also suggesting that it is a distributary branch. The main channel belt is around 250 m wide and narrows to 200 m downstream of the branching point, whereas the subordinate channel belt is about 80 m wide (Fig. 22C). Mean paleocurrent directions changed from northwest-directed south of the interpreted branching point to northeast-directed north of the interpreted branching point (Fig. 22C).

On the southern side of the canyon, four cross sections (cross sections 1, 2, 3 and 4) cut through the main channel system at different angles (Fig. 22C). They were analyzed to show the channel belt geometry and internal facies architecture. Cross section 5 on the northern side of the canyon cuts through the main channel belt in a general strike direction. Cross sections 6 and 7 cut through the subordinate channel belt in a strike and oblique direction respectively. Cross section 8 cuts through the crevasse splay deposits fed by the subordinate channel. Cross section 9 shows the levee facies associated with the main channel belt. The internal bedding geometry and facies relationships of the main channel belt, subordinate channel belt, crevasse splay and levees are illustrated and described below in more detail with respect to each of these cross sections.

3.6.1 Main Channel Belt Exposed on the Southern Cliff

Cross section 1 (Figs. 29 and 30)

Description: Cross section 1 shows an oblique (SE-N) view of the main channel belt (Fig. 22C). A basal erosional surface cuts into adjacent planar bedded strata and muddy deposits below, and shallows toward the southeast (Fig. 29). Internally, it is composed of medium-grained sandstones with meter-scale inclined beds locally capped by dune-scale cross beds of FA1 (Figs. 29 and 30). In the middle part of the cross section, where Section 2 and Section 3 are located, the large scale inclined beds dip toward the north, with some internal beds dipping in the opposite direction (Fig. 29). A minor erosional surface is identified on the northern side of the cross section (Fig. 29). Although late tectonic normal faults obscure the detailed bedding in part of the outcrop, macroforms generally appear to accrete toward the north, as correlated

with the measured sections (Fig. 30).

Correlation of measured sections also shows that Parasequence 5a is regionally capped by the transgressive lag facies (FA7) (Fig. 30).

Interpretation: The distributary channel belt deposits are interpreted to cut into adjacent levee deposits and muddy bayfill deposits below. Where the basal erosional surface shallows upward toward the southeast, it is interpreted to be the southeastern cutbank. The southeastern part of the channel belt, where the channel shallows upward, is possibly composed of unit bar deposits, which are capped by the dune-scale cross beds (Fig. 29). The large inclined beds are interpreted to be point bars accreting toward the north.

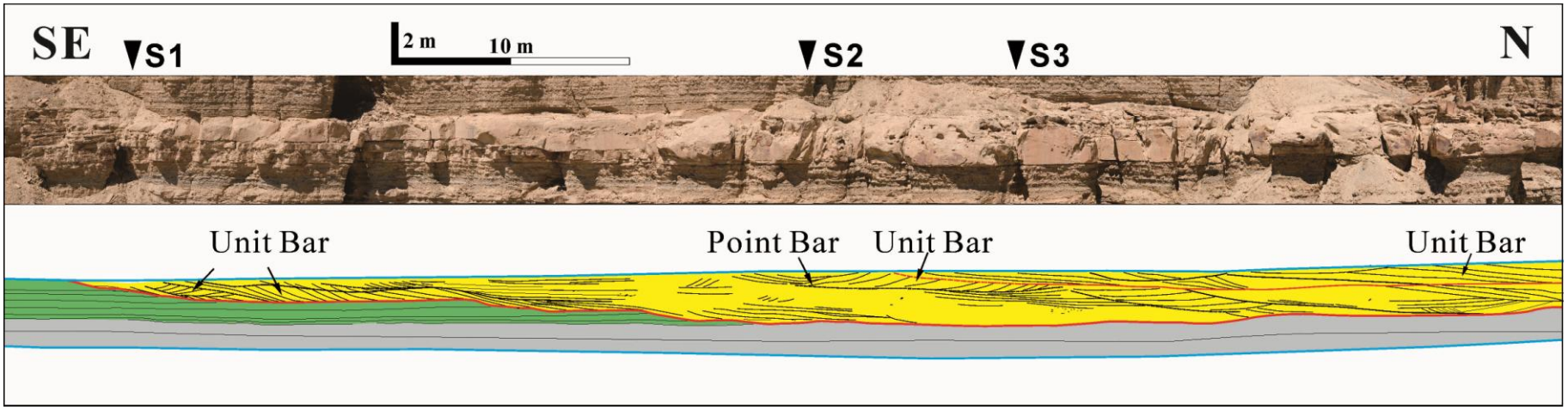

Figure 29. A) Photomosaic and bedding diagram of cross section 1, which cuts through the main channel belt in an oblique direction, showing the geometry, internal minor erosional surfaces and facies architecture of the eastern part of the main channel belt. The eastern cut bank of the main channel belt cuts into planar bedded levee deposits to the southwest. See Figure 22C for the location of the cross section. See Figure 30B for the legends.

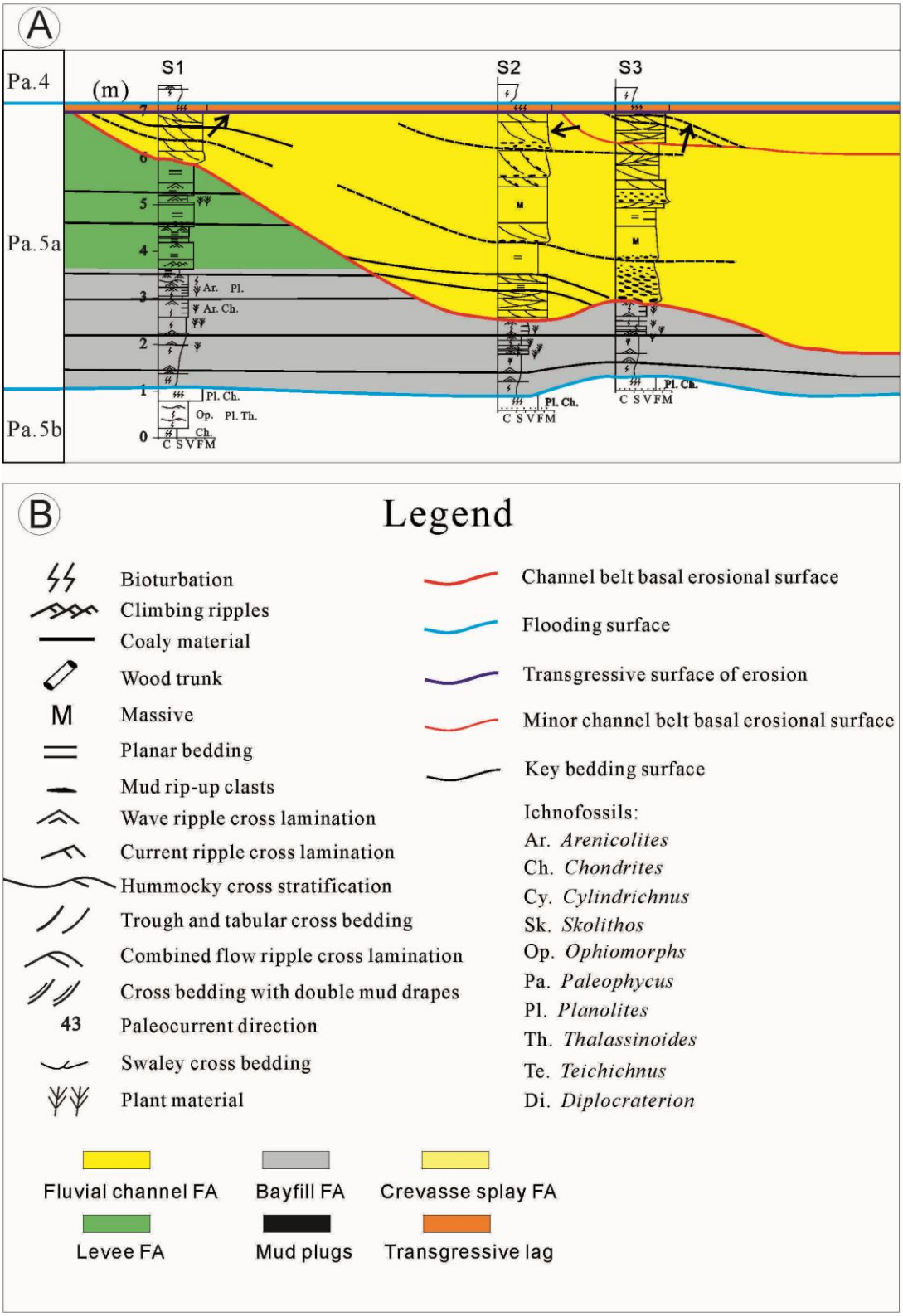

Figure 30. Correlation of measured sections showing facies and strata, bounding surfaces through cross section 1. Large inclined surfaces mainly dip toward north. B) Facies key for the geological sections and bedding diagrams presented in this study.

Cross section 9 (E-W) (Fig. 31)

Description: Cross section 9 is located just east of cross section 1 (Fig. 22C). It shows a general strike view of the facies laterally adjacent to and associated with the main channel belt recognized in cross section 1. The eastern cut bank of the main channel belt can be seen on the western side of cross section 9 (Fig. 31). The erosional surface cuts into planar-bedded very fine-grained sandstone of FA3, which becomes thinner and muddier away from the channel belt (Fig. 31). This dramatic thinning, from 2-3 m to less than 1 m of the planar bedded sandstone occurred over a distance less than 200 m (Fig. 31).

Interpretation: The whole Parasequence 5a in cross section 9 is interpreted to be levee facies which thin and pinch out away from the main channel belt (Fig. 22C).

Cross section 2 (Figs. 32 and 33)

Description: Cross section 2 shows an oblique-strike (E-SW) view of the main channel belt (Fig. 22C). The channel belt sandbody is about 5 meters thick and is separated by a minor erosional surface into two storeys (Fig. 32). The lower storey is composed of 5 meter-thick inclined beds, with internal dune-scale cross bedding (FA1), which accrete toward the east (Figs. 32 and 33). A large inclined bed on the western side of the outcrop is composed of meter-scale cross beds (illustrated with large individual dashed lines) with bedding surfaces dipping in an opposite direction to the dip of the large inclined beds (Fig. 32). A thin muddy bar drape underlies the large inclined unit (Fig. 32). A mud plug (FA2) is identified right below the internal erosional surface on the eastern side of the cross section (Fig. 32).

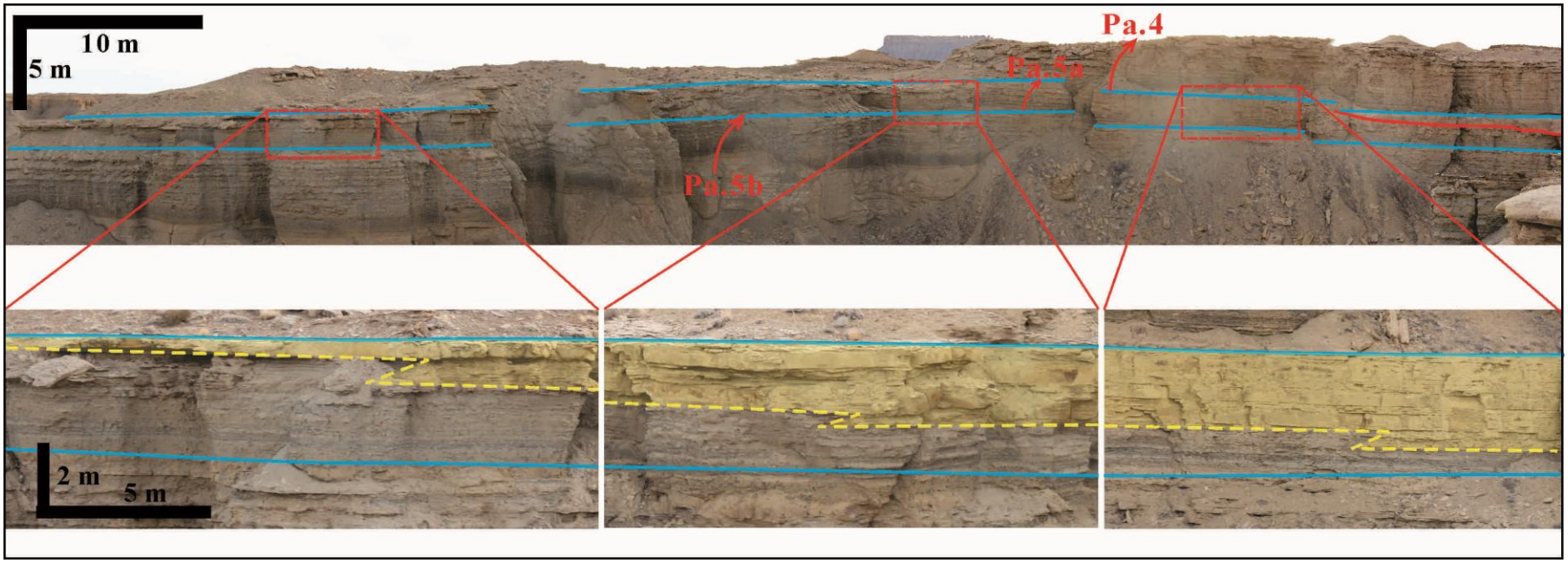

Figure 31. Photomosaic of cross section 9 east of cross section 1 showing the lateral pinch out of levee deposits associated with the main channel belt illustrated in Figure 30. Three parasequences are shown in the photomosaic (Parasequence 5b, 5a and 4, marked in red arrows). The top and base of Parasequence 5a (flooding surfaces) are drawn with blue solid lines. Detailed interpretations of facies-association composition are shown in the lower three photos. Levee facies were shaded in light yellow. Bayfill facies were shaded in grey. Notice the thinning of the levee deposits and corresponding thickening of the muddy, heterolithic bayfill deposits from west to east, which is illustrated schematically with a yellow dashed shazam line. See Figure 22C for the location of the cross section.

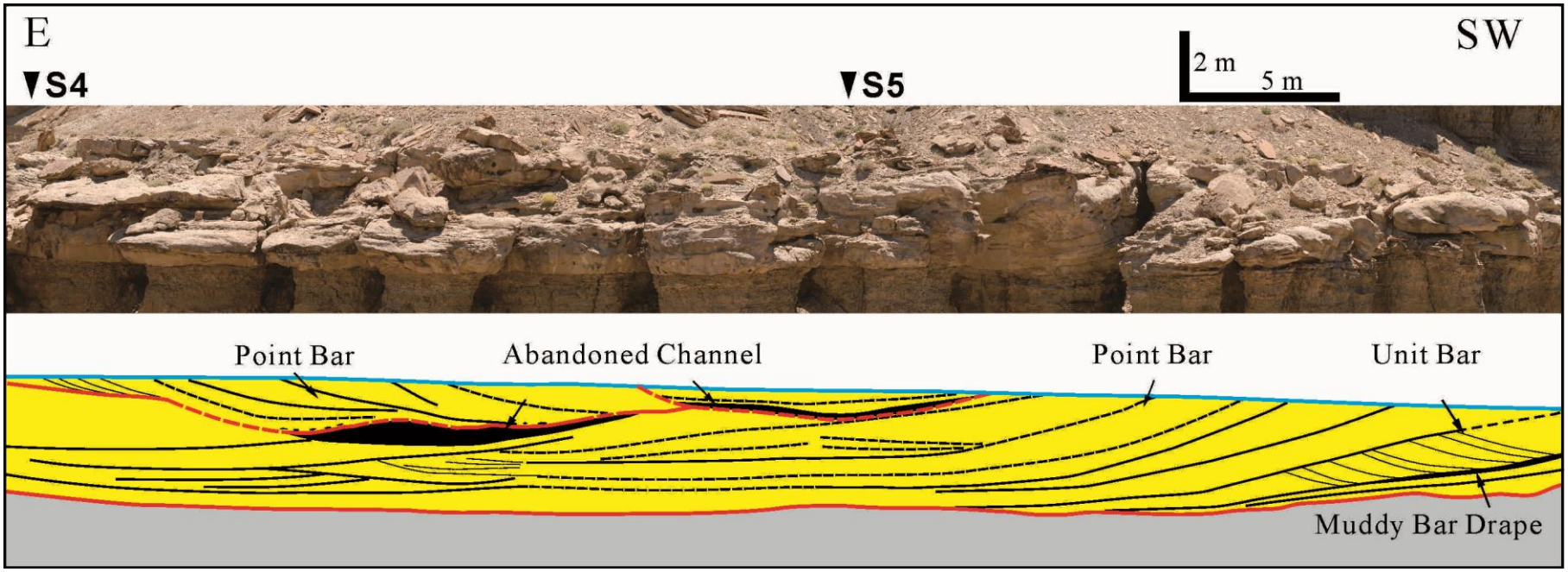

Figure 32. Photomosaic and bedding diagram of cross section 2, which cuts through the main channel belt in a general strike direction, showing the geometry, internal minor erosional surfaces and facies architecuture. Two storeys can be seen, with the lower channel storey filled with bars accreting toward the northeast. The left upper channel storey cuts into the lower storey and was filled with bars accreting toward the west. See Figure 22C for the location of the cross section.

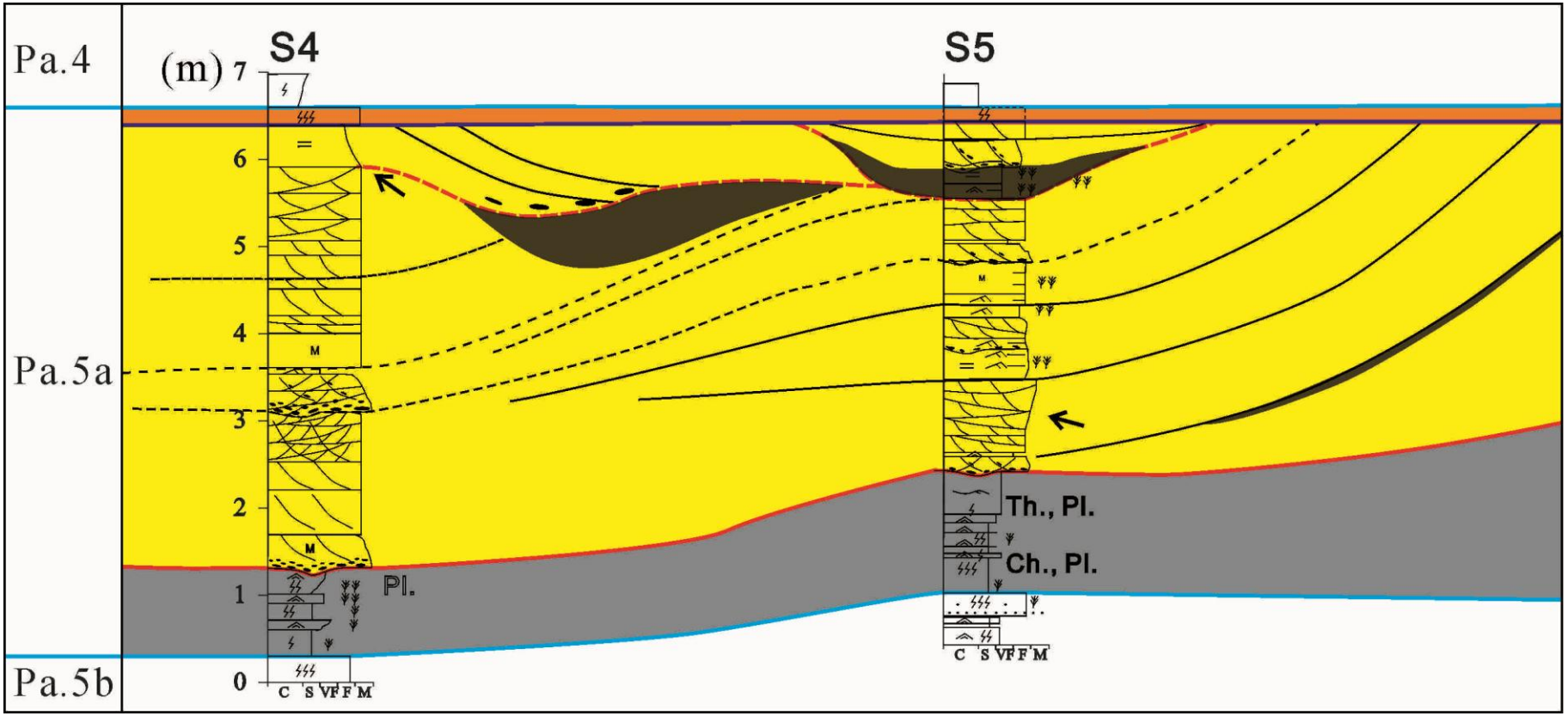

Figure 33. Correlation of measured sections showing facies and strata, bounding surfaces through cross section 2.

The lower storey is erosionally cut by the upper storey, which is filled with meter-scale cross beds, of FA1 which dip toward the west, opposite from the large inclined beds in the lower channel storey (Fig. 32). These meter-scale cross beds are internally composed of dune-scale cross beds and rippled beds. At the western end of the upper storey, a U-shaped channel form contains a lining mudstone which is overlain by some planar- and ripple-cross-laminated fine-grained sandstone (FA2) (Figs. 32 and 33). These strata onlap the channel form and passively filled it (Figs. 32 and 33). Paleocurrent directions are generally toward north and northwest (Figs. 22C and 33).

Interpretation: The channel belt is interpreted to have two channel storeys separated by the internal minor erosional surface. The lower storey is composed of eastward accreting point bars and the upper storey is composed of westward accreting point bars. Two mud plugs are interpreted to be abandoned channel deposits associated with these two channel storeys. The thin mudstone draping the point bars on the western side of the cross section is interpreted to be deposits formed during a waning river flood.

Cross section 3 (Figs. 34 and 35)

Description: Cross section 3 shows an oblique (SW-NE) view of the western side of the main channel belt (Fig. 22C). The northeast part of the channel belt is characterized by a few large inclined beds between sections 7 and 8, dipping northeast (Fig. 35). These large inclined beds are sometimes separated from each other by thin mudstone layers, which continuously drape the entire foreset of the macroforms (Fig. 35). A U-shaped channel form, at the top of section 7, is filled mostly with muddy heterolithic deposits of FA 2, which onlap the U-shaped channel form (Fig. 35). The

U-shaped channel form truncates adjacent strata from both sides and is not conformable with the accreting large inclined unit on the right. The southwestern part of the channel belt is characterized by multiple erosional surfaces (Fig. 34). A deep scour is obvious between section 8 and section 9, which almost cut through the whole sandbody. Internally, the northeastern part of the channel scour is filled with meter-scale cross-bedded sandstone, (FA1) with inclined beds dipping toward the south. Other parts of the channel scour are mostly filled with dune-scale cross beds with minor erosional surfaces. A U-shaped channel form is seen between Sections 9 and 10 and is filled with a meter thick carbonaceous silty mudstone (FA2), which is overlain by meter thick cross bedded sandstone (Figs. 34 and 35). The U-shaped channel form cuts into strata on the left and it is conformable with the strata on the right. The mudstone in the U-shaped channel form is overlain by some cross-bedded medium-grained sandstones.

Interpretation: The large inclined cross beds between Section 7 and 8 are interpreted to be point bars accreting toward northeast. The U-shaped channel form at Section 7 is interpreted to be a chute channel due to its lateral relationship with adjacent strata (Bridge 2006) The coarsening upward pattern as indicated by measured section 7 (Fig. 35), may indicate that the chute channel fill comprises mouth bars, deposited at the point where the chute channel becomes unconfined. Mudstones draping large inclined beds are interpreted to be deposited during inter-flood periods. Meter-scale cross beds are interpreted to be unit bars (Fig. 34). The U-shaped channel form on the southwest part of the channel belt, which is filled with mudstone overlain by cross bedded sandstone is interpreted to be the result of channel abandonment followed by river rejuvenation.

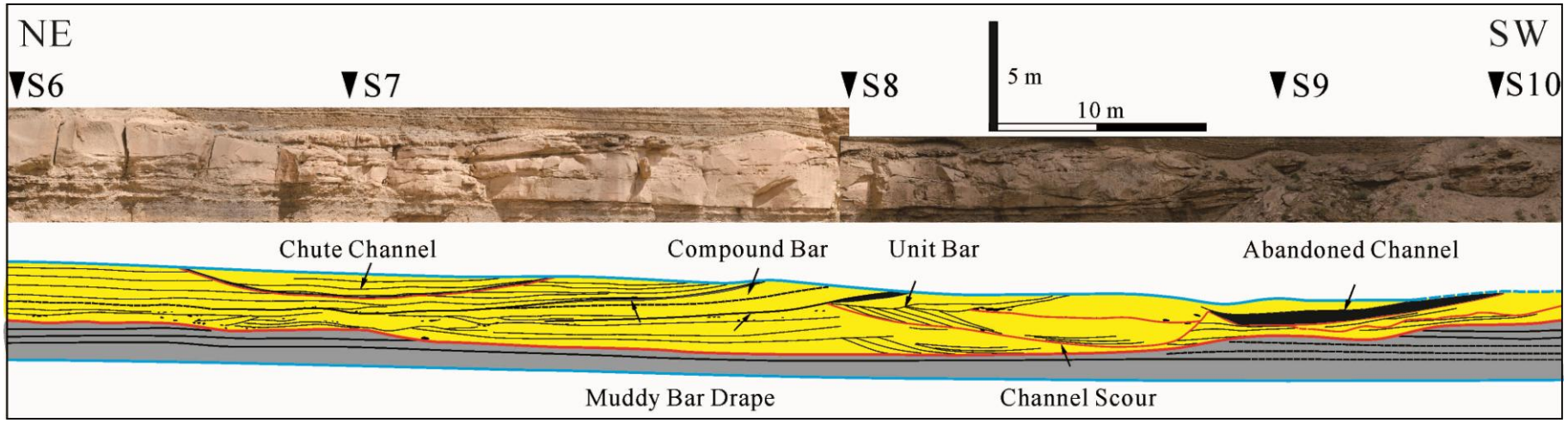

Figure 34. Photomosaic and bedding diagram of cross section 3, which cuts through the main channel belt in a general oblique direction, showing the geometry of the channel belt, internal minor erosional surfaces and facies architecture. The U-shaped concave-up erosional surface located at the upper left part of the channel belt is interpreted to be a chute channel. Bars generally accreting toward the north are present between section 7 and section 8. Multiple minor erosional surfaces can be seen in the southwestern part of the channel belt. See Figure 22C for the location of the cross section.

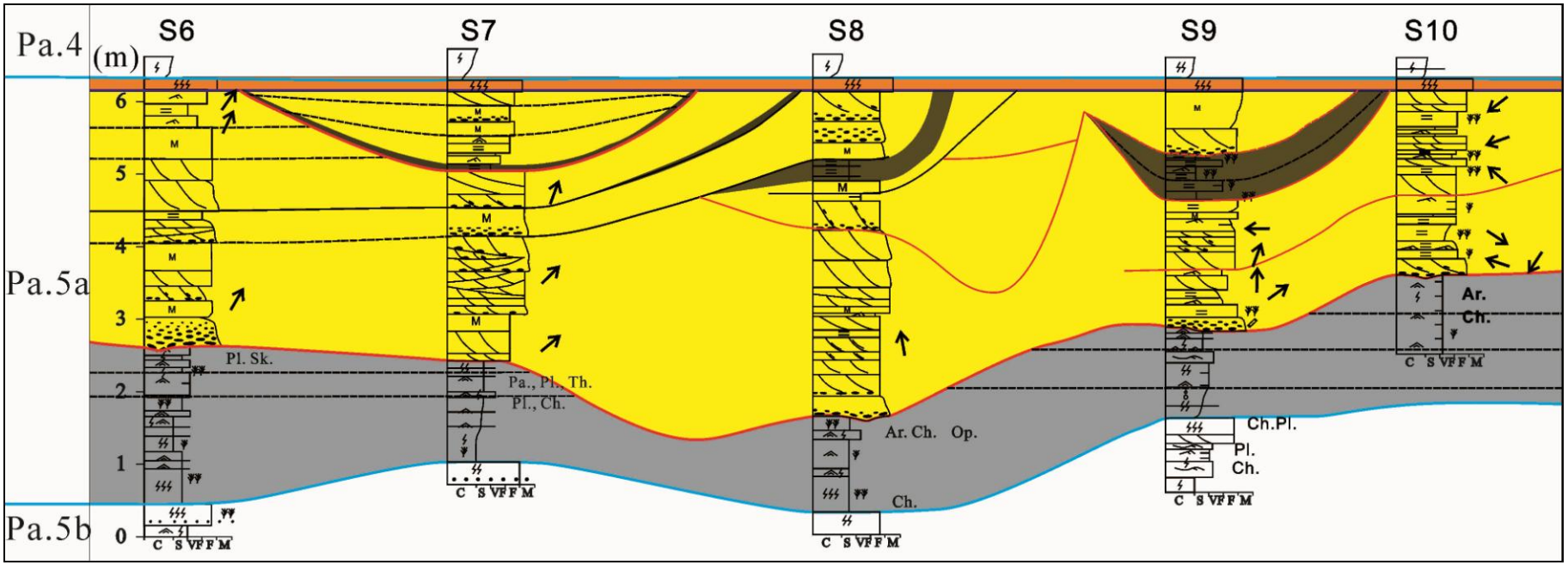

Figure 35. Correlation of measured sections showing facies and strata, bounding surfaces in cross section 3. See Figure 22C for the location of the cross section.

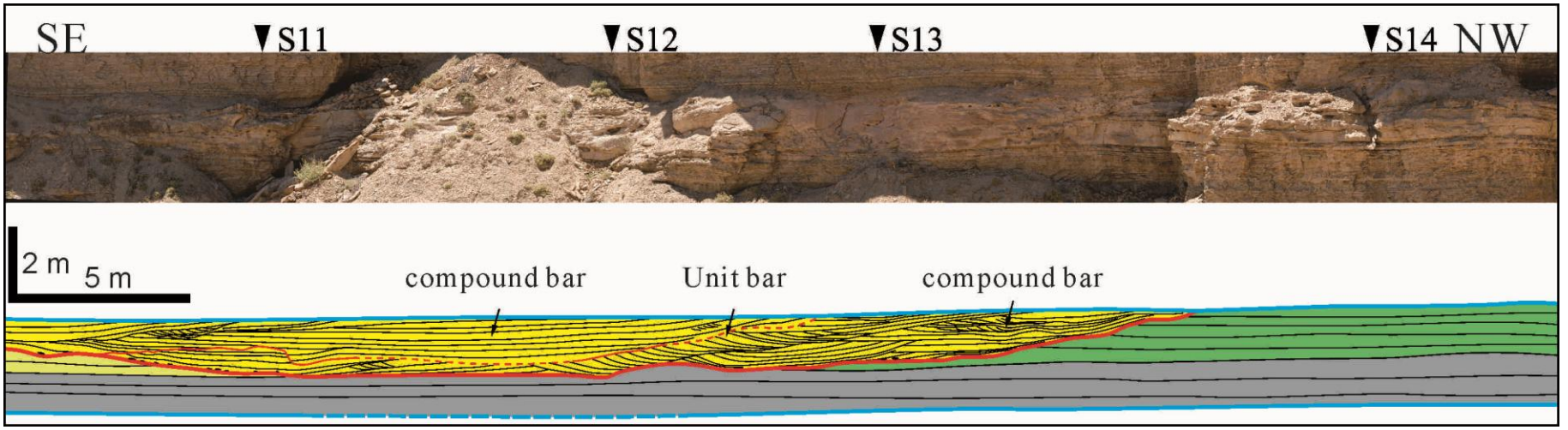

Figure 36. Photomosaic and bedding diagram of cross section 4, which cuts the main channel belt in a general strike direction on the western side, showing the geometry, internal erosional surface and facies architecture of this part of the main channel belt. See Figure 22C for the location of the cross section.

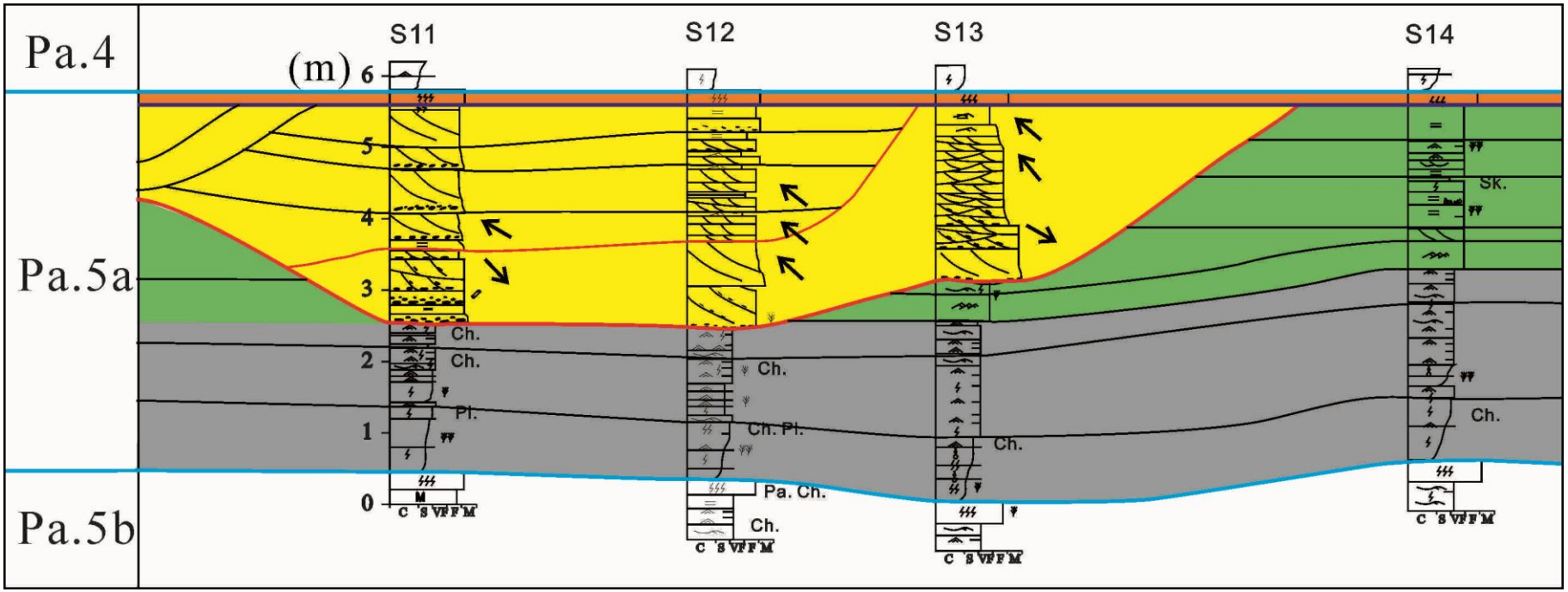

Figure 37. Correlation of measured sections showing facies and strata, bounding surfaces in cross section 4. See Figure 22C for the location of the cross section.

Cross section 4 (Figs. 36 and 37)

Description: Cross section 4 shows a more or less strike (SE-NW) view of the main channel belt (Fig. 22C). It shows the western margin and cut bank of the main channel belt and shallowing of the channel belt toward the east (Fig. 36). Internally, a minor erosional surface separates this part of the main channel belt into two different storeys, as shown in the bedding diagram (marked with a red line in Fig. 36) and in the correlated cross sections (Fig. 37). The lower storey is mainly preserved on the northwestern side of the channel belt. It is composed of meter-scale cross beds and large-scale inclined beds (FA1), which generally dip toward the west. The upper storey is composed of mostly dune-scale cross beds, with the larger scale bed set surfaces gently dipping toward the southeast (Fig. 36). The inclined beds in the lower storey are clearly truncated by the upper storey (Fig. 36).

Interpretation: The channel belt is composed of two storeys separated by the internal erosional surface. The lower storey is interpreted to be filled with compound bar deposits with a possible northwest accretion component. The upper storey is interpreted to comprise point bars with a southeast accretion component.

3.6.2 Main Channel Belt Exposed on the Northern Cliff

Cross section 5 (Figs. 38 and 39)

Description: cross section 5 shows a complete strike (W-E-S) view of the main channel belt (Fig. 22C). A complete U-shaped channel form can be seen, which defines the entire main channel belt. The western and eastern cut banks are respectively located at section 24 and the middle of section 31 and 32 (Figs. 22C, 38 and 39). It is thickest in its western part and thins toward the eastern margin.

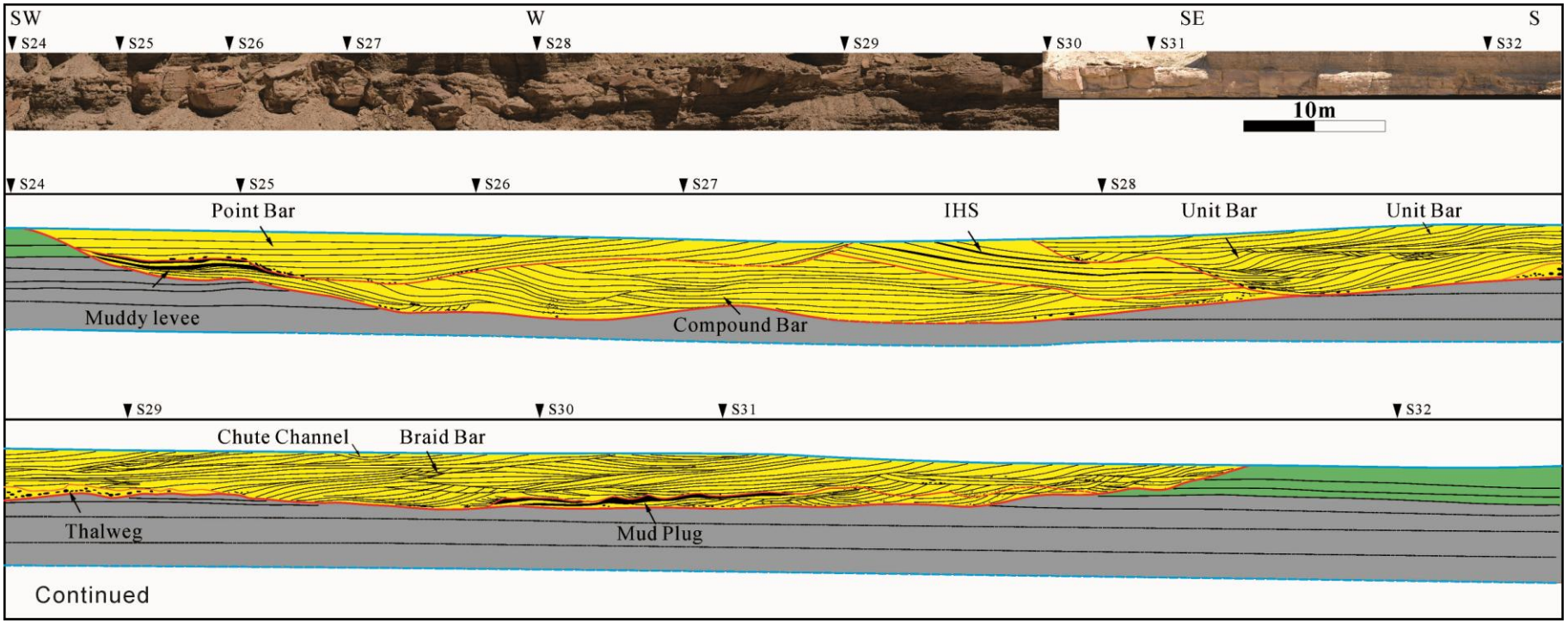

Figure 38. Photomosaic and bedding diagram of cross section 5, showing a general strike view of the main channel belt on the northern side of the gully. Detailed facies architecture is shown in the lower bedding diagram. The channel belt erosionally cuts into the underlying bayfill deposits and adjacent levee deposits. Internally, it shows a multi-lateral stacking pattern. See Figure 22C for the location of the cross section.

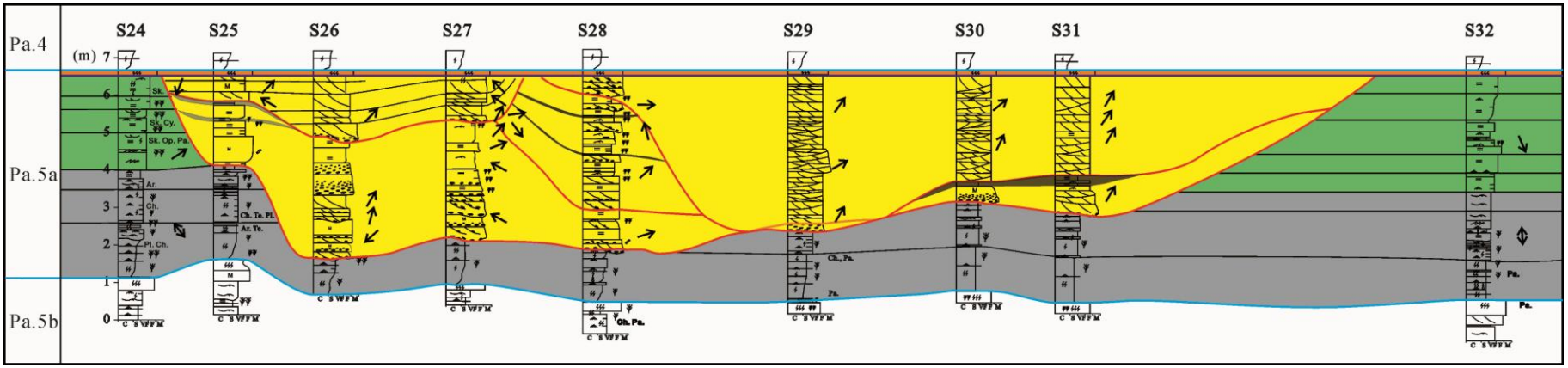

Figure 39. Correlation of measured sections showing facies and strata, bounding surfaces in cross section 5. See Figure 22C for the location of the cross section.

A U-shaped channel form (Fig. 38, from section 24 to section 27) truncates the strata below. There are abundant rip-up mud clasts above the basal erosional surface (Fig. 38). Internally, it is filled with large inclined beds accreting toward the west (Fig. 38). The apparent dip angles of these inclined beds decreases toward the west. Measured sections show that the decrease of dip angle is also associated with decreasing grain size (Fig. 39). This U-shaped channel form cuts into another storey below, which is composed of large inclined beds (FA1) accreting to the east on the western part and large-scale low angle beds on the eastern part (Fig. 39). The westernmost part of the lower channel belt is composed of heterolithic interbedded sandstone and mudstone (FA2). Between Sections 29 and 31, some eastward-dipping large inclined beds are bounded below and above by two erosional surfaces. They are muddy and heterolithic in their upper part and become uniformly sandy toward the channel base and east (Fig. 40). They form inclined heterolithic stratification (IHS). Another U-shaped channel form is observed from section 28 to the eastern cut bank of the main channel belt (Fig 38). At the western part of the channel form, between section 28 and section 29, it is filled with at least three storeys of meter-scale cross bedded sandstone (FA1). These meter-scale cross beds range from 1-2 m in thickness, and 1 to 10 m in width. They uniformly dip toward the west. At the top these large cross beds, some decimeter-scale scours are filled with trough cross-bedded medium-grained sandstone. To the east, between section 29 and 31, large inclined beds dipping in opposite directions show a mounded geometry and a bidirectional downlapping pattern (Fig. 38). Two mud plugs (FA2) are present in the channel belt deposit and are illustrated in the bedding diagram (Fig. 38) and correlation of measured sections (Fig. 39). They are both present at the base of an erosional surface the southern part of the channel belt.

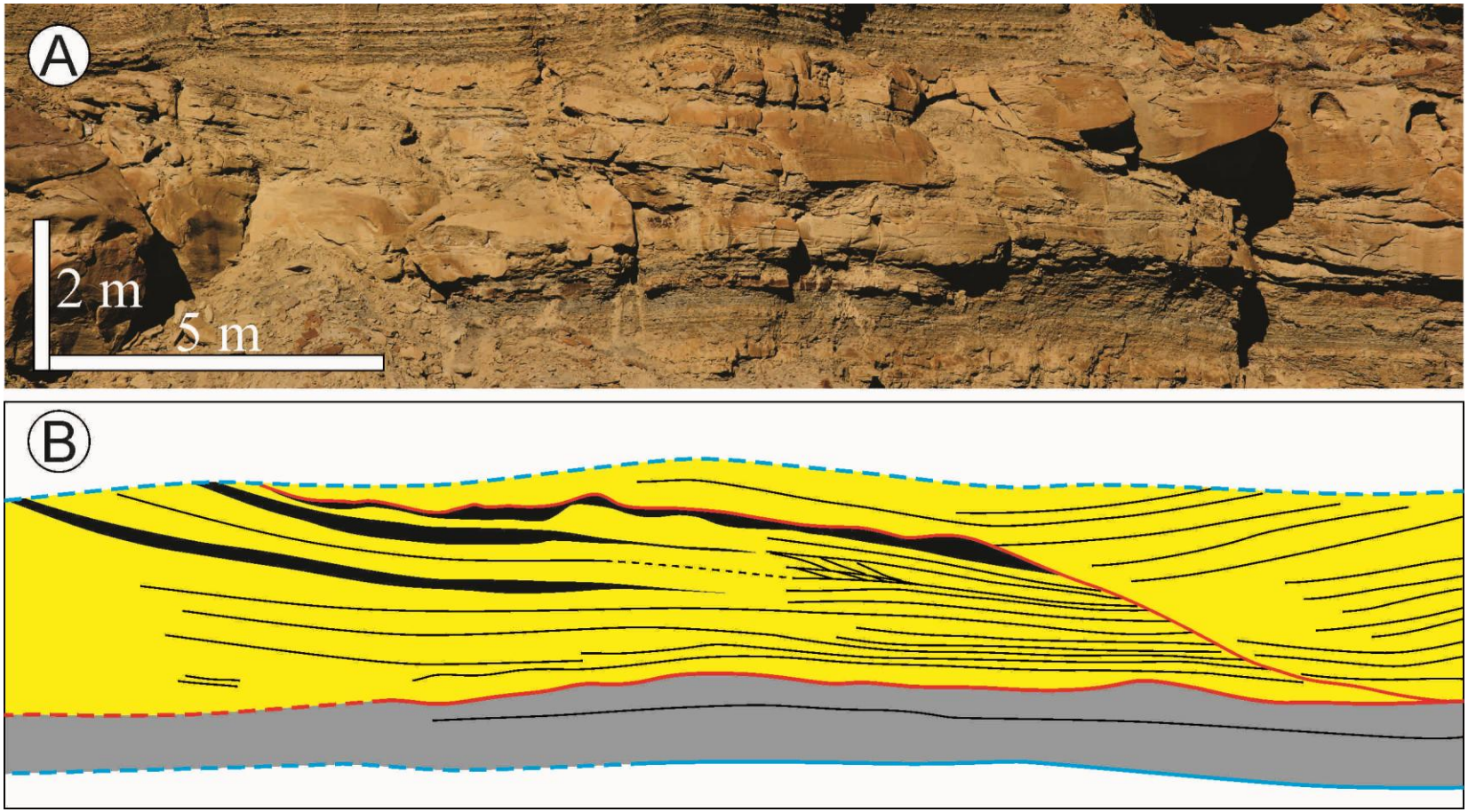

Figure 40. Inclined heterolithic strata in cross section 5 between section 22 and 23. A) Detailed photo of inclined heterolithic strata. B) Bedding diagram of photo A, showing the muddy strata dip half way down the channel depth and pinched out.

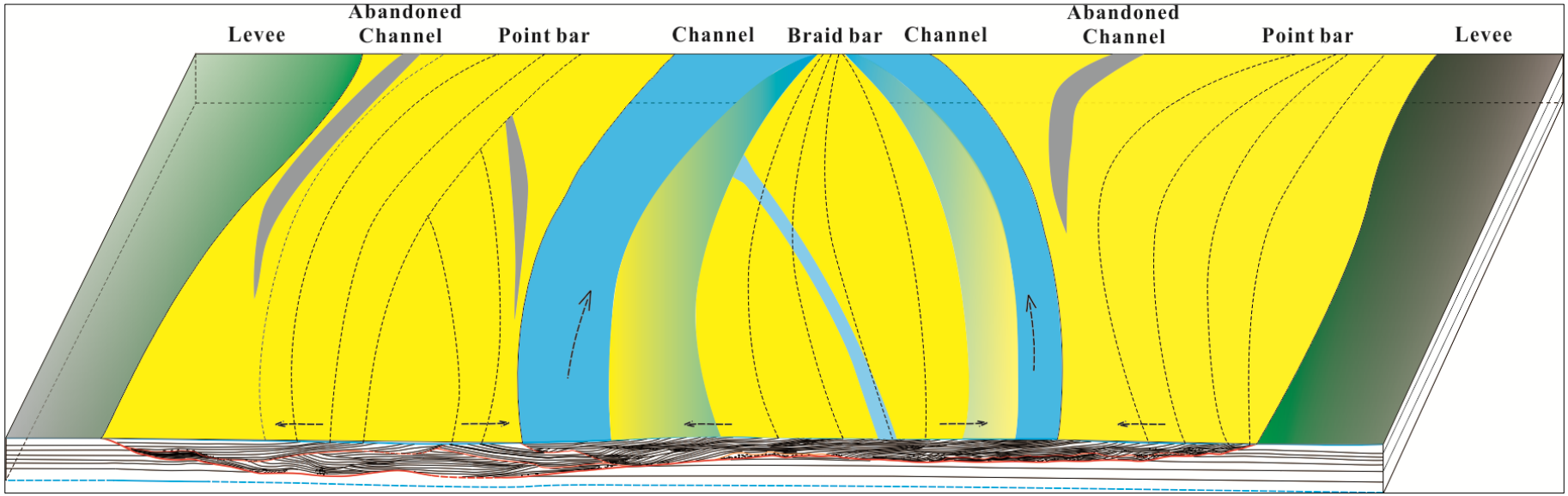

Figure 41. Block diagram of a paleogeographic reconstruction based on information from cross section 5. A braided river pattern is illustrated.

Interpretation: The large inclined beds preserved at the upper western part of the main channel belt are interpreted to be formed as a southwest accreting point bar (Fig. 38, from section 24 to section 27). The decrease of the apparent dip angles of these inclined beds toward the west and associated decrease in grain size (Fig. 39) indicates a gradual abandonment of the channel. The strata below this channel belt are interpreted to be compound bars with muddy levee deposits at the southwest wing of the sub-channel belt (Fig. 38). The inclined heterolithic beds between Sections 29 and 31 are similar to the IHS documented by Smith (1987), Jordan and Pryor (1992), and Corbeanu et al. (2004), and may indicate a tidally influenced meandering channel deposit. The meter-scale cross beds between Sections 28 and 29 are interpreted to be unit bars. The small scours cutting into the unit bars are interpreted to be low flow stage secondary channels (Bridge 2003; Bridge 2006). The inclined beds between Sections 29 and 31 are interpreted to be braid bar deposits based on their mounded geometry and bidirectional downlapping pattern (Bridge 2003; Adams and Bhattacharya 2005; Bridge 2006). In summary, the main channel belt downstream of the branching point shows a multistory and multi-lateral pattern. It is mainly composed of point bars accreting toward the west with local braid bars in the middle part, which indicates a dominantly meandering channel with local braided threads (Fig. 41).

3.6.3 Subordinate Channel Belt

Cross section 7 (Fig. 42)

Description: Cross section 7 shows an oblique (NW-SE) view of the subordinate channel belt looking upstream (Fig. 22C). A U-shaped channel form confines the channel belt. It erosionally cuts into muddy bayfill deposits below and adjacent levee facies. Hummocky and swaley cross-stratified sandstone is observed at Section 20. Loading structure can be seen in the thin sandstone layers below the channel belt. Internally, large-scale inclined beds dip uniformly toward the northwest, with the apparent dip angles decreasing with accretion of the beds (Fig. 42). The large inclined beds (FA1) are composed of mostly dune-scale cross beds and less abundant planar beds, rippled beds and massive sandstone (Fig. 43). The cross beds composing the large inclined beds may dip in a direction perpendicular to the large inclined beds. From the location of section 22 to the northwest cutbank, a U-shaped channel form can be seen, which is passively filled with muddy cross laminated sandstone and cross-bedded sandstone (FA2) (Figs. 42 and 43). A centimeter thick concave-up channel-lining mudstone drapes the channel form (Figs. 42 and 43). This channel form is conformable with the beds to the southeast and filled with relatively fine-grained sediment.

Interpretation: The geometry of the large inclined beds and their accretion pattern indicate that a meandering channel was gradually filled by lateral accretion of a point bar and temporarily abandoned and then reoccupied. The concave geometry of the inclined beds marks the start of abandonment. The hummocky and swaley cross stratified sandstone at Section 20 is interpreted to be shoreface deposits. The localized characteristic indicates that the shoreface deposits could be a minor wave-reworked

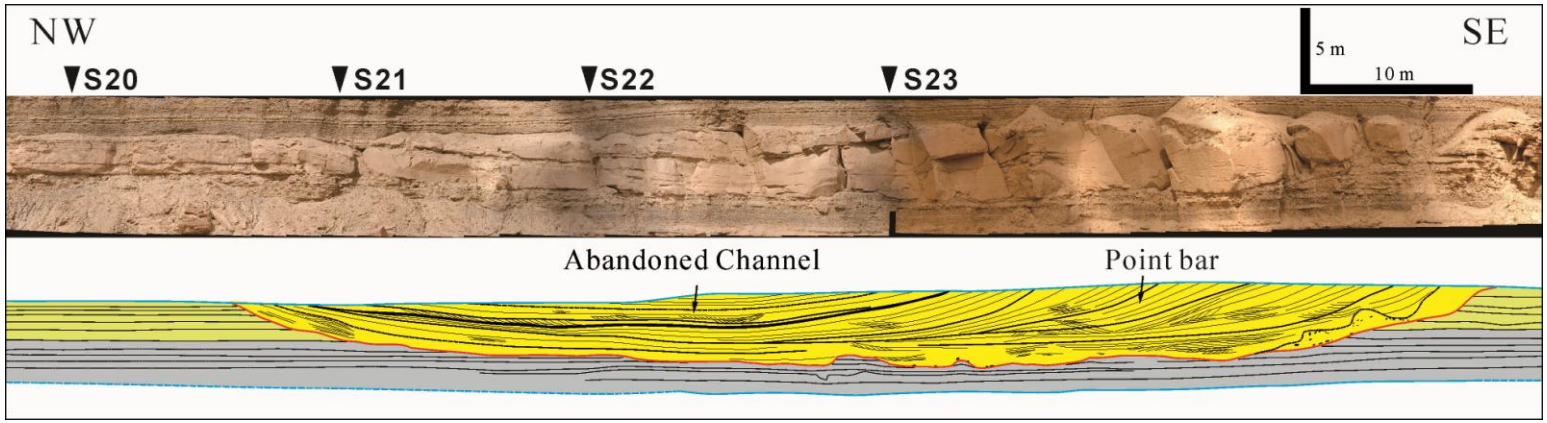

Figure 42. Photomosaic and bedding diagram of CS 7, which cuts through the subordinate channel belt in an oblique direction, showing the geometry of the channel belt and detailed facies architecture. Note the soft sediment deformation below the channel deposits. See Figure 22C for location of the cross section.

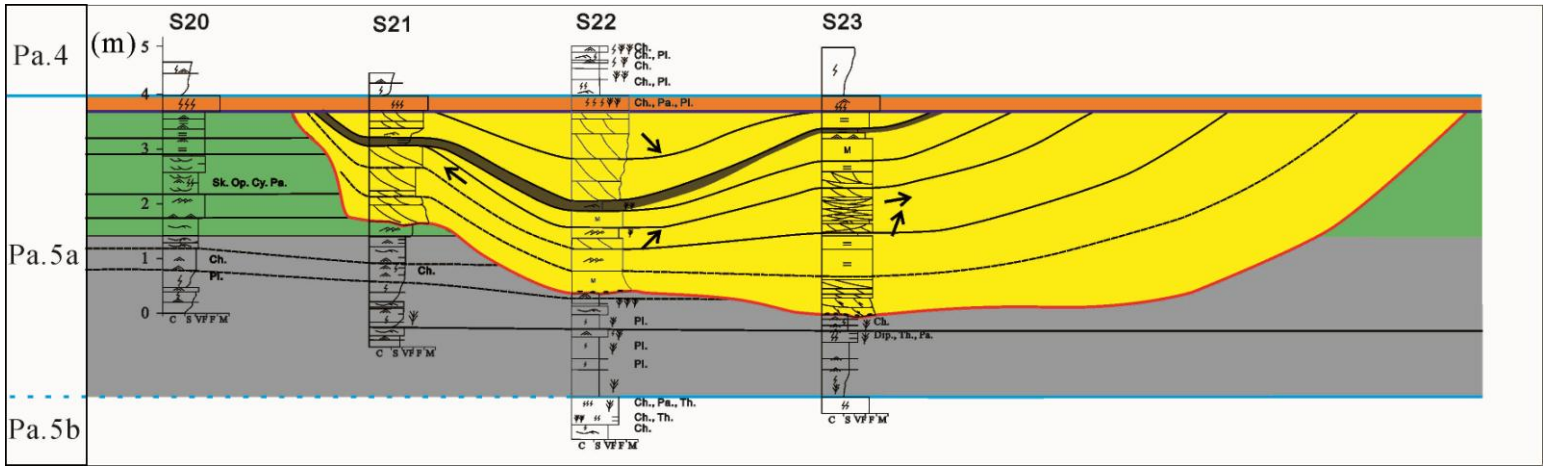

Figure 43. Correlation of measured sections showing facies and bounding surfaces along CS 7. See Figure 22C for the location of the cross section.

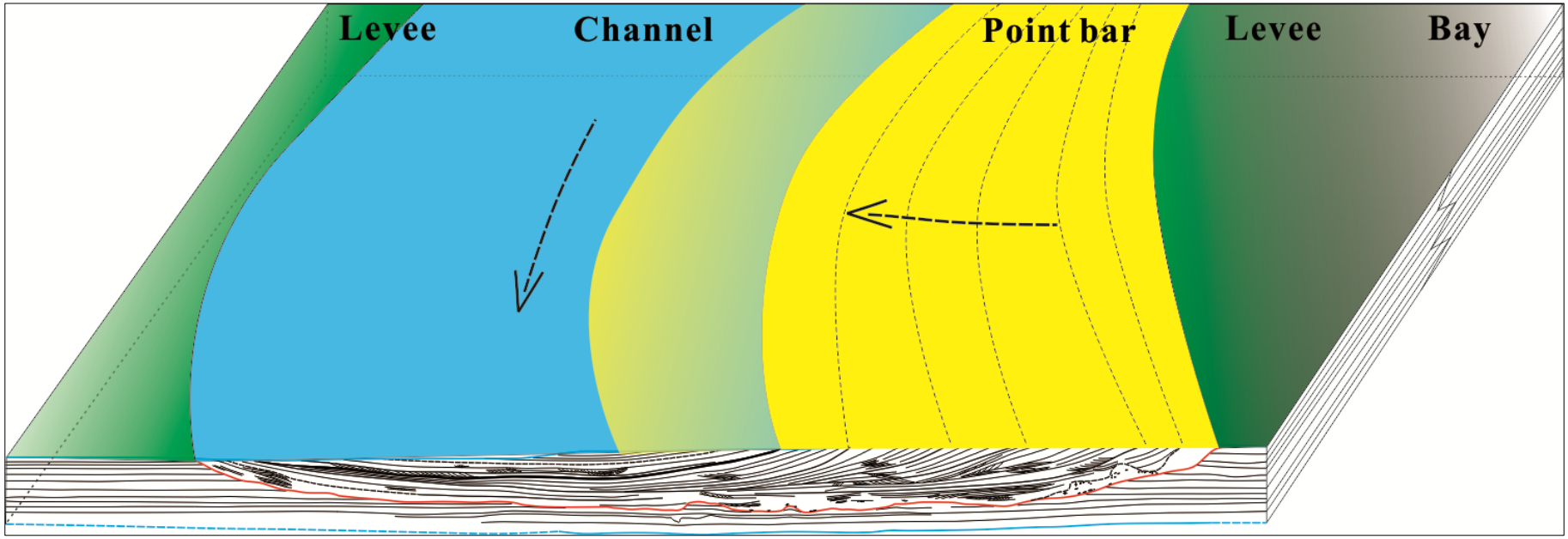

Figure 44. Block diagram showing a paleogeographic reconstruction based on cross section 7. A typical meandering river pattern is illustrated.

split, close to the shoreline of a semi-closed inter-distributary bay. The geometry of the large inclined beds and their accretion pattern indicate that a meandering channel was gradually filled by lateral accretion of a point bar and temporarily abandoned and then reoccupied (Fig. 43).

Cross section 6 (Fig. 45)

Description: Cross section 6 shows a generally strike (S-N) view of the subordinate channel belt looking downstream (Fig. 22C). It shows a U-shaped channel geometry (Fig. 45). The base of the channel belt is characterized by abundant rip-up mud-clasts. A minor erosional surface separates the channel belt into two storeys (Fig. 45). The major younger channel belt is also composed of large inclined beds dipping toward the north. The dip angle of the large inclined beds decreases with their lateral accretion (Fig. 45). At the northern part of the channel belt, inclined beds become concave upward. Cross beds are the major component of these large inclined beds (Fig. 45).

Interpretation: The subordinated channel belt is separated by the minor internal erosional surface into two channel belts. The geometry, facies association and lateral accretion pattern indicate that the major younger channel belt was gradually filled by lateral accretion of a point bar in accordance with the observation and interpretation from cross section 7.

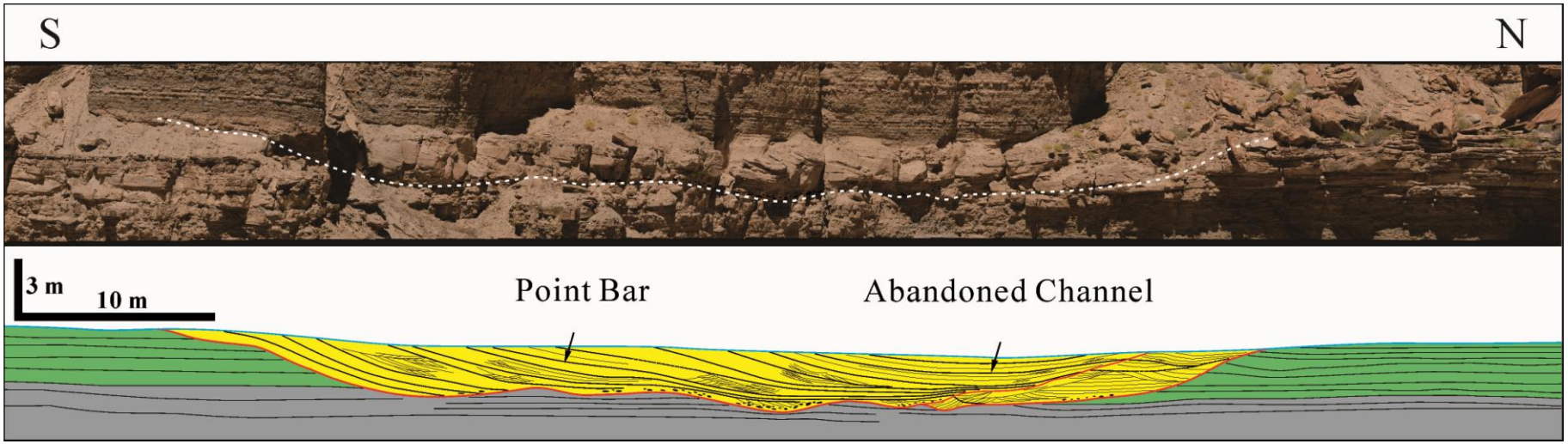

Figure 45. Photomosaic and detailed bedding diagram of cross section 6, which cuts through the subordinate channel belt in an oblique view, showing the geometry of the channel belt and internal facies organization. Large inclined surfaces dipping toward the north are interpreted to be lateral accretion of point bar deposits. See Figure 22C for the location of the cross section.

Cross section 8 (W-E) (Fig. 46)

Description: Cross section 8 shows a correlation of measured sections through the west of the subordinate channel belt described above (Fig. 22C). It shows a general coarsening upward succession (Fig. 46). A planar bedded and rippled sandstone on top of the cross section thins toward the west. Below the planar bedded sandstone, a wedge-shaped sandstone is composed of very fine-grained sandstone with current- and wave-ripple cross lamination, HCS, and planar beds and thin mudstones.

Interpretation: The top planar bedded sandstone is interpreted to be levee deposits and the wedge shaped sandstone with thin mudstone is interpreted to be crevasse splay deposits fed by the subordinate channel.

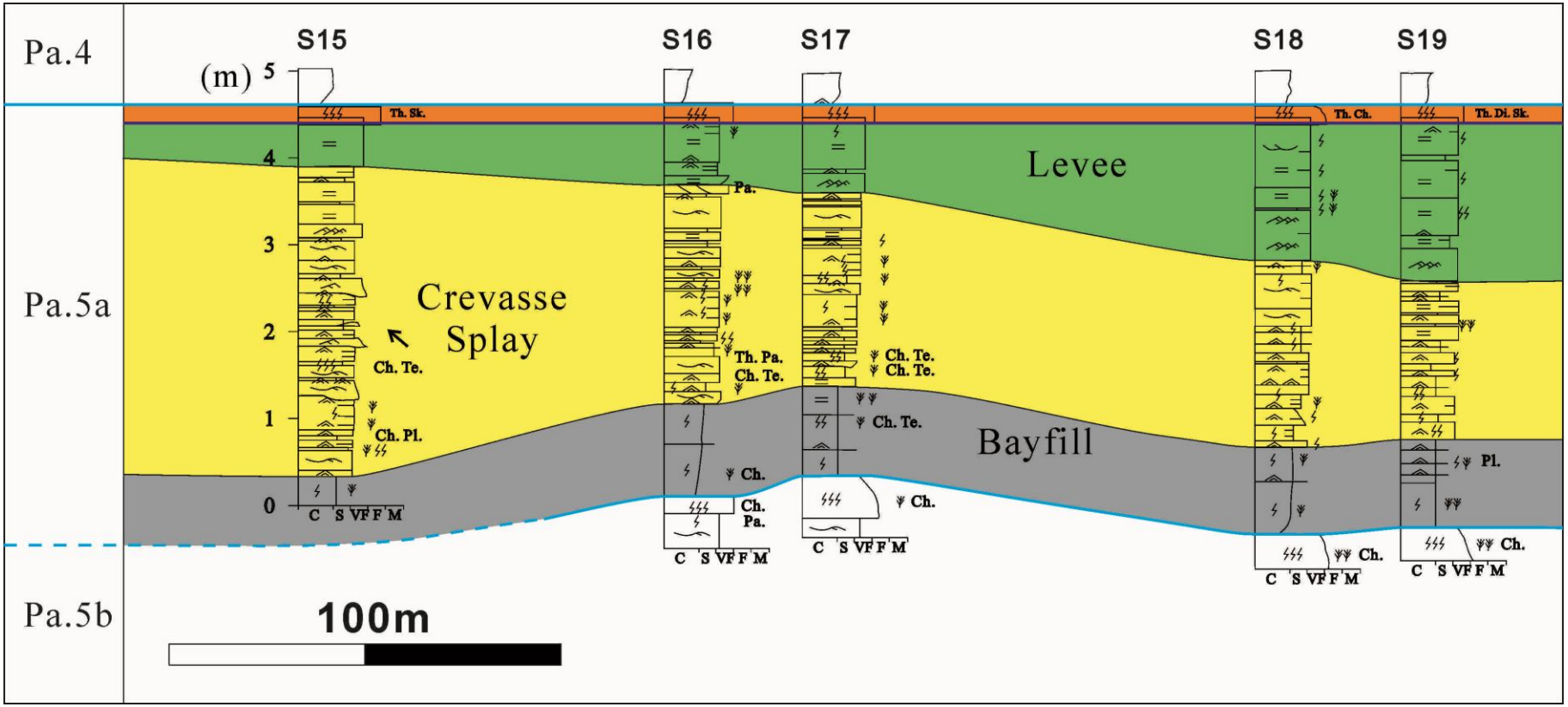

Figure 46. Correlation of measured sections of cross section 8 showing the facies and strata of crevasse splay and levee deposits to the west of the subordinate channel belt. It shows that the levee facies associated with the subordinate channel belt thins away from it. The thickening of the sandy facies toward the west is interpreted to have resulted from progradation of crevasse splay deposits. See Figure 22C for the location of the cross section.

3.7 Estimates of Channel Geometry and Water Discharge

The arrangement of the 2-D outcrop faces makes it possible to obtain accurate channel and channel belt dimensions as summarized in TABLE 3. The channel belt widths are estimated to be 250 m by correlating cut banks across the canyon and reconstructing the channel belt plan view and measuring the widths perpendicular to the channel belt axes. The subordinate channel belt is about 80 m in width. The channel belt thicknesses are observed from the measured sections through the sandbody and from photomosaics. Bar heights and widths are estimated from cross sections and detailed bedding diagrams (cross section 3 for main channel belt upstream of branching, cross section 2 for main channel belt downstream of branching and cross section 7 for the subordinate channel belt). When the channel belt is not cut in a strike view, for example the subordinate channel belt, apparent channel and bar dimensions are projected according to the channel axis to get the true widths. Formative channel widths are either estimated to be 1.5* the maximum bar width or completely preserved abandoned channel forms (Allen 1965). High-stage channel depth are estimated to be 1.25 * the maximum bar height (Bridge 2003). The values in TABLE 3 show that the channel belts and formative channel dimensions are generally larger for the main channel belt downstream of branching than the subordinate channel belt, indicating an uneven branching pattern.

The water discharge of rivers within each channel belt can be estimated with the method described by Bhattacharya and Tye (2004) and Bhattacharya and MacEachern (2009) with the following equation:

Q=65%*A*U

where A=average cross section area of the channel (width*depth), 65% is a coefficient for estimating the U-shaped channel geometry from a rectangle, and U=average velocity of the river.

Channel widths and depths are estimated as before and maximum values are used. For the average river velocity, the method of Rubin and McCulloch (1980) is used. Flow velocity for each channel belt is estimated based on grain size (medium-grained sand), bedform type (dunes) and water depths (Fig. 47). The result of estimated water discharges are summarized in TABLE 3.

The maximum water discharge for the main channel belt upstream of branching is estimated to be 70-130 m^3/s (TABLE 3). Mulder and Syvitski (1995) argued that rivers with an average discharge of less than 6000 m^3/s may produce hyperpycnal flows during large seasonal floods. Distributary channels feeding the Ferron Notom delta, which are close to the Sevier Orogen (c. 200-300 km) and draining a relatively small basin (Bhattacharya and Tye 2004) were probably small, sediment-rich, "dirty" rivers experiencing large seasonal floods (Bhattacharya and MacEachern 2009). Consequently, hyperpycnal flows have been hypothesized to be an important process in building the delta system in delta front and prodelta environments. Evidence of hyperpycnal flows has been documented in prodelta facies of Parasequence 6a of the Ferron Notom delta (Li 2009; Zhu 2010).

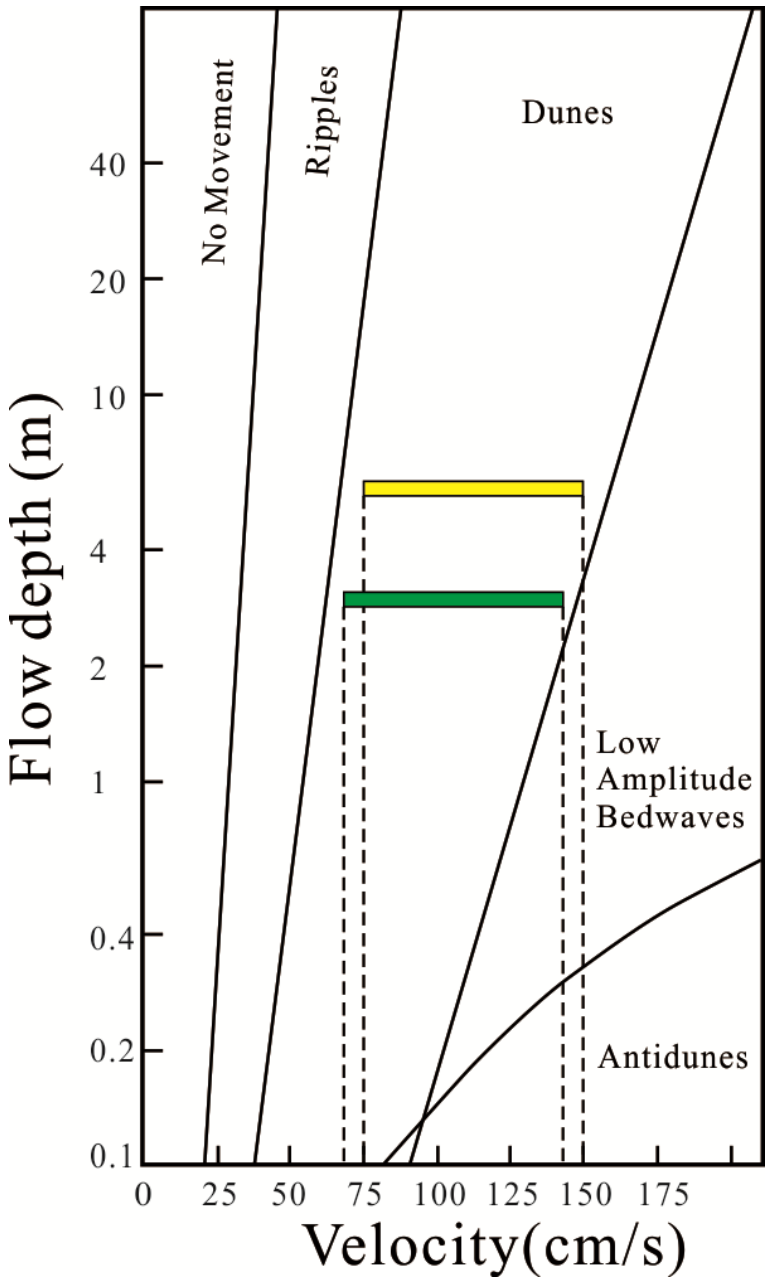

Figure 47. Velocity plot for different channel belts. Velocity for the main channel belt landward of bifurcation falls in the range of 750-150 cm/s (yellow bar); velocity plot for the subordinate channel falls in the range of 80-155 cm/s (green bar). Method from Bhattacharya and Tye (2004).

Li et al. (2010) estimated the maximum water discharge of the trunk channel of the Notom delta to be 1290 m^3/s from studying the fluvial system in Parasequence 3 of Sequence 1. Delta distributary networks are characterized by successive downstream bifurcations, which split the river discharge. Yalin (1992) suggested that with each bifurcation or avulsion the channel width and depth reduce as $B_{k+1} \approx 0.7 B_k$ and $h_{k+1} \approx 0.8 h_k$ respectively. Where B=channel width, h is channel depth and k is channel order (k=1 represents the trunk river before branching). Assuming the water velocity does not change during bifurcation, water discharge decreases by $Q_{k+1} \approx 0.56\ Q_k$. The order of the main channel belt in this study can be estimated by solving the following function $170 = 1290 * 0.56^{(k-1)}$, which gives the result that k lies between 3 and 4. Considering that the water velocity will probably decrease at each branching point, water discharge may decrease faster than that expressed in the equation. Consequently, the main channel belt upstream of the branching point is estimated to have been a 4^{th} order channel in the distributary channel system.

TABLE. 3—Summarization of channel belt and estimated channel dimensions and river velocity and water discharge

		Maximum Width (m)	Maximum Thickness (m)	Aspect ratio (width/thickness)	Maximum Bar height	Maximum Bar width	Channel width from maximum bar width or complete channel form (m)	Estimated high stage channel depth from maximum bar height(m)	Estimated peak river velocity（cm/s）	Estimated water discharge (m^3/s)
Main channel belt	Upstream of branching	250	5	50	4	24	~35	~5	~75-150	85-170
	Downstream of branching	200	5	40	4	20	~30	~5	~75-150	70-145
Subordinate channel belt		80	4	20	3.2	10	~20	~4	~65-140	30-70

3.8 Paleogeographic Reconstruction

Based on analysis of channel belt and channel and bar geometry, a paleogeography of the study area is reconstructed (Fig. 48). An asymmetrical branching pattern is indicated as a subordinated channel or relative smaller width branching away from the main channel. The dominant meandering fluvial pattern of the main channel belt is interpreted based on the observation that most of the macroforms dip in a uniform direction. The braided fluvial pattern is based on the observation of bi-directional downlapping bar deposits in the main channel belt. The meander loops are drawn according to the dip directions of the large inclined beds seen on the cross sections. The chute channel is drawn based on the chute channel recognized from cross section 3 (Fig. 34). Two abandoned channels are drawn to illustrate the abandoned channel facies. The fading green color illustrates the thinning of the levee deposits away from the channel belts and pinching out into bayfill deposits (Fig. 31).

The subordinate channel is interpreted to be a typical meandering channel. The crevasse splay facies are present northwest of the location of bifurcation. Paleocurrent directions, as indicated by current ripples in crevasse splay deposits, are to the northwest, which is in agreement with the trend of the subordinate channel. Due to the limitation of outcrop exposure, the dimensions of the crevasse splay deposits can not be accurately estimated. Consequently, the reconstruction of the crevasse splay is schematic. A localized wave-formed barrier spit (shoreface) is interpreted and illustrated in the paleogeographic reconstruction (Fig. 48).

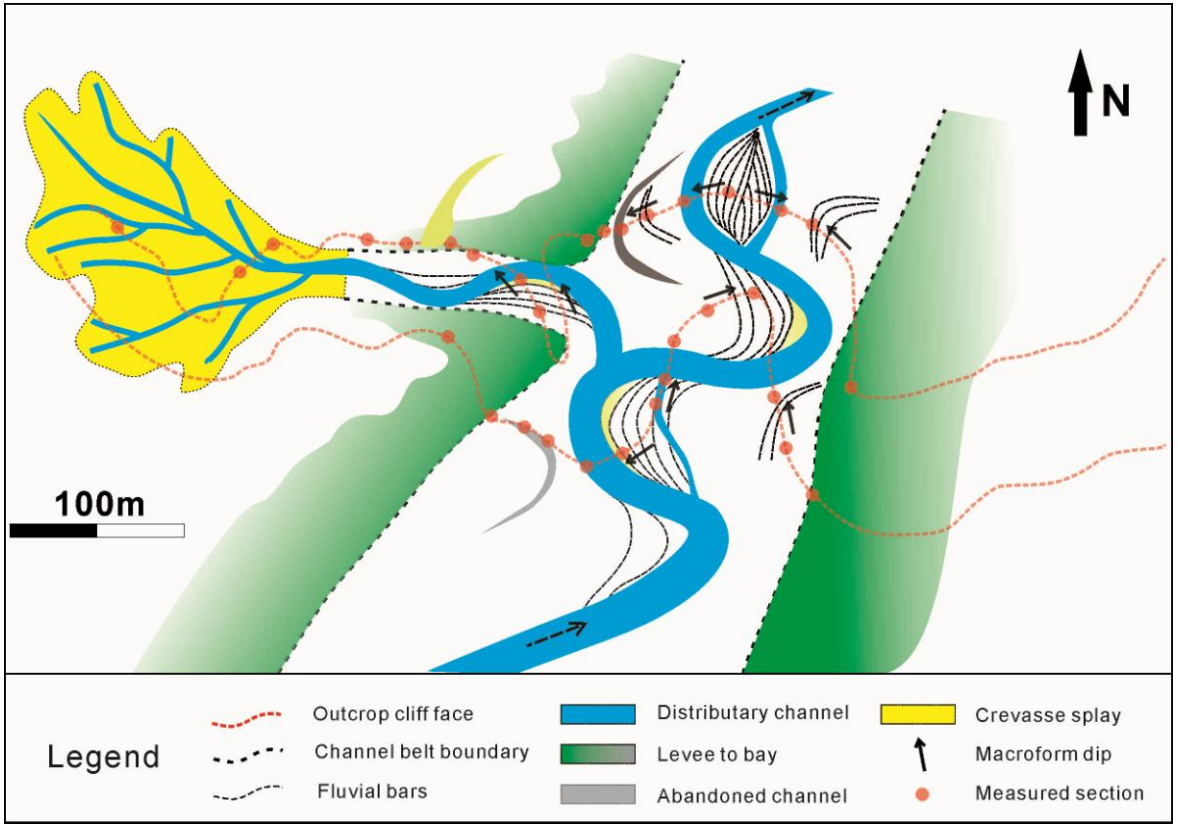

Figure 48. Paleogeographic reconstruction of the study area based on correlation of measured sections (Figs. 30, 33, 35, 37, 39, 43, and 46), detailed bedding diagram (Figs. 29, 31, 32, 34, 36, 38, 40, 42, and 45), facies interpretation (Figs. 23, 24, 25, and 26), paleocurrent information (Fig. 22C) and macroform dip information. Overall, it shows a distributary channel system with a crevasse splay associated with the subordinate branch of the distributary channel. A main channel belt flowed toward the north east with natural levees thinning away from the channel. The main channel was a meandering river with multiple chutes and a possible braided thread. Abandoned channels are common in the main channel belt.

3.9 Discussion

Deltaic distributary channel networks are built from two fundamental processes: avulsion and bifurcation around mouth bars (Olariu and Bhattacharya 2006; Jerolmack and Swenson 2007). Based on the discussion above, we argue that the branching documented in this study is a partial avulsion, in the sense of Slingerland (2004), instead of a bifurcation. Avulsion, versus bifurcation, is also thought to be more important in delta plain, versus terminal distributary channels. Studies of terminal distributary channels in the Ferron Notom delta (e.g. Garza, 2009; Zhu, 2010 and Ahmed, in review), suggest that bifurcation is the dominant process at the delta front.

Distributary channels on lower delta plains are traditionally regarded as characterized by straight streams (Coleman and Prior, 1982). The paleogeographic reconstruction of this study (Fig. 48) shows that the main channel belt is a dominantly meandering fluvial system with local braided threads and the subordinate channel belt is a meandering fluvial system. This indicates that the channel belt in question cannot be simply classified as a meandering fluvial system or braided system (Ethridge, 2010), but shows mainly point bars with subordinate braid bars.

The typical laterally accretion patterns documented in this study suggest that a certain amount of expansion and translation occurred during the evolution of these lower-delta-plain distributary channels. The width/thickness ratios of the distributary channel belts (20-50), however, are small compared to those typical fluvial systems (Reynold 1999; Gibling 2006). This suggests that these lower delta-plain distributary channels are short lived and relatively stable as indicated by Coleman and Prior

(1982), especially in comparison to the wider channel belts observed in the fully fluvial part of the Ferron Notom delta (Li et al. 2010).

Key heterogeneities include many of the elements described by Lynds and Hajek (2005) including abandoned channel deposits, channel-lining mudstone, and inclined heterolithic strata (Fig. 49). Other mudstone facies include channel-floor mud plugs, intra-channel levees, and mud-chip conglomerates (Fig. 49). Abandoned channel fills are common, although they typically contain both mudstone and sandstone and do not completely compartmentalize the channel belt within which they lie, both of which suggest gradual, versus abrupt abandonment. The dimensions of these mudstone facies are summarized in TABLE 4. The mudstone facies associated with these distributary channel belts are quite different from those seen in the purely fluvial parts of the Ferron Notom Delta. In particular, they lack coals, paleosols, and the organic-rich mudstones that are common in upper delta plain and floodplain environment. The bayfill facies resemble floodplain lake deposits, but are generally thicker and more laterally extensive.

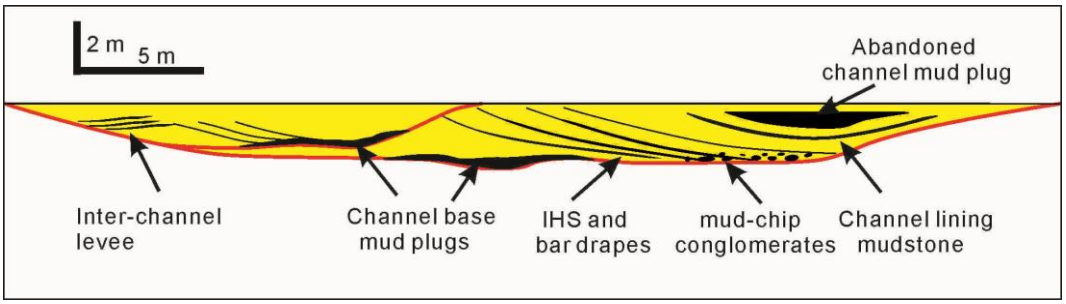

Figure 49. Schematic diagram showing muddy facies identified in the distributary channel belts.

TABLE 4. —Dimensions of mudstone facies

Mudstone facies	Width	Thickness
Muddy levees	10-20 m	5-20 cm
Channel floor mud plugs	10-30 m	10-30 cm
Inclined heterolithic strata	5-20 m	5-40 cm
Channel lining mudstone	20-30 m	10-15 cm
Abandoned channel deposits	20-25 m	50-100 cm

3.10 Conclusions

1) A lower delta-plain distributary system resulting from partial avulsion is documented using multiple 3-D outcrop exposures in an ancient deltaic depositional system. The main channel belt, upstream of avulsion, has an estimated discharge about 70-130 m^3/s. Based on empirical equations and previous study of the major fluvial rivers in the Ferron Notom delta, the channel in this study is estimated to be a 4^{th} order branch of the deltaic distributary network.
2) High resolution photomosaics, detailed bedding diagram, and cross sections of correlated measured section are made to illustrate internal facies architectures of distributary channel deposits and their associated levee, bayfill and crevasse splay deposits. Distributary channels are composed of mostly dune-scale cross beds and individual bedded unit bars, which may combine to form compound bars. Distributary channels cut into adjacent levee deposits and muddy bayfill deposits below. Levee deposits are composed of planer bedded and climbing rippled sandstone, which thin and pinch out away laterally from the channel over a distance of less than 200 m. Crevasse splay deposits are present where crevasse channels become unconfined. They are characterized by an upward coarsening pattern and are

composed of wave and current cross-laminated sandstone and locally hummocky cross-stratified sandstone.

3) This lower delta-plain distributary channel system is characterized by the presence of tidal signatures, sporadic marine burrowing in the channel, bayfill and crevasse splay deposits that are associated with the channels.
4) Based on the study of macroforms, the main distributary channel is reconstructed to be a dominantly meandering river with a locally braided reach. The avulsive channel is interpreted to be a typical meandering river. Significant expansion and translation may occur in lower-delta-plain distributary channels.
5) Lower delta-plain distributary channel deposits show four mudstone types, including abandoned channel deposits, muddy bar drapes, inclined heterolithic strata (IHS), and muddy levee deposits, which account for about 5% of the total channel deposits and form potential local barriers. Inclined heterolithic strata and muddy bar drapes are interpreted to be deposited in response to tidal processes in a lower delta-plain environment.

CHAPTER 4 Facies Architectural Study of River-dominated Mouth-Bar Deposits in a Crevasse Delta in the Cretaceous Ferron Notom Delta, South Central Utah

4.1 Introduction

Distributary mouth bars are an essential component in building a deltaic wedge (Wright 1977; Bhattacharya 2006; Gani and Bhattacharya 2007; Bhattacharya 2010). They form when a river enters a standing body of water and become unconfined, depositing sediments at the river mouth as a result of deconcentration of outflow momentum and loss of its competence to carry sediment (Bates 1953; Coleman and Prior 1982; Bhattacharya 2006). The external morphology and internal facies distribution largely depend on the density contrast between issuing and ambient water, water depth, bottom slope or the physical position of the delta and marine processes (Wright and Coleman 1974; Bhattacharya 2006; Bhattacharya 2010). In river-dominated environments, where marine influence (wave/tide) is lacking or weak (e.g. bayhead deltas, crevasse splays), three primary forces may dominant at the river mouth: 1) inertia and associated turbulent diffusion, which is favored by high outflow velocity, little or no density contrast between issuing and ambient water, and relative large water depth at the river mouth; 2) friction between the effluent and sea floor, which is favored by shallow water depths immediately seaward of the river mouth, and 3) buoyancy with a high water depth and high density contrast between issuing and ambient water (Wright 1977; Coleman and Prior 1982). Based mostly on modern

examples and theoretical concepts, Wright (1977) proposed models for mouth bars deposited under these three dominant effluent forces, showing that they are characterized by different morphology and lithofacies distribution patterns. Knowledge about the internal facies architecture, and heterogeneity of mouth-bar deposits, however, is lacking. Abundant modern case studies (Wright and Coleman 1974; Kostaschuk 1985; Fielding et al. 2005; Wellner et al. 2005; Fan et al. 2006), theoretical modeling (Edmonds and Slingerland 2007; Seybold et al. 2007; Dolgopolova and Mikhailov 2008; Hoyal and Sheets 2009) and flume studies (Hoyal et al. 2003) have contributed to our understanding of the processes of mouth-bar formation and their evolutionary patterns. However, detailed facies architectural and heterogeneity analysis of mouth-bar deposits is best be done with ancient deposits using extensive and laterally continuous outcrop exposures (Olariu and Bhattacharya 2006; Enge et al. 2010; Schomacker et al. 2010). Studies that relate facies architectural elements to different river effluent forces are rare (Martinsen 1990; Turner and Tester 2006; Ahmed et al. in review).

This chapter presents detailed facies architectural study of distributary mouth bars deposited in a river-dominated marine crevasse delta within the Cretaceous Ferron Sandstone in central Utah. This study is an attempt to show how river-mouth processes documented in modern examples can be explained by facies architecture documented with ancient examples.

4.2 Geological Setting

The Ferron Sandstone Member of the Mancos Shale Formation was formed as a result of the continued thrusting of the Sevier orogenic belt to the west and associated

subsidence of the Cordilleran foreland basin, as sediments were shed from the highland to the seaway eastward during Late Turonian (Hale 1972; Cotter 1975; DeCelles and Giles 1996) (Fig. 1A). Three fluvial-deltaic complexes were identified in the Ferron Sandstone, namely the “Last Chance”, “Notom”, and “Vernal” deltas, which prograded in a general east to northeast direction at the western margin of the Cretaceous Western Interior Seaway (Hale and Van De Graaff 1964; Hale 1972; Hill 1982) (Fig. 1B). This study focuses on the Notom Delta, which is well exposed in the north of the Henry Mountains in south central Utah (Fig. 50). A recent sequence stratigraphic study of the Notom Delta documented 6 sequences, 18 parasequence sets and 43 parasequences (Zhu et al. 2012) (Fig. 51). This study focuses on Parasequence set 6 in Sequence 2 (Fig. 51B). In Sequence 2, Parasequence set 6 (including Parasequence 6a, 6b and 6c) is characterized by a progradational and aggradational pattern, and forms a progradation-aggradation (PA) accommodation succession (Fig. 51A) (Li et al. 2011; Zhu et al. 2012). Parasequence set 7 below Parasequence set 6 shows a descending regressive nature of the shoreline and suggests deposition during a relative sea-level fall. Consequently, Parasequence set 7 is interpreted to be the falling stage systems tract of Sequence 2 showing a degradational accommodation succession (Fig. 51A). Parasequences set 5 and 4 above Parasequence set 6 show an aggradational and progradational stacking pattern and thus are interpreted to be the transgressive and highstand systems tract of Sequence 2 (Zhu et al. 2012). The landward part of Parasequence set 6 comprises an incised valley system (Li et al. 2010), and is interpreted to be the feeder for the seaward part of Parasequence set 6.

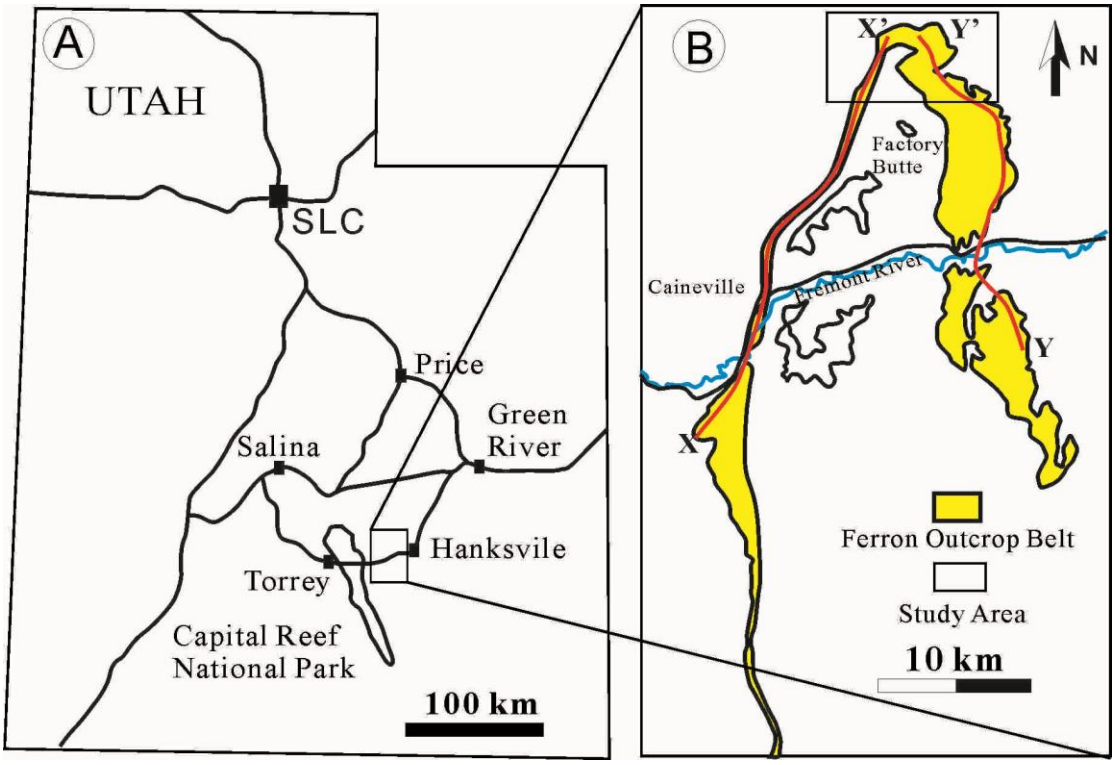

Figure 50. Basemap of the study area. A) Basemap showing Utah and the location of the Ferron Notom delta outcrop, which is marked with a black rectangle. B) Basemap showing the distribution of the Ferron Notom delta outcrop and the location of this study area, which is marked with a black rectangle. XX' and YY' mark the locations of cross sections shown in Figure 51.

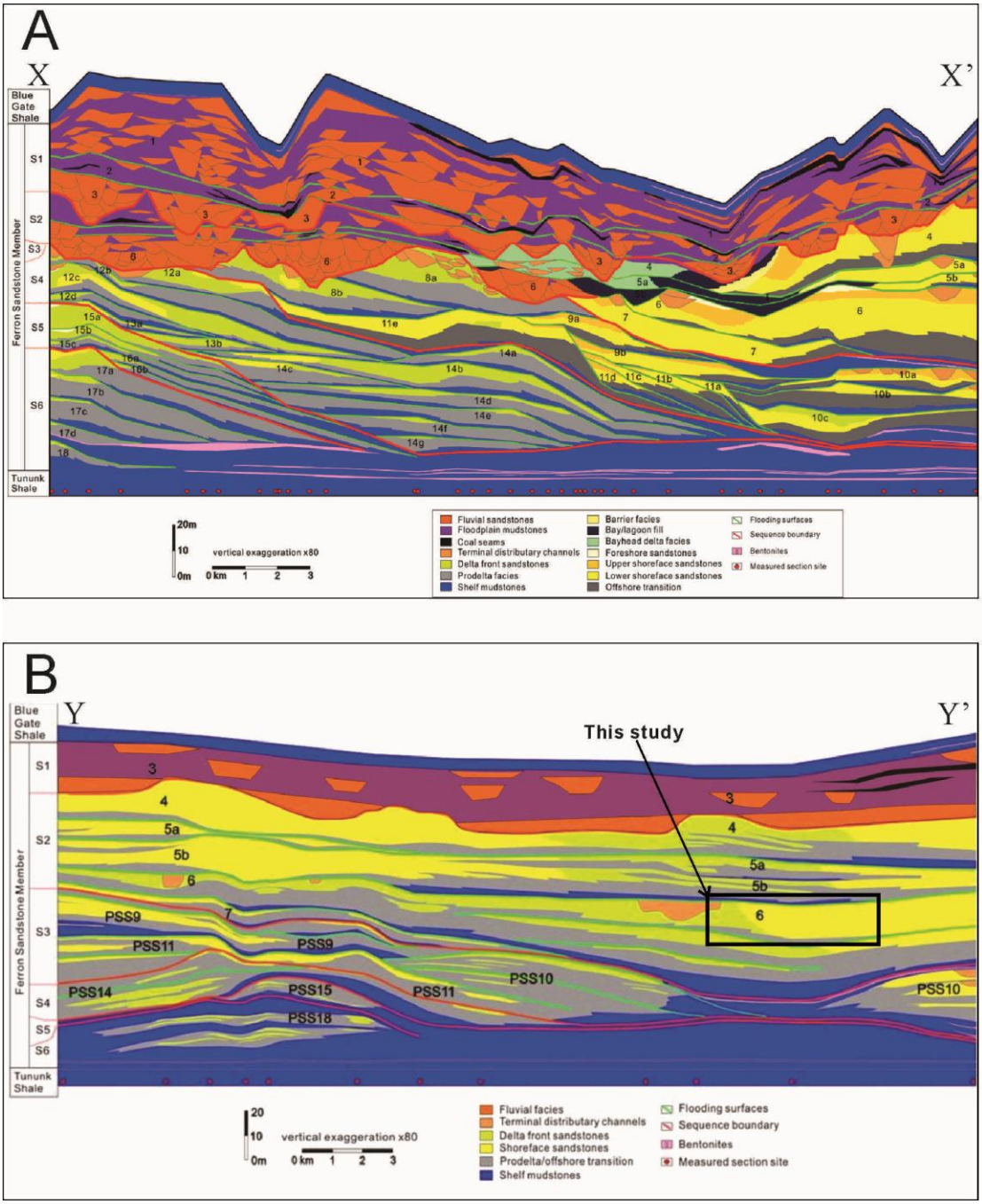

Figure 51. Cross sections showing the regional sequence stratigraphy of the Ferron Notom Delta. A) Oblique depositional dip sequence stratigraphy of the Notom Delta by Zhu, 2010, B) Oblique depositional strike sequence stratigraphy of the Notom delta by Li, 2009. Parasequence set 6 of Sequence 2, marked with a black rectangle, is the focus of this study. See Figure 50B for the locations of the two cross sections.

4.3 Previous Studies

Li et al. (2011) interpreted Parasequence 6a in Sequence 2 to be an asymmetrical delta, which is composed of a sandy shoreface on the updrift side with waves approaching the shoreline from the northeast producing northwest and southeast longshore currents. There are two problems with this interpretation. Firstly, the transition between the shoreface and the river-dominated delta front was not well elucidated due to sparse data collection. Secondly, the absence of muddy lagoonal and bayfill deposits which are commonly associated with downdrift side of modern asymmetrical deltas (Li et al. 2011), are not documented in the Notom Delta (Bhattacharya and Giosan 2003). An alternative interpretation of Parasequence 6a by Zhu (2010) with the same data set is that it is a river-dominated delta that prograded northeast into a semi-closed bay protected by a wave-dominated barrier system. The absence of muddy lagoonal and bayfill deposits in the delta is explained with this bayhead delta model. However, the facies architecture of the river-dominated delta and the transition between river-dominated delta and wave/storm-dominated shoreface have not been well documented. Garza (2010) and Ahmed et al. (in review) showed evidence of mouth-bar complexes that prograded toward the northwest to west in the river-dominated delta-front part of Parasequence 6a in the Coalmine Wash area, while the regional delta prograded northeast. Detailed facies architectural study of these mouth-bar deposits provides insights into their evolutionary patterns and depositional processes. Based on their accretion pattern or slope trajectory, unit bars are grouped into aggradational and progradational bar assemblages, which comprise bar complexes and finally build a delta lobe (Garza 2010). Two types of bars are recognized, including detached inertia-dominated bars which lie in the lower part of

the parasequence and are primarily composed of planar beds, and friction-dominated mouth bars which lie in the upper part of the parasequence and are mainly composed of dune-scale cross beds (Ahmed et al. in review). The upward change from inertia- to friction-dominated bars result from filling of accommodation and consequent decrease of water depth (Ahmed et al. in review). This paper presents an integration of previous work on Parasequence 6a and attempts to provide insights on the transition between the shoreface and river-dominated delta front and the relationship between the river-dominated mouth bars documented by Garza (2010) and Ahmed et al. (in review) and the regional delta.

4.4 Methodology and Data Set

This study will focus on the northern part of the Ferron outcrop belt close to Factory Butte northwest of Hanksville (Figs. 50 and 52).

Data used for this study were collected in the field by measuring detailed sedimentological sections, in which lithology, sedimentary structures, grain size, bed thickness, paleocurrent direction, and trace fossils were recorded. Gigapan hardware and software and telephoto zoom lenses were used to compose centimeter to a few millimeter resolution photomosaics, which were in turn used to make detailed bedding diagrams, illustrating internal bed geometry and facies architecture. Paleocurrent data measured from directions of cross stratification of angle of repose and “rib and furrow” structures were plotted on rose diagrams with a program named “Georient”. The dip information of clinoforms was recorded and plotted on Google Earth.

In total, 18 measured sections (Fig. 51), 9 photomosaics (Figs. 52B and 52C). 10 dips of mouth-bar clinoforms and about a thousand paleocurrent measurements were collected. Nine bedding diagrams and 2 correlated measured sections were made.

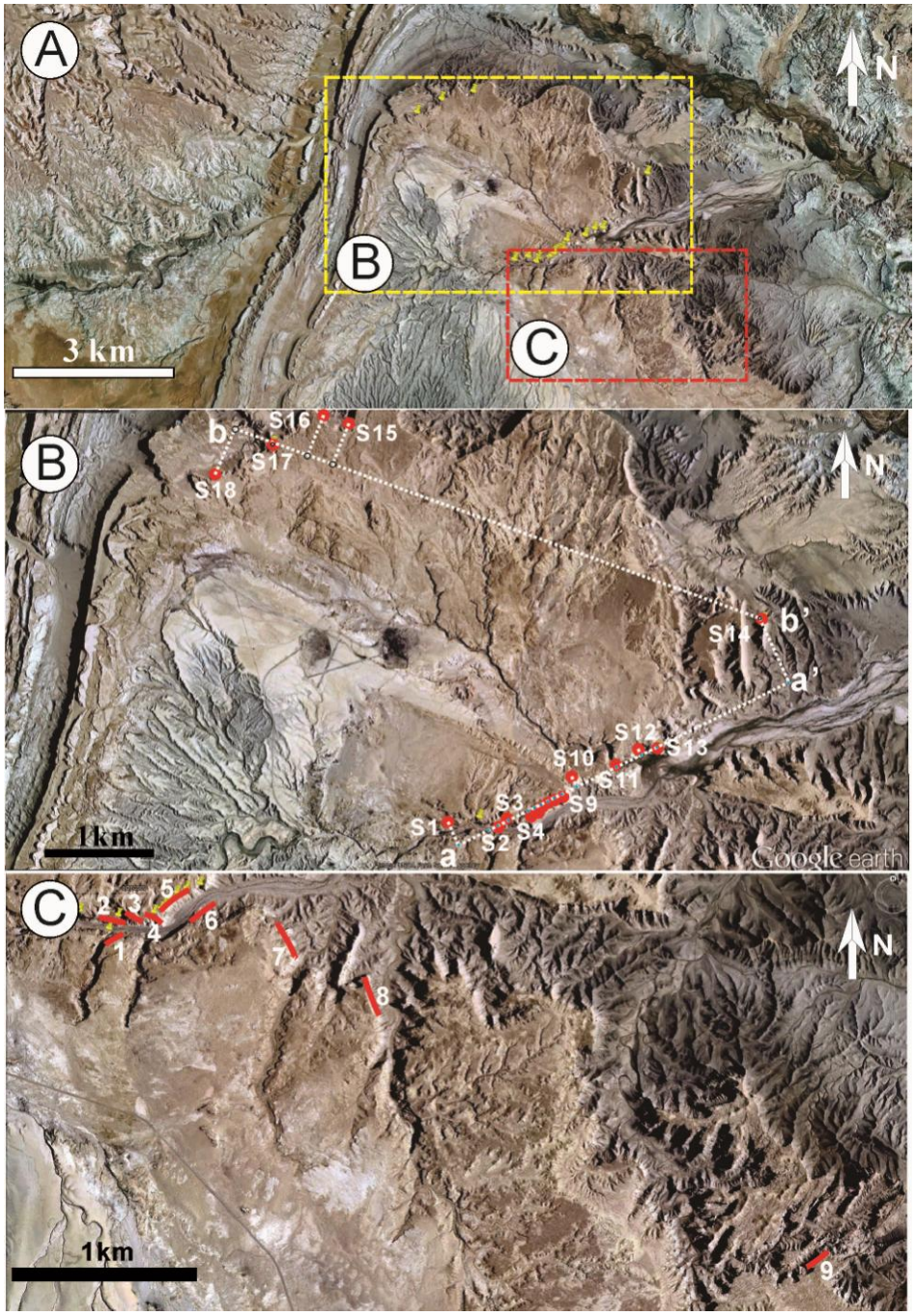

Figure 52. A) Google Earth image showing the study area. Yellow and red rectangles mark the locations of basemaps shown in Figures 52B and 52C respectively. B) Google Earth image showing the locations of measured sections and locations of cross sections a-a' and b-b'. Red dots indicate the locations of measured sections. See Figures 52A and 50 for the location of the basemap. C) Google Earth image showing the locations of photomosaics and bedding diagrams. Red lines mark the locations of photomosaics. See Figures 52A and 50 for the location of the basemap.

4.5 Facies Analysis

Parasequence 6a is about 20 m thick and is characterized by a general coarsening upward pattern (Figs. 53 and 54). Seven facies are identified in Parasequence 6a based on their lithology, sedimentary structures, ichnofacies, geometry, and vertical and lateral relationships. The fluvial dominated part includes prodelta, distal delta-front, proximal delta-front, and terminal distributary channel deposits (Figs. 53 and 54). The wave/storm-dominated part includes shelf, lower shoreface and upper shoreface. Proximal delta-front and terminal distributary channel facies are the focus of this study. Detailed analysis of other deltaic facies and shoreface deposits can be found in Garza (2010), Li et al. (2011), and Ahmed et al. (in review).

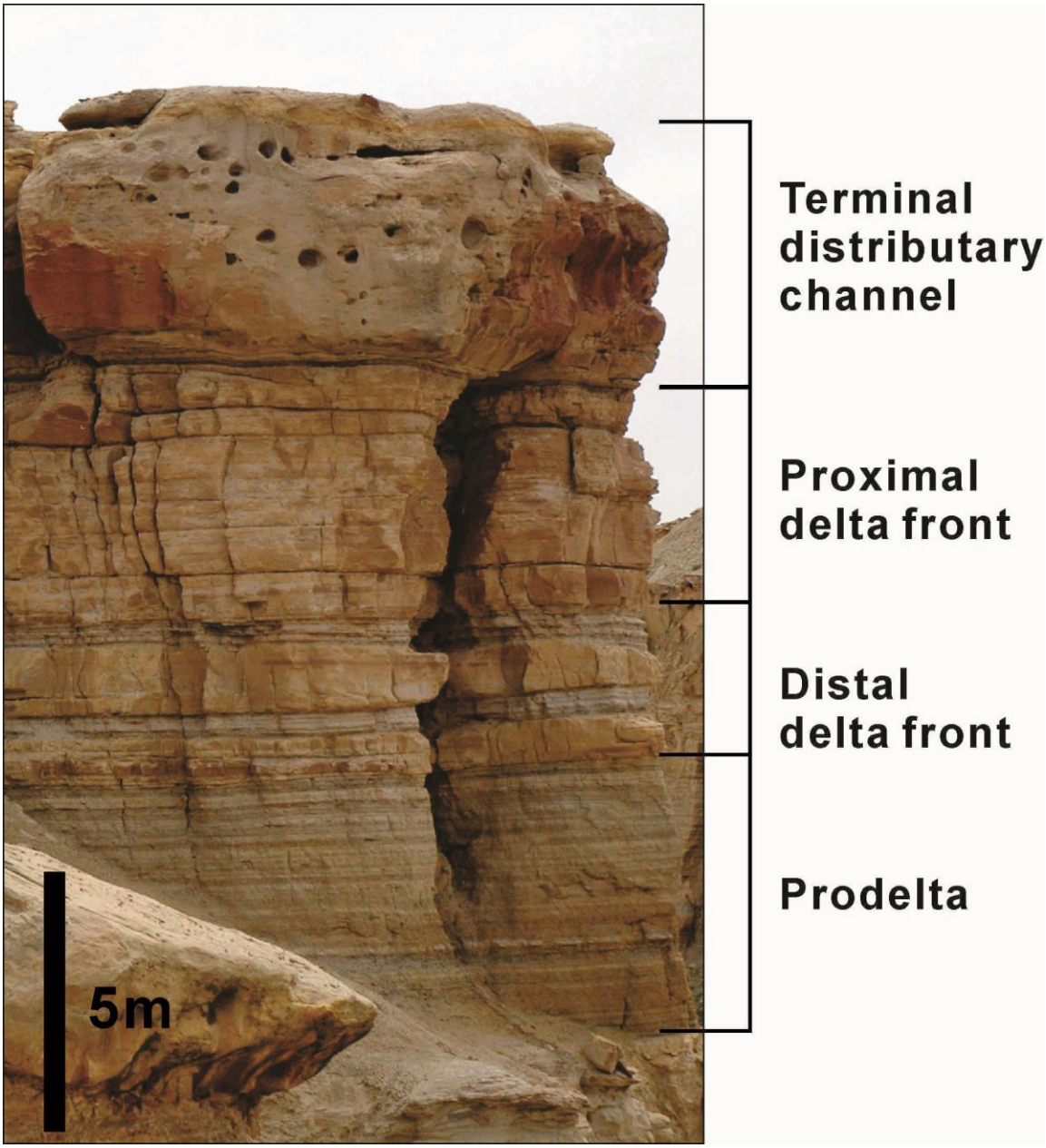

Figure 53. Photo showing a complete vertical section of the river-dominated part of Parasequence 6a. A general coarsening upward trend can be seen. It is subdivided into four facies from base to top: muddy prodelta, heterolithic distal delta-front, sandy proximal delta-front and terminal distributary channel deposits.

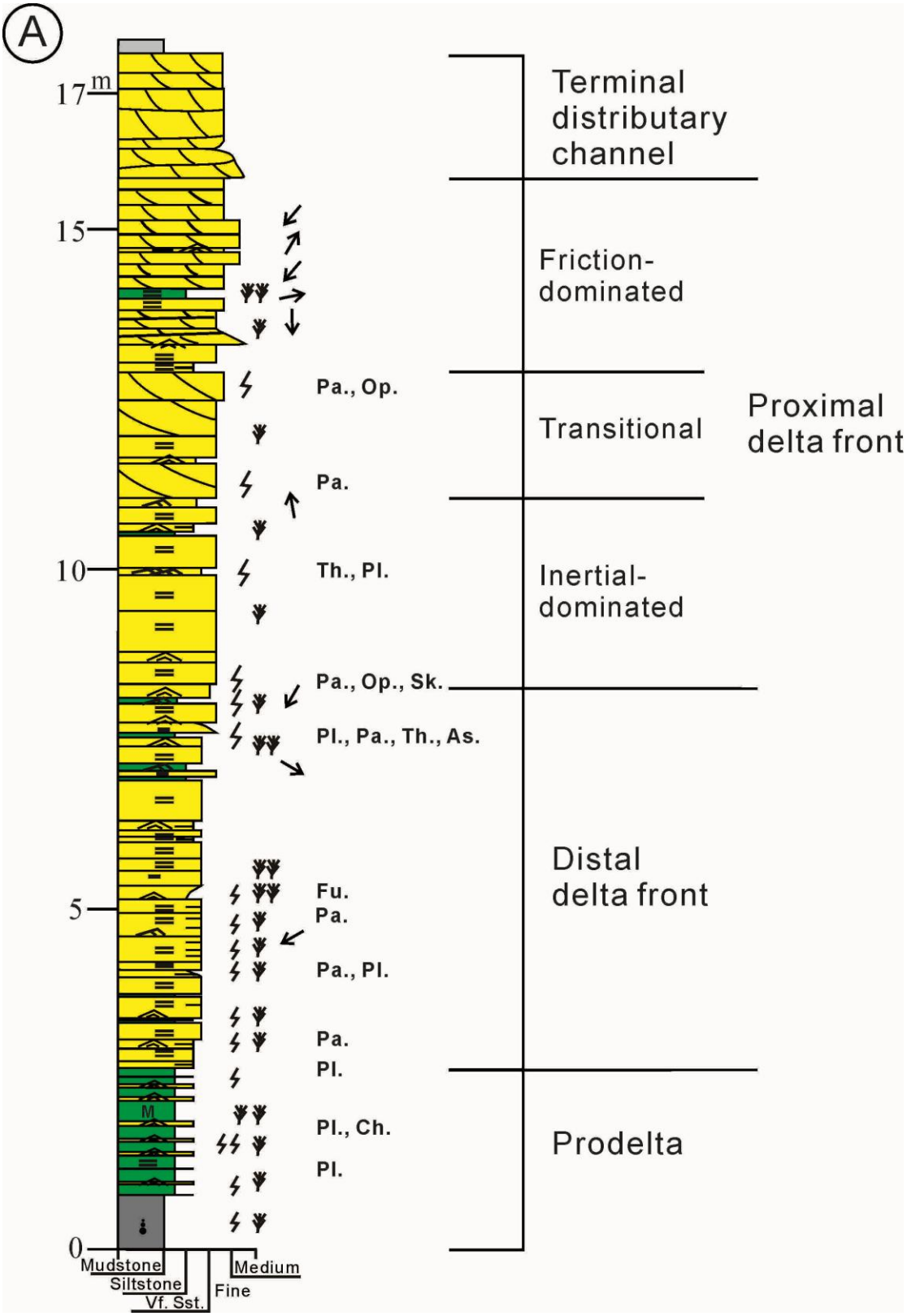
A
17 m
15
10
5
0
Pa., Op.
Pa.
Th., Pl.
Pa., Op., Sk.
Pl., Pa., Th., As.
Fu.
Pa.
Pa., Pl.
Pa.
Pl.
Pl., Ch.
Pl.
M
Terminal distributary channel
Friction-dominated
Transitional
Proximal delta front
Inertial-dominated
Distal delta front
Prodelta
Mudstone
Siltstone
Vf. Sst.
Fine
Medium

Figure 54. A) A type measured section in the river-dominated delta showing the detailed facies. The whole section is divided into four facies including: prodelta, distal delta front, proximal delta front and terminal distributary channel. The proximal delta-front facies is subdivided into inertia-dominated, transitional and friction-dominated facies. B) Legend for the measured sections shown in Figure 54A. The same legend is used for the following sections in this chapter.

4.5.1 Prodelta

Description: Prodelta facies are present at the basal part of the coarsening upward succession in Parasequence 6a. They are mostly composed of laminated mudstone and siltstone with occasional interbedded thin layers of laminated very fine-grained sandstone (Figs. 54 and 55A). Mudstones can be massive or graded. Normal grading is very common with laminated muddy siltstone grading upward into massive mudstone (Fig. 55B). Some of the normally graded successions are characterized by an erosional base which cuts into the mudstone below (Fig. 55B). Inverse grading is not as common as normal grading, but when present, is mostly associated with normal grading above with either an erosional or conformable 54oundary (Fig. 55A). Dewatering cracks are seen locally in the mudstone (Fig. 55C). The mudstone is generally lightly bioturbated (BI of 0-2) with some beds showing intense bioturbation (Fig. 55D). Carbonaceous material is abundant (Fig. 54A). Thin layers of sandstone are mostly wave-cross laminated (Fig. 55B).

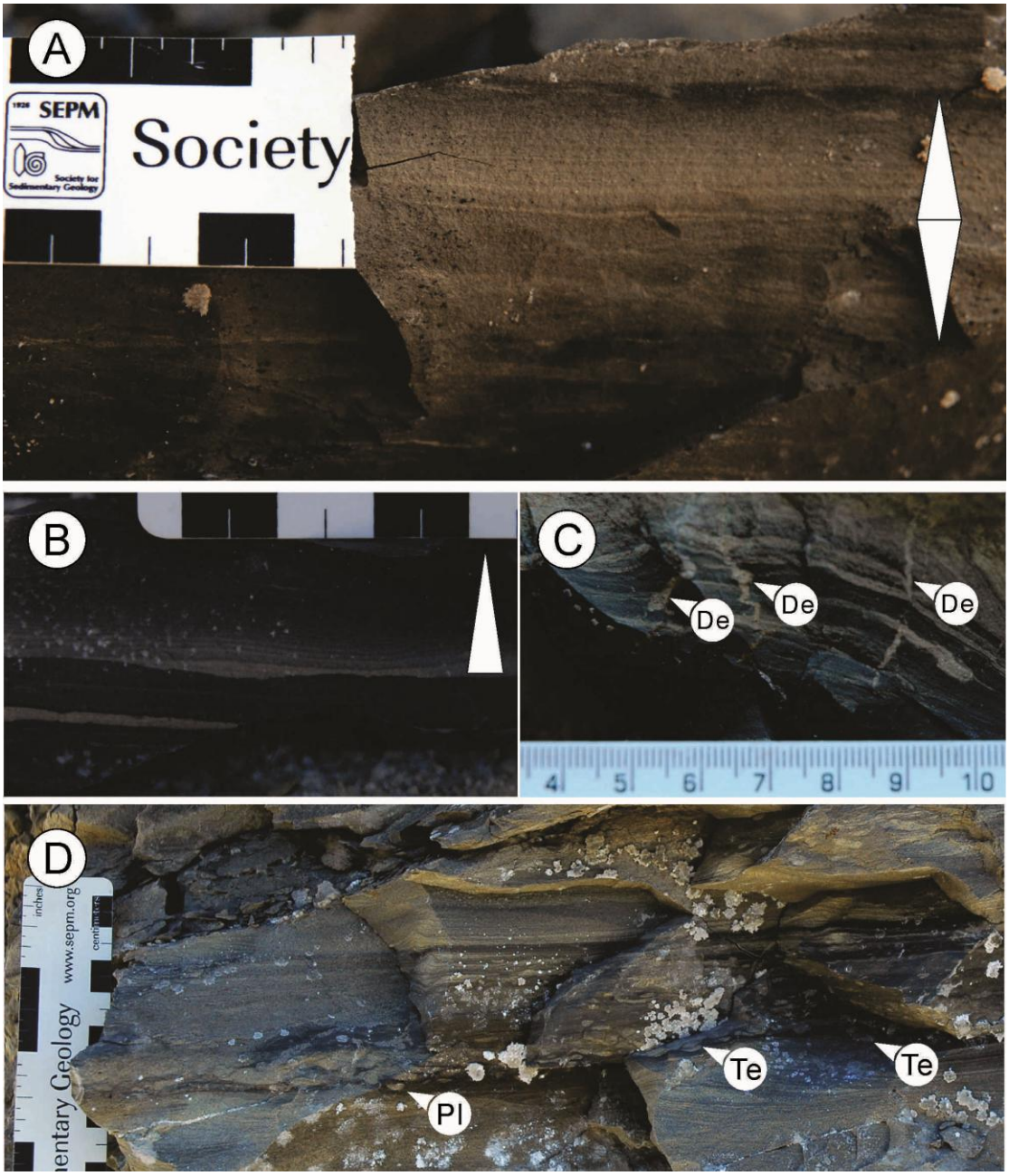

Figure 55. Muddy prodelta facies. A) A thin laminated bed showing inverse grading overlain by normal grading. B) Mudstone interbedded with laminated very fine-grained sandstone. The upper part of the section is characterized by a normally graded bed, as marked with the white triangle, where laminated very fine-grained sandstone grades upward to muddy siltstone and then to silty mudstone and mudstone with clear contacts. The base of the very fine grained sandstone is characterized by a minor erosional surface as marked with a small white arrow. C) Laminated silty mudstone with dewatering cracks. D) Laminated silty mudstone interbedded with bioturbated mudstone. Pl. *Planolites*, Te. *Teichichnus*.

Interpretation: The muddy facies described above are interpreted to be deposited in a river-dominated and wave-influenced prodelta environment. The low bioturbation indicates a stressed environment, due to fresh water input and high sedimentation rate (MacEachern et al. 2005). The presence of dewatering cracks suggests high sedimentation rate and possible salinity fluctuation close to the river mouth. Massive mudstone is interpreted to be deposited out of suspension in a buoyancy-dominated setting (Nemec 1995). Normally graded beds are interpreted to be turbidite deposits, with laminated siltstone and massive mudstone respectively representing Tc and Te Bouma sequences (Bouma and Scott 1964). However, when normal grading is associated with inverse grading below, together they are interpreted to be deposited by hyperpycnal turbidity currents related to river floods (Mulder et al. 2001; Mulder et al. 2003). Inverse grading is the product of waxing flow and normal grading is the result of waning flow. The occasional erosional contact in between indicates a flood event of exceptionally high magnitude, when deposition stopped and erosion occurred (Mulder et al. 2001; Mulder et al. 2003; Bhattacharya and MacEachern 2009).

4.5.2 Distal Delta Front

Description: Muddy prodelta facies grade upward to heterolithic interbedded sandstone and silty mudstone (Figs. 53 and 54). Silty mudstone is massive (Fig. 56A) and locally contains ball and pillow structures and growth faults (Fig. 56B). Thin bedded (in centimeters) sandstones are both current- and wave-ripple cross laminated (Figs. 56C, 56E and 56F). Thick bedded (in decimeters) sandstones are planar laminated capped by cross-laminated sandstone (Figs. 56, 56D and 56E). Current ripples are locally climbing (Fig. 56F). Individual sandstone beds is up to a few hundred meters. BI ranges from 0 to 2. *Planolites* and *Paleophycus* are common.

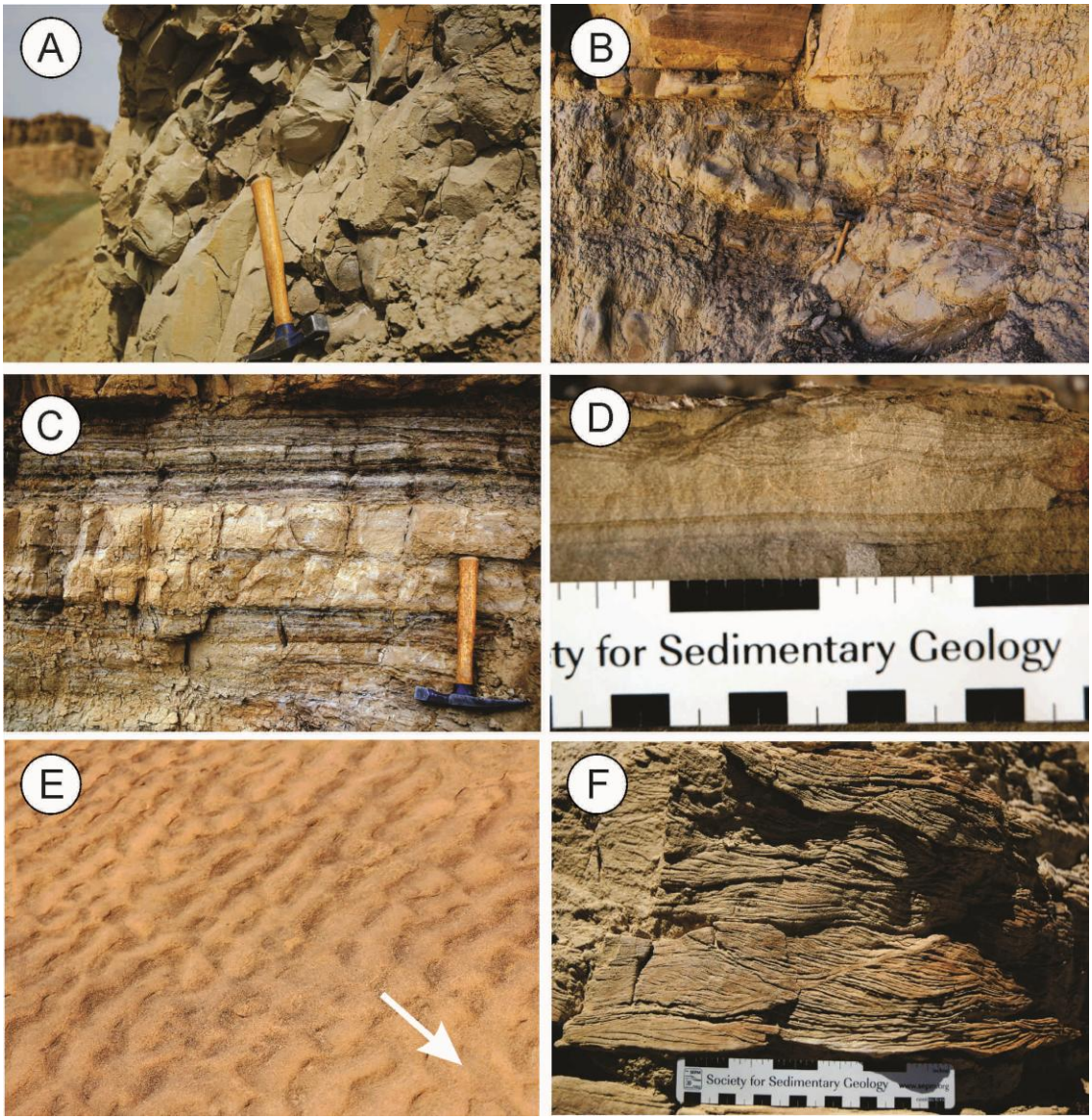

Figure 56. Distal delta-front facies. A) Massive siltstone. B) Deformed and faulted siltstone. Notice the hammer as a scale.The fault beneath the hammer. C) Heterolithic interbedded very fine-grained silty sandstone and silty mudstone. The sandstone is mostly planar bedded. D). Planar bedded sandstone capped by wave-cross laminated sandstone. E) Current ripples in plan view. Paleocurrent direction is toward the lower right as indicated by the arrow. F) Climbing ripples with the climbing angle ranging from 30-60 degrees.

Interpretation: The heterolithic facies described above is interpreted to be deposited in a distal delta-front environment. The massive siltstone characterized by ball and pillow structures and growth faults is interpreted to be slump deposits resulting from gravity flows similar to those described in the Mississippi delta front

(Lindsy et al. 1984). Soft sediment deformation and climbing ripples both indicate a relatively fast rate of sedimentation. The planar bedded sandstone is interpreted to be distal delta-frontal splays. The low bioturbation index and limited variety of trace fossils indicate a stressed environment, probably close to a river mouth (MacEachern et al. 2005; MacEachern et al. 2010).

4.5.3 Proximal Delta Front

Heterolithic distal delta-front facies grade upward into sandy proximal delta-front facies (Figs. 53 and 54). The sandy proximal delta-front facies are subdivided into three subfacies including basal planar beds, middle low-angle cross beds and upper dune-scale cross beds (Fig. 54).

Basal planar beds:

Description: The basal planar beds are composed of fine-grained sandstone (56A). Beds are commonly more than 1 meter thick and can be traced laterally for more than a few hundred meters. Some of the planar beds are not truly planar but show small-scale undulating geometry (Fig. 57B). In places, current ripples grade upward into planar beds, which in turn grade upward into current ripples again (Fig. 58). Current ripples dip offshore. These planar beds are in general lightly bioturbated with a BI ranging from 0-2. Common *ichnogenera* are *Ophiomorpha* (Fig. 59A), *Skolithos* (Figs. 59B and 59C), *Palaeophycus* (Fig. 59C), *Cylindrichnus*, and *Planolites*.

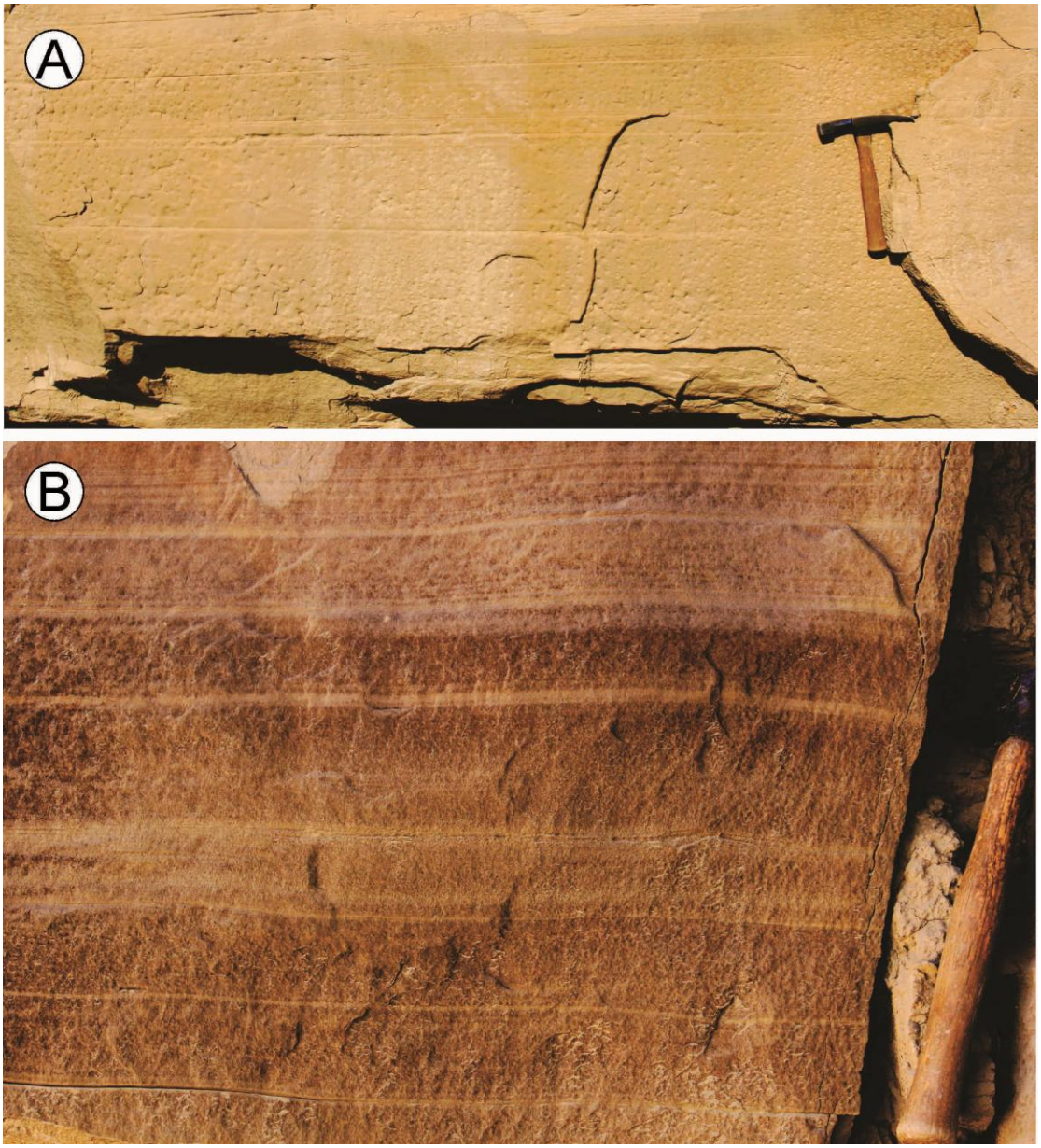

Figure 57. Inertia-dominated delta-front facies. A) Planar laminated fine-grained sandstone. B) Quasi-planar laminated fine-grained sandstone, notice that the planar beds show some gentle undulation.

Interpretation: The planar beds are interpreted to be deposited in an inertia-dominated river mouth during a storm/flood event similar to those described by Martinsen et al. (1990). These planar beds lie about 10 m below the top of Parasequence 6a, and were probably deposited in a water depth of about 10 m, which favors the dominance of inertial forces (Wright 1977). The dilution of the sea water

around the delta by fresh water from the river also possibly reduced the density contrast between the issuing and ambient water (Bhattacharya and MacEachern 2009). The current ripples dipping offshore (including climbing ripples) indicate unidirectional flow from the river and wave ripples indicate storm/wave influence. The undulating planar beds are termed quasi-planar laminations (Arnott 1993)，indicating possibly uni-directional and undulating combined flow, linked to storms. The ripple-planar-ripple facies successions are interpreted to indicate the waxing and waning of hyperpycnal flow deposits, similar to those described in the Pennsylvanian Minturn Formation (Lamb et al. 2008; Myrow et al. 2008) and the Panther Tongue Formation (Olariu et al. 2009). The detached nature of these sandstones from the river mouth and their internal traction-dominated structures (quasi-planar and current ripples cross lamination) indicate that there were enough inertia in the river flow which displaced the sea water away and deposited sediments further seaward of river mouth. Consequently, we interpret these planar beds to be inertia-dominated bars as proposed by Wright (1977).The trace fossil assemblage is interpreted to represent a *Skolithos* ichnofacies (MacEachern et al. 2005; MacEachern et al. 2010). However, the sparse burrowing and limited variety of ichnogenera indicate an environment that is more stressed compared to a normal shoreface setting (MacEachern et al. 2005).

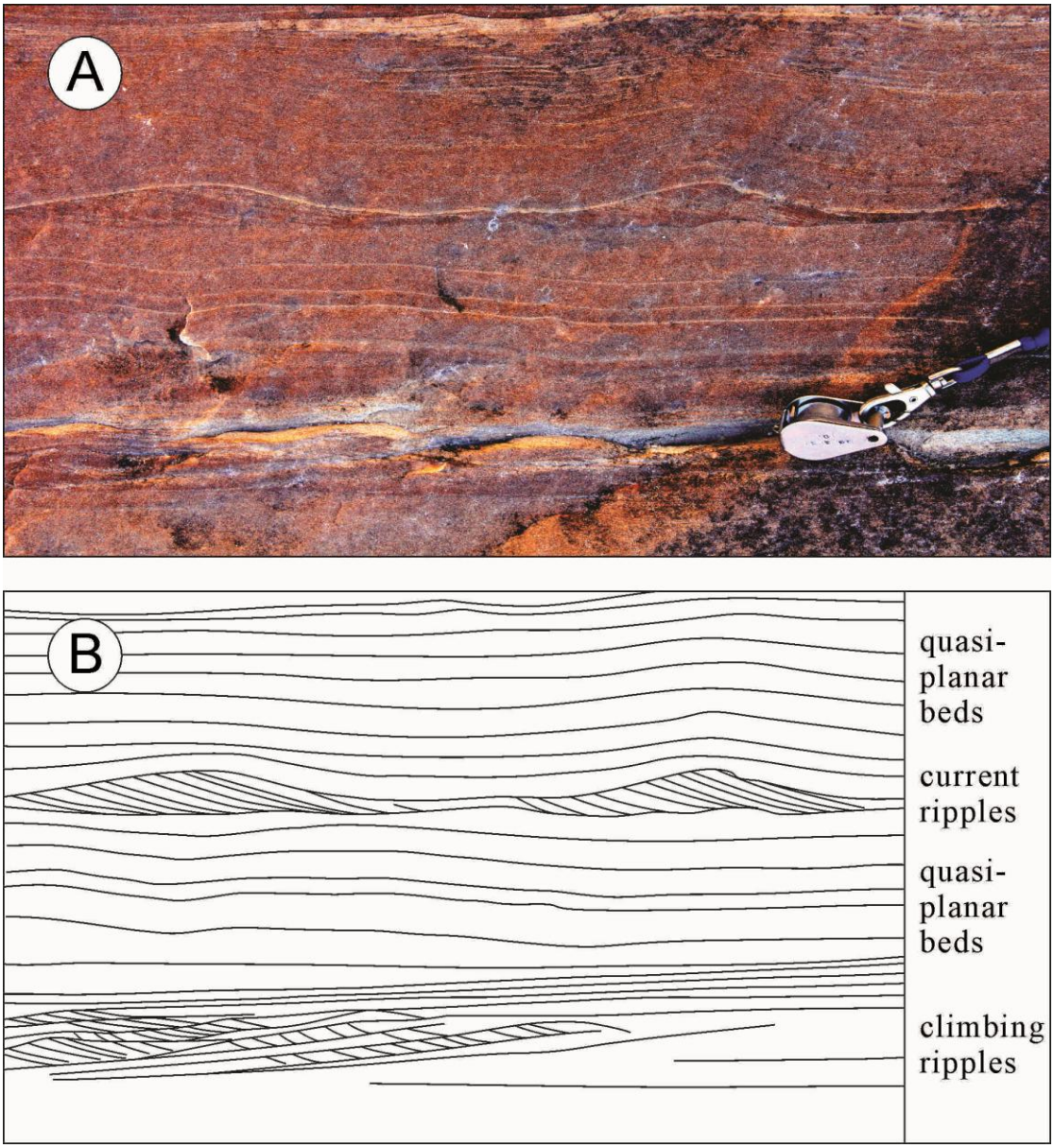

Figure 58. Inertia-dominated delta front facies. A) Current ripples grade upward into quasi-planar beds which are overlain by current ripples, and capped by quasi-planar beds. All the current ripples dip offshore. B) Line drawing of the bedding shown in photo 57A.

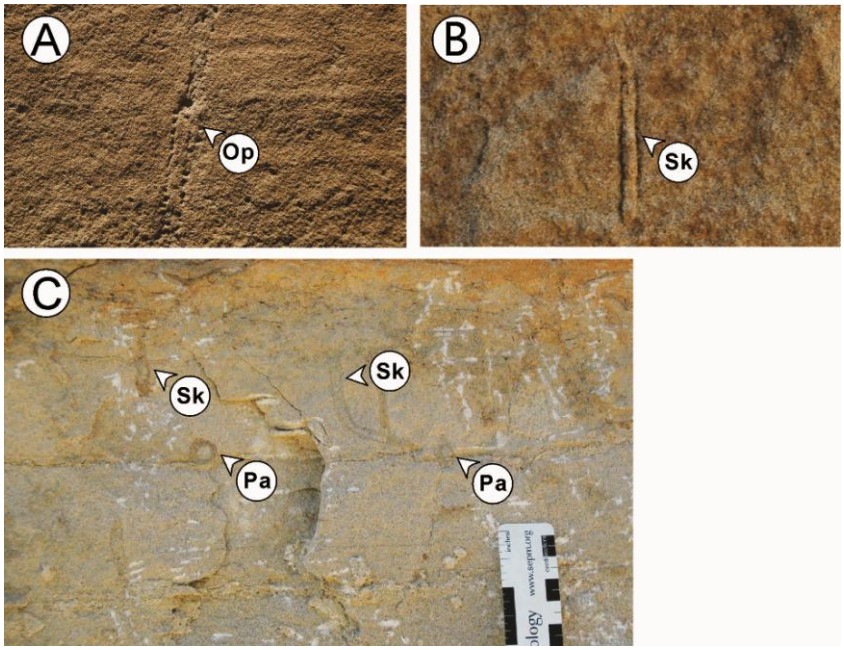

Figure 59. Bioturbation seen in the proximal delta front facies. A) *Ophiomorpha* B) *Skolithos* C) *Skolithos* and *Paleophycus*.

Upper dune-scale cross beds

Description: The upper part of the proximal delta front is composed of fine- to medium-grained, dune-scale cross-bedded sandstone (Figs. 53 and 54). These cross beds are commonly less than 30 cm thick and no more than a few tens of meters long (Fig. 60). Minor erosional surfaces can be seen locally (Fig. 60). Trace fossils are very rare.

Interpretation: The dune-scale cross beds at the upper part of a coarsening upward succession are interpreted to be deposited in a friction-dominated environment, similar to those documented by Turner and Tester (2006). They are estimated to have been deposited subaqueously, in a water depth less than a few meters. The shallowing of the water resulted from the filling of the accommodation by deposition of the underlying prodelta, distal delta-front, and proximal delta-front facies. These cross beds are interpreted to be friction-dominated mouth bars, as proposed by Wright (1977).

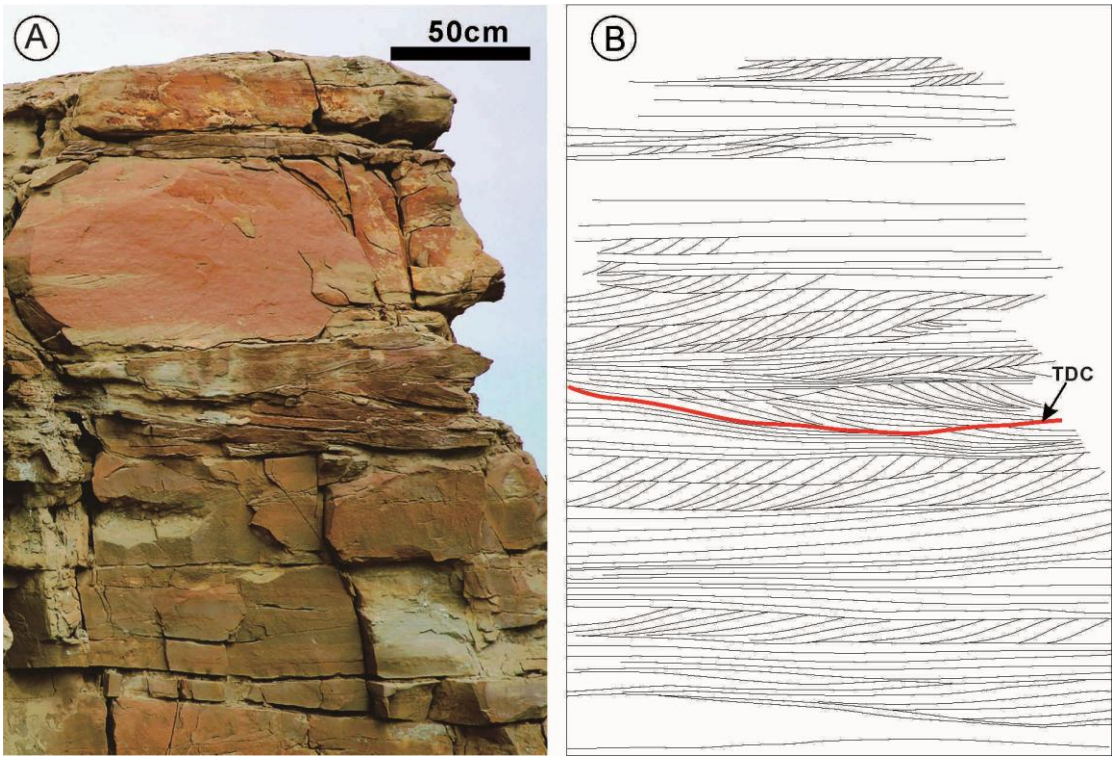

Figure 60. Friction-dominated delta-front deposits. A) photo showing the upper part of Parasequence 6a, which is dominantly dune-scale cross beds B) Bedding diagram drawn based on photo in Figure 60A. Two minor scour surfaces are marked with red lines, which are candidates for terminal distributary channels.

Middle low-angle cross beds (Transitional facies)

Description: In between the planar bedded inertia-dominated mouth bars and dune-scale cross-bedded friction-dominated mouth bars are large-scale low angle cross beds (Fig. 54). Figure 61 shows a typical example of one such cross bed set. It is about 1.5 m thick and a few tens of meters wide. It is composed of a coarsening upward pattern changing from silty fine-grained sandstone up to fine- to medium-grained sandstone. It thins and gets finer toward the left. Internally it is composed of multiple coupled inverse and normal graded cycles (Fig. 62). These cross bed sets show a gradual decrease in dimensions (thickness and lateral extent) and increase in dip angles. Figure 63 shows some examples of these cross-bed sets, which are more than 1 meter thick at the basal part of the succession and Figure

64shows some examples with decreased thicknesses further up the succession. Detailed bedding diagram of large outcrops in Figure 65 also shows an example of this. The large-scale low-angle cross sets are commonly less than a few tens of meters wide. The contacts between these bed sets can be conformable or erosional (Figs. 63 and 63). Thin-bedded massive mudstone layers are locally seen separating these bed sets (Fig. 66). Some of the mud layers may be cut out locally by the upper bed set (Fig. 65A). The lateral offset between these cross-bed sets are obvious (Fig. 64). Mud plugs are commonly seen at the back of cross-bed sets (Fig. 64). Biturbation is similar to that observed in the lower planar beds.

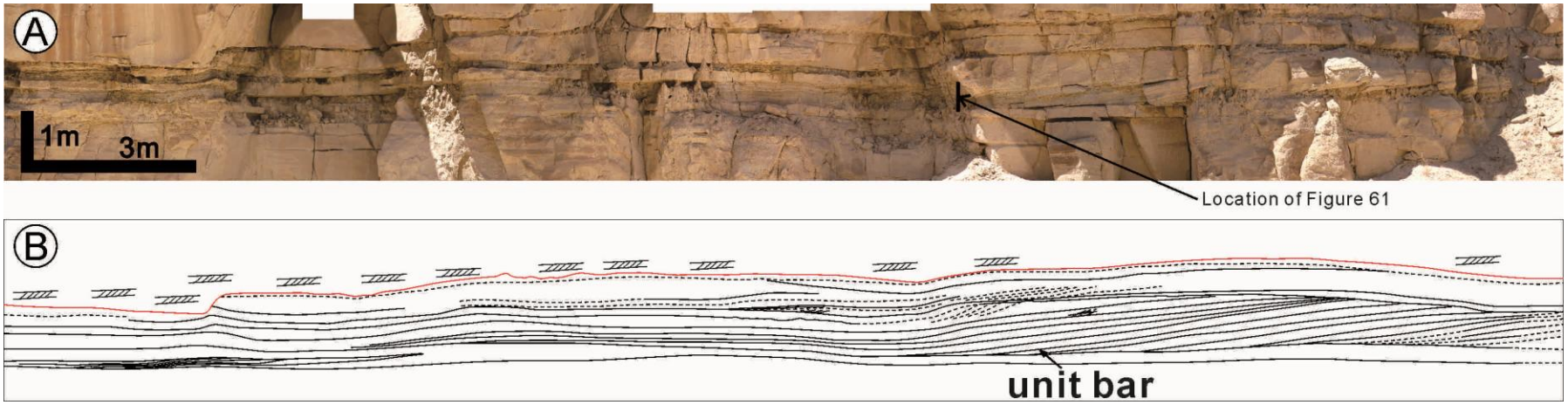

Figure 61. Unit bar. A) Photomosaic showing an example of a unit bar. B) Bedding diagram of Photo 61A. Meter-thick low angle cross beds accrete and thin toward the left. Also note that the bar is sandy on the right and fines toward the left. Locally these large cross beds are compound and are composed of dune-scale cross beds.

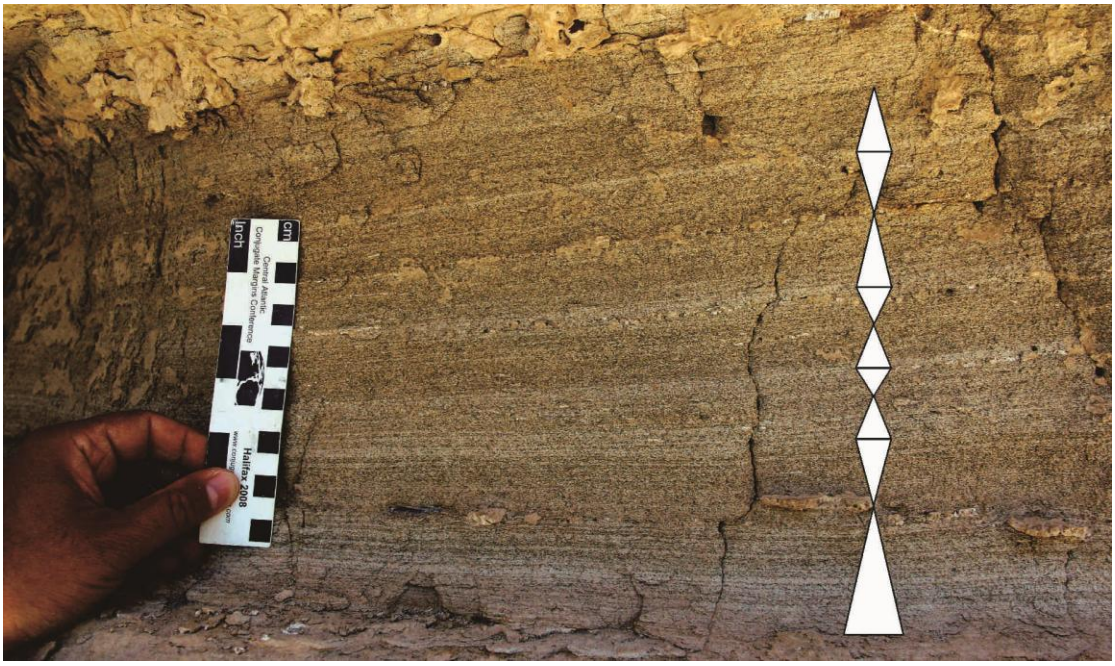

Figure 62. A photo showing the internal facies in the unit bar deposits shown in Figure 61. Cycles of inversely graded bed overlain by normally graded bed are marked with white triangles. Each association of inversely graded bed and normally graded bed is interpreted to result from separate flood event, with the inversely graded bed representing waxing flood deposits and the normally graded bed representing waning flood deposits. See Figure 61 for location of the photo.

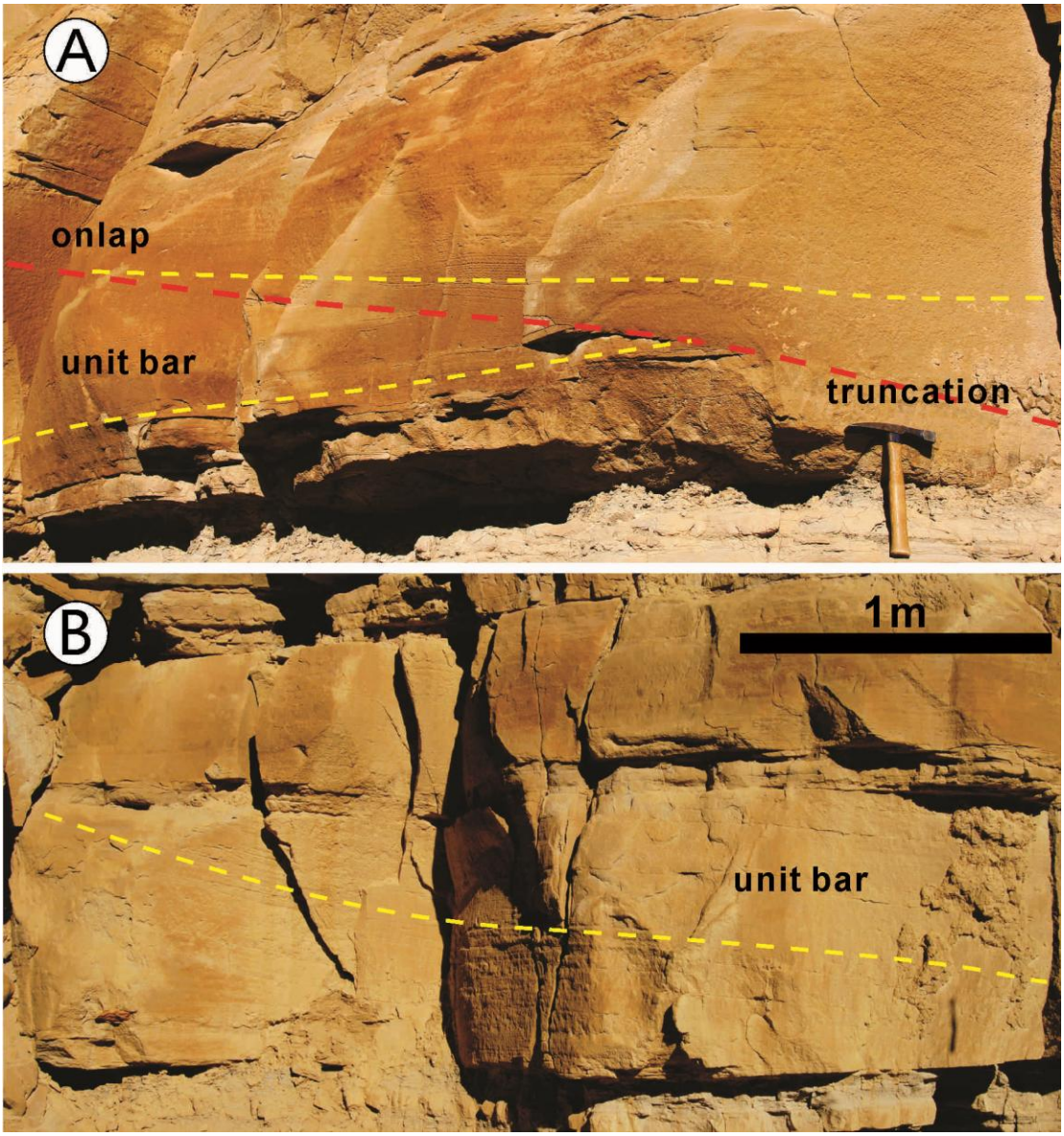

Figure 63. Large-scale low-angle cross-bed sets observed between inertia-dominated facies and friction-dominated facies. A) Photo and line drawing showing the architectural relationship of the low-angle cross-bed sets. The upper cross-bed set truncates and onlaps the cross-bed set. B) Low-angle cross-bed sets conformably overlie each other. All of these large-scale low-angle cross-sets are interpreted to be unit bar deposits.

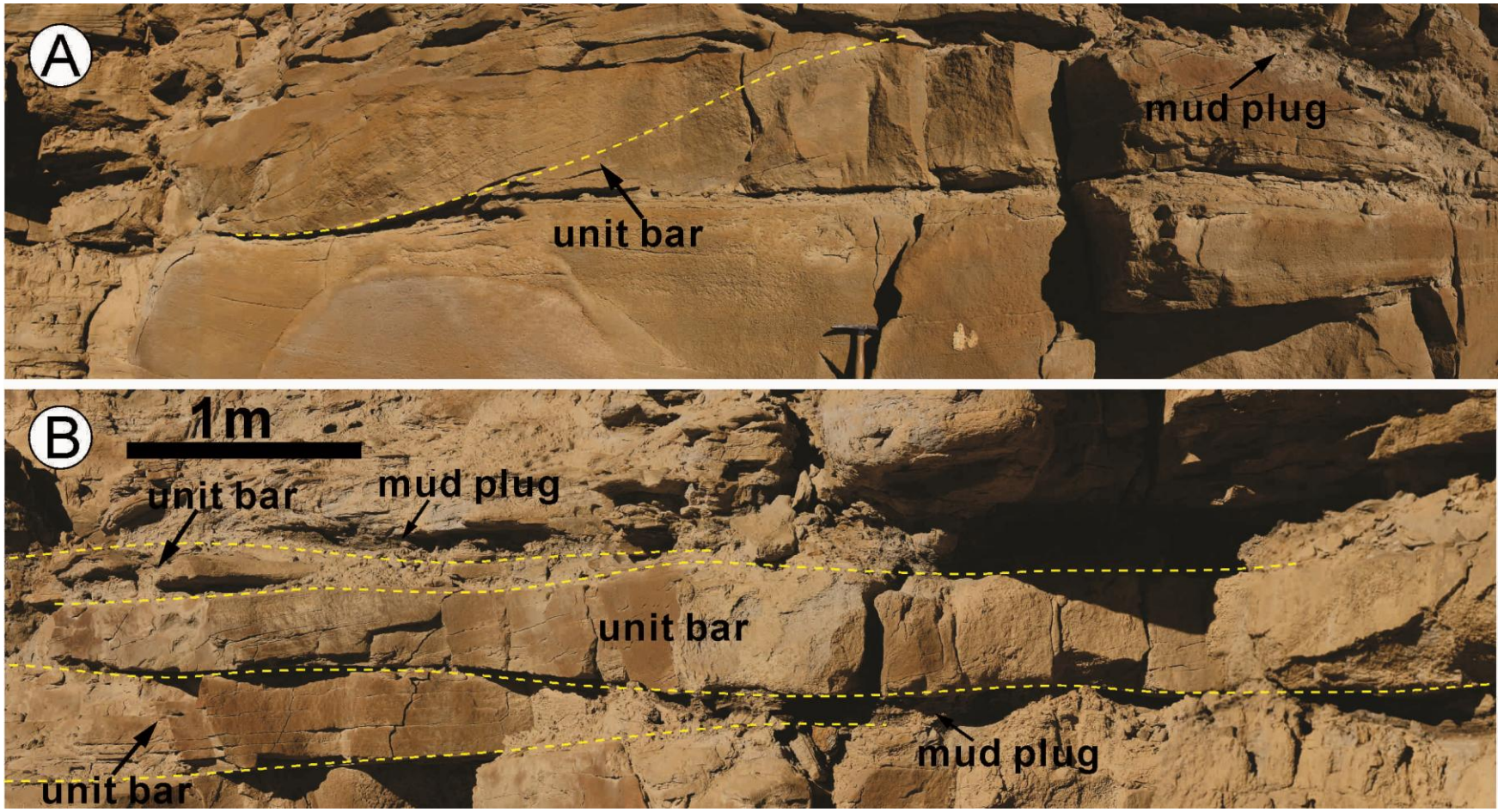

Figure 64. Photos and line drawings of large-scale low-angle cross-bed sets with smaller thicknesses and widths compared to those shown in Figure 63. A) An example of a unit bar with a mud plug at the back of the the cross-bed set. B) Three examples of unit bars with mud plugs at their back. Notice the overlapping pattern of these cross-bed sets.

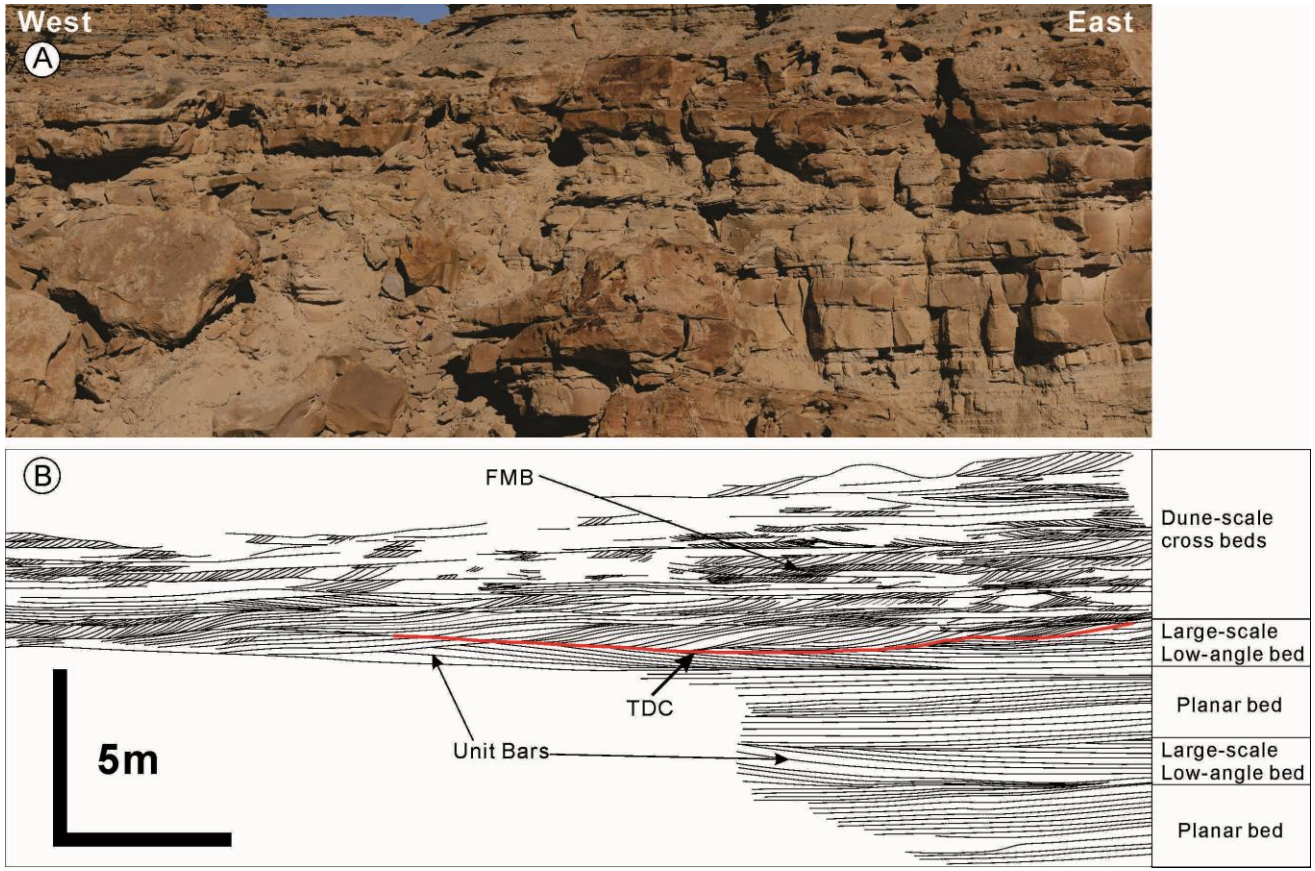

Figure 65. Cross section 2 A) Photomosaic of cross section 2. B) Bedding diagram based on the photomosaic in Figure 65A showing a systematic upward change of sedimentary facies from basal planar beds to large-scale low-angle cross-bed sets which decrease in dimensions upward into dune-scale cross beds. An erosional surface in the middle part of the photo is traced with a red line, which is interpreted to be a terminal distributary channel. The terminal distributary channel is filled with unit mouth bars that accrete toward the west and then aggrade. See Figure 52C for the location of the cross section. TDC: terminal distributary channel, FMB: Friction-dominated mouth bar.

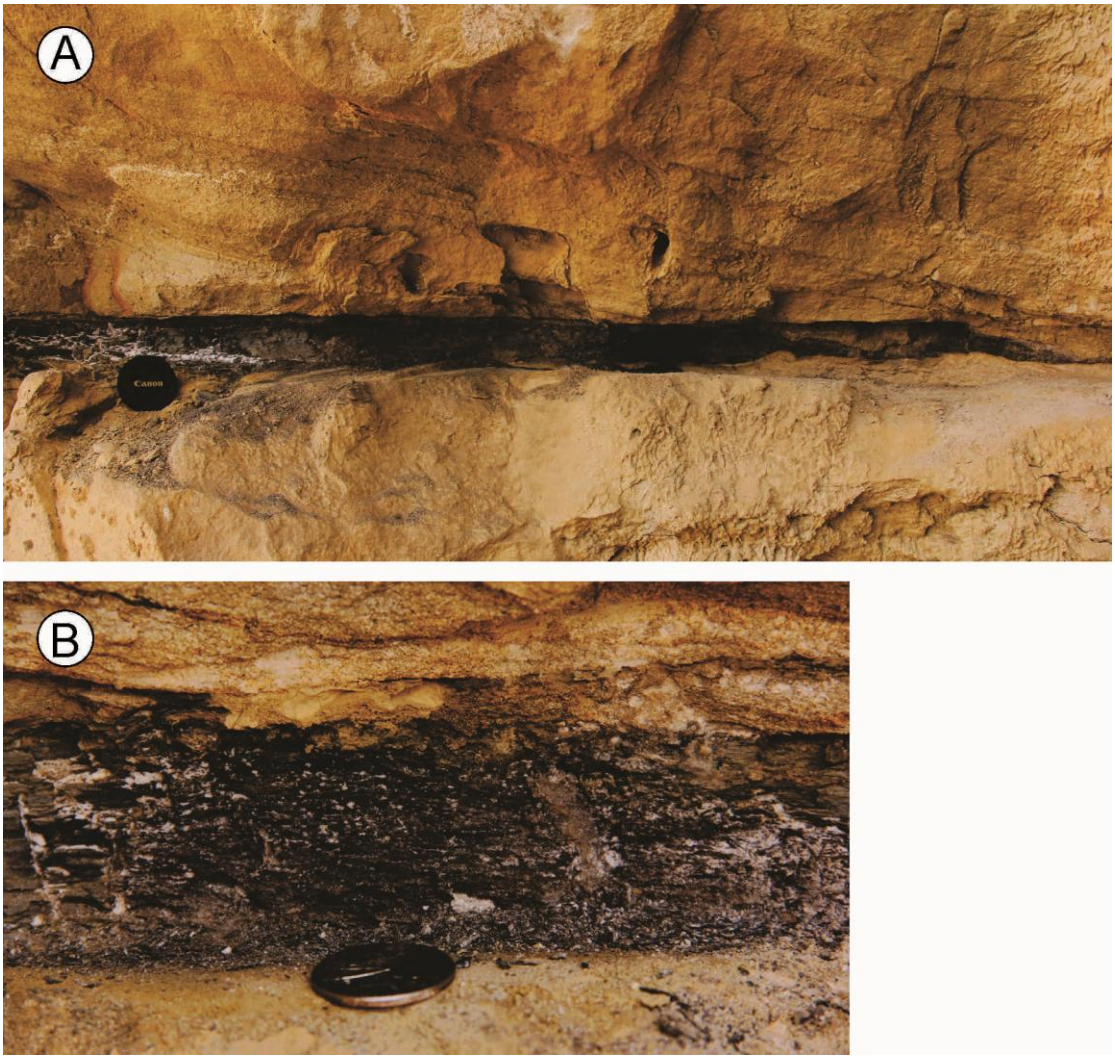

Figure 66. Mud drapes between mouth-bar deposits. A) A centimeter-thick mudstone drape separating two unit mouth bars (Notice the foresets in the upper unit). The mudstone on the right part of the photo was partially eroded away by the upper unit. B) A close up of the mudstone in A. The mudstone bed is more than 3 cm thick and internally shows no sedimentary structures. It is interpreted to be deposited out of suspension possibly as a fluid mud during river low stage.

Interpretation: The large-scale low-angle cross-beds described above are interpreted to represent the transitional facies from inertia-dominated bars below and friction-dominated facies above. The decrease of cross-set dimension (thickness and extent) is interpreted to result from increasing dominance of frictional forces in response to a gradual decrease of water depth due to the filling of the accommodation by the delta. Upward increase in sediment grain sizes may also contributed to the

decreasing of cross bed set dimensions. The lenticular upward-coarsening cross set shown in Figure 16 represents a basic and essential element in building the delta. These cross sets are termed unit mouth bars similar to those "effluent-generated microdelta-type unit bars" described by Nemec et al. (1988). The upward-coarsening, lateral fining and thinning of these unit mouth bars mimic a microdelta to some extent. The internal inverse and normal graded cycles may indicate multiple flood events with inversed graded beds representing waxing flood deposits and normal graded beds representing waning flood deposits (Mulder et al. 2001; Mulder et al. 2003). The offlapping of these unit mouth bars is interpreted to be the result of their aggradation and progradation. Aggradational and progradational unit mouth bars are grouped into mouth-bar assemblages (Ahmed et al. in review). The thin mudstone layers separating unit-mouth bars or mouth-bar assemblages are interpreted to be deposited out of suspension during lower river stages. The erosion of some of the mudstones indicates that possibly a lot of the mudstones deposited during the low river stages were eroded away by subsequent flood events. Mud plugs at the back of unit mouth bars are interpreted to be the remains of waning floods. They were preserved only because they were deposited in physiographically low areas scoured during the previous flood event.

4.5.4 Terminal Distributary Channel Deposits

Description: They are characterized by a basal erosional surface and occur at the upper part of the coarsening upward facies succession (Figs. 65, 67, 68 and 69). However, the erosional boundaries are commonly poorly defined with one clear erosional edges (cut banks) on one side and the other side laterally conformable with

the adjacent mouth-bar deposits (Figs. 67 and 68). Erosional surfaces have relief of less than 5 m (commonly around 2 to 3 meters) and widths of less than a few tens of meters. Internally they are filled with dune-scale cross-bedded sandstone and sometimes with meter-scale inclined beds (Figs. 65, 67, 68 and 69). The channel fill may or may not show a fining upward trend (Fig. 54A). Locally, the erosional surface is partially filled with mudstones and the mudstone is conformable with the adjacent large inclined beds (Fig. 68).

Interpretation: These erosional surfaces are interpreted to be terminal distributary channels, similar to those documented in the Cretaceous Panther Tongue Sandstone (Olariu et al. 2005; Olariu and Bhattacharya 2006). The sandy fill of the terminal distributary channels is interpreted to be formed by lateral accretion of mouth bars. The mudstone fill of some of the terminal distributary channels is interpreted to be abandoned channel deposits.

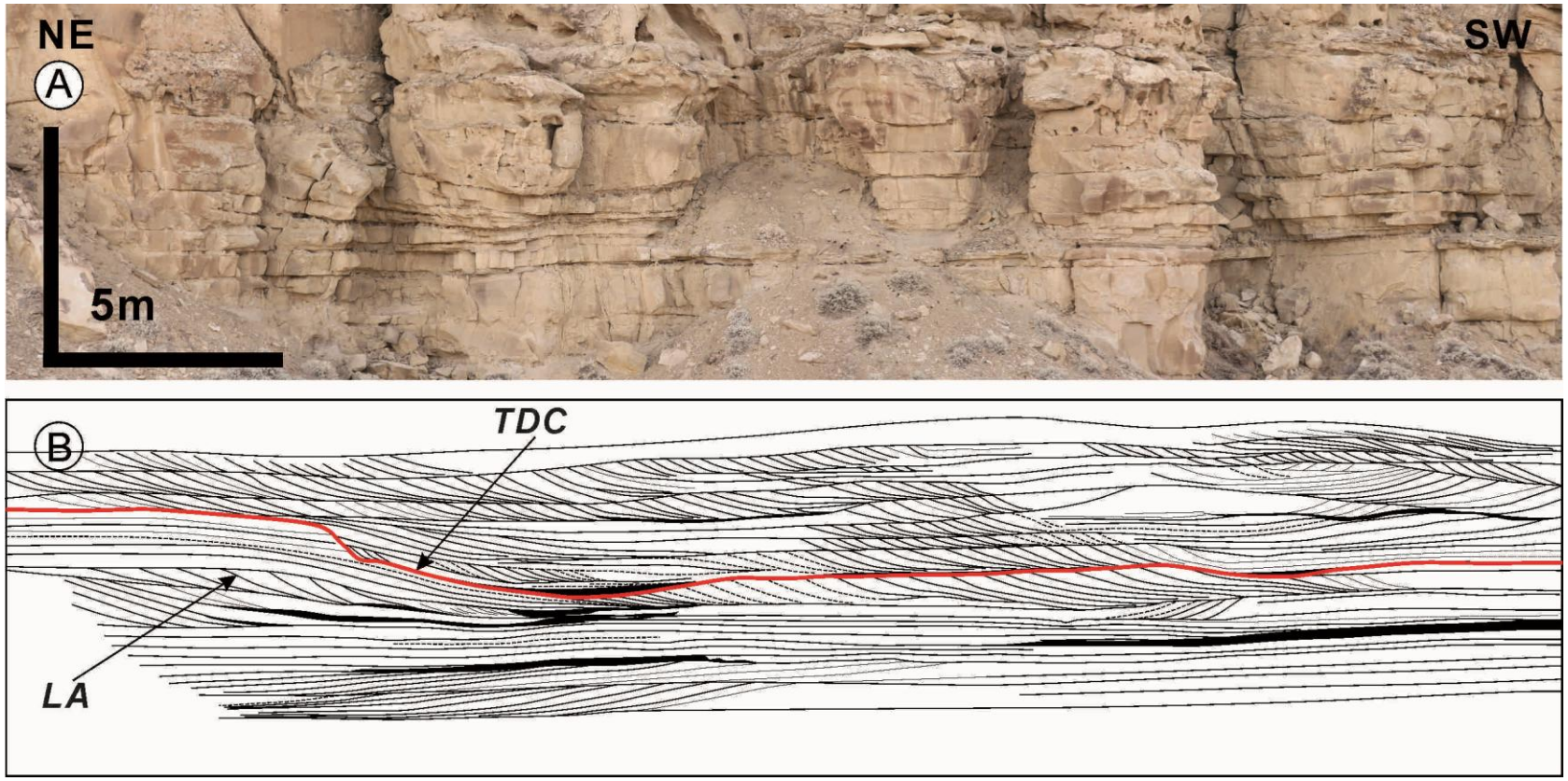

Figure 67. A) Photomosaic of cross section 1. B) Bedding diagram of cross section 1. Clinoforms dip toward the southwest at the lower left part of the outcrop. A terminal distributary channel is marked with a red line, which cuts down into the mouth-bar deposits on the northeast side of the outcrop. The erosional relief is about 3 meters on the northeast side and gradually decreases toward the southwest, where it becomes more or less conformable with the mouth-bar deposits. See Figure 52C for location of the cross section. LA: lateral accretion.

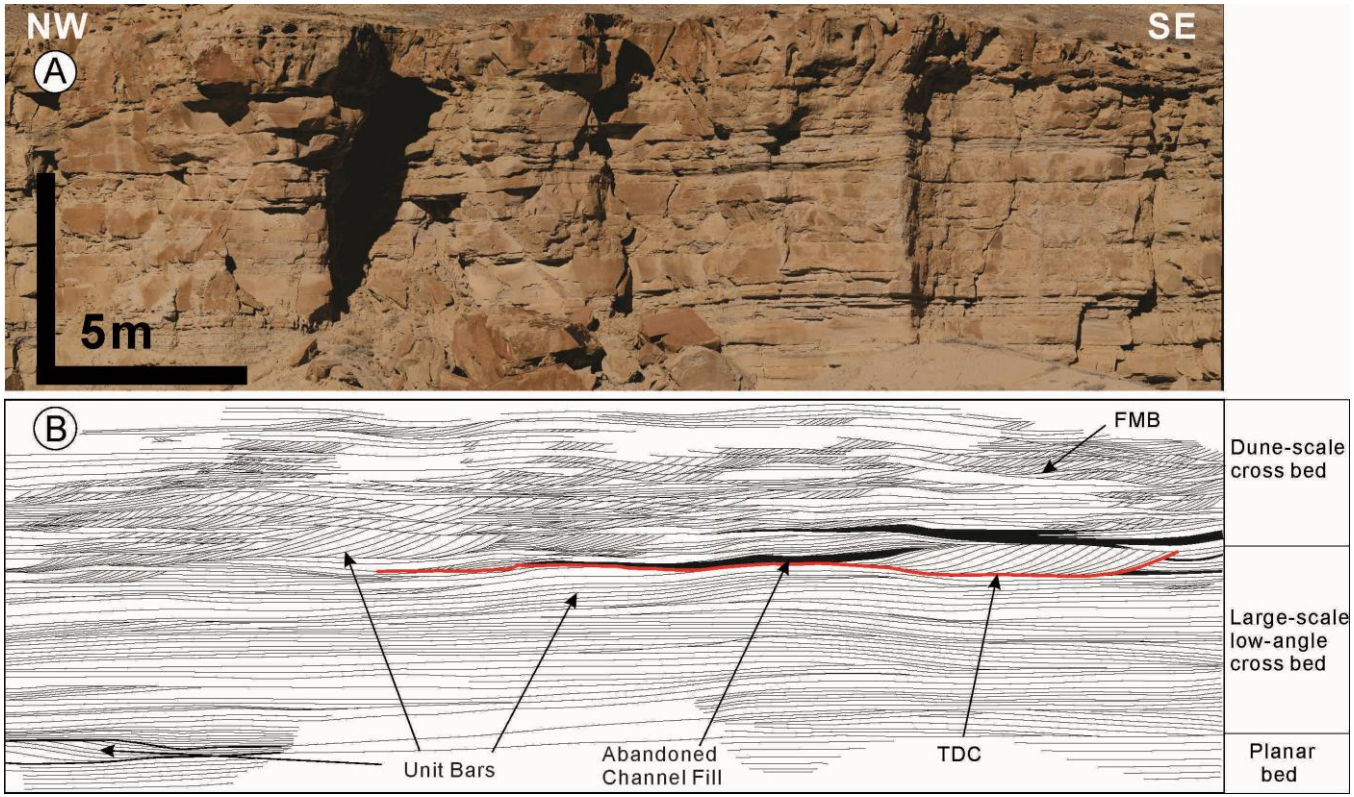

Figure 68. A) Photomosaic of cross section 3. B) Bedding diagram of cross section 3. A regular decrease in cross-set dimensions from the base of the cross section to the top can be seen. In the middle part of the cross section, an erosional surface with a relief of about 2 m is interpreted to be a terminal distributary channel and is marked with a red line. The terminal distributary channel is conformable with the mouth bars to the southeast, which are composed of cross-bed sets about 2 m thick and accrete toward the northwest. The terminal distributary channel is overlain by a mud plug, which is interpreted to be abandoned channel deposits. Above the abandoned channel a muddy facies can be seen. It is interpreted to be the bottom sets of mouth bars. See Figure 52C for location of the cross section.

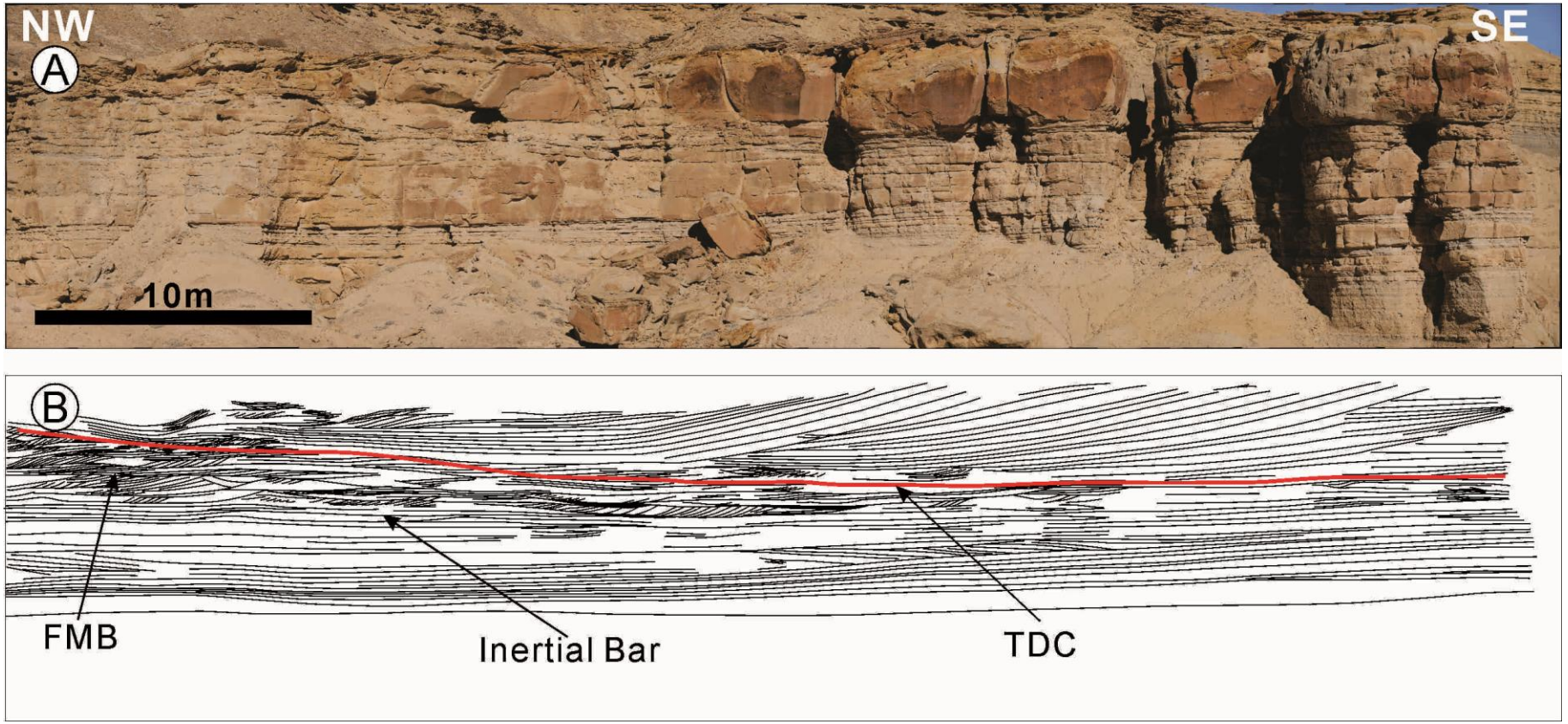

Figure 69. A) Photomosaic of cross section 4. B) Bedding diagram of cross section 4. An erosional surface with relief of about 5 m is marked with a red line, which is interpreted to be a terminal distributary channel. The channel is filled with large-scale inclined cross beds, which are interpreted to be laterally accreting mouth bars. The terminal distributary channel cuts down into the mouth-bar deposits below, which thicken from the southeast toward the northwest. See Figure 52C for the location of the cross section.

4.5.5 Shoreface

Description: They are characterized by a general coarsening upward pattern (Fig. 70). The shoreface succession is sandier than the deltaic succession and in general more intensely bioturbated (Figs. 54A and 70). Three lithofacies are identified. The basal part of the succession is composed of moderately to highly bioturbated planar and wave-laminated mudstone and muddy siltstone (Fig. 70). Above the mudstone and siltstone is a thick package of sandstone about 8~10 meters, which is characterized by moderate bioturbation and hummocky cross stratification. The top of the succession is composed of mostly dune-scale cross beds with varying degrees of bioturbation.

Interpretation: The whole coarsening upward succession is interpreted to represent a typical shoreface depositional environment, based on the combination of lithofacies and generally highly bioturbated nature. The basal intensely bioturbated mudstone and siltstone is interpreted to be continental shelf deposits. The hummocky cross-stratified sandstone is interpreted to be storm-dominated shoreface deposits which is overlain by dune-scale cross-bedded upper shoreface deposits (Fig. 70). Detailed facies description and interpretation can be found in Li et al. (2011).

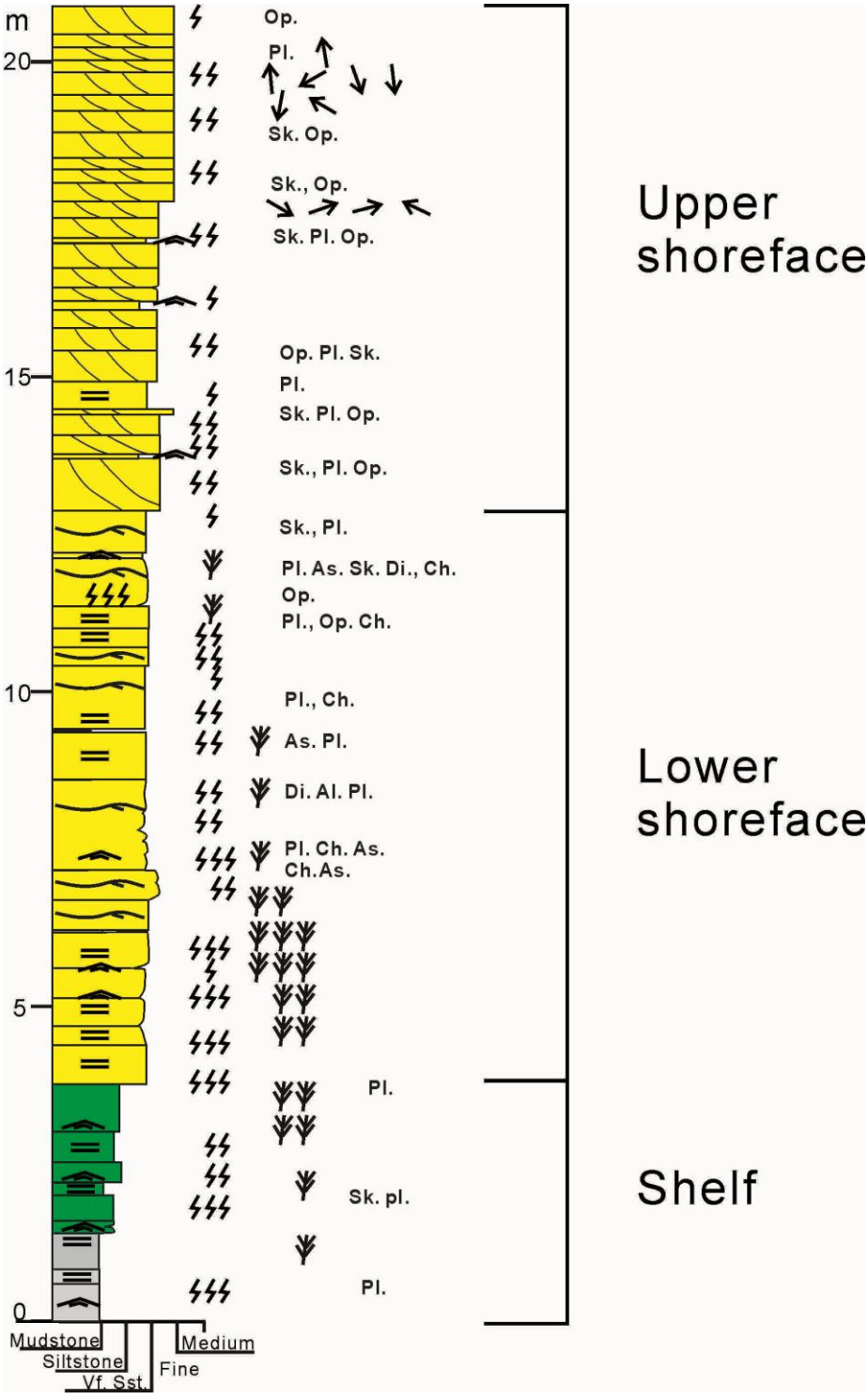

Figure 70. A type measured section from the shoreface deposits in Parasequence 6a. It is divided into three facies: the muddy shelf, hummocky cross-stratified lower shoreface and dune-scale cross-bedded upper shoreface. In general this succession is moderately to highly bioturbated. See Figure 54 for legend.

4.6 Evidence for a Crevasse Delta

4.6.1 Paleocurrent Data

Integrated paleocurrent data collected from Li, et al. (2011), Ahmed, et al. (in review), Garza (2010), and this study are shown in Figure 71. In total, about 1500 paleocurrent measurements were collected and plotted in 10 rose diagrams (Fig. 71). Parasequence 6a in the Skyline Rim area is interpreted by Li, et al. 2011 and Zhu, 2010 to be river-dominated delta-front deposits. Paleocurrents in the Skyline Rim area are generally toward the northeast, as indicated by N1, N2, N3, and N4 (Fig. 71). The gradual change of paleocurrent directions from east to northeast (from N1 to N4) is interpreted to indicate a radiating pattern, typical of a river-dominated delta lobe (Bhattacharya 2006; Bhattacharya 2010). Based on previous facies analysis and the paleocurrent data from this study, a generally northeastward prograding delta is indicated. Parasequence 6a in the Coalmine Wash area is also interpreted to be river-dominated delta-front deposits by Garza (2010) and Ahmed, et al. (in review), which is in accordance with this study as shown in the following section. Paleocurrents, as indicated by N5, N6, and N7 in the Coalmine Wash area, are toward the west and southwest, indicating a delta lobe prograding west to southwest (Fig. 71). Paleocurrent data in N8 is characterized by a bimodal pattern, with a component pointing northeast and one component pointing southwest. The northeast-oriented component is interpreted to be measured from the northeastward prograding delta, as indicated by N1 to N4, while the southwest-oriented component is from the westward prograding delta, as suggested by N5, N6 and N7. N9, and N10 are plotted from paleocurrent data measured from the shoreface-dominated part of the delta. N9 are

measurements of strikes of wave-ripple crests, indicating that the waves were approaching the shoreline from a general northeast direction. N10 are measurements of dips of dune-scale cross beds within the shoreface deposits. It shows a bimodal pattern. This is interpreted to indicate that southwestward approaching waves broke on a shoreline, favoring longshore transport toward the northwest and southeast. N9 and N10 both indicate waves were from the northeast.

It is shown in this study that the paleocurrents from the wave-dominated shoreface system are characterized by a bimodal pattern, while paleocurrents from a river-dominated delta are characterized by a general unidirectional pattern (Fig. 71). A radiating pattern may be recongnized in a river-dominated delta lobe.

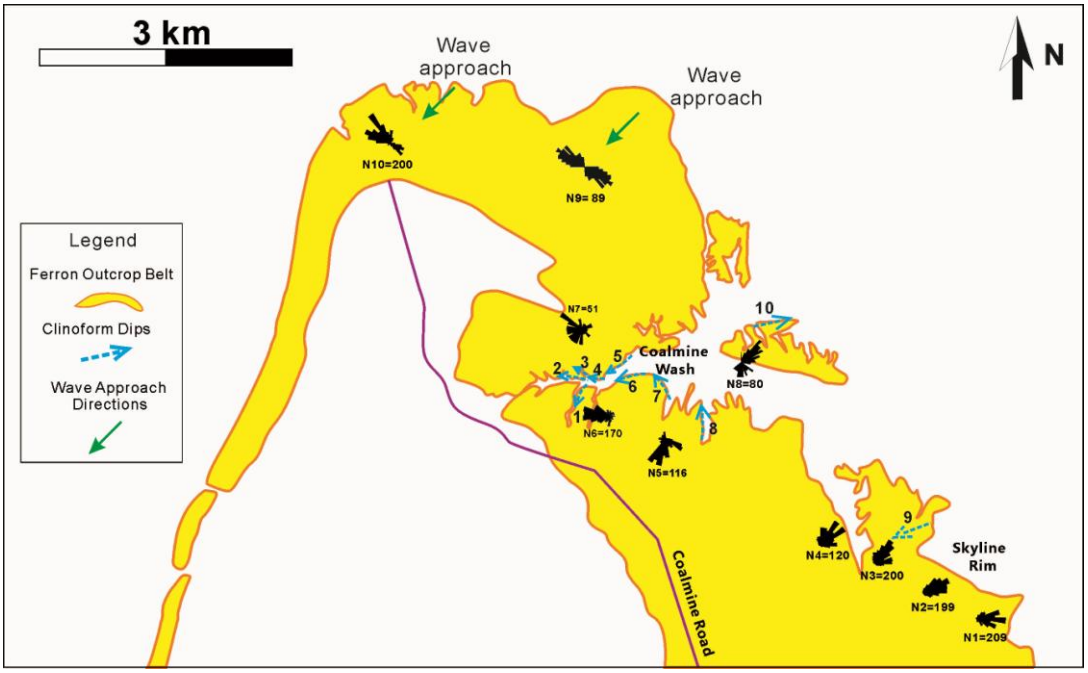

Figure 71. Basemap of the study area showing the Ferron outcrop belt, paleocurrent data and clinoform data. Paleocurrent data shown in rose diagrams. Rose diagram N9 is plotted from measurements of strikes of wave crests. Other rose diagrams are plotted from measurements from rib and furrow structures and angle-of-repose cross beds. Blue arrows indicate dips of clinoforms. The numbers of clinoforms are in accordance with the numbers of cross sections shown in Figure 52C. Green arrows indicate wave approach directions. Data are from Li et al. (2011), Ahmed (2011), Garza (2010) and this study.

4.6.2 Clinoform Data

Ten clinoform dips were collected in the river-dominated delta front part of the delta and they were plotted on the map (Fig. 71). Green arrows point toward the direction of the dips of clinoforms. These clinoforms are interpreted to have been formed by mouth-bar accretion. They are 2 to 8 meters high with dip angles ranging from 5^0-12^0, similar to the deltaic clinoforms documented in previous studies (Olariu et al. 2005; Bhattacharya 2010; Schomacker et al. 2010). Detailed facies architectural analysis of these mouth-bar deposits are in the following section.

Clinoforms at cross section 1, close to N6 dip, toward the southwest, which is perpendicular to the paleocurrent direction which is northwest (Figs. 67 and 71). Similarly, clinoforms at cross sections 7 and 8, dip toward the northwest. It is perpendicular to the southwest paleocurrent direction (Fig. 71). Clinoforms at cross sections 1, 7, and 8 are interpreted to indicate lateral accretion of mouth-bar deposits. As indicated by a green arrow, clinoforms at cross section 9, close to N3 dip, toward the southwest, which is opposite to the paleocurrent direction (northeast) (Fig. 71). Consequently, Clinoforms at cross section 9 are interpreted to represent upstream accretion of mouth bars. Clinoforms at cross sections 2, 3, 4, 5, and 6 dip generally west, which is in general accordance with the paleocurrent direction and consequently are interpreted to be downstream accretion of mouth-bar deposits. Clinoforms at cross section 11, close to N8, dip east and is in accordance with the paleocurrent data. They are also interpreted to be downstream accretion of mouth-bar deposits. However, notice that clinoforms at cross section 11 and those at cross section 4, 5, and 6 dip toward almost opposite directions, even though they are just a few hundred meters away.

4.6.3 Depositional Facies

Two composite cross sections were made to show the depositional facies in the study area. Cross section a-a’ is in an oblique-dip orientation (Fig. 712) and cross section b-b’ is in an oblique-strike direction (Fig. 73).

A typical deltaic succession is interpreted and correlated from S1 to S8 in cross section a-a’, based on the common presence of current-ripple cross lamination, graded beds (especially inverse grading), unidirectional-dipping cross beds, and clinoforms (Fig. 72). They are in general lightly bioturbated with limited *ichnogenera*. They were divided into muddy prodelta, heterolithic delta-front, planar bedded inertia-dominated mouth-bar, cross bedded friction-dominated mouth-bar and terminal distributary channels deposits. Even though wave-ripple cross lamination and hummocky cross stratification can be locally seen, wave and storm influence are limited. This river-dominated succession changes over a short distance northeastward into a shoreface system from S11 to S14 (Fig. 72), which is characterized by abundant wave-ripple cross lamination, hummocky cross stratification (HCS) and a more highly bioturbated nature (BI ranges from 0 to 6). A basinward (east) pinch out of the shoreface system is illustrated from S13 to S14 (Fig. 72). S9 and S10 show a mix of storm/wave-influence as indicated by wave-ripple cross lamination and HCS, and river influence, as indicated by current-ripple cross lamination. They are interpreted to be interfingering of river-dominated delta-front and wave-dominated lower shoreface deposits, and represent the transitional facies between a river-dominated delta and wave/storm-dominated shoreface (Fig. 72).

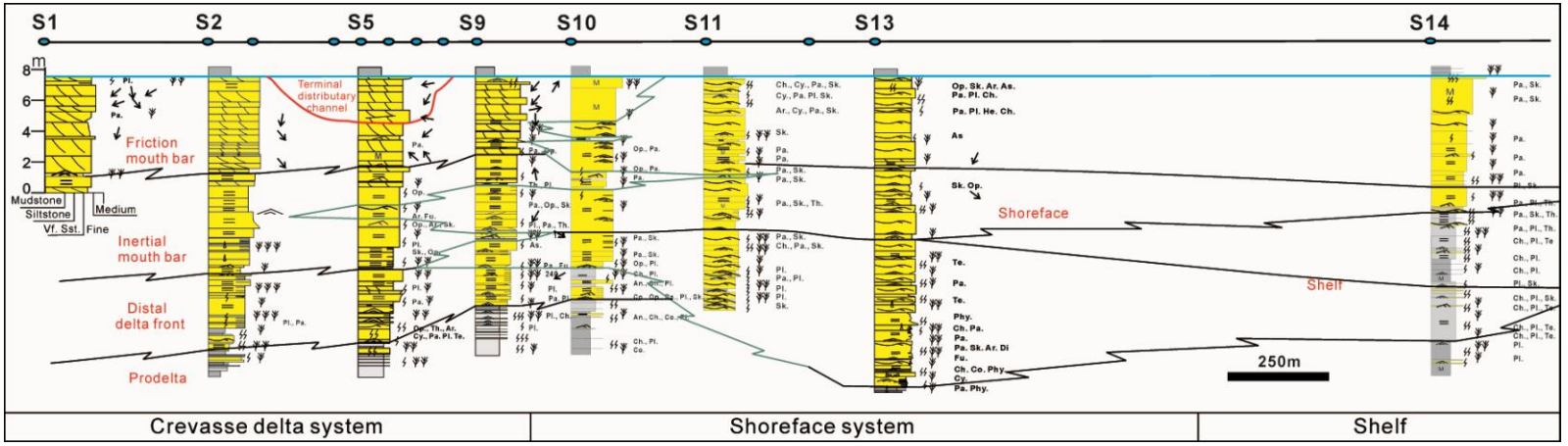

Figure 72. Oblique-dip cross section a-a'. Correlation of measured sections shows the transition of river-dominated delta front facies into wave/storm-dominated shoreface toward the east. See Figure 52B for the location of the cross section.

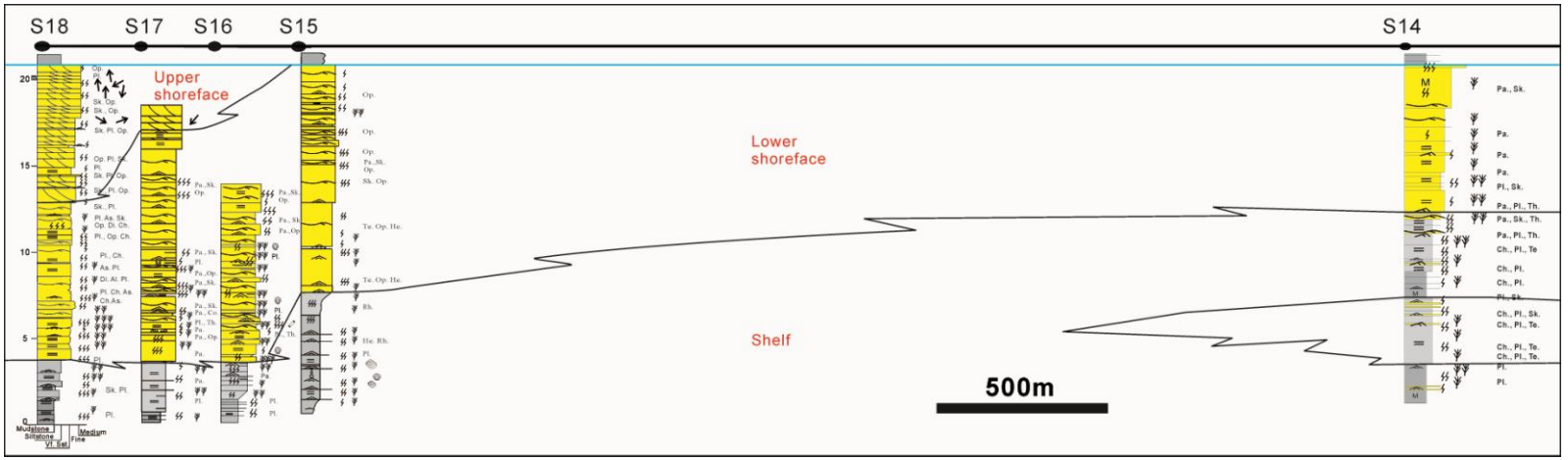

Figure 73. Oblique-strike cross section b-b'. Correlation of measured sections show detailed facies of a shoreface system. See Figure 52B for the location of the cross section. sandstone.

A typical shoreface succession is interpreted and correlated in cross section b-b' (Fig. 73). It is divided into a bioturbated muddy shelf, which passes upward into hummocky cross-stratified lower shoreface overlain by cross-bedded upper shoreface. A gradual lateral transition of upper shoreface to lower shoreface and to shelf from S18 to S14 is also illustrated (Fig. 73).

A detailed paleogeography is constructed based on paleocurrent data, clinoform data, depositional facies analysis from this study, and previous studies, (Fig. 74). A regional delta prograded toward the northeast and a shoreface system in a northwest-southeast orientation are recognized, which are the same as interpretated by Li et al. (2011) and Zhu et al. (2012). However, the regional delta is river-dominated and show no obvious southeastward deflection, as indicated by the radiating pattern of the paleocurrents (Fig. 71). A crevasse delta prograding toward the west is interpreted in the Coalmine Wash area based on the fact it prograded in the opposite direction to the regional deltaic system. A distributary channel is interpreted to have branched away from the trunk river and fed the crevasse delta. The river-dominated nature of the crevasse delta and its closeness and sharp facies change to the shoreface system, indicates that the crevasse delta was probably partially protected by a wave-formed barrier system toward the northwest (Fig. 74).

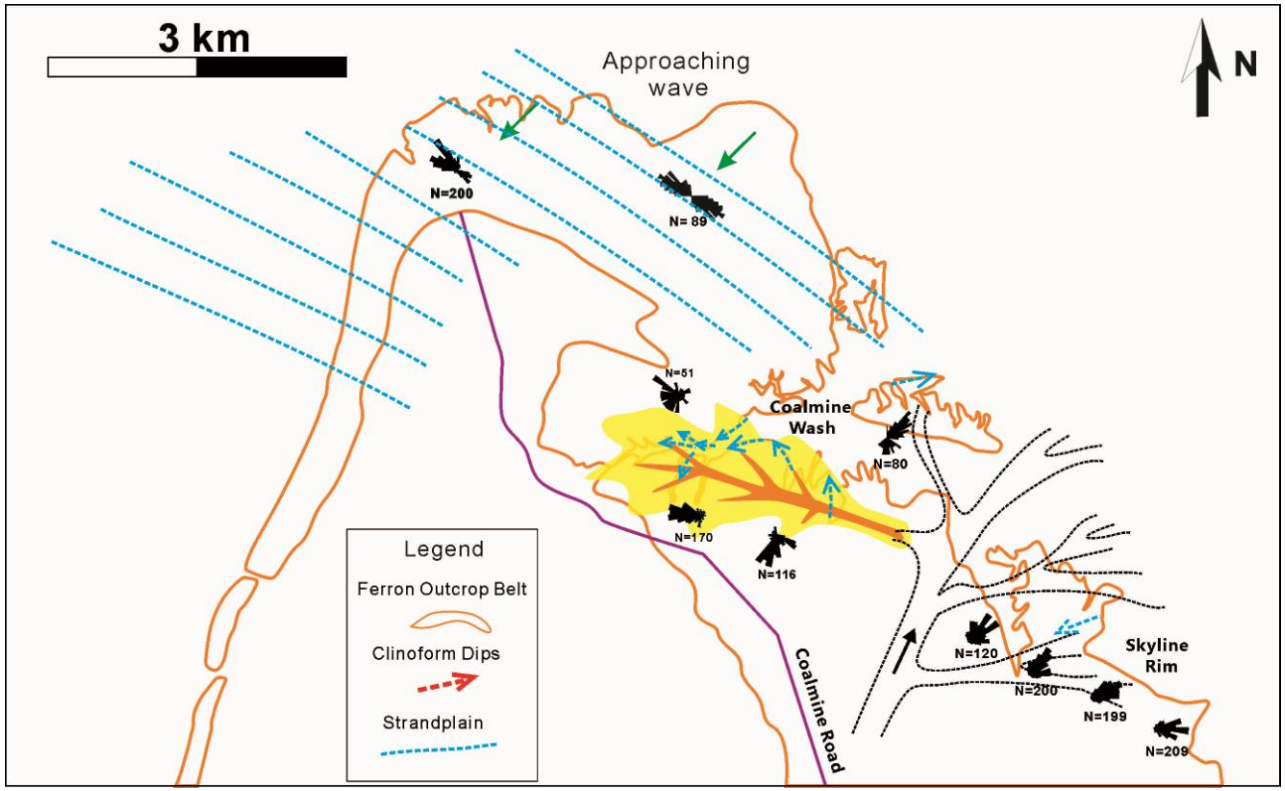

Figure 74. Schematic paleogeographic reconstruction of Parasequence 6a, based on paleocurrent data, clinform data, and depositional facies analysis in this study. It shows that a regional delta prograded toward the northeast. A crevasse delta, prograding toward the west and northwest, was fed by a distributary channel branching away from the trunk channel. The crevasse delta was partially protected by a barrier system to the northeast, where wave approached the shoreline from the northeast.

4.7 Mouth-bar Facies Architecture

4.7.1 Mouth-bar Accretion Pattern

Facies architectural analysis and paleocurrent data show that mouth bars in the Ferron Notom Delta accreted downstream, laterally and upstream.

Lateral accretion: Lateral accretion is the most commonly mouth-bar accretion pattern in this study. It accounts for more than 50% of all mouth bars and is present mostly at the upper part of the parasequence. Cross sections 1, 2, 3, 7, and 8 show examples of lateral accretion of mouth bars, with clinoform dip direction perpendicular to paleocurrent directions (Figs. 65, 67, 68, 71, 75, and 76). For example, in cross section 1, mouth bars accreted toward the southwest, following the migration of the terminal distributary channel (Fig. 67). Paleocurrent direction is out of the outcrop toward the northwest (Fig. 71).

Upstream accretion: Only one example of upstream accretion was observed and accounts for about 10% of mouth-bar deposits. It is present at the top of the parasequence and is characterized by opposite dip directions of cross beds and clinoforms. In cross section 9, clinoforms dip towards the west and the cross beds composing the clinothems dip toward the east (Figs. 71 and 77). Consequently, the mouth bars accreted in an opposite direction to the river flow direction and thus are interpreted to represent upstream accretion. Similar accretion patterns have been documented in the Atchafalaya delta (Van Heerden and Roberts 1988; Olariu and Bhattacharya 2006), the Wax Lake delta (Wellner et al. 2005), the Last Chance Delta (Bhattacharya and Davies 2004) and the Panther Tongue (Olariu et al. 2005). Numerical experiments show that upstream accretion represents the late stage of

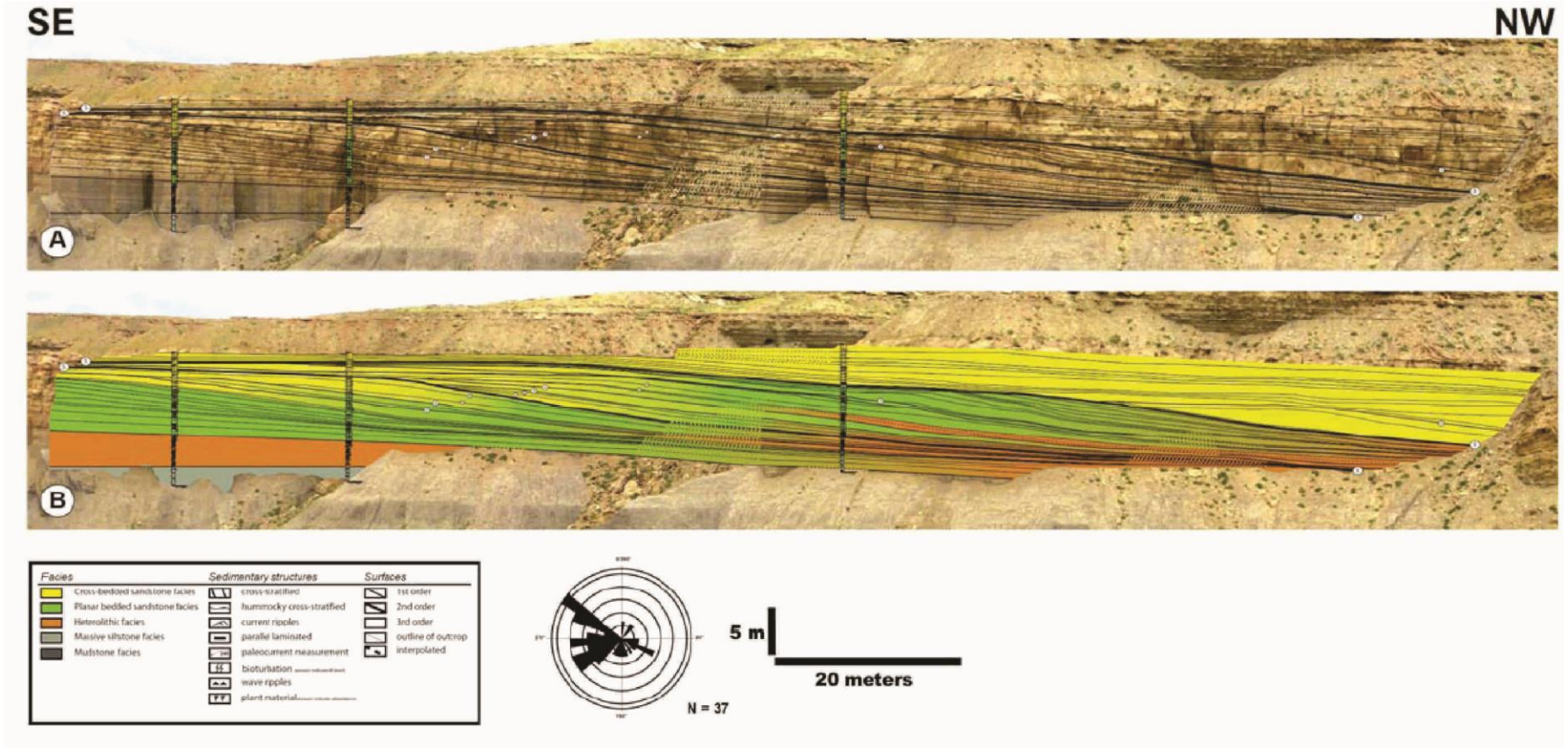

Figure 75. A). Photomosaic and B) Bedding diagram of cross section 7 showing that clinoforms dip toward the northwest and paleocurrents are toward the southwest, indicating lateral accretion of mouth bars. From Ahmed et al. in review. See Figure 52C for location of the cross section.

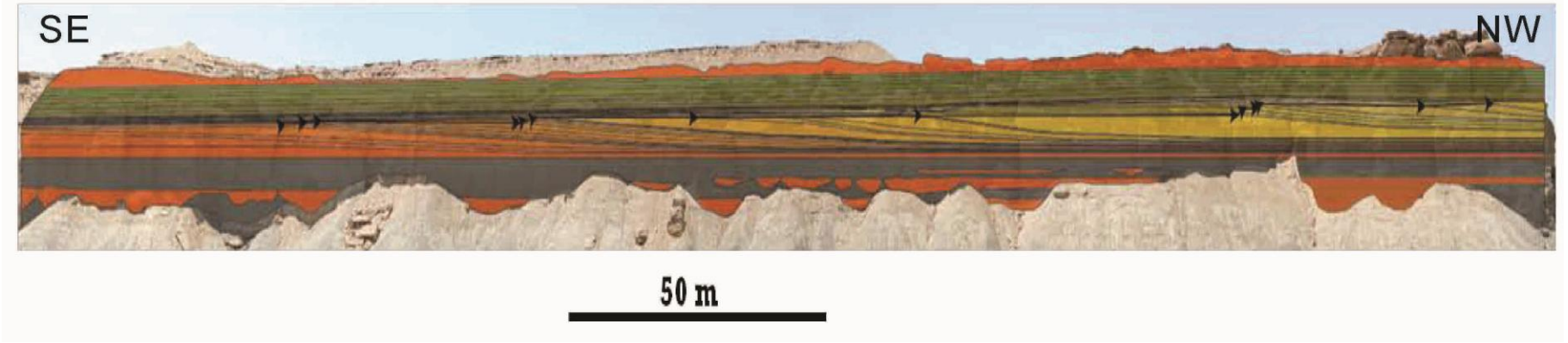

Figure 76. A). Photomosaic and B) Bedding diagram of cross section 8 showing clinoforms dipping toward the northwest. From Garza (2011). See Figure 52C for location of the cross section.

mouth bar evolution (Edmonds and Slingerland 2007). It is likely to result in choking andsubsequent abandonment of distributary channels and may trigger upstream avulsion (Bhattacharya and Davies 2004; Edmonds and Slingerland 2007). In cross section 9, the mouth-bar deposits are underlain by an erosional surface, which is interpreted to be terminal distributary channels.

Downstream accretion: Downstream accretion accounts for about 40% of the mouth-bar facies in this study. It is characterized by the same dip directions of clinoforms and cross beds. Cross sections 4, 5, 6, and 10 show examples of downstream accretion (Fig. 69, 71, 78 and 79). In cross section 5, clinoforms dip toward the west with paleocurrents toward southwest (Figs. 78 and 71). In cross section 6, clinforms dip toward the west and paleocurrent direction is west as well (Fig. 79).

Figure 80 shows a schematic model illustrating mouth-bar accretion pattern as observed in this study. Friction-dominated bars are deposited at the river mouth and in relatively shallow water. They are composed of mostly cross beds. The inner side (upstream) of these friction-dominated mouth bars is characterized by upstream accretion, while the outer side (downstream) of the mouth bars is characterized by downstream and lateral accretion. Inertial bars are fed by hyperpycnal flows, which bypassed the river mouth and deposited at the foot of the slope. They are characterized by large-scale low-angle clinoforms and are internally composed of planar and quasi-planar beds.

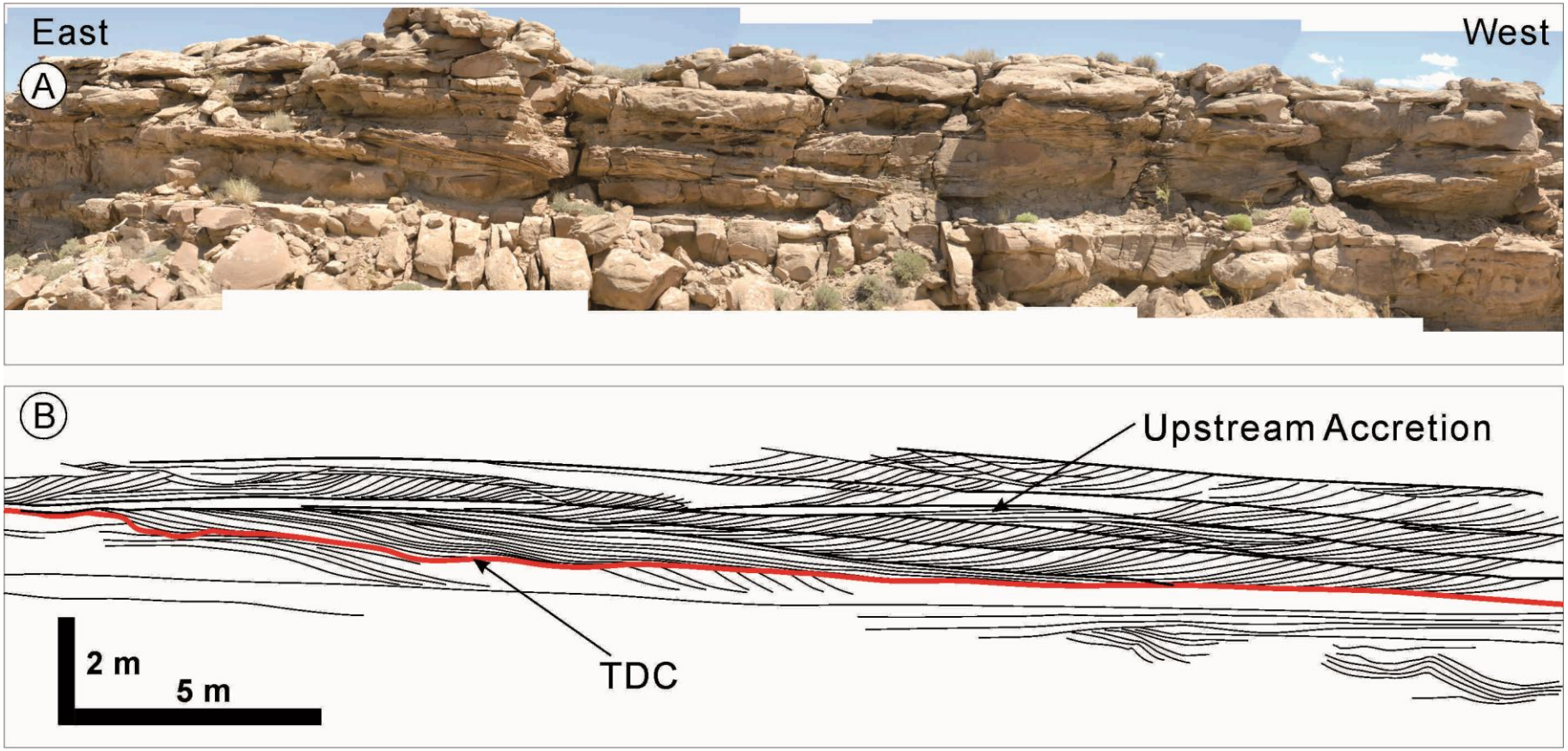

Figure 77. A). Photomosaic and B) Bedding diagram of cross section 9 showing a terminal distributary channel as marked with a red line. The terminal distributary channel is filled with upstream accreting mouth-bar deposits with accretion surfaces dipping toward the right and internal cross beds dipping toward the left. See Figure 52C for location of the cross section.

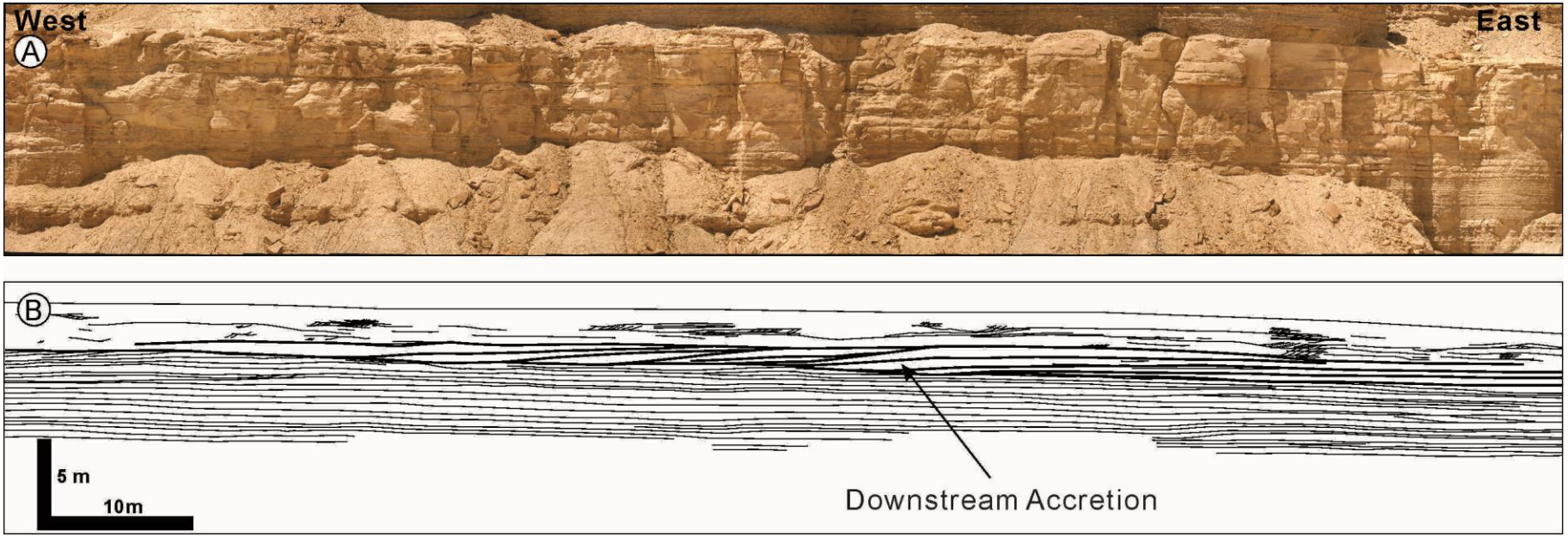

Figure 78. A) Photomosaic of cross section 5 B) Bedding diagram of cross section 5 showing an example of downstream accretion of mouth bars. The basal planar beds change up to meter-scale clinoforms accreting toward the west. Paleocurrent direction is also toward the west. See Figure 52C for the location of the cross section. See Figure 72 for the paleocurrent pattern in this area.

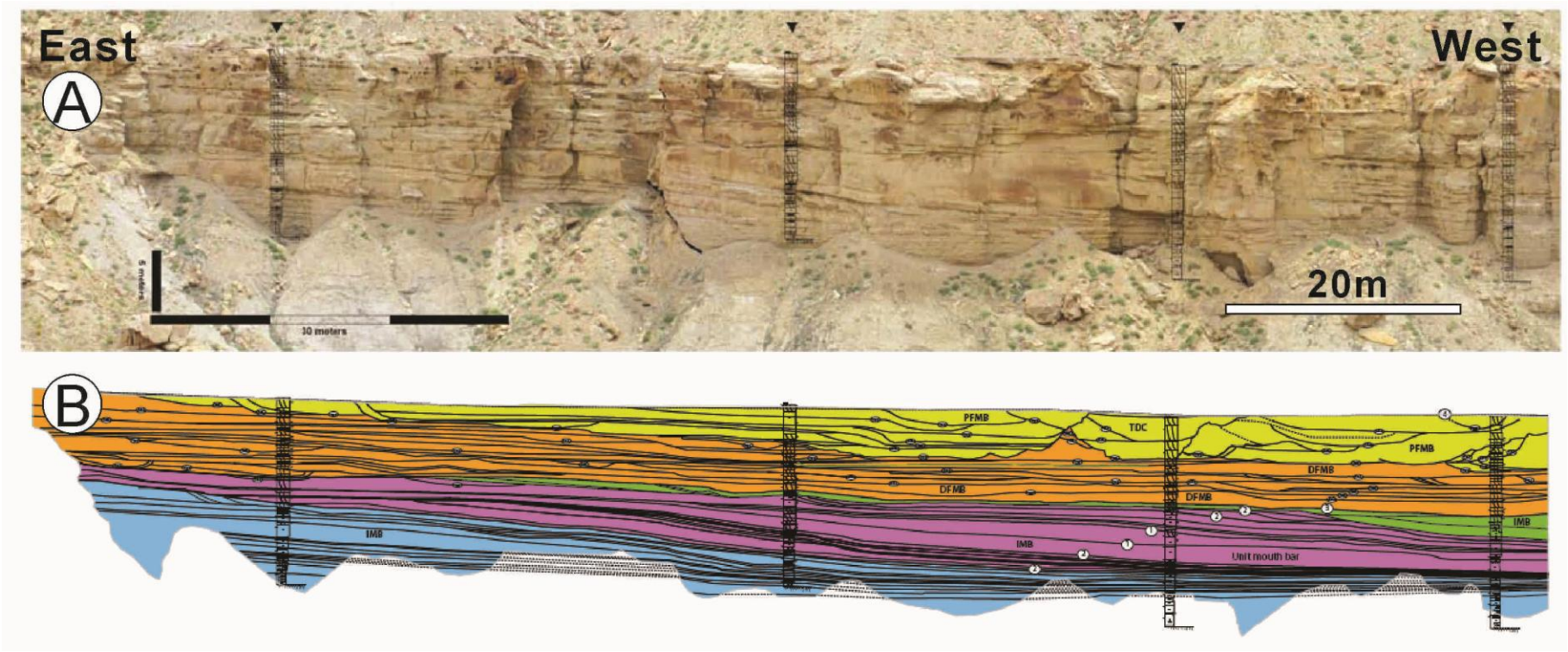

Figure 79. A). Photomosaic and B) Bedding diagram of cross section 6 showing that clinoforms dip toward the northwest. The paleocurrent is toward the northwest (Fig. 71) which indicates that these mouth bars accreted downstream. From Ahmed et al. in review. See Figure 52C for location of the cross section.

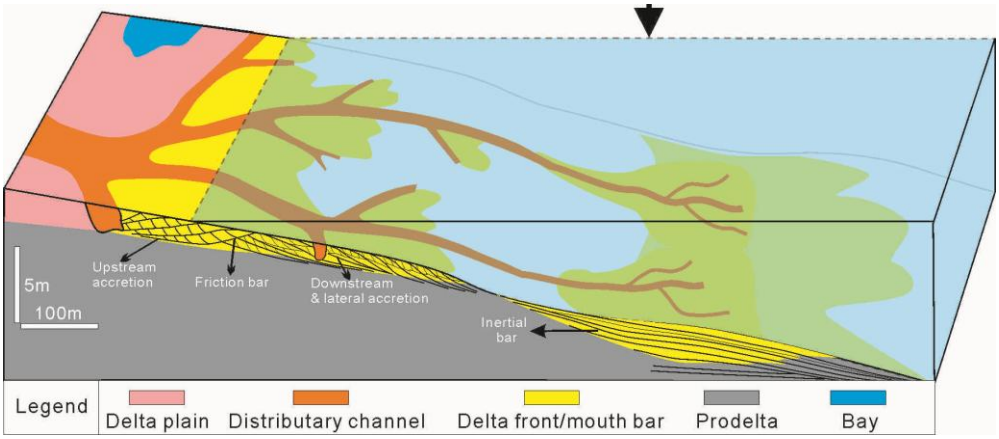

Figure 80. Block diagram illustrating mouth-bar depositional models and accretion patterns.

4.7.2 Mouth-bar Depositional Processes

The coupled inverse and normal graded beds observed in both prodela mudstone and delta-front sandstones and the ripple-planar-ripple successions in the delta-front sandstones suggest hyperpycnal deposits (Mulder et al. 2001; Mulder et al. 2003; Lamb et al. 2008; Myrow et al. 2008; Bhattacharya and MacEachern 2009; Olariu et al. 2009). The traction-dominated structures (planar bedding and ripple cross lamination) and the detached nature indicate that these hyperpycnal flows are inertia-dominated. Also, the inertial bars are assumed to scale to the thickness of the hyperpycnal plume. Maximum depth of terminal distributary channels is thought to be about 5 m. Consequently, the flow thickness of the hyperpycnal plume is probably less than 5 m, which is much less than their inferred depositional depth (10 m).

Wright (1977) pointed out that the degree to which the river effluent is turbulent or buoyant depends on the densimentric Froude number ***F'*** given in the following equation:

$$F' = U/\sqrt{\gamma g h'}$$

Where U is the mean velocity of the outflow and

$$\gamma = 1 - \rho_f / \rho_s$$

where ρ_f and ρ_s are respectively the density of effluent and ambient fluids; g is acceleration of gravity; h' is the depth of the density interface. Inertia and turbulence are suppressed when F' is close to or less than 1. Turbulence and inertia increase in importance as F' exceeds 1.

The average density for sea water ρ_s =1.025 kg/m^3. The critical sediment concentration for plunging plumes in the marine environments range from 36-43 kg/m^3 (Mulder et al. 2003). We take the average of 40 kg/m^3, which yields 1.04 kg/m^3 for the density of the sediment loaded fresh water.

calculating γ=1.04-1.025=0.015

g$\approx$10 m/s^2 and h$'$=5 m as indicated by the deepest terminal distributary channels identified in this study and U is estimated to be 1.5 m/s using the method by Bhattacharya and Tye (2004) and then calculating

F'=5/$\sqrt{0.015 * 10 * 5}$=1.73, which indicates that the flow is supercritical.

In actuality, the density of ambient water surrounding a delta is probably less than the average density for sea water, due to the mixing and dilution by fresh river water (Mulder et al. 2003; Bhattacharya and MacEachern 2009). The critical suspended concentrations of the river plume for hyperpycnal flows could be much lower than normal values when convective instability is considered (Mulder et al. 2003). Consequently, γ could be much smaller than the normal value, which makes F'>>1. When F'>1, the hyperpycnal flow is inertia- and turbulence-dominated (Bhattacharya 2010; Ahmed et al. in review).

The inertia-dominated bars are interpreted to have been deposited in about 10 m of water. The progradation and aggradation of these planar bedded and large-scale

low-angle clinothems resulted in shallowing of the water seaward of the river mouth. Over this platform built up by these inertial bars, river plumes are dominated by frictional forces. Distributary channels became bifurcation-dominated and started shifting laterally (Olariu and Bhattacharya 2006; Turner and Tester 2006; Ahmed et al. in review). Upstream accretion occurred in this stage of mouth-bar evolution, which resulted in choking of some distributary channel and abandonment of associated mouth bar or delta lobes (Bhattacharya and Davies 2004; Edmonds and Slingerland 2007) (Fig. 80).

4.7.3 Mouth-bar and Terminal Distributary Channel Geometries

Inertia-dominated bars are commonly about 1-5 meter thick and at least a few hundred meters long. They are characterized by low-angle clinoforms. Friction-dominated mouth bars are 2-3 meter thick and no more than a few tens of meters long. The dimensions of these bar features are analogous to the smallest scale unit mouth bars that were documented in Wax Lake delta (Wellner et al. 2005). Based on the examples in this study, terminal distributary channel deposits are less than 5 meter thick and less than a few tens of meters wide. The width/thickness ratio of terminal distributary channels range from 10 to 20. They are relatively small compared to the lower delta-plain distributary channel in the Notom delta (20-50) (Li and Bhattacharya in review) and those pure fluvial channels in the alluvial plain and incised valley systems (Li et al. 2010).

4.8 Discussion

4.8.1 Paleogeographic Reconstruction

A new paleogeograpic reconstruction is made based on this study (Fig. 81C). Comparing with the two previously proposed models by Li et al. (2011) (Fig. 81A) and Zhu (2010) (Fig. 81B), there are a few aspects that make this interpretation more convincing.

Firstly, the paleocurrent data of the river-dominated part of the delta indicates a radiating pattern, which is typical of a river-dominated delta. In contrast to the asymmetrical model by Li et al. (2011) where he showed mouth bars greatly deflected toward the southeast due to longshore current. Paleocurrent data in this study do not indicate any obvious deflection of the delta (Fig. 74).

Secondly, Li et al. (2011) explained that the absence of lagoonal and bayfill deposits was due to the following transgression, which reworked previous fine-grained deposits on the top part of the delta. However, the distributary channel facies, upstream accretion of mouth bars, and the clinoform geometries documented in this study indicate that the delta was top-preserved instead of top-truncated. This indicates that, if there were muddy and lagoonal and bayfill deposits, they would be preserved in the rock record instead of being winnowed away (Fig. 81).

Thirdly, the thickness and dimension of the crevasse delta documented in this study makes it unlikely to be a bayhead delta that prograded into a lower delta-plain lagoon, as is commonly seen in down drift side of modern asymmetrical deltas. Instead, we interpreted it to be part of the main delta, which prograded into a large bay.

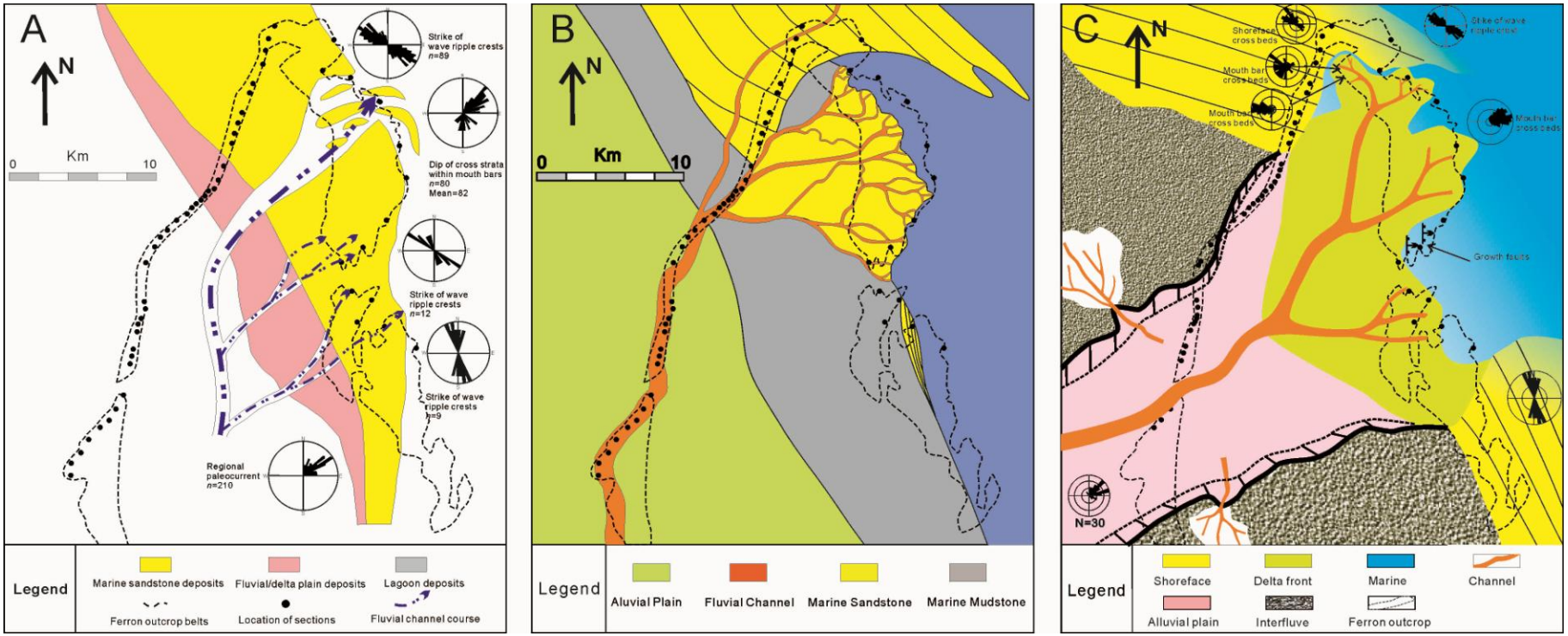

Figure 81. Schematic diagrams showing the evolution of paleogeographic reconstruction evolution of Parasequence 6a. A) Asymetrical delta model proposed by Li et al. (2010). B) Bayhead delta model proposed by Zhu (2010). C) Bayhead delta model based on this study with more details than the one proposed by Zhu (2010).

4.8.2 Heterogeneity of Delta-front Deposits

Four different types of mudstones are identified in this study based on facies analysis from detailed bedding diagrams and measured sections. Their geometry and architectural relationships with delta-front mouth-bar deposits are shown in a conceptual model (Fig. 82).

The first type of muddy facies is distal delta-front and prodelta mudstone (Figs. 55, 56 and 82). They are relatively thick (some more than 1 meter thick) and extensive (up to hundreds of meters). They are interpreted to be deposited partially out of suspension and partially from turbidity currents.

The second type of mudstone is mud plugs deposited at the back side of unit bars (Figs. 64 and 82). They are confined to the scour of the back side of the mouth bars, with a thickness of centimeters to a few decimeters and lateral extent of less than a few meters. They are interpreted to be deposits of suspension fall out of fine-grained sediments and survived the following flood event. They were deposited and only preserved in a topographic low area.

The third type of mudstone is mud drapes separating mouth bars (Figs. 66 and 82). They are interpreted to be deposited out of suspension (Nemec 1995). Some of these mudstones are possibly fluid muds. Fluid mud deposits are characterized by homogeneous and structureless mudstone layers, with a thickness >0.5 cm (in contrast to those deposited slowly out of suspension, which are commonly thinner). They may drape the lower part of the foresets of mouth bars or separate the whole mouth-bar assemblage (Figs. 67 and 82). Their dimensions depend on mouth-bar and bar-assemblage dimensions. They commonly have a thickness larger than a few

centimeters and lateral extent larger than a few meters. They are interpreted to be deposited during the low stage of the associated river, during which the mixing of salt water and fresh water-induced flocculation of clays.

The fourth type of muddy facies is abandoned terminal distributary channel deposits (Figs. 68 and 82). They may or may not show a channel form due to later compaction. They are conformable with lateral mouth-bar deposits at least from one side. They have a thickness of tens of centimeters and lateral extent of up to ten meters. They are commonly developed in response to upstream accretion of mouth bars further downstream, which block the channel (Olariu and Bhattacharya 2006).

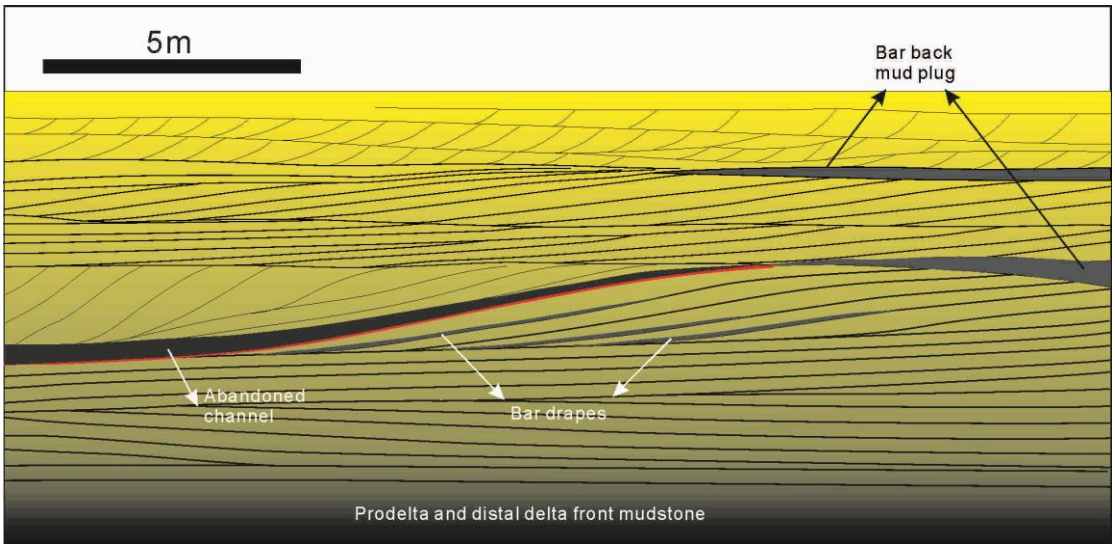

Figure 82. A schematic diagram showing the mudstone facies identified in the delta-front mouth-bar deposits.

4.9 Conclusions

1) A river-dominated crevasse delta is mapped with measured sections, paleocurrents, and clinoforms. It prograded toward the west while the regional delta prograded toward the northeast. It was partially protected from marine-influence by a wave-formed barrier shoreface system.

2) Four facies are identified in the river-dominated part of the delta: they are muddy prodelta, heterolithic distal delta front, and sandy proximal delta front.

3) The proximal delta-front facies is divided into basal planar-bedded sandstone, which is interpreted to be inertia-dominated mouth bars, upper dune-scale cross bedded sandstone, which is interpreted to be friction-dominated mouth bars, and large-scale low-angle cross-bedded sandstone, which is interpreted to be transitional facies between inertia-dominated and friction-dominated facies.

4) Coupled inverse grading and normal grading, and ripple-planar-ripple successions indicate that hyperpycnal flow deposition played an important role in building a delta lobe. These hyperpycnal flows are inertia-dominated based on the fact that their deposits are detached from the river mouth and are characterized by traction-dominated structures.

5) A systematic decrease in dimensions of the cross-bed sets is documented in the transitional large-scale low-angle cross-bed sets, which is interpreted to be mainly due to the gradual aggradation and shallowing of the water (the depth of the interface of effluent and ambient water) and consequently increasing dominance of frictional forces.

6) Inertial bars are characterized by downstream accretion, friction-dominated mouth bars show lateral, downstream and upstream accretion. Upstream accretion is only observed on the top of the parasequence in the friction-dominated facies.

7) The heterogeneity of delta-front deposits is mainly from the result of four types of muddy facies. They are distal delta-front and prodelta mudstone, mouth-bar drapes deposited from suspension or fluid muds, mouth-bar back mud plugs, and abandoned channel deposits.

CHAPTER 5 Conclusions

This study presents detailed facies architectural study of incised valley systems, distributary channel systems, and delta-front mouth-bar deposits from the Cretaceous Ferron Notom Delta.

The compound incised valley system study provides evidence that they are more complex than existing models. This study shows that they are possibly filled during the subsidiary transgressions during a long term relative sea-level fall, which is different from conventional understanding that they are exclusively degradational during relative sea-level fall.

The lower delta-plain distributary channel system study, documented a branching distributary channel system. Detailed facies architectural study reveals its internal facies varability and relationship with associated levee, bay and crevasse delta facies. A new method of estimating the branching order of deltaic distributary systems is developed and for the first time applied in this study.

Detailed facies architectural study in Parasequence 6a, together with paleocurrent data and clinoform data enabled mapping of a crevasse delta. This study documented examples of mouth-bar accretion patterns (downstream, upstream and lateral) that are analogues to middle-sized modern deltas. Inertia and friction effluent forces are interpreted. This study provides evidence that supports the bayhead delta model and not the asymmetrical model proposed by previous studies.

ADAMS, M.M., and BHATTACHARYA, J.P., 2005, No change in fluvial style across a sequence boundary, Cretaceous Blackhawk and Castlegate Formation of central Utah, U.S.A.: Journal of Sedimentary Research, v. 75, p. 1038-1051.

AHMED, S., BHATTACHARYA, J.P., GARZA, D., and LI, Y., in review, Construction of an inertia- to friction-influenced delta front, Turonian Ferron Sandstone, Utah: Journal of Sedimentary Research.

AINSWORTH, R.B., and WALKER, R.G., 1994, Control of estuarine valley-fill deposition by fluctuations of relative sea-level, Cretaceous Bearpaw-Horseshoe canyon transition, Drumheller, Alberta, Canada, *in* Dalrymple, R.W., Boyd, R., and Zaitlin, B.A., eds., Incised-Valley Systems: Origin and Sedimentary Sequences: SEPM, Special Publication 51, p. 159-174.

AITKEN, J.F., and FLINT, S.S., 1994, High-frenquency sequences and the nature of incised-valley fills in fluival systems of the breathitt group (Pennsylvanian), Appalachian foreland basin, eastern Kentucky, *in* Dalrymple, R.W., Boyd, R., and Zaitlin, B.A., eds., Incised-Valley Systems: Origin and Sedimentary Sequences: SEPM, Special Publication 51, p. 344-359.

ALLEN, G.P., and POSAMENTIER, H.W., 1993, Sequence stratigraphy and facies models of an incised valley fill: the Gironde estuary, France: Journal of Sedimentary Petrology, v. 63, p. 378-391.

ALLEN, J.R.L., 1965, The sedimentation and paleogeography of the Old Red Sandstone of Anglesy, North Wales: Proceedings of the Yorkshare Geological Society, v. 35, p. 139-185.

ALLEN, J.R.L., 1973, A classification of climbing ripples: Journal of Geological Society London, v. 129, p. 537-541.

ARDIES, G.W., DALRYMPLE, R.W., and ZAITLIN, B.A., 2002, Controls on the geometry of incised valleys in the Basal Quartz Unit (Lower Cretaceous), Western Canada sedimentary basin: Journal of Sedimentary Research, v. 72, p. 602-618.

ARMSTRONG, R.L., 1968, Sevier orogenic belt in Nevada and Utah: Geological Society of America Bulletin, v. 79, p. 429-458.

ARNOTT, R.W.C., 1993, Quasi-planar-laminated sandstone beds of the Lower Cretaceous Bootlegger Member, North-central Montana: evidence of combined-flow sedimentation: Journal of Sedimentary Petrology, v. 63, p. 488-494.

ASHLEY, G.M., and SHERIDAN, R.E., 1994, Depositional model for valley fills on a passive continental margin, *in* Dalrymple, R.W., Boyd, R., and Zaitlin, B.A., eds., Incised-Valley Systems: Origin and Sedimentary Sequences: SEPM, Special Publication 51, p. 266-285.

AZEREDO, A.C., WRIGHT, V.P., and RAMALHO, M.M., 2002, The middle-late Jurassic forced regression and disconformity in central Portugal: eustatic, tectonic and climatic effects on a carbondate ramp system: Sedimentology, v. 49, p. 1339-1370.

BARTON, M.D., TYLER, N., and ANGLE, E.S., 2004, Facies arthitecture and permeability structure of Valley-Fill sandstone bodies, Cretaceous Ferron Sandstone, Utah, *in* Chidsey, T.C., Adams, R.D., and Morris, T.H., eds., The Fluvial-deltaic Ferron Sandstone: Regional to Wellbore Analog Studies and Application to Reservoir Modeling: AAPG Studies in Geology 50, p. 383-404.

BATES, C.C., 1953, Rational theory of delta formation: AAPG Bulletin, v. 37, p. 2119-2162.

BELKNAP, D.F., KRAFT, J.C., and DUNN, R.K., 1994, Transgressive valley-fill lithosomes: Delaware and Maine, *in* Dalrymple, R.W., Boyd, R., and Zaitlin, B.A., eds., Incised-Valley Systems: Origin and Sedimentary Sequences: SEPM, Special Publication 51, p. 304-320.

BEST, J.L., ASHWORTH, P.J., BRISTOW, C.S., and RODEN, J., 2003, Three-dimensional sedimentary architecture of a large mid channel sand braid bar, Jamuna River, Bangladesh: Journal of Sedimentary Research, v. 73, p. 516-530.

BHATTACHARYA, J.P., 2006, Deltas, *in* Walker, R.G., and Posamentier, H., eds., Facies Models Revisited SEPM, Special Publication No. 84, p. 237-292.

BHATTACHARYA, J.P., 2010, Deltas, *in* James, N.P., and Dalrymple, R.W., eds., Facies Models 4: The Geological Associaion of Canada, p. 232-264.

BHATTACHARYA, J.P., 2011, Practical problems in the application of the sequence stratigraphic method and key surfaces: integrating observations from ancient fluival-deltaic wedges with Quaternary and modelling studies: Sedimentology, v. 58, p. 120-169.

BHATTACHARYA, J.P., and DAVIES, R.K., 2004, Sedimentology and structure of growth faults at the base of the Ferron Sandstone Member along Muddy Creek, Utah: Searching for modern Ferron analogs and applications to subsurface interpretation, *in* Chidsey, T.C., Adams, R.D., and Morris, T.H. eds, The Fluvial-deltaic Ferron Sandstone: Regional to Wellbore Scale Outcrop

Analog Studies and Applications to Reservoir Modeling, v. AAPG Studies in Geology 50, p. 279-304.

BHATTACHARYA, J.P., and GIOSAN, L., 2003, Wave-influenced deltas: geomorphological implications for facies reconstruction: Sedimentology, v. 50, p. 187-210.

BHATTACHARYA, J.P., and MACEACHERN, J.A., 2009, Hyperpycnal rivers and prodeltaic shelves in the Cretaceous Seaway of North America: Journal of Sedimentary Research, v. 79, p. 184-209.

BHATTACHARYA, J.P., and TYE, R.S., 2004, Searching for modern Ferron analogs and applications to subsurface interpretation, *in* Chidsey, T.C., Adams, R.D., and Morris, T.H. eds, The Fluvial-deltaic Ferron Sandstone: Regional to Wellbore Scale Outcrop Analog Studies and Applications to Reservoir Modeling: AAPG Studies in Geology 50, p. 39-57.

BLUM, M.D., 1993, Genesis and architecture of incised valley fill sequences: A late Quaternary example from the Colorado River, gulf coastal plain of Texas, *in* Weimer, P., and Posamentier, H.W., eds., Siliciclastic Sequence Stratigraphy: Recent Developments and Applications: AAPG Memoir 58, p. 259-283.

BLUM, M.D., and ASLAN, A., 2006, Signatures of climate vs. sea-level change within incised valley-fill successions: Quaternary examples from the Texas Gulf Coast: Sedimentary Geology, v. 190, p. 177-211.

BLUM, M.D., and VALASTRO, S.J., 1994, Late Quaternary sedimentation, lower Colorado River, Gulf Coastal Plain of Texas: Geological Society of America Bulletin, v. 106, p. 1002-1016.

BOUMA, A.H., and SCOTT, E., 1964, Sedimentology of some flysch deposits. A graphic approach to facies interpretation: Amsterdam, Elsevier, 168 p.

BOYD, R., DALRYMPLE, R.W., and ZAITLIN, B.A., 2006, Estuarine and incised valley facies models, *in* Walker, R.G., and Posamentier, H., eds., Facies Models Revisited: SEPM, Special Publication 84, p. 171-235.

BOYD, R., and DIESSEL, C.F., 1994, The application of sequence stratigraphy to non-marine clastics and coal: Second High Resolution Sequence Stratigraphy Conference, Tremp, Proceedings, p. 13-20 (Referred from Boyd et al. 2006).

BRIDGE, J.S., 2000, The geometry, flow patterns and sedimentary processes of Devonian rivers and coasts, New York and Pennsylvaina, USA, *in* Friend, P.F. and Williams, B.P.J. eds., New Perspectives on the Old Red Sandstone: Geological Society of London, Special Publication 180, p. 85-108.

BRIDGE, J.S., 2003, Rivers and Floodplains: Forms, Processes, and Sedimentary Record.: Oxford U.K., Blckwell Science, 491 p.

BRIDGE, J.S., 2006, Fluvial facies models: recent developments, *in* Walker, R.G., and Posamentier, H. eds, Facies Model Revisited: SEPM, Special Publication 84, p. 83-168.

CHERVEN, V.B., 1978, Fluvial and deltaic facies in the Sentinel Butte Formation central Williston basin: Journal of Sedimentary Petrology, v. 48, p. 159-170.

CLIFTON, H.E., 2006, A reexamination of facies models for clastic shoreline, *in* Walker, R.G., and Posamentier, H. eds, Facies Model Revisited: SEPM, Special Publication 84, p. 293-337.

COLEMAN, J.M., and PRIOR, D.B., 1982, Deltaic environments of deposition, *in S*cholle, P.A., and Spearing, D., Sandstone Depositional Environments: AAPG Memoir v. 31, p. 139-178.

CORBEANU, R.M., WIZEVICH, M.C., BHATTACHARYA, J.P., ZENG, X., and MCMECHAN, G.A., 2004, Three-dimensional architecture of ancient lower delta-plain point bars using ground-penetrating radar, Cretaceous Ferron Sandstone, Utah, *in* Chidsey, T.C., Adams, R.D., and Morris, T.H., eds., The Fluvial-deltaic Ferron Sandstone: Regional to Wellbore Scale Outcrop Analog Studies and Applications to Reservoir Modeling: AAPG Studies in Geology v. 50, p. 427-449.

COTTER, E., 1975, Deltaic deposits in the Upper Cretaceous Ferron Sandstone, Utah, *in* Broussard M.L.S. ed., Deltas, Models for Exploration: Houston Geological Society, p. 471-484.

DALRYMPLE, R., ZAITLIN, B.A., and BOYD, R., 1992, Estuarine facies models: conceptual basis and stratigraphic implications: Journal of Sedimentary Petrology, v. 62, p. 1130-1146.

DALRYMPLE, R.W., 2010, Tidal depositional systems, *in* James, N.P. and Dalrymple, R.W., eds., Facies Models 4: The Geological Associaion of Canada, p. 201-231.

DALRYMPLE, R.W., BOYD, R., and ZAITLIN, B.A., 1994, History of research, types and internal organization of incised-valley systems: introduction to the volume, *in* Dalrymple, R.W., Boyd, R., and Zaitlin, B.A., eds., Incised-Valley Systems: Origin and Sedimentary Sequences: SEPM, Special Publication 51, p. 3-10.

DALRYMPLE, R.W., and CHOI, K., 2007, Morphologic and facies trends through the fluvial-marine transition in tide-domianted depositional systems: A schematic framework for enviromental and sequence-stratigraphic interpretation: Earth-Science Reviews, v. 81, p. 135-174.

DECELLES, P.G., and GILES, K.A., 1996, Foreland basin system: Basin Research, v. 8, p. 105-123.

DOLGOPOLOVA, E.N., and MIKHAILOV, V.N., 2008, Mathematical modeling of the formation and progradation of a river mouth bar into a sea: case study of Danube delta branches: Water Resources, v. 35, p. 287-296.

DUMARS, A.J., 2002, Distributary mouth bar formation and channel bifurcation in the Wax Lake Delta, Atchafalaya Bay, Louisiana [unpublished M. S. thesis]: Louisiana State University, Baton Rouge, Louisiana, 94 p.

EDMONDS, D.A., HOYAL, D.C.J.D., SHEETS, B.A., and SLINGERLAND, R.L., 2009, Predicting delta avulsions:Implications for coastal wetland restoration: Geology, v. 37, p. 759-762.

EDMONDS, D.A., and SLINGERLAND, R.L., 2007, Mechanics of river mouth bar formation: Implications for the morphodynamics of delta distributray networks: Journal of Geophysical Research, v. 112, p. 1-14.

EDMONDS, D.A., and SLINGERLAND, R.L., 2008, Stability of delta distributary networks and their bifurcations: Water Resources Research, v. 44, p. 1-13.

ELLIOTT, T., 1976, The morphology, magnitude and regime of a carboniferous fluvial-distributray channel: Journal of Sedimentary Petrology, v. 46, p. 70-76.

ENGE, H.D., HOWELL, J.A., and BUCKLEY, S.J., 2010, The geometry and internal architecture of stream mouth bars in the Panther Tongue and the Ferron Sandstoen Members, Utah, U.S.A.: Journal of Sedimentary Research, v. 80, p. 1018-1031.

ETHRIDGE, F.G., 2010, Interpretation of ancient fluvial channel deposits: review and recommendations, *in* Davison, S.K., Leleu, S. and North, C.P. eds., From River to Rock Record: The Preservation of Fluvial Sediments and Their Subsequent Interpretation: SEPM, Special Publication 97, p. 9-36.

FAMUBODE, O.A., BHATTACHARYA, J.P., D'OUZA, D.C., and MONTES, O.A., 2012, Response to accomodation change in channel belt distribution, floodplains, and paleosols: Cretaceous Ferron-Notom Delta, Utah: AAPG Annual Meeting Poster Session.

FAN, H., HUANG, H., ZENG, T.Q., and WANG, K., 2006, River mouth bar formation, riverbed aggradation and channel migration in the modern Huanghe (Yellow) river delta, China: Geomorphology, v. 74, p. 124-136.

FIELDING, C.R., 1984, Upper delta plain lacustrine and fluviolacustrine facies from the Westphalian of the Durham coalfield, NE England: Sedimentology, v. 31, p. 547-567.

FIELDING, C.R., 2010, Planform and facies variability in asymmetric deltas: Facies analysis and depositional architecture of the Turonian Ferron Sandstone in the western Henry Mountains, South-Central Utah, U.S.A.: Journal of Sedimentary Research, v. 80, p. 455-479.

FIELDING, C.R., TUUEMAN, J.D., and ALEXANDER, J., 2005, Sharp-based, flood-dominatd mouth bar sands from the Burdekin river delta of northeastern Australia: extendign the spectrum of mouth-bar facies, geometry , and stacking patterns: Journal of Sedimentary Research, v. 75, p. 55-66.

FITZSIMMONS, R., and JOHNSON, S., 2000, Force regressions: recognition, architecture and genesis in the Campanian of Bighorn Basin, Wyoming, *in* Hunt, D., Gawthorpe, R.L., eds., Sedimentary Responses to Forced Regressions: Geological Society of London, Special Publication 172, p. 113-139.

GANI, M.R., and BHATTACHARYA, J.P., 2007, Basic building blocks and process variability of a Cretaceous Delta: internal facies architecture reveals a more dynamic interaction of river, wave, and tidal processes than is indicated by exteranl shape: Journal of Sedimentary Research, v. 77, p. 284-302.

GARDNER, M.H., 1995, Tectonic and eustatic controls on the strata architecture of mid-Cretaceous stratigraphic sequences, central western interior foreland basin o North America, *in* S.L. Dorobek and G.M.Ross, eds., Stratigraphic Evolution of Foreland Basins: SEPM, Special Publication 52, p. 243-281.

GARRISON, J.R., and VAN DEN BERGH, T.C.V., 2006, Effects of sedimentation rate, rate of relative rise in sea level, and duration of sea-level cycle on the filling of incised valleys: examples of filled and "overfilled" incised valleys from the upper-Ferron Sandstone, Last Chance Delta, east-centeral Utah, U.S.A, *in* Dalrymple, R.W., Leckie, D.A., and Tillman, R.W., eds., Incised

Valleys in Time and Space: SEPM, Special Publication 85, p. 220-239.
GARZA, D., 2010, 3-D facies architecture and mouth bar development of a Food-, Storm-dominated Delta: Cretaceous Ferron Sandstone, Utah [unpublished M.S. thesis]: University of Houston, Houston, TX, 78 p.
GIBLING, M.R., 2006, Width and thickness of fluvial channel bodies and valley fills in the geological record: a literature complilation and classification: Journal of Sedimentary Research, v. 76, p. 731-770.
GOODBRED, S.L.J., and KUEHL, S.A., 2000, Enormous Ganges–Brahmaputra sediment discharge strengthened early Holocene monsoon: Geology, v. 28, p. 1083-1086.
HALE, L.A., 1972, Depositional history of the Ferron Sandstone, central Utah, *in* Baer, J.L., and Callaghan, E. eds., Plateau-basin and Range Transition Zone: Utah Geologic Association Publication 2, p. 115–138.
HALE, L.A., and VAN DE GRAAFF, F.R., 1964, Cretaceous stratigraphy and facies patterns-northeastern Utah and adjacent areas: Intermountain Association Petroleum Geologists Guidebook, 13th Annual Field Conference, p. 115-138.
HAMBERG, L., and NIELSEN, L.H., 2000, Shingled, sharp-based shoreface sanstones: depositional response to stepwised force regression in a shallow basin, Upper Triassic Gassum Formation, Denmark, *in* Hunt, D., and Gawthorpe, R.L., eds., Sedimentary Responses to Forced Regressions: Geological Society of London, Special Publication 172, p. 69-89.
HAMILTON, W.D., SCOTT, D., MARSDEN, G., and BAXTER, B., 2001, Structural and stratigraphic influences on reservoir compartmentalization in low accommodation settings: Basal Quartz A Sandstone, Alderson Lower Mannville "D4D" Pool: Canadian Society of Petroleum Geologist, Annual Convention, Calgary, Program and Abstracts.
HARTLEY, A.J., WEISSMANN, G.S., NICHOLS, G.J., and WARWICK, G.L., 2010, Large distributive fluvial systems: characteristics, distribution, and constrols on development: Journal of Sedimentary Research, v. 80, p. 167-183.
HELLAND-HANSEN, W., and GJELBERG, J.G., 1994, Conceptual basis and variablity in sequence stratigraphy: a different perspective: Sedimentary Geology, v. 92, p. 31-52.
HILL, R.B., 1982, Depositional environments of the Upper Cretaceous Ferron Sandstone south of Notom, Wayne County, Utah: Brigham Young University Geological Study, v. 29, p. 59-83.
HOLBROOK, J.M., and BHATTACHARYA, J.P., in press, Reappraisal of the sequence boudary in time and space: case and considerations for an SU (Subaerial Unconformity) that is not a sediment bypass surface, a time barrier, or an unconformity: Earth and Science Reviews.
HOLBROOK, J.M., SCOTT, R.W., and OBOH-IKUENOBE, F.E., 2006, Base-level buffers and buttresses: a model for upstream versus downstream control on fluvial geometry and architecture within sequences: Journal of Sedimentary Research, v. 76, p. 162-174.
HOPKINS, J.C., 1984, Channel-fill deposits formed by aggradation in deeply scoured, superimposed distributaries of the lower Kootenai Formation (Cretaceous): J. Sed. Petrol., v. 55, p. 42-53.
HOYAL, D.C.J.D., and SHEETS, B.A., 2009, Morphodynamic evolution of experimental cohesive deltas: Journal of Geophysical Research, v. 114, p. 1-18.
HOYAL, D.C.J.D., VAN WAGONER, J., ADAIR, N.L., DEFFENBAUGH, M., LI, D., SUN, T., HUH, C., and GIFFIN, D.E., 2003, Sedimentation from jets: a depositional model for clastic deposits of all scales and environments: AAPG Annual Meeting Extended Abstracts.
IMBRIE, J., HAYS, J.D., and MARTINSON, D.G., 1984, The orbital theory of Pleistocene climate: support from a revised chronology of the marine oxygen isotope record, *in* A.L. Berger ed., Milankovitch and Climate: Reidel Publishing Company, Dordrecht, The Netherlands, p. 269-305.
JEROLMACK, D.J., and SWENSON, J.B., 2007, Scaling relationships and evolution of distributary networks on wave-influenced deltas: Geophysical Research Letters, v. 34, p. 1-5.
JORDAN, D.W., and PRYOR, W.A., 1992, Hierarchical levels of heterogeneity in a Mississippi river meander belt and application to reservoir systems: AAPG Bulletin, v. 76, p. 1601-1624.
KOSTASCHUK, R.A., 1985, River mouth processes in a fjord-delta, British Columbia, Canada: Marine Geology, v. 69, p. 1-23.
LAMB, M.P., MYROW, P.M., LUKENS, C., HOUCK, K., and STRAUSS, J., 2008, Deposits from wave-influenced trubidity currents: Pennsylvanian Minturn Formation, Colorado, U.S.A.: Journal of Sedimentary Research, v. 78, p. 480-498.
LECLAIR, S.F., and BRIDGE, J.S., 2001, Quantitative interpretation of sedimentary structures formed by

river dunes: Journal of Sedimentary Research, v. 71, p. 713-716.
LI, W., 2009, Valleys, facies and sequence stratigraphy of the Ferron Notom Delta, Capital Reef, Utah [unpublished PhD thesis]: University of Houston, Houston, Texas, 139 p.
LI, W., and BHATTACHARYA, J.P., 2011, Architecture and depositional proceses of a forced regressive series in the Turonian Ferron "Notom Delta", southern Utah, U.S.A.: Marine and Petroleum Geology, v. 28, p. 1517-1529.
LI, W., BHATTACHARYA, J.P., and CAMPBELL, C., 2010, Temporal evolution of fluvial systle in a compound incised-valley fill, Ferron "Notom Delta," Henry Mountains region, Utah (U.S.A): Journal of Sedimentary Research, v. 80, p. 529-549.
LI, W., BHATTACHARYA, J.P., ZHU, Y., and GARZA, D., 2011, Evaluating delta asymmetry using three-dimentional facies architecture and ichnological analysis, Ferron 'Notom Delta', Capital Reef, Utah, USA: Sedimentology, v. 58, p. 478-507.
LI, Y., and BHATTACHARYA, J.P., in review, Facies architectural study of a stepped forced regressive compund incisedv valley system in the Ferron Notom Delta, southern Utah, U.S.A.: Journal of Sedimentary Research.
LI, Y., and BHATTACHARYA, J.P., in review, Facies architecture, branching pattern, and paleodischarge of a lower delta-plain distributary channel system in the Cretaceous Ferron Notom Delta, southern Utah, U.S.A.: Sedimentology.
LINDSY, J.F., PRIOR, D.B., and COLEMAN, J.M., 1984, Distributary-mouth bar development and role of submarine landslides in delta growth, South Pass, Mississippi Delta: AAPG Bulletin, v. 68, p. 1732-1743.
LYNDS, R., and HAJEK, E., 2005, Conceptual model for predicting mudstone dimensions in sandy braided-river reserviors: AAPG Bull., v. 90, p. 1273-1288.
MACEACHERN, J.A., BANN, K.L., BHATTACHARYA, J.P., and HOWELL, C.D., 2005, Ichnology of deltas: organism responses to the dynamic interplay of rivers, waves, stroms and tides, *in* Giosan, L., and Bhattacharya, J.P. eds., River Deltas: Concepts, Models and Examples: SEPM, Special Publication 83, p. 49-85.
MACEACHERN, J.A., PEMBERTON, S.G., GINGRAS, M.K., and BANN, K.L., 2010, Ichnology and facies models, *in* James, N.P. and Dalrymple, R.W., eds., Facies Models 4: The Geological Associaion of Canada, p. 19-58.
MARTINSEN, O.J., 1990, Fluvial, inertia-dominated deltaic deposition in the Namurian (Carboniferous) of northern England: Sedimentology, v. 37, p. 1099-1113.
MARTINSEN, O.J., 1994, Evolution of an incised valley fill, the Pine Ridge Sandstone of southeastern Wyoming, U.S.A.: systematic sedimentary response to relative sea-level change, *in* Dalrymple, R.W., Boyd, R., and Zaitlin, B.A., eds., Incised-Valley Systems: Origin and Sedimentary Sequences: SEPM, Special Publication 51, p. 109-128.
MAYNARD, J.R., FELDMAN, H.R., and ALWAY, R., 2010, From bars to valleys: the sedimentology and seismic geomorphology of fluvial to estuarine incised-valley fills of the Grand Rapids formation (Lower Cretaceous), Iron River field, Alberta, Canada: Journal of Sedimentary Research, v. 80, p. 611-638.
MIALL, A.D., 1985, Architectural-element analysis: a new method of facies analysis applied to fluvial deposits: Earth-Science Reviews, v. 22, p. 261-308.
MIALL, A.D., 1996, The Geology of Fluival Deposits: Sedimentray Facies, Basin Analysis and Petroleum Geology: Heidelgerg, Springer-Verlag Inc., 582 p.
MIALL, A.D., 2010, Alluvial deposits, *in* James, N.P. and Dalrymple, R.W., eds., Facies Model Revisited: SEPM, Special Publication 90, p. 105-137.
MIALL, A.D., and ARUSH, M., 2001, Cryptic sequence boundaries in braided fluvial successions: Sedimentology, v. 48, p. 971-985.
MULDER, T., MIGEON, S., SAVOYE, B., and FAUGERES, J.C., 2001, Inversely graded turbidite sequences in the deep Mediterranean: a record of deposits from flood-generated trubidity current?: Geo-Marine Letters, v. 21, p. 86-93.
MULDER, T., and SYVITSKI, J.P.M., 1995, Tubidity currents generated at river mouths during exceptional discharges to the world's oceans: Journal of Geology, v. 103, p. 285-299.
MULDER, T., SYVITSKI, J.P.M., MIGEON, S., FAUGERES, J.C., and SAVOYE, B., 2003, Marine hyperpycnal flows: initiation, behavior and related deposits. A review: Marine and Petroleum Geology, v. 20, p. 861-882.
MYROW, P.M., LUKENS, C., LAMB, M.P., HOUCK, K., and STRAUSS, J., 2008, Dynamics of a

transgressive prodeltaic system: implications for geography and climate within a Pennsylvanian intracratonic basin, Colorado, U.S.A.: Journal of Sedimentary Research, v. 78, p. 512-528.

NEMEC, W., 1995, The dynamics of deltaic suspension plumes, *in* Oti, M.N., and Postma, G., eds., Geology of Deltas: Rptterdam, Balkema, p. 31-93.

NORTH, C.P., and WARWICK, G.L., 2007, Fluvial fans, myths, concepthions, and the end of terminal fan model: Journal of Sedimentary Research, v. 77, p. 693-701.

OLARIU, C., and BHATTACHARYA, J.P., 2006, Terminal distributary channels and delta front architecture of river-dominated delta systems: Journal of Sedimentary Research, v. 76, p. 212-233.

OLARIU, C., BHATTACHARYA, J.P., XU, X., AIKEN, C.L.V., ZENG, X., and MCMECHAN, G.A., 2005, Integrated study of ancient delta front deposits, using outcrop, ground penetrating radar and three dimension photorealistic data: Cretaceous Panther Tongue Sandstone, Utah, *in* Giosan, L., and Bhattacharya, J.P., eds., River Deltas: Concepts, Models, Examples: SEPM, Special Publication 83, p. 155-178.

OLARIU, C., STEEL, R.J., and PETTER, A.L., 2009, Delta-front hyperpycnal bed geometry and implications for reservior modeling: Cretaceous Panther Tongue delta, Book Cliffs, Utah: AAPG Bulletin, v. 94, p. 819-845.

PATTISON, S.A.J., and WALKER, R.G., 1998, Multiphase transgressive filling of an incised valley and shoreface complex, Viking Formation, Sundance-Edson area, Alberta: Bulletin of Canadian Petroleum Geology, v. 46, p. 89-105.

PLINK-BJORKLUND, P., and STEEL, R., 2006, Incised valley on an Eocene coastal plain and shelf, Spitsbergen-part of a linked shelf-slope system, *in* Dalrymple R.W., Leckie, D.A. and Tillman, R.W., eds., Incised Valleys in Time and Space: SEPM, Special Publication 85, p. 281-307.

PLINT, A.G., 1988, Sharp-based shoreface sequences and "offshore bars" in the Cardium Formation of Alberta: their relationship to relative changes in sea level, *in* Wilgus, C.K., Hastings, C.G., Kendall, C.G.St.C., Posamentier, H.W., Ross, C.A., and Van Wagoner, J.C., eds., Sea-level Changes: An Integreated Approach: SEPM, Special Publication 42, p. 357-370.

PLINT, G., 2010, Wave- and storm-dominated shoreline and shallow-marine systems, *in* Janmes, N.P., and Dalrymple, R.W., eds., Facies Model Revisited: SEPM, Special Publication 90, p. 167-199.

POSAMENTIER, H.W., and ALLEN, G.P., 1999, Siliciclastic Sequence Stratigraphy: Concepts and Applications: SEPM, Concepts in Sedimentology and Paleontology, v. 7, 210 p.

POSAMENTIER, H.W., ALLEN, G.P., JAMES, D.P., and TESSON, M., 1992, Forced regressions in a sequence stratigraphic framework: concepts, examples, and exploration significance: AAPG Bulletin, v. 76, p. 1687-1709.

POSAMENTIER, H.W., JERVEY, M.T., and VAIL, P.R., 1988, Eustatic constrols on clastic deposition I —conceptual framework, *in* Wilgus, C.K., Hastings, B.S., Kendall, C.G.St.C., Posamentier, H.W., Ross, C.A., and Van Wagoner, J.C., eds., Sea-Level Changes: An Integrated Approach: SEPM, Special Publication 42, p. 109-124.

RAHMANI, R.A., 1988, Estuarine tidal channel and nearshore sedimentation of a late Cretaceous epicontinental sea, Drumheller, Alberta, Canada, *in* de Boer, P. L., van Gelder, A., and Nio, S. D., eds., Tide-influenced Sedimentary Environments and Facies: Boston, Reidel Publishing, 433-481 p.

REESINK, A.J.H., and BRIDGE, J.S., 2011, Evidence of bedform superimposition and flow unsteadiness in unit-bar deposits, south Saskatchewan river, Canada: Journal of Sedimentary Research, v. 81, p. 814-840.

REYNOLD, A.D., 1999, Dimensions of paralic sandstone bodies: AAPG Bulletin, v. 83, p. 211-229.

RICE, S.P., CHURCH, M., WOOLDRIDGE, C.L., and EDWARD, J.H., 2008, Morphology and evolution of bars in a wandering gravel-bed river; lower Fraser river, British Columbia, Canada: Sedimentology, v. 56, p. 1-28.

RUBIN, D.M., and MCCULLOCH, D.S., 1980, Single and superimposed bedforms-a synthesis of San Francisco Bay and flume observations: Sedimentary Geology, v. 26, p. 207-231.

RYER, T.A., and ANDERSON, P.B., 2004, Facies of the Ferron Sandstone, East-Central Utah, *in* Chidsey, T.C., Adams R.D.and T.H. Morris, eds., The Fluvial-deltaic Ferron Sandstone: Regional to Wellbore Scale Outcrop Analog Studies and Applications to Reservoir Modeling.: AAPG Studies in Geology, v. 50, p. 59-78.

SAMBROOK SMITH, G.H., ASHWORTH, P.J., BEST, J.L., WOODWARDS, J., and SIMPSON, C.J., 2006, The

sedimentology and alluvial architecture of the sandy braided South Saskatchewan River, Canada: Sedimentology, v. 53, p. 413-434.

SCHOMACKER, E.R., KJEMPERUD, A.V., NYSTUEN, J.P., and JAHREN, J.S., 2010, Recognition and significance of sharp-based mouth bar deposits in the Eocene Green River formation, Uinta basin, Utah: Sedimentology, v. 57, p. 1069-1087.

SEYBOLD, H., ANDRADE, J.J.S., and HERRMANN, H.J., 2007, Modeling river delta formation: Proceedings of the National Academy of Sciences of the United States of America, v. 104, p. 16804-16809.

SHACKLETON, N.J., 1987, Oxygen isogopes, ice volume, and sea level: Quaternary Science Reviews, v. 6, p. 183-190.

SHANLEY, K.W., and MCCABE, P.J., 1993, Alluvial architecture in a sequence stratigraphic framework: a case history from the Upper Cretaceous of southern Utah, USA, in Flint, S.S., and Bryant, I.D., eds., The geological Modelling of hydrocarbon reservoirs and outcrop analogues: International Association of Sedimentology, Special Publication 15, p. 21-55.

SIMMS, A.R., ANDERSON, J.B., TAHA, Z.P., and RODRIGUEZ, A.B., 2006, Overfilled versus underfilled incised valleys: examples from the quaternary Gulf of Mexico, *in* Dalrymple R.W., Leckie, D.A., and Tillman, R.W., eds., Incised Valleys in Time and Space: SEPM, Special publication 85, p. 117-139.

SLINGERLAND, R.L., and SMITH, N.D., 2004, River avulsions and their deposits: Annual Review of Earth and Planetary Sciences, v. 32, p. 257-285.

SMITH, N., 1974, Sedimentology and bar formation in the upper Kicking Horse River, a braided outwash stream: The Journal of Geology, v. 82, p. 205-223.

STRONG, N., and PAOLA, C., 2008, Valleys that never were: time surfaces versus stratigraphic surfaces: Journal of Sedimentary Research, v. 78, p. 579-593.

TAMURA, T., NANAYAMA, F., and SAITO, Y., 2007, Intra-shoreface erosion in response to rapid sea-level fall: depositional record of a tectonically uplifted strand plain, Pacific coast of Japan: Sedimentology, v. 54, p. 1149-1162.

TURNER, B.R., and TESTER, G.N., 2006, The Table Rocks sandstone: a fluvial, friction-dominated lobate mouth bar sandbody in the Westphalian B Coal Measures, NE England: Sedimentary Geology, v. 190, p. 97-119.

VAKARELOV, B.K., BHATTACHARYA, J.P., and NEBRIGIC, D.D., 2006, Importance of high-frequency tectonic sequences during greeenhouse times of Earth history: Geology, v. 34, p. 797-800.

VAN HEERDEN, I.L., and ROBERTS, H., 1988, Facies development of Atchafalaya Delta, Louisiana: a modern bayhead delta: AAPG Bulletin, v. 72, p. 439-453.

VAN WAGONER, J.C., MITCHUM, R.M., CAMPION, K.M., and RAHMANIAN, V.D., 1990, Silicilsastic sequence stratigraphy in well logs, core, and outcrops: concepts for high-resolution correlation of time and facies: American Association of Petroleum Geologists, Methods in Exploration Series, v. 7, 55 p.

VISSER, M.J., 1980, Neap-spring cycles reflected in Holocene subtidal large-sclae bedform deposits: A preliminary note: Geological Society of America Bulletin, v. 8, p. 543-546.

WELLNER, R., BEAUBOUEF, R., VAN WAGONER, J., ROBERTS, H., and SUN, T., 2005, Jet-plume depositional bodies-the primary building blocks of Wax Lake Delta: The Gulf Coast Association of Geological Societies, v. 55, p. 867-909.

WESCOTT, W.A., 1993, Geomorphic thresholds and complex response of fluvial systems-some implications for sequence stratigraphy: AAPG Bulletin, v. 77, p. 1208-1218.

WILLIAMS, G.D., and STELCK, C.R., 1975, Speculations on the Cretaceous paleogeography of North America, *in* Calwell, W.G.E. ed., The Cretaceous System in the Wetern Interior of North America: The Geological Associaion of Canada Special Paper 13, p. 1-20.

WILLIS, A., 2000, Tectonic control of nested sequence architecture in the Sego Sandstone, Neslen Formation and Upper Castlegate Sandstone (Upper Cretaceous), Sevier Foreland Basin, Utah, USA: Sedimentary Geology, v. 136, p. 277-317.

WILLIS, B.J., 1997, Architecture of fluvial-dominated valley-fill deposits in the Cretaceous Fall River Formation: Sedimentology, v. 44, p. 735-757.

WILSON, C.W.J., 1948, Channels and channel-filling sediments of richmond age in south-central Tennessee: Geological Society of America Bulletin v. 59, p. 733-766.

WRIGHT, L.D., 1977, Sediment transport and deposition at river mouths: A synthesis: Geological society of America Bulletin, v. 88, p. 857-868.

WRIGHT, L.D., and COLEMAN, J.M., 1974, Mississippi river mouth processes: effluent dynamics and morphologic development: Journal of Geology, v. 82, p. 751-778.

YALIN, M.S., 1992, River Mechanics: Oxford, U.K., Pergamon Press, 220 p.

YOSHIDA, 2000, Sequence and facies architecture of the upper Blackhawk Formation and the Lower Castlegate Sandstone (Upper Cretaceous), Book Cliffs, Utah, USA: Sedimentary Geology, v. 136.

ZAITLIN, B.A., DALRYMPLE, R., and BOYD, R., 1994, The stratigraphic organization of incised-valley systems associated with relative sea-level change, *in* Dalrymple, R.W., Boyd, R., and Zaitlin, B.A., eds., Incised-Valley Systems: Origin and Sedimentary Sequences: SEPM, Special Publication 51, p. 45-60.

ZHU, Y., 2010, Sequence stratigraphy and facies architecture of the Cretaceous Ferron Notom delta complex, South-Central Utah, USA [unpublished PhD thesis]: University of Houston, Houston, TX, 155 p.

ZHU, Y., BHATTACHARYA, J.P., LI, W., LAPEN, T.J., JICHA, B.R., and SINGER, B.S., 2012, Milankovitch-scale sequence stratigraphy and stepped forced regressions of the Turonian Ferron Notom deltaic complex, south-central Utah, U.S.A.: Journal of Sedimentary Research, v. 82, p. 723-746.